ELUCIDATING THE THERAPEUTIC POTENTIAL OF TRANSCRANIAL PULSE STIMULATION IN DEPRESSION

QIN PING

PhD

The Hong Kong Polytechnic University

2026

The Hong Kong Polytechnic University

Department of Rehabilitation Sciences

Elucidating the therapeutic potential of transcranial pulse stimulation in depression

QIN PING

A thesis submitted in partial fulfilment of the requirements for the degree of Doctor of Philosophy

December 2025

CERTIFICATE OF ORIGINALITY

I hereby declare that this thesis is my own work and that, to the best of my knowledge and belief, it reproduces no material previously published or written, nor material that has been accepted for the award of any other degree or diploma, except where due acknowledgement has been made in the text.

_____ _____ (Signed)

QIN PING _____ (Name of student)

Abstract

Background: Transcranial pulse stimulation (TPS) is a novel, non-invasive brain stimulation technique that uses shock waves to modulate brain function. Preliminary evidence suggests its potential for alleviating depressive symptoms, but no randomized, double-blind, sham-controlled trials have yet confirmed its antidepressive efficacy in major depressive disorder (MDD). Furthermore, the potential of TPS as a combined therapy and its capability to effectively target deeper brain regions associated with depression, such as the dorsal anterior cingulate cortex (dACC) and anterior insula cortex (AIC), remain unexplored.

Methods: This thesis comprises four studies. Study 1 was a systematic review investigating the efficacy and safety of low-intensity transcranial ultrasound stimulation (LITUS). Study 2 was a randomized, double-blind, sham-controlled trial evaluating the clinical and neural effects of TPS in 80 patients with MDD. Study 3 was a randomized, single-blind, crossover pilot trial in 34 healthy individuals examining the behavioral aftereffects of a single TPS session. Study 4 was a randomized, single-blind, sham-controlled pilot trial in 60 healthy individuals testing the feasibility and modulation effects of TPS targeting the dACC and AIC.

Main findings: The systematic review (Study 1) found LITUS to be therapeutically effective for various conditions with a favorable safety profile. In patients with MDD (Study 2), active TPS produced a significantly greater reduction in depression severity compared to sham ($p = 0.048$) and significantly increased resting-state functional connectivity (rsFC) within the left dorsolateral prefrontal cortex

(lDLPFC), as well as between lDLPFC and the left orbitofrontal, superior medial prefrontal, pregenual anterior cingulate, posterior cingulate cortices, and bilateral precuneus and calcarine cortex. Study 3 showed that a single session of TPS of the primary motor cortex did not yield superior behavioral effects compared with a control TPS session of the vertex in healthy individuals. Study 4 demonstrated the feasibility and efficacy of TPS application to dACC and AIC over 2 weeks. Results showed that dACC-TPS reduced risk-taking behavior, whereas AIC-TPS increased it, as measured by the balloon analog risk task. Target-specific TPS-induced rsFC changes were observed following both dACC and AIC stimulation compared to sham. Specifically, dACC stimulation enhanced dACC-seeded rsFC with the bilateral ventrolateral prefrontal, right dorsolateral prefrontal, and right dorsomedial prefrontal cortices. In contrast, AIC stimulation resulted in decreased AIC-seeded rsFC with the right middle and inferior frontal (opercular and triangular parts), right precentral gyrus, right supramarginal, right posterior superior temporal, the left posterior middle temporal, left superior and middle occipital cortices, left middle cingulate cortex, and left cuneus.

Discussions and Conclusions: This research establishes TPS as a safe, well-tolerated, and effective intervention for MDD, with demonstrable neuromodulation effects on depression-relevant brain circuits. However, a single TPS session did not demonstrate sufficient utility in modulating behavior. Conversely, multiple TPS sessions targeting the dACC and AIC were feasible and safe in healthy adults, modulating risk-taking behaviors and producing target-specific neuromodulatory effects. These findings

provide a strong foundation for future studies to optimize TPS protocols, explore the dACC and AIC as novel therapeutic targets, and further investigate the underlying neural mechanisms of depression treatment.

Research Outputs Related to this Report

A. Journal publications during the PhD study period (arising from this thesis):

1. **Qin, P. P.**, Jin, M., Xia, A. W., Li, A. S., Lin, T. T., Liu, Y., Kan, R. L., Zhang, B. B., & Kranz, G. S. (2024). The effectiveness and safety of low-intensity transcranial ultrasound stimulation: A systematic review of human and animal studies. *Neuroscience and biobehavioral reviews*, *156*, 105501. https://doi.org/10.1016/j.neubiorev.2023.105501
2. **Qin, P. P.**, Chak, I. K., Kan, R. L., Jin, M. X., Zhang, B. B., Xia, A. W., Lin, T. T., Wang, S. X., Liu, J. H., Cheung, T., & Kranz, G. S. (2025). Effects of Transcranial Pulse Stimulation of the Primary Motor Cortex on Motor Performance in Healthy Adults: A Randomized Crossover Pilot Study. *CNS neuroscience & therapeutics*, *31*(12), e70711. https://doi.org/10.1002/cns.70711
3. **Qin, P. P.**, Jin, M. X., Kan, R. L., Chak, I. K., Zhang, B. B., Xia, A. W., Lin, T. T., Wang, S. X., Liu, J. H., Cheung, T., & Kranz, G. S. (2026) Prefrontal Transcranial Pulse Stimulation for Major Depressive Disorder: A Randomized Clinical Trial. *JAMA Network Open* (submitted, under 3rd review)

B. Manuscripts during the PhD study period (arising from this thesis):

1. **Qin, P.P.,** et al. Efficacy and safety of transcranial pulse stimulation of the dorsal anterior cingulate cortex and anterior insula cortex in healthy adults: A prospective, randomized, sham-controlled, pilot trial.

Manuscript in preparation.

C. Conference presentations during the PhD study period (arising from this thesis)

1. Li, A. S., **Qin, P. P.**, et al. (2023). An innovative method for precision targeting of brain regions for transcranial pulse stimulation. Presented at the 13th Pan-Pacific Conference on Rehabilitation (13th PPCR) as a traditional oral presentation.
2. **Qin, P. P.,** Xia, A. W., Jin, M., Li, A. S., Lin, T. T., Kranz, G. S. (2023). Efficacy and safety of low-intensity transcranial ultrasound stimulation: A systematic review of human and animal studies. Presented at the 13th Pan-Pacific Conference on Rehabilitation (13th PPCR) as a traditional oral presentation.
3. **Qin, P. P.**, Li, A. S., Xia, A. W., Jin, M., Zhang, B. B., Kan, R. L., Lin, T. T., & Kranz, G. S. (2024). Transcranial pulse stimulation for the treatment of major depressive disorder: A randomized, double-blind, sham-controlled, pilot trial. Presented at the International College of Neuropsychopharmacology (CINP 2024) as a poster presentation.
4. **Qin, P. P.**, Jin, M., Xia, A. W., Chau, W. M., Li, A. S., Zhang, B. B., Kan, R. L., Lin, T. T., & Kranz, G. S. (2024). Neuromodulatory effects of transcranial pulse stimulation. Presented at the 1st Meeting of the Neuromodulation Society in China Great Bay Area as a poster presentation.
5. **Qin, P. P.** & Kranz, G. S. (2024). Elucidating the potential of transcranial pulse stimulation (TPS) to treat depression – from mechanisms to clinical response. Presented at the 1st International

TPS Symposium as a keynote speaker.

6. **Qin, P. P.**, Chau, W. M., Jin, M., Chak, K.Y., Lin, T. T., Xia, A. W., Zhang, B. B., Kan, R. L., & Kranz, G. S. (2024). Transcranial pulse stimulation for the treatment of major depressive disorder: A randomized, double-blind, sham-controlled, pilot trial. Presented at the 1st Annual Conference on Teaching and Learning Innovative Conference in Rehabilitation Sciences as a poster presentation.
7. **Qin, P. P.**, Chau, W. M., Jin, M., Chak, K.Y., Lin, T. T., Xia, A. W., Zhang, B. B., Kan, R. L., & Kranz, G. S. (2025). Effectiveness of transcranial pulse stimulation for major depression: Preliminary evidence for clinical response and neuroimaging mechanisms. Presented at the 36th International College of Neuropsychopharmacology (CINP 2025) as an oral presentation.
8. **Qin, P. P.**, Chau, W. M., Chak, K.Y., Lin, T. T., Jin, M., Xia, A. W., Zhang, B. B., Kan, R. L., & Kranz, G. S. (2025). Therapeutic and neural effects of transcranial pulse stimulation. Presented at the Focused Ultrasound Neuromodulation Conference (FUN25) as a poster presentation.
9. **Qin, P. P.**, Chak, K.Y., Lin, T. T., Jin, M., Kan, R. L., Zhang, B. B., Xia, A. W., Wang, S. X., Yuan, T., Bergmann, T. O., Padberg, F., & Kranz, G. S. (2026). Target-specific neuromodulatory effects of transcranial pulse stimulation of the anterior cingulate cortex and anterior insular cortex. Presented at the 2nd Congress of Neuromodulation Society in Greater Bay Area as a distinguished speaker

D. Journal publications during the PhD study period (not arising from this thesis):

1. Cai, C. X.[#], **Qin, P. P.**[#], Liu, C. Y., Cai, P., & Wei, X. (2026). Postoperative Telerehabilitation in Patients With Hip Fracture: Systematic Review and Meta-Analysis. *JMIR mHealth and uHealth*, *14*, e77341. https://doi.org/10.2196/77341 ([#] contributed equally)
2. Jin, M. X., **Qin, P. P.**, Xia, A. W. L., Kan, R. L. D., Zhang, B. B. B., Tang, A. H. P., Li, A. S. M., Lin, T. T. Z., Giron, C. G., Pei, J. J., & Kranz, G. S. (2024). Neurophysiological and neuroimaging markers of repetitive transcranial magnetic stimulation treatment response in major depressive disorder: A systematic review and meta-analysis of predictive modeling studies. *Neuroscience and biobehavioral reviews*, *162*, 105695. https://doi.org/10.1016/j.neubiorev.2024.105695
3. Jin, M., Xia, A. W. L., Chau, W. M. W., Shi, N. M. X. Y., **Qin, P. P.**, Zhang, B. B. B., Kan, R. L. D., Tang, A. H. P., Lin, T. T. Z., Wang, S. X., Chung, D. W. S., Padberg, F., & Kranz, G. S. (2026). Acute prefrontal hemodynamic responses to intermittent theta burst stimulation correlate with current depression and episode recurrence: A cross-sectional study. *Psychiatry and clinical neurosciences*, 10.1111/pcn.70066. Advance online publication. https://doi.org/10.1111/pcn.70066
4. Kan, R. L. D., Lin, T. T. Z., Zhang, B. B. B., Giron, C. G., Jin, M., **Qin, P. P. I.**, Xia, A. W. L., Chan, S. K. W., Chau, B. K. H., & Kranz, G. S. (2023). Moderators of stimulation-induced neural excitability in the left DLPFC: A concurrent iTBS/fNIRS case study. *Brain*

stimulation, *16*(5), 1445–1447. https://doi.org/10.1016/j.brs.2023.09.015

5. Kan, R. L. D., Zhang, B. B. B., Lin, T. T. Z., Tang, A. H. P., Xia, A. W. L., **Qin, P. P.** I., Jin, M., Fong, K. N. K., Becker, B., Yau, S. Y., & Kranz, G. S. (2024). Sex differences in brain excitability revealed by concurrent iTBS/fNIRS. *Asian journal of psychiatry*, *96*, 104043. https://doi.org/10.1016/j.ajp.2024.104043
6. Kan, R. L. D., Tang, A. H. P., **Qin, P. P.**, Jin, M., Xia, A. W. L., Zhang, B. B. B., Lin, T. T. Z., Wang, S. X., Lin, J. J., Yeung, M. K., Chan, S. K. W., Li, F., Vila-Rodriguez, F., Fong, K. N. K., Padberg, F., & Kranz, G. S. (2026). Utilizing stimulation-evoked hemodynamic activity to predict antidepressant response to intermittent theta-burst stimulation in adults with major depression. *Journal of affective disorders*, 121631. Advance online publication. https://doi.org/10.1016/j.jad.2026.121631
7. Shu, T., Yang, H., Zhao, G., Jin, M., **Qin, P. P.**, Xie, C., Guan, Y., Xian, P., Chen, L., Hou, J., & Kan, R. L. (2025). Prediction models for functional outcomes in prolonged disorders of consciousness: a systematic review and meta-analysis. *Journal of neuroengineering and rehabilitation*, *22*(1), 259. https://doi.org/10.1186/s12984-025-01802-w
8. Wei, X., Zhou, P., Wei, Y., Wu, D., **Qin, P.**, Zhang, Y., Zhu, J., Ren, Z., Li, H., & Zhang, Y. (2024). Comparison of Occupational Performance in Immersive Virtual and Real Environments Among Patients With Stroke: Observational Randomized Crossover Pilot Study. *JMIR*

serious games, *12*, e58388. https://doi.org/10.2196/58388

9. Xia, A. W. L., Jin, M., **Qin, P. P. I.**, Kan, R. L. D., Zhang, B. B. B., Giron, C. G., Lin, T. T. Z., Li, A. S. M., & Kranz, G. S. (2024). Instantaneous effects of prefrontal transcranial magnetic stimulation on brain oxygenation: A systematic review. *NeuroImage*, *293*, 120618. https://doi.org/10.1016/j.neuroimage.2024.120618
10. Xia, A. W. L., Jin, M., Zhang, B. B. B., Kan, R. L. D., Lin, T. T. Z., **Qin, P. P.**, Wang, X., Chau, W. M. W., Shi, N. M. X. Y., Kannan, P., Lu, E. Y., Yuan, T., Jiaqi Zhang, J., & Kranz, G. S. (2025). Investigating the hemodynamic response to iTBS of the left DLPFC: A concurrent iTBS/fNIRS study. *Brain stimulation*, *18*(2), 235–245. https://doi.org/10.1016/j.brs.2025.02.008
11. Xia, A. W., Jin, M., **Qin, P. P.,** Chak, I. K. Y., Zhang, B. B., Kan, R. L. D., Wang, S. X., Lin, T. T. Z., Shi, N. M. X. Y., Lam, V., Chau, W. M. W., Tang, A. H. P., Williams, N., Padberg, F., & Kranz, G. S. (2026). Temporal variation of brain hemodynamics with accelerated iTBS for depression: A single-case concurrent TMS/fNIRS study. Brain stimulation, 19(1), 103020. https://doi.org/10.1016/j.brs.2025.103020

E: Awards to the student during the PhD study period (arising from this thesis):

1. The Student Encouragement Award at the 35th International College of Neuropsychopharmacology (CINP 2024), May 23rd -27th 2024, Tokyo, Japan.
2. The best poster award (the third prize) and traveling award at the 1st Meeting of the Neuromodulation Society in China Great Bay Area,

June 7th-8th 2024, Zhuhai, China.

3. The best poster presentation (bronze award) at the 1st Annual Conference on Teaching and Learning Innovative Conference in Rehabilitation Sciences, December 9th-10th 2024, Hong Kong, China.
4. The 2nd runner-up at the 3rd 3-minute thesis competition (Department of Rehabilitation Science, PolyU), May 21st 2025, Hong Kong, China.
5. The President's Special Commendation at the 36th International College of Neuropsychopharmacology (CINP 2025), June 15th-18th 2025, Melbourne, Australia.

Acknowledgements

I want to sincerely thank my chief supervisor, Dr. Georg Kranz. During my PhD journey, I have gained much more from him than just academic knowledge, brilliant research ideas, and research skills. His positive outlook on life and research, his calming demeanor, his encouraging words, his genuine concern for my physical and mental health, and his focus on work-life balance have all played a crucial role in easing my anxiety and offering great support. I believe these lessons will benefit me not only in my academic career but also throughout my life.

I also want to thank my co-supervisor, Dr. Bolton Chau, and all my teammates. Without their help and support, this journey would not have been easy or joyful. Special thanks go to Jimmy JIN, Rebecca KAN, Bingbing Zhang, and Adam XIA for their assistance with the research projects and for sharing research ideas with me daily. I am also grateful to Tim LIN for developing the targeting method for the TPS studies; to Ivan Chak for conducting TPS follow-up treatments, depression assessments, and data collection for Study 4, as well as organizing the data for Study 4; to Wanda Chau for depression assessments and for referring patients with major depressive disorder; and to Ami Li for depression assessments.

I am grateful to the University Research Facility in Behavioral and Systems Neuroscience for providing the facilities for my experiments. Special thanks to Dr. Celia Dong and Ms. Sophia Ho for their kindness in conducting the magnetic resonance imaging measurements for my participants. I extend my thanks to the Nursing School for supporting the

use of transcranial pulse stimulation. Most importantly, I wish to express my heartfelt thanks to all the participants in the study, without whom this research would not have been possible.

Last but not least, I want to thank my family— especially my parents and husband— for their unconditional love. Their help in caring for my son allowed me to work without concern. Thank you also to all my friends for their love and care, which have helped shape the person I am today.

Table of Contents

Chapter 1 General Introduction.....27

1.1 Major depressive disorder.....27

1.2 Non-invasive brain stimulation for MDD.....28

1.3 Transcranial pulse stimulation.....28

1.4 TPS for depression treatment.....32

1.5 Exploring new treatment strategies by investigating TPS's aftereffects and deeper brain modulation.....33

1.6 Aims and objectives of the research.....34

1.7 Implications of the research.....35

1.8 References.....35

Chapter 2 Literature review: The effectiveness and safety of low-intensity transcranial ultrasound stimulation – A systematic review of human and animal studies (Study 1)* 41

2.1 General introduction of this literature review.....41

2.2 Abstract.....41

2.3 Introduction.....42

2.4 Methods.....44

2.4.1 Search strategy.....44

2.4.2 Inclusion and exclusion criteria.....45

2.4.3 Selection of studies and data extraction.....46

2.4.4 Assessment of risk of bias in included studies.....46

2.4.5 Strategy for qualitative synthesis.....47

2.5 Results.....47

2.5.1 Study selection and study characteristics.....47

2.5.2 Risk of bias within included studies.....72

2.5.3 Neuromodulation effects of LITUS.....79

2.5.3.1 Clinical and pre-clinical outcomes.....81

2.5.3.2 Neurophysiological outcomes.....84

2.5.3.3 Neuroimaging outcomes.....86

2.5.3.4 Histological and biological outcomes.....89

2.5.4 Adverse effects reported in the included studies.....92
2.6 Discussion.....94
2.7 Conclusions.....99
2.8 References.....99
Chapter 3 Transcranial pulse stimulation for major depressive disorder: A randomized, double-blind, sham-controlled clinical trial (Study 2).....109
3.1 Introduction.....109
3.2 Methods.....110
3.2.1 Study overview.....111
3.2.2 Sample size.....111
3.2.3 Inclusion and exclusion criteria.....112
3.2.4 Randomization and allocation concealment.....112
3.2.5 TPS procedure and blinding.....113
3.2.6 Clinical outcome measures.....114
3.2.7 Neuroimaging measures.....115
3.2.8 Statistical analysis.....115
3.3 Study results.....117
3.3.1 Participant characteristics.....117
3.3.2 Clinical outcomes.....120
3.3.2.1 Primary outcomes.....120
3.3.2.2 Secondary outcomes.....121
3.3.2.2.1 Changes in HAMD-17 and PHQ-9 scores.....121
3.3.2.2.2 Response and remission rates.....126
3.3.2.3 Safety.....126
3.3.2.4 Integrity of the blind.....128
3.3.3 Neuroimaging outcomes.....128
3.3.3.1 lDLPFC-seeded rsFC changes.....128
3.3.3.2 Association between lDLPFC-seeded rsFC changes and treatment response.....133
3.3.4 Open-label treatment.....135
3.3.5 3-month follow-up.....135

3.4 Discussion....136
3.4.1 The feasibility and clinical efficacy of TPS for treating major depression....136
3.4.2 The neural effects of lDLPFC-TPS....137
3.4.3 Implementation of standardized MNI-coordinate targeting....138
3.4.4 Study limitations....138
3.5 References....139
Chapter 4: Effects of transcranial pulse stimulation of the primary motor cortex on motor performance in healthy adults: A randomized crossover pilot study (Study 3)* 144
4.1 Introduction....144
4.2 Methods....146
4.2.1 Study overview....146
4.2.2 Sample size....147
4.2.3 Inclusion and exclusion criteria....148
4.2.4 Randomization, allocation concealment, and blinding....148
4.2.5 TPS procedure....149
4.2.5.1 Locating stimulation targets....149
4.2.5.2 TPS parameters and administration....150
4.2.6 Behavioral assessment....152
4.2.7 Statistical analysis....154
4.3 Study results....154
4.3.1 Participants' characteristics....154
4.3.2 NHPT performance....155
4.3.3 SRTT performance....157
4.3.4 Integrity of the blind....159
4.3.5 Safety....159
4.4 Discussion....161
4.4.1 The feasibility and behavioral effects of a single-session TPS....161
4.4.2 Study limitations....162

4.4.3 Implications for future studies....163
4.5 References....164
Chapter 5: Efficacy and safety of transcranial stimulation of the dorsal cingulate cortex and anterior insula cortex in healthy adults: A prospective, randomized, sham-controlled, pilot trial (Study 4)..167
5.1 Introduction....167
5.2 Methods....170
5.2.1 Study overview....170
5.2.2 Sample size....172
5.2.3 Inclusion and exclusion criteria....172
5.2.4 Randomization and allocation concealment....172
5.2.5 TPS procedure and blinding....173
5.2.6 Psychological measurements....175
5.2.7 MRI measurements....177
5.2.8 Statistical analysis....178
5.3 Study results....179
5.3.1 Participants' characteristics....179
5.3.2 Task performance and mood....182
5.3.2.1 Counting Stroop task performance....182
5.3.2.2 BART performance....182
5.3.2.3 GNGT performance....185
5.3.2.4 RMET performance....186
5.3.2.5 Mood....186
5.3.3 Rs-fMRI findings....186
5.3.3.1 Seed-based rsFC changes following TPS....187
5.3.3.2 Association between changes in target-seeded rsFC and changes in psychological assessment....196
5.3.4 Self-perception of TPS's efficacy....198
5.3.5 TPS Safety....198
5.4 Discussion....201
5.4.1 Feasibility and safety of TPS for stimulating the dACC and AIC....201

5.4.2 Stimulation effects on behavioral performance 202
5.4.3 Stimulation effects on rsFC 202
5.4.4 Study limitations 204
5.4.5 Future research direction 204
5.5 References 205
Chapter 6 Conclusions and Suggestions for Future Research 211
Appendices 212
Table S1. Search strategy of MEDLINE through PubMed 212
Table S2. Search strategy of Embase through Embase 212
Table S3. Search strategy of CENTRAL through Cochrane Library.212
Table S4. Search strategy of CINAHL through EBSCOHost 212
Table S5. Search strategy of WOS through Web of Science 212
The treatment compliance in Study 2 212
Table S6. Changes in MADRS scores from baseline to Week 2 and from Week 2 to posttreatment (Week 4) 2123
Table S7. Correlation analysis between the rsFC changes in significant clusters for the Group x Time interaction effect and improved MADRS scores in Study 2 2124
Figure S1. Reaction time interference (incongruent vs. neutral trials) in the counting Stroop task 2126
Figure S2. Accuracy interference (neutral vs. incongruent trials) in the counting Stroop task 212
Figure S3. False alarm rate (FAR) in No-Go trials in the Go/No-Go test (GNGT) with 50% No-Go trials 2128
Figure S4. False alarm rate (FAR) in No-Go trials in the Go/No-Go test (GNGT) with 20% No-Go trials 2129
Figure S5. Scores of the reading mind in the eyes test (RMET) in individual groups 212
Figure S6. Subjective happiness scale (SHS) scores in individual groups 212
Figure S7. Warwick-Edinburgh mental well-being scale (WEMWBS) scores in individual groups. 2122

Figure S8. Profile of mood scale (POMS) scores in individual groups 2123

Table S8. Rs-FC results displaying AIC-seeded clusters with a significant interaction effect (dACC vs. sham x post-TPS vs. pre-TPS) and the corresponding post-hoc analyses (completers: n = 18 dACC group; n = 18 sham group) in Study 4.....2124

Figure S9. AIC-seeded rsFC changes in clusters showing significant interaction effects (dACC vs. sham x post-TPS vs. pre-TPS) in Study 4. 2128

Table S9. RsFC results displaying dACC-seeded clusters with a significant interaction effect (AIC vs. sham x post-TPS vs. pre-TPS) and the corresponding post-hoc analysis (completers: n=17 AIC group; n=18 sham group) in Study 4 212

Figure S10. dACC-seeded rsFC changes in clusters showing significant interaction effects (AIC vs. sham x post-TPS vs. pre-TPS) in Study 4 21233

List of Figures

Figure 1. Study selection process of the systematic review (Study 1)..... 48
Figure 2. Risk of bias assessment for the included studies (Study 1)..... 73
Figure 3. Neuromodulation effects of LITUS in human subjects (Study 1)..... 79
Figure 4. Neuromodulation effects of LITUS in healthy animals (Study 1) 80
Figure 5. Neuromodulation effects of LITUS in animal disease models (Study 1).... 81
Figure 6. Study procedure of Study 2 111
Figure 7. CONSORT flow diagram for Study 2 118
Figure 8. Montgomery-Åsberg Depression Rating Scale (MADRS) score changes in the active and sham groups. 121
Figure 9. Hamilton depression scale-17 (HAMD-17) score changes in the active and sham groups 122
Figure 10. Patient health questionnaire-9 (PHQ-9) score changes in the active and sham groups 123
Figure 11. Clusters with significantly enhanced lDLPFC-seeded resting-state functional connectivity after the active TPS (results from post-hoc analysis of significant Group x Time interaction effect) 133
Figure 12. Experimental design of Study 3..... 147
Figure 13. Procedure for marking the hotspot in the right primary motor cortex..... 150
Figure 14. TPS handpiece positioning for (left) hotspot in the right primary motor cortex and (right) vertex stimulation..... 152
Figure 15. Changes in left-hand NHPT performance over time after the active and control TPS 156
Figure 16. Changes in left-hand SRTT performance over time after the active and control TPS 158
Figure 17. Study procedure of Study 4 171
Figure 18. Stimulation targets in Study 4 175
Figure 19. Average number of pumps in the BART..... 184
Figure 20. Adjusted average number of pumps in the BART. 184
Figure 21. Number of exploded balloons in the BART..... 185
Figure 22. dACC-seeded rsFC changes in clusters showing a significant interaction effect (dACC vs. sham x post-TPS vs. pre-TPS)..... 190
Figure 23. AIC-seeded rsFC changes in clusters showing significant interaction effects (AIC vs. sham x post-TPS vs. pre-TPS)..... 194

List of Tables

Table 1. Characteristics of included human studies 49
Table 2. Characteristics of included animal studies 51
Table 3. Full breakdown of study quality assessment for the included human studies using the Cochrane Risk of Bias 2 tool for randomized trials and for randomized crossover trials 74
Table 4. Full breakdown of study quality assessment for the included animal studies using the Systematic Review Center for Laboratory Animal Experimentation Risk of Bias tool. 76
Table 5. Demographic and clinical characteristics of participants in Study 2 119
Table 6. Linear mixed model analysis of change from baseline to post-treatment by Group interaction and the post-hoc analyses in Study 2 124
Table 7. Adverse events occurred in Study 2 126
Table 8. Rs-fMRI results displaying significant clusters for the group x time interaction effect for the completers (n=33 active; n=33 sham). 130
Table 9. Baseline characteristics of participants (completers, n = 34) in Study 3 154
Table 10. The numerical data of NHPT for both visits for the left hand 156
Table 11. The numerical data of SRTT for both visits for the left hand 158
Table 12. Adverse events occurred in Study 3 159
Table 13. Baseline characteristics of participants (n = 60) in Study 4 180
Table 14. Rs-FC results displaying clusters with a significant interaction effect (dACC vs. sham x post vs. pre) and the corresponding post-hoc analyses (completers: n=18 dACC group; n=18 sham group) 188
Table 15. Rs-FC results displaying clusters with a significant interaction effect (AIC vs. sham x post vs. pre) and the corresponding post-hoc analysis (completers: n=17 AIC group; n=18 sham group). 192
Table 16. Adverse events occurred during the experimental period in Study 4 199

List of Abbreviations

AD: Alzheimer’s disease;

ADHD: attention deficit hyperactivity disorder;

AEPs: auditory evoked potentials;

AIC: anterior insula cortex;

ASD: autism spectrum disorder;

BART: balloon analog risk task;

BDNF: brain-derived neurotrophic factor;

dACC: dorsal anterior cingulate cortex;

DC: duty cycle;

DLPFC: dorsolateral prefrontal cortex;

DMN: default mode network;

DTI: diffusion tensor imaging;

EEG: electroencephalography;

EFD: energy flux densities;

EMG: electromyography;

ESWT: low-energy extracorporeal shock wave therapy;

FAR: false alarm rate;

FDI: first dorsal interosseous;

fTUS: focused transcranial ultrasound stimulation;

GDNF: glial cell line-derived neurotrophic factor;

GLMM: Generalized Linear Mixed Models;

GNGT: Go/No-Go test;

HAMD-17: Hamilton depression scale-17;

ICF: intracortical facilitation;

I_{SPTA}: maximum spatial-peak-temporal-average intensity;

I_{SPPA}: maximum spatial-peak-pulse-average intensity;

ITT: intention-to-treat;

LCN: lateral cerebellar nucleus;

lDLPFC: left dorsolateral prefrontal cortex;

LFP: local field potential;

LITUS: low-intensity transcranial ultrasound stimulation;

LMM: linear mixed model;

MADRS: Montgomery-Åsberg Depression Rating Scale;

MCI: mild cognitive impairment;

MDD: major depressive disorder;

MEG: magnetoencephalogram;

MEPs: motor-evoked potentials;

MI: mechanical index;

MINI: Mini International Neuropsychiatric Interview;

MNI: Montreal Neurological Institute;

MPFC: medial prefrontal cortex;

MRI: magnetic resonance imaging;

NHPT: nine-hole peg test;

NIBS: non-invasive brain stimulation;

TBI: traumatic brain injury;

tDCS: transcranial direct current stimulation;

tb-fTUS: theta-burst focused transcranial ultrasound stimulation;

TES: transcranial electrical stimulation;

TMS: transcranial magnetic stimulation;

TI: thermal index;

TPS: transcranial pulse stimulation;

PD: Parkinson's disease;

PET: positron emission tomography;

PHQ-9: patient health questionnaire-9;

POMS: Profile of Mood States;

RT: reaction time;

RCT: randomized controlled trial;

rM1: right primary motor cortex;

RMET: reading the mind in the eyes test;

rsFC: resting-state functional connectivity;

rs-fMRI: resting-state functional magnetic resonance imaging;

S1: the primary somatosensory cortex;

SEPs: somatosensory evoked potentials;

SHS: Subjective Happiness Scale;

SICI: short-interval intracortical inhibition;

SN: salience network;

SPM12: Statistical Parametric Mapping 12;

SRTT: simple reaction time task;

STN: subthalamic nucleus;

unfocused TUS: unfocused transcranial ultrasound stimulation;

VLPFC: ventrolateral prefrontal cortex;

VEPs: visual evoked potentials

WEMWBS: Warwick-Edinburgh Mental Well-Being Scale

Chapter 1 General Introduction

1.1 Major depressive disorder

Major depressive disorder (MDD) is a global disease with a high disease burden (Mathers, 2008) and a lifetime prevalence ranging from 2 to 21% (Gutierrez-Rojas et al., 2020). Clinically, MDD is characterized by a persistently depressed mood or loss of interest or pleasure for at least two weeks, accompanied by changes in affect, cognition, or neurovegetative functions (American Psychiatric Association and Association, 2013). Neuroimaging studies have identified structural and functional abnormalities in patients with MDD compared to healthy controls. Reported findings include decreased cortical thickness in the medial prefrontal cortex, orbitofrontal cortex, anterior and posterior cingulate cortex, insula, and temporal lobes (Schmaal et al., 2017), as well as reduced volumes in the ventromedial striatum and hippocampus (Schmaal et al., 2016; Drevets, Price, and Furey, 2008). Most of these abnormal structures exhibit a decrease in glucose metabolism and cerebral blood flow (Drevets, Price, and Furey, 2008). Furthermore, resting-state functional magnetic resonance imaging (rs-fMRI) studies reveal that patients with MDD exhibit network deficits within the frontoparietal network, between frontoparietal and parietal regions of the dorsal attention network, and between the affective network and medial prefrontal cortex (MPFC). Conversely, MDD is associated with hyperconnectivity within the default mode network (DMN), as well as between the DMN and MPFC, hippocampus, and dorsolateral prefrontal

cortex (DLPFC) (Kaiser et al., 2015). Together, these structural and functional circuit abnormalities provide a mechanistic basis for the development of precise neuromodulatory treatments for MDD.

1.2 Non-invasive brain stimulation for MDD

Treatment strategies for MDD include pharmacotherapy, psychotherapy, electroconvulsive therapy, deep brain stimulation, and non-invasive brain stimulation (NIBS) (Kupfer, Frank, and Phillips, 2012). Among these, NIBS techniques such as transcranial magnetic stimulation (TMS) and transcranial direct current stimulation (tDCS) have been extensively studied as adjunctive therapies due to their noninvasiveness and promising clinical efficacy (Lefaucheur et al., 2020; Wang, 2019). The left DLPFC is the most common target for NIBS in MDD. Aside from its established effectiveness in alleviating depressive symptoms, neuroimaging studies also highlight the critical role of the left DLPFC. For instance, a cognitive dyscontrol biotype of depression is characterized by hypoactivation of the DLPFC (Williams, 2016), and increased DLPFC activity has been shown during recovery from depressive symptoms in depressed patients (Koenigs and Grafman, 2009).

1.3 Transcranial pulse stimulation

Transcranial pulse stimulation (TPS) (NEUROLITH, Storz Medical AG, Tagerwilen, Switzerland) is a novel CE-approved NIBS technique that utilizes shock waves to modulate brain function (Truong et al., 2022), developed from focused low-energy extracorporeal shock waves (Lohse-

Busch et al., 2014; Lohse-Busch, Reime, and Falland, 2014). Unlike focused transcranial ultrasound stimulation (fTUS), which delivers periodic sonication waves of 500-700 kHz with long sonication trains, TPS delivers single, high-pressure, short-duration (3 μs) shockwave pulses. Each pulse consists of a large positive peak amplitude followed by a small, negative-amplitude pulse, thereby avoiding the hazardous brain heating and secondary stimulation maxima (Sarica et al., 2022). The energy flux densities (EFD) of TPS pulses range from 0.01- 0.25 mJ/ mm^2, with pulse frequencies of 1 - 8 Hz and a maximum peak pressure of 25 MPa. These parameters yield a maximum spatial-peak-temporal-average intensity (I_{SPTA}) of 100 mW/cm^2, a maximum spatial-peak-pulse-average intensity (I_{SPPA}) of 111 W/cm^2, a mechanical index (MI) of 10.95, and a thermal index (TI) < 0.7 (Matt et al., 2022). Although no guideline or safety profile has been established for therapeutic transcranial ultrasound, reference limits are available from the FDA guideline for diagnostic ultrasound ($I_{SPTA\text{-}max}$ = 720m W/cm^2; $I_{SPTA\text{-}max}$ = 94m W/cm^2 for cephalic use; $I_{SPPA\text{-}max}$ = 190 W/cm^2; MI_{max} = 1.9; TI_{max} = 6) (Food and Administration, 2019), and from the International Electro-technical Commission (IEC standard 60601-2-5) for physiotherapy ultrasound equipment ($I_{SPTA\text{-}max}$ = 3 W/cm^2) (Duck, 2007). The current TPS system restricts the maximum EFD for human application to 1 mJ/mm^2 per second (EFD_{max} = 0.2 mJ/ mm^2 at a pulse frequency of 5 Hz; EFD_{max} = 0.25 mJ/ mm^2 at a pulse frequency of 4 Hz), representing a much lower safety threshold than preclinical data suggest (Beisteiner et al., 2020).

The TPS device comprises a mobile TPS handpiece (Neuro handpiece), a near-infrared MR-based navigation system (Polaris Vicra System by Northern Digital Inc.), and a touchscreen interface. Pulses emitted from the handpiece generate a highly focused energy zone within the brain through the skull (Beisteiner et al., 2020). The focus size is 5 mm x 5 mm x 56 mm, with the long axis perpendicular to the skull. Therapeutic penetration depth of the pulses (depth of the focus's center) can be adjusted using an additional stand-off device: 35 mm with a long stand-off device (15 mm), 43.4 mm with a short stand-off device (6.6 mm), and 50 mm without a stand-off device. An in-vitro study indicated that shock waves can be distorted by the skull, resulting in a lateral focal shift of 4-5 mm, with cranial attenuation of pressure and intensity of approximately 85% (Beisteiner et al., 2020).

The safety, feasibility, and efficacy of TPS have been first investigated in healthy subjects (Beisteiner et al., 2020; Matt et al., 2022) and patients with Alzheimer's disease (AD) (Beisteiner et al., 2020; Cont et al., 2022). A randomized, sham-controlled, within-subject study in healthy subjects demonstrated that 10, 100, and 1000 TPS pulses applied to the primary somatosensory cortex modulated neuronal activity, as measured by median nerve somatosensory evoked potentials (Beisteiner et al., 2020). Another randomized, sham-controlled, crossover study in healthy subjects demonstrated that three TPS sessions (1000 pulses each) induced structural and functional brain changes, as indicated by diffusion-tensor imaging and rs-fMRI (Matt et al., 2022). The first uncontrolled TPS clinical pilot study provided preliminary evidence of TPS's effectiveness

in patients with AD (Beisteiner et al., 2020). Neuropsychological scores improved significantly after 6-12 treatment sessions over 2-4 weeks, with effects lasting up to three months. Improvements correlated with increased functional connectivity within the memory network (Beisteiner et al., 2020) and increased cortical thickness in the left superior parietal lobule within the DMN (Popescu, Pernet, and Beisteiner, 2021). Notably, a recent randomized controlled trial further demonstrated therapeutic and neuromodulatory effects of a 2-week TPS treatment in younger patients with AD (Matt et al., 2025). Animal studies corroborate these findings, showing instantaneous and immediate aftereffects of TPS. Specifically, TPS enhanced microvascular networks during stimulation in AD mouse brains (Karakatsani, Nozdriukhin, et al., 2025) and modulated the resting-state functional connectivity (rsFC) in both AD and wild-type mice (Karakatsani, Gezginer, et al., 2025).

Lately, more and more TPS clinical studies have emerged and demonstrated feasibility and therapeutic potential in various disease cohorts including mild cognitive impairment (MCI) (Fong et al., 2023; Lo et al., 2024), depression (Cheung, Li, Ho, et al., 2023), Parkinson's disease (PD) (Osou et al., 2024; Manganotti et al., 2025), attention deficit hyperactivity disorder (ADHD) (Cheung et al., 2024), and autism spectrum disorder (ASD) (Cheung, Li, Lam, et al., 2023).

Mechanistically, TPS differs from fTUS and unfocused transcranial ultrasound stimulation (unfocused TUS) (Qin et al., 2024). Holding the intrinsic properties of shockwaves, TPS mechanically stimulates cell metabolism through mechanotransduction (d'Agostino et al., 2015). This

process promotes neurogenesis and angiogenesis by upregulating brain-derived neurotrophic factor and vascular endothelial growth factor (Ito, Fukumoto, and Shimokawa, 2009; Matsuda et al., 2020; Sun et al., 2006; Yahata et al., 2016), and exerts anti-inflammatory effects by stimulating endothelial nitrogen oxide release (Mariotto et al., 2009).

1.4 TPS for depression treatment

The first TPS clinical trial by Beisteiner et al. (Beisteiner et al., 2020) mentioned above provided initial evidence of its antidepressive effects. Following 2-4 weeks of TPS treatment, administered three sessions per week, patients with AD exhibited significant alleviation of depressive symptoms, accompanied by normalization of functional connectivity between the salience and ventromedial networks (Matt, Dorl, and Beisteiner, 2022). These findings paved the way for TPS research in the field of mental health. More recently, an open-label pilot randomized controlled trial (RCT) evaluated the antidepressive effect of TPS in adults with depressive symptoms (Cheung, Li, Ho, et al., 2023). The results showed that six TPS sessions (300 pulses per session) delivered to the left DLPFC over two weeks significantly reduced the depressive symptoms compared to a waitlist control group. However, the results of existing TPS studies on depression should be interpreted with caution. Potential biases include placebo effects, lack of blinding of assessors and participants, heterogeneity of study populations, imprecise targeting, and limited sample size. Therefore, a double-blind, sham-controlled RCT with a larger sample size is required to validate the effectiveness of TPS

in patients with MDD. Furthermore, the underlying mechanisms of TPS's therapeutic effects in MDD remain unclear and warrant further investigation.

1.5 Exploring new treatment strategies by investigating TPS's aftereffects and deeper brain modulation

Although most studies have applied multiple TPS sessions to broad cortical regions and reported promising therapeutic effects, the majority were uncontrolled trials. This reliance on large-scale stimulation leaves the region-specific modulatory effects and underlying neuromodulatory mechanisms unclear. RCTs targeting specific brain regions are therefore essential to elucidate stimulation-induced modulation. To date, only three RCTs have investigated the target-specific neuromodulatory and behavioral effects of TPS. Beisteiner et al. demonstrated that a single-session TPS of the primary somatosensory cortex (S1) induced immediate changes in somatosensory evoked potentials in healthy individuals (Beisteiner et al., 2020). Matt et al. showed that three S1-TPS sessions enhanced global sensorimotor efficiency for up to one week (Matt et al., 2022). One recent clinical trial found that a single session of TPS applied to the primary motor cortex significantly reduced tremor amplitude in PD patients immediately following stimulation, compared with sham stimulation (Manganotti et al., 2025). Although the above-mentioned studies showed promising neurophysiological and behavioral effects, the aftereffects of a single-session TPS remain insufficiently explored.

Investigating such aftereffects could inform novel treatment strategies, including psychotherapy combined with TPS for depression.

On the other hand, TPS's ability to non-invasively stimulate deeper brain regions holds substantial potential for research and clinical applications in mental health. However, no studies have yet established its feasibility or efficacy in modulating such regions. The dorsal anterior cingulate cortex (dACC) and the anterior insula cortex (AIC) are two major nodes of the salience network (SN), which integrates internal and external stimuli to guide attention and behaviors (Menon and Uddin, 2010). Dysfunction of this SN has been implicated in the pathophysiology of various mental disorders, including depression, anxiety, ASD, obsessive-compulsive disorder, post-traumatic stress disorder, and schizophrenia (Goldstein-Piekarski et al., 2022; Segal et al., 2023). Given TPS's capacity to target deeper brain regions and the relevance of the dACC and AIC to mental health, we aim to investigate the feasibility and modulatory effects of TPS on the dACC and AIC, providing evidence for TPS as a deeper brain stimulation technique and to identify additional therapeutic targets for depression.

1.6 Aims and objectives of the research

To address the research gaps identified above, this project aims to (1) summarize existing evidence from both human and animal studies on the effectiveness and safety of low-intensity transcranial ultrasound stimulation (LITUS); (2) evaluate the antidepressive effect of left DLPFC-TPS in MDD patients; (3) assess TPS-induced changes in brain

circuits using rs-fMRI in MDD patients; (4) examine the aftereffects of a single-session TPS in healthy individuals; and (5) test the feasibility and efficacy of stimulating deeper brain regions with TPS by targeting dACC and AIC in healthy individuals.

1.7 Implications of the research

This project is the first worldwide application of a randomized, double-blind, sham-controlled TPS trial in patients with MDD. It determines TPS as a novel LITUS technique for the treatment of depression and potentially benefits patients with MDD included in the current trial. Secondly, this project is the first investigation of TPS-induced changes in rsFC in MDD patients, thereby advancing understanding of its neural effects in MDD patients. Thirdly, it is the first investigation of the aftereffects (up to 40 minutes post-stimulation) of TPS on motor behavior, thereby leading to a better understanding of TPS's modulatory effects. Fourthly, the project is the first investigation of TPS-induced deeper brain stimulation, demonstrating both behavioral and neuromodulatory effects on deeper brain regions. These findings will provide evidence on the feasibility and capability of deeper brain stimulation with TPS and identify additional therapeutic targets for depression.

1.8 References

American Psychiatric Association, DSMTF, and American Psychiatric Association. 2013. *Diagnostic and statistical manual of mental disorders: DSM-5* (American psychiatric association Washington, DC).

Beisteiner, R., E. Matt, C. Fan, H. Baldysiak, M. Schonfeld, T. Philippi Novak, A. Amini, T. Aslan, R. Reinecke, J. Lehrner, A. Weber, U. Reime, C. Goldenstedt, E. Marlinghaus, M. Hallett, and H. Lohse-Busch. 2020. 'Transcranial Pulse Stimulation with Ultrasound in Alzheimer's Disease-A New Navigated Focal Brain Therapy', *Adv Sci (Weinh)*, 7: 1902583.

Cheung, T., T. M. H. Li, Y. S. Ho, G. Kranz, K. N. K. Fong, S. F. Leung, S. C. Lam, W. F. Yeung, J. Y. T. Lam, K. H. Fong, R. Beisteiner, Y. T. Xiang, and C. P. W. Cheng. 2023. 'Effects of Transcranial Pulse Stimulation (TPS) on Adults with Symptoms of Depression-A Pilot Randomized Controlled Trial', *Int J Environ Res Public Health*, 20.

Cheung, T., T. M. H. Li, J. Y. T. Lam, K. H. Fong, L. Y. Chiu, Y. S. Ho, A. C. Tse, C. T. Li, C. P. Cheng, and R. Beisteiner. 2023. 'Effects of transcranial pulse stimulation on autism spectrum disorder: a double-blind, randomized, sham-controlled trial', *Brain Commun*, 5: fcad226.

Cheung, T., B. K. Yee, B. Chau, J. Y. T. Lam, K. H. Fong, H. Lo, T. M. H. Li, A. M. Li, L. Sun, R. Beisteiner, and C. P. W. Cheng. 2024. 'Efficacy and safety of transcranial pulse stimulation in young adolescents with attention-deficit/hyperactivity disorder: a pilot, randomized, double-blind, sham-controlled trial', *Front Neurol*, 15: 1364270.

Cont, C., N. Stute, A. Galli, C. Schulte, K. Logmin, C. Trenado, and L. Wojtecki. 2022. 'Retrospective real-world pilot data on transcranial pulse stimulation in mild to severe Alzheimer's patients', *Front Neurol*, 13: 948204.

d'Agostino, M. C., K. Craig, E. Tibalt, and S. Respizzi. 2015. 'Shock wave as biological therapeutic tool: From mechanical stimulation to recovery and healing, through mechanotransduction', *Int J Surg*, 24: 147-53.

Drevets, W. C., J. L. Price, and M. L. Furey. 2008. 'Brain structural and functional abnormalities in mood disorders: implications for neurocircuitry models of depression', *Brain Struct Funct*, 213: 93-118.

Duck, F. A. 2007. 'Medical and non-medical protection standards for ultrasound and infrasound', *Prog Biophys Mol Biol*, 93: 176-91.

Fong, T. K. H., T. Cheung, S. T. J. Ngan, K. Tong, W. Y. V. Lui, W. C. Chan, C. S. M. Wong, and C. P. W. Cheng. 2023. 'Transcranial pulse stimulation in the treatment of mild neurocognitive disorders', *Ann Clin Transl Neurol*, 10: 1885-90.

Food, and Drug Administration. 2019. 'Marketing clearance of diagnostic ultrasound systems and transducers', *Guidance for Industry and Food and Drug Administration Staff. Available online: https://www. fda. gov/media/71100/download (accessed on 19 April 2021)*.

Goldstein-Piekarski, A. N., T. M. Ball, Z. Samara, B. R. Staveland, A. S. Keller, S. L. Fleming, K. A. Grisanzio, B. Holt-Gosselin, P. Stetz, J. Ma, and L. M. Williams.

2022. 'Mapping Neural Circuit Biotypes to Symptoms and Behavioral Dimensions of Depression and Anxiety', *Biol Psychiatry*, 91: 561-71.

Gutierrez-Rojas, L., A. Porras-Segovia, H. Dunne, N. Andrade-Gonzalez, and J. A. Cervilla. 2020. 'Prevalence and correlates of major depressive disorder: a systematic review', *Braz J Psychiatry*, 42: 657-72.

Hameroff, S., M. Trakas, C. Duffield, E. Annabi, M. B. Gerace, P. Boyle, A. Lucas, Q. Amos, A. Buadu, and J. J. Badal. 2013. 'Transcranial ultrasound (TUS) effects on mental states: a pilot study', *Brain Stimul*, 6: 409-15.

Ito, K., Y. Fukumoto, and H. Shimokawa. 2009. 'Extracorporeal shock wave therapy as a new and non-invasive angiogenic strategy', *Tohoku J Exp Med*, 219: 1-9.

Jia, X. Z., J. Wang, H. Y. Sun, H. Zhang, W. Liao, Z. Wang, C. G. Yan, X. W. Song, and Y. F. Zang. 2019. 'RESTplus: an improved toolkit for resting-state functional magnetic resonance imaging data processing', *Sci Bull (Beijing)*, 64: 953-54.

Kaiser, R. H., J. R. Andrews-Hanna, T. D. Wager, and D. A. Pizzagalli. 2015. 'Large-Scale Network Dysfunction in Major Depressive Disorder: A Meta-analysis of Resting-State Functional Connectivity', *JAMA Psychiatry*, 72: 603-11.

Karakatsani, M. E., I. Gezginer, D. Nozdriukhin, S. Tiemann, H. A. I. Yoshihara, R. Storz, M. Belau, R. Ni, X. L. Dean-Ben, and D. Razansky. 2025. 'Transcranial pulse stimulation modulates neuronal activity and functional network dynamics', *Brain Stimul*, 18: 1834-42.

Karakatsani, Maria Eleni, Daniil Nozdriukhin, Savannah Tiemann, Hikari A. I. Yoshihara, Rafael Storz, Markus Belau, Ruiqing Ni, Daniel Razansky, and Xosé Luís Deán-Ben. 2025. 'Multimodal imaging of murine cerebrovascular dynamics induced by transcranial pulse stimulation', *Alzheimer's & Dementia*, 21.

Koenigs, Michael, and Jordan Grafman. 2009. 'The functional neuroanatomy of depression: Distinct roles for ventromedial and dorsolateral prefrontal cortex', *Behavioural Brain Research*, 201: 239-43.

Kupfer, D. J., E. Frank, and M. L. Phillips. 2012. 'Major depressive disorder: new clinical, neurobiological, and treatment perspectives', *Lancet*, 379: 1045-55.

Lee, T. M. C., L. Liang, W. K. Hou, A. H. Y. Tse, and C. C. H. Chan. 2023. 'The Chinese "Reading the Mind in the Eyes" Test: A study with normal adults, and adults with Asperger syndrome/high-functioning autism', *Asian J Psychiatr*, 89: 103785.

Lefaucheur, J. P., A. Aleman, C. Baeken, D. H. Benninger, J. Brunelin, V. Di Lazzaro, S. R. Filipovic, C. Grefkes, A. Hasan, F. C. Hummel, S. K. Jaaskelainen, B. Langguth, L. Leocani, A. Londero, R. Nardone, J. P. Nguyen, T. Nyffeler, A. J. Oliveira-Maia, A. Oliviero, F. Padberg, U. Palm, W. Paulus, E. Poulet, A. Quartarone, F. Rachid, I. Rektorova, S. Rossi, H. Sahlsten, M. Schecklmann, D. Szekely, and U. Ziemann. 2020. 'Evidence-based guidelines on the therapeutic use of repetitive transcranial

magnetic stimulation (rTMS): An update (2014-2018)', *Clin Neurophysiol*, 131: 474-528.

Lo, H. K., T. K. Fong, T. Cheung, S. J. Ngan, W. V. Lui, W. C. Chan, C. S. Wong, T. K. Wong, and C. P. Cheng. 2024. 'Enhanced Cognition and Modulation of Brain Connectivity in Mild Neurocognitive Disorder: The Promise of Transcranial Pulse Stimulation', *Biomedicines*, 12.

Lohse-Busch, H., E. Marlinghaus, U. Reime, and U. Mowis. 2014. 'Focused low-energy extracorporeal shock waves with distally symmetric polyneuropathy (DSPNP): a pilot study', *NeuroRehabilitation*, 35: 227-33.

Lohse-Busch, H., U. Reime, and R. Falland. 2014. 'Symptomatic treatment of unresponsive wakefulness syndrome with transcranially focused extracorporeal shock waves', *NeuroRehabilitation*, 35: 235-44.

Manganotti, P., M. Liccari, T. Maria Isabella Lombardo, J. Della Toffola, V. Cenacchi, M. Catalan, and P. Busan. 2025. 'Effect of a single session of transcranial pulse stimulation (TPS) on resting tremor in patients with Parkinson's disease', *Brain Res*, 1850: 149405.

Mariotto, S., A. C. de Prati, E. Cavalieri, E. Amelio, E. Marlinghaus, and H. Suzuki. 2009. 'Extracorporeal shock wave therapy in inflammatory diseases: molecular mechanism that triggers anti-inflammatory action', *Curr Med Chem*, 16: 2366-72.

Mathers, Colin. 2008. *The global burden of disease: 2004 update* (World Health Organization).

Matsuda, M., H. Kanno, T. Sugaya, S. Yamaya, K. Yahata, K. Handa, T. Shindo, H. Shimokawa, H. Ozawa, and E. Itoi. 2020. 'Low-energy extracorporeal shock wave therapy promotes BDNF expression and improves functional recovery after spinal cord injury in rats', *Exp Neurol*, 328: 113251.

Matt, E., G. Dorl, and R. Beisteiner. 2022. 'Transcranial pulse stimulation (TPS) improves depression in AD patients on state-of-the-art treatment', *Alzheimers Dement (N Y)*, 8: e12245.

Matt, E., L. Kaindl, S. Tenk, A. Egger, T. Kolarova, N. Karahasanovic, A. Amini, A. Arslan, K. Saricicek, A. Weber, and R. Beisteiner. 2022. 'First evidence of long-term effects of transcranial pulse stimulation (TPS) on the human brain', *J Transl Med*, 20: 26.

Matt, Eva, Michael Mitterwallner, Sonja Radjenovic, Daria Grigoryeva, Alexandra Weber, Elisabeth Stögmann, Alina Domitner, Anna Zettl, Sarah Osou, and Roland Beisteiner. 2025. 'Ultrasound Neuromodulation With Transcranial Pulse Stimulation in Alzheimer Disease', *JAMA Network Open*, 8.

Menon, V., and L. Q. Uddin. 2010. 'Saliency, switching, attention and control: a network model of insula function', *Brain Struct Funct*, 214: 655-67.

Osou, S., S. Radjenovic, L. Bender, M. Gaal, A. Zettl, G. Dorl, E. Matt, and R. Beisteiner. 2024. 'Novel ultrasound neuromodulation therapy with transcranial pulse stimulation (TPS) in Parkinson's disease: a first retrospective analysis', *J Neurol*, 271: 1462-68.

Popescu, T., C. Pernet, and R. Beisteiner. 2021. 'Transcranial ultrasound pulse stimulation reduces cortical atrophy in Alzheimer's patients: A follow-up study', *Alzheimers Dement (N Y)*, 7: e12121.

Qin, P. P., M. Jin, A. W. Xia, A. S. Li, T. T. Lin, Y. Liu, R. L. Kan, B. B. Zhang, and G. S. Kranz. 2024. 'The effectiveness and safety of low-intensity transcranial ultrasound stimulation: A systematic review of human and animal studies', *Neurosci Biobehav Rev*, 156: 105501.

Rao, H., M. Korczykowski, J. Pluta, A. Hoang, and J. A. Detre. 2008. 'Neural correlates of voluntary and involuntary risk taking in the human brain: an fMRI Study of the Balloon Analog Risk Task (BART)', *Neuroimage*, 42: 902-10.

Sarica, C., J. F. Nankoo, A. Fomenko, T. C. Grippe, K. Yamamoto, N. Samuel, V. Milano, A. Vetkas, G. Darmani, M. N. Cizmeci, A. M. Lozano, and R. Chen. 2022. 'Human Studies of Transcranial Ultrasound neuromodulation: A systematic review of effectiveness and safety', *Brain Stimul*, 15: 737-46.

Schmaal, L., D. P. Hibar, P. G. Samann, G. B. Hall, B. T. Baune, N. Jahanshad, J. W. Cheung, T. G. M. van Erp, D. Bos, M. A. Ikram, M. W. Vernooij, W. J. Niessen, H. Tiemeier, A. Hofman, K. Wittfeld, H. J. Grabe, D. Janowitz, R. Bulow, M. Selonke, H. Volzke, D. Grotegerd, U. Dannlowski, V. Arolt, N. Opel, W. Heindel, H. Kugel, D. Hoehn, M. Czisch, B. Couvy-Duchesne, M. E. Renteria, L. T. Strike, M. J. Wright, N. T. Mills, G. I. de Zubicaray, K. L. McMahon, S. E. Medland, N. G. Martin, N. A. Gillespie, R. Goya-Maldonado, O. Gruber, B. Kramer, S. N. Hatton, J. Lagopoulos, I. B. Hickie, T. Frodl, A. Carballedo, E. M. Frey, L. S. van Velzen, Bwjh Penninx, M. J. van Tol, N. J. van der Wee, C. G. Davey, B. J. Harrison, B. Mwangi, B. Cao, J. C. Soares, I. M. Veer, H. Walter, D. Schoepf, B. Zurowski, C. Konrad, E. Schramm, C. Normann, K. Schnell, M. D. Sacchet, I. H. Gotlib, G. M. MacQueen, B. R. Godlewska, T. Nickson, A. M. McIntosh, M. Papmeyer, H. C. Whalley, J. Hall, J. E. Sussmann, M. Li, M. Walter, L. Aftanas, I. Brack, N. A. Bokhan, P. M. Thompson, and D. J. Veltman. 2017. 'Cortical abnormalities in adults and adolescents with major depression based on brain scans from 20 cohorts worldwide in the ENIGMA Major Depressive Disorder Working Group', *Mol Psychiatry*, 22: 900-09.

Schmaal, L., D. J. Veltman, T. G. van Erp, P. G. Samann, T. Frodl, N. Jahanshad, E. Loehrer, H. Tiemeier, A. Hofman, W. J. Niessen, M. W. Vernooij, M. A. Ikram, K. Wittfeld, H. J. Grabe, A. Block, K. Hegenscheid, H. Volzke, D. Hoehn, M. Czisch, J. Lagopoulos, S. N. Hatton, I. B. Hickie, R. Goya-Maldonado, B. Kramer, O. Gruber, B. Couvy-Duchesne, M. E. Renteria, L. T. Strike, N. T. Mills, G. I. de Zubicaray, K.

L. McMahon, S. E. Medland, N. G. Martin, N. A. Gillespie, M. J. Wright, G. B. Hall, G. M. MacQueen, E. M. Frey, A. Carballedo, L. S. van Velzen, M. J. van Tol, N. J. van der Wee, I. M. Veer, H. Walter, K. Schnell, E. Schramm, C. Normann, D. Schoepf, C. Konrad, B. Zurowski, T. Nickson, A. M. McIntosh, M. Papmeyer, H. C. Whalley, J. E. Sussmann, B. R. Godlewska, P. J. Cowen, F. H. Fischer, M. Rose, B. W. Penninx, P. M. Thompson, and D. P. Hibar. 2016. 'Subcortical brain alterations in major depressive disorder: findings from the ENIGMA Major Depressive Disorder working group', *Mol Psychiatry*, 21: 806-12.

Segal, A., L. Parkes, K. Aquino, S. M. Kia, T. Wolfers, B. Franke, M. Hoogman, C. F. Beckmann, L. T. Westlye, O. A. Andreassen, A. Zalesky, B. J. Harrison, C. G. Davey, C. Soriano-Mas, N. Cardoner, J. Tiego, M. Yucel, L. Braganza, C. Suo, M. Berk, S. Cotton, M. A. Bellgrove, A. F. Marquand, and A. Fornito. 2023. 'Regional, circuit and network heterogeneity of brain abnormalities in psychiatric disorders', *Nat Neurosci*, 26: 1613-29.

Sun, Y., K. Jin, J. T. Childs, L. Xie, X. O. Mao, and D. A. Greenberg. 2006. 'Vascular endothelial growth factor-B (VEGFB) stimulates neurogenesis: evidence from knockout mice and growth factor administration', *Dev Biol*, 289: 329-35.

Truong, D. Q., C. Thomas, B. M. Hampstead, and A. Datta. 2022. 'Comparison of Transcranial Focused Ultrasound and Transcranial Pulse Stimulation for Neuromodulation: A Computational Study', *Neuromodulation*, 25: 606-13.

Wang, Y. 2019. 'Transcranial direct current stimulation for the treatment of major depressive disorder: A meta-analysis of randomized controlled trials', *Psychiatry Res*, 276: 186-90.

Williams, Leanne M. 2016. 'Precision psychiatry: a neural circuit taxonomy for depression and anxiety', *The Lancet Psychiatry*, 3: 472-80.

Wischnewski, M., and D. J. Schutter. 2015. 'Efficacy and Time Course of Theta Burst Stimulation in Healthy Humans', *Brain Stimul*, 8: 685-92.

Yahata, K., H. Kanno, H. Ozawa, S. Yamaya, S. Tateda, K. Ito, H. Shimokawa, and E. Itoi. 2016. 'Low-energy extracorporeal shock wave therapy for promotion of vascular endothelial growth factor expression and angiogenesis and improvement of locomotor and sensory functions after spinal cord injury', *J Neurosurg Spine*, 25: 745-55.

Zeng, K., G. Darmani, A. Fomenko, X. Xia, S. Tran, J. F. Nankoo, Y. Shamli Oghli, Y. Wang, A. M. Lozano, and R. Chen. 2022. 'Induction of Human Motor Cortex Plasticity by Theta Burst Transcranial Ultrasound Stimulation', *Ann Neurol*, 91: 238-52.

Chapter 2 Literature review: The effectiveness and safety of low-intensity transcranial ultrasound stimulation – A systematic review of human and animal studies (Study 1)*

*Published in *Neuroscience and Biobehavioral Reviews* in December 2024

2.1 General introduction of this literature review

TPS is one of the LITUS techniques that utilizes ultra-short ultrasound - shockwaves to modulate the brain. To enhance understanding of the modulatory effects of LITUS and TPS, a literature review was conducted to examine LITUS applications in both clinical and preclinical settings. This literature review has been published in Neuroscience and Biobehavioral Reviews (Qin et al., 2024).

2.2 Abstract

Low-intensity transcranial ultrasound stimulation (LITUS) is a novel non-invasive neuromodulation technique. We conducted a systematic review to evaluate current evidence on the efficacy and safety of LITUS neuromodulation. Five databases were searched from inception to May 31, 2023. Randomized controlled human trials and controlled animal studies were included. The neuromodulation effects of LITUS on clinical or pre-clinical, neurophysiological, neuroimaging, histological and biochemical outcomes, and adverse events were summarized. In total, 11 human studies and 44 animal studies were identified. Overall, LITUS alleviates various symptoms and modulates associated brain circuits

without major side effects. Future research needs to establish a solid therapeutic framework for LITUS.

2.3 Introduction

Low-intensity transcranial ultrasound stimulation (LITUS) is a newly developed non-invasive brain stimulation (NIBS) technique that offers promising neuromodulation by acoustic energy transmitted into the brain parenchyma. LITUS typically reaches deeper brain regions with a high spatial resolution than transcranial magnetic stimulation (TMS) or transcranial electrical stimulation (TES), which sparks interest in the field (Fomenko et al., 2018). Unlike high-intensity transcranial focused ultrasound, which mediates brain function through thermal effects or ablation of diseased brain structure, LITUS aims to modulate neuronal activity through a non-thermal mechanism with minimal risk of tissue damage (Fini and Tyler, 2017; Tsui et al., 2005). Such a kind of neuromodulation through multiple ultrasound pulses is referred to as sonication in the LITUS literature.

LITUS has developed rapidly in recent years. In 2008, an ex vivo study first discovered the excitatory modulation effect of LITUS on neuronal activity and brain networks by using a low-intensity (temporal average intensity, I_{TA} < 300m W/cm^2), low-frequency (< 0.65M Hz) ultrasonic stimulation (Tyler et al., 2008). Two years later, similar low-intensity, low-frequency ultrasound waves were applied to mouse brains through the skull, and ultrasound-elicited neuronal activity was detected in the motor cortex and hippocampus (Tufail et al., 2010). The first LITUS

human study was conducted in 2013. Higher frequency (8M Hz), and low acoustic intensity (I_{TA} < 152m W/cm^2) unfocused ultrasound was used to target the posterior frontal cortex in patients with chronic pain. The treatment group showed a significant improvement in mood compared to the placebo group (Hameroff et al., 2013). Since then, an increasing number of studies have emerged with extensive applications of LITUS in both animals and humans. However, to date, there is no guideline on the therapeutic use of LITUS. To establish the safety margin and to promote the therapeutic use of ultrasound as a NIBS technique, most studies determined the stimulated intensity based on the FDA recommendation for diagnostic ultrasound with spatial-peak temporal average intensity (I_{SPTA}) < 720m W/cm^2 and spatial-peak pulse average intensity (I_{SPPA}) < 190 W/cm^2 (FDA, 2019), or based on the recommendation of the International Electro-technical Commission (IEC standard 60601-2-5) for physiotherapeutic ultrasound devices with I_{SPTA} < 3 W/cm^2 (Duck, 2007). Here, I_{SPPA} stands for the average pulse intensity at the spatial maximum position, relating to the short-term mechanical bio-effect. I_{SPTA} means the temporal average intensity at the spatial maximum position relating to the thermal bio-effect (Fomenko et al., 2018). In addition, LITUS has been classified into the following three types : (1) focused transcranial ultrasound stimulation (fTUS): performed with focused ultrasound transducers (Darmani et al., 2022); (2) unfocused transcranial ultrasound stimulation (unfocused TUS): performed with unfocused ultrasound transducers (Darmani et al., 2022); (3) transcranial pulse stimulation (TPS): performed with a device generating single ultrashort ultrasound

pulses (3 μs) at frequencies of 1-5 Hz, with I_{SPTA} = 100m W/cm^2 and I_{SPPA} = 111 W/cm^2 (Matt et al., 2022).

Previous systematic reviews summarized studies that revealed transcranial ultrasound stimulation effects on brain excitability and behavior (Sarica et al., 2022; Wang et al., 2019). However, the included studies had highly heterogeneous study designs, including randomized controlled design, within-subject design, uncontrolled design, and case reports, which limited the interpretation of this novel technique for its implementation in clinical and research settings. Moreover, within-subject studies with no adequate washout period were also included, which may introduce carryover effects, as compelling evidence showed that one LITUS session can induce a long-lasting neuromodulation effect for up to 40 minutes (Gibson et al., 2018; Hameroff et al., 2013; Zeng et al., 2022). Therefore, the present study aimed to systematically review and synthesize randomized controlled human trials and in vivo controlled animal studies to investigate the neuromodulation effects and side effects of LITUS.

2.4 Methods

This systematic review followed the standards established in the Preferred Reporting Items for Systematic Reviews and Meta-Analysis (PRISMA) Statement (Page et al., 2021), and was registered on PROSPERO (CRD42023399150).

2.4.1 Search strategy

MEDLINE (via PubMed), Embase (via Embase), CENTRAL (in the Cochrane Library), CINAHL (via EBSCOHost), and WOS (via Web of Science) were searched from database inception to May 31, 2023. The language was limited to English and Chinese. The following keywords were used: “low intensity transcranial ultrasound”, “transcranial focused ultrasound”, “transcranial unfocused ultrasound”, “low intensity transcranial focused ultrasound”, “transcranial pulse stimulation”, “transcranial ultrasound”, “focused ultrasound”, “transcranial”, “ultrasound”, “neuromodulation”. See Appendices (Table S1-S5) for the detailed search strategy. Reference lists of relevant reviews and included studies were searched to identify potential records.

2.4.2 Inclusion and exclusion criteria

Studies were eligible for inclusion if they (1) were human studies with a randomized controlled design (including crossover design) or were controlled animal studies (inclusion was not limited to the randomized controlled design for animal studies as randomization in animal studies is not standardized) (Hooijmans et al., 2014); (2) used LITUS to modulate brain function through mechanical effect; here, we included studies that reported the use of low-intensity TUS or non-thermal TUS, or studies that used acoustic intensity that met FDA or IEC recommendations (Duck, 2007; FDA, 2019); (3) had a blank control group or sham control group; (4) had outcomes of interests including clinical or pre-clinical, neurophysiological, neuroimaging, histological and biochemical findings. Studies were excluded if they (1) used LITUS to open the blood-brain

barrier in combination with microbubble injection for substance delivery; (2) conducted repeated measures without a washout time greater than 40 minutes.

2.4.3 Selection of studies and data extraction

Two reviewers (PQ & WLX) independently screened the titles and abstracts. The full text was assessed using inclusion and exclusion criteria. Any disagreements between the two reviewers were solved through discussion with the third reviewer (MXJ). Data was extracted by two independent reviewers (PQ & WLX) and recorded in a standardized form. The following information was extracted: (1) characteristics of subjects or animal models; (2) type of LITUS and control; (3) treatment parameters of LITUS (e.g., total intervention sessions, stimulation target and sonication parameters); (4) outcome measures; (5) main results of LITUS neuromodulation effects; (6) side effects of LITUS. Any disagreements between the two reviewers were solved through discussion with the third reviewer (MXJ).

2.4.4 Assessment of risk of bias in included studies

Two reviewers (PQ & WLX) independently assessed the risk of bias for each study. We used the Cochrane Risk of Bias 2 tool (Cochrane RoB 2.0) to assess the risk of bias for human studies, which comprises six domains: randomization process, period and carryover effects (applicable for crossover trials), deviations from the intended intervention, missing outcome data, measurement of the outcome, and selection of the reported

result (Sterne et al., 2019). We used the Systematic Review Center for Laboratory Animal Experimentation risk of bias (SYRCLE's RoB) tool for animal experiments and assessed selection bias, performance bias, detection bias, attrition bias, reporting bias and other biases (Hooijmans et al., 2014). Any disagreements between the two reviewers were solved by consulting the third reviewer (MXJ).

2.4.5 Strategy for qualitative synthesis

Given the high heterogeneity of the included studies, it was not possible to perform meta-analyses (Cochrane, 2022). The neuromodulation outcomes of LITUS were categorized into four domains: clinical and pre-clinical, neurophysiological, neuroimaging, and histological and biochemical results. Studies with the same outcome of interest were grouped, and the comparative results between the LITUS group and the control group were summarized. In addition, the adverse effects associated with LITUS reported in individual studies were summarized.

2.5 Results

2.5.1 Study selection and study characteristics

The original search of the databases identified 1618 records and 180 studies were retrieved for full-text review. A total of 11 human studies and 44 animal studies were included in this systematic review. The study selection process is shown in Figure 1.

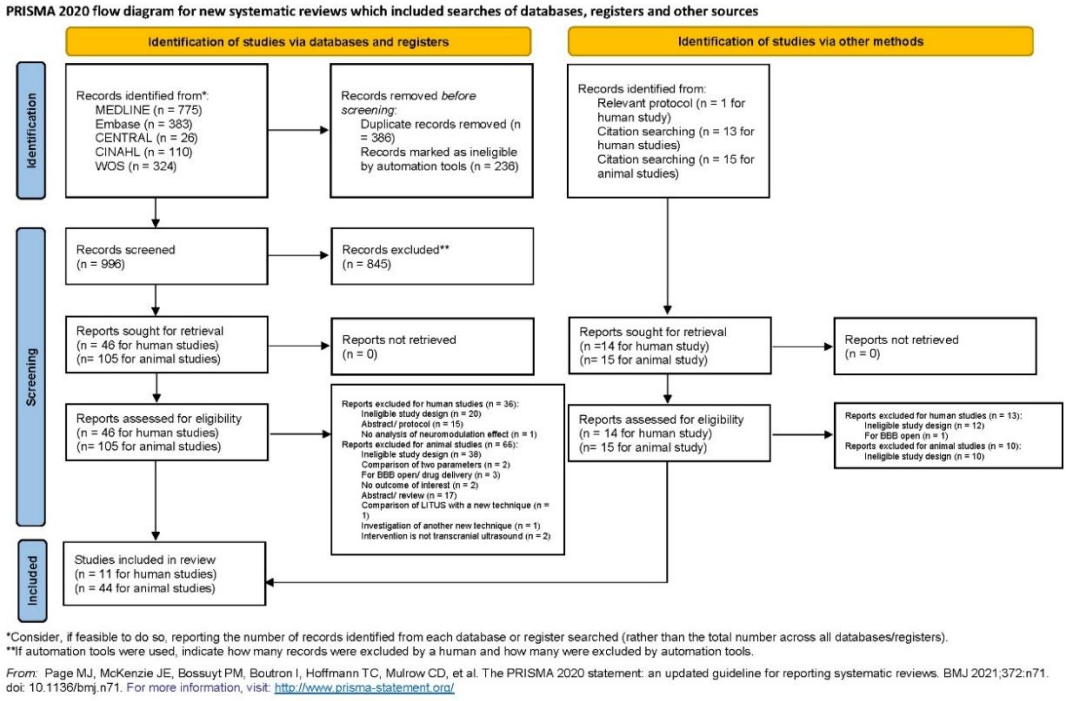

Figure 1. Study selection process of the systematic review (Study 1)

Table 1 shows detailed characteristics of individual human studies. Eight of eleven human studies included healthy subjects, two studies included patients with depression, and one study included patients with chronic pain. Table 2 shows detailed characteristics of individual animal studies. Various disease models were used in animal studies, including Parkinson's disease (PD), depression, epilepsy, pain, ischemic brain injury, demyelination, Alzheimer's disease (AD), attention deficit hyperactivity disorder (ADHD), traumatic brain injury (TBI), hypertension, schizophrenia, sleep disorder, addictive disorder, and essential tremor.

Table 1. Characteristics of included human studies

Study	Type of subjects	Grouping (sample size)	Characteristics of LITUS			Main outcomes			Reported adverse effect
			Target	Stimulation sessions	Parameters	Outcome measures	Timepoint of outcome measurements	Main results (experimental group compared to the control group)	
Matt 2022	Healthy subjects	TPS; Sham; (n=12 in the crossover study)	Left primary somatosensory cortex	4 min/ session; 3 sessions in consecutive 3 days	Pulse frequency: 4 Hz; Energy level: 0.25 mJ/mm^2; I_{SPTA}: 100 mW/cm^2; I_{SPPA}: 111 W/cm^2; Number of pulses in a session: 1000; MI: 10.95	sMRI DTI Rs-fMRI	Around 1 week after stimulation	No significant difference in grey matter volume between groups A decrease in axial diffusivity in the primary somatosensory cortex and primary motor cortex An increase in global efficiency in the left sensorimotor network	sMRI did not reveal any signs of bleeding, edema, or other morphological alterations after the TPS and the sham TPS
Cheung 2023	Patients with major depression	TPS (n=15); No TPS (n=15)	Left dorsal lateral prefrontal cortex	1.25-1.6 min/ session; 3 sessions/week for 2 weeks	Pulse frequency: 3-4 Hz; Energy level: 0.2-0.25 mJ/mm^2; I_{SPTA}: 100 mW/cm^2; I_{SPPA}: 111 W/cm^2; Number of pulses in a session: 300; MI: 10.95	HDRS-17	At stimulation endpoint	A decrease in score	4% subjects reported headaches; One subject experienced nausea and vomiting
Badran 2020	Healthy subjects	fTUS; Sham; (n=19 in the crossover study)	Right anterior thalamus	10 min/ session; 2 sessions in one day with a 10-min interval	F_0: 0.65 MHz; I_{SPTA}: 995 mW/cm^2; I_{SPTA}: 719 mW/cm^2 (after the attenuation through the skull); I_{SPPA}: 19.9 W/cm^2; I_{SPPA}: 14.38 W/cm^2 (after the attenuation through the skull); SD: 30 s; Trials of sonication: 10; ISI: 30 s; PRF: 10 Hz; PD: 5 ms; DC: 5%; Number of pulses in a sonication: 300; Peak rarefactional pressure 0.72 MPa; MI: 0.89	QST	At stimulation endpoint	An increase in thermal pain threshold	No adverse events were observed throughout the experiment
Samuel 2022	Healthy subjects	tb-fTUS; Sham; (n=15 in	Left motor cortex	80 s/ session; 1 session	F_0: 0.5 MHz; I_{SPTA}: 230 mW/cm^2; I_{SPPA}: 2.26 W/cm^2; SD: 80 s; PRF: 5 Hz; PD: 20 ms; DC:	MEP induced by TMS	At stimulation endpoint	An increase in MEP amplitude	

		the crossover study)			10%; Number of pulses in a sonication: 400; Peak rarefactional pressure: NR; MI: NR	SICI induced by TMS MEG		A decrease in SICI An increase in alpha spectral power in right sensorimotor/frontal cortex and an increase in beta spectral power in right sensorimotor/parieto-occipital cortex	No subjects reported any adverse effects throughout the experiment
Sanguinetti 2020	Healthy subjects	fTUS (n=24); Sham (n=24)	Right inferior frontal gyrus	30 s/ session; 1 session	F_0: 0.5 MHz; I_{SPTA}: 130 mW/cm^2; I_{SPPA}: 54 W/cm^2; I_{SPPA}: 16.2 W/cm^2 (after the attenuation through the skull); SD: 30 s; PRF: 40 Hz; PD: 0.065 ms; DC: 0.26%; Number of pulses in a sonication: 1200; Peak rarefactional pressure: 1.27 MPa; MI: 1.8	VAMS	10 minutes, 20 minutes, and 30 minutes after stimulation	An increase in global affect score 20 minutes and 30 minutes after stimulation	NR
Zeng 2022	Healthy subjects	tb-fTUS; Sham; (n=15 in the crossover study)	Left motor cortex	80 s/ session; 1 session	F_0: 0.5 MHz; I_{SPTA}: 230 mW/cm^2; I_{SPPA}: 2.26 W/cm^2; SD: 80 s; PRF: 5 Hz; PD: 20 ms; DC: 10%; Number of pulses in a sonication: 400; Peak rarefactional pressure: NR; MI: NR	MEP induced by TMS SICI induced by TMS ICF induced by TMS	5 minutes, 30 minutes, and 60 minutes after stimulation	An increase in MEP amplitude 5 minutes and 30 minutes after stimulation A decrease in SICI 5 minutes and 30 minutes after stimulation An increase in ICF 5 minutes after stimulation	No subjects reported any adverse effects throughout the experiments
	Healthy subjects	tb-fTUS; Sham; (n=12 in the crossover study)	Left motor cortex	80 s/ session; 1 session	F_0: 0.5 MHz; I_{SPTA}: 230 mW/cm^2 ; I_{SPPA}: 2.26 W/cm^2; SD: 80 s; PRF: 5 Hz; PD: 20 ms; DC: 10%; Number of pulses in a sonication: 400; Peak rarefactional pressure: NR; MI: NR	Visuomotor task	10 minutes after stimulation	A decrease in movement time	
Zhang 2022a	Healthy subjects	fTUS; Sham; (n=20 in the	Left motor cortex	10 min/ session; 1 session	F_0: 0.8 MHz; Intensity: 1.2 W/cm^2; SD: 1 s; Trials of sonication: 200; ISI: 2 s; PRF: NR;	Finger tapping test	At stimulation endpoint	An increase in score	

		crossover study)			PD: NR; DC: NR; Number of pulses in a sonication: NR; Peak rarefactional pressure: NR; MI: NR	MEP induced by TMS		A decrease in MEP latency and an increase in MEP amplitude	No significant difference of discomfort score between groups
Reznik 2020	Patients with mild to moderate depression	fTUS (n=12); Sham (n=12)	Right frontal-temporal cortex	30 s/ session; 5 sessions in a week	F_0: 0.5 MHz; I_{SPTA}: 71 mW/cm^2; I_{SPPA}: 14 W/cm^2; SD: 30 s; PRF: NR; PD: NR; DC: NR; Number of pulses in sonication: NR; Peak rarefactional pressure: 0.65 MPa; MI: 0.9	PSWQ	At stimulation endpoint	A decrease in score	NR
Gibson 2018	Healthy subjects	unfocused TUS (n=19); Sham (n=21)	Left motor cortex	2 min/ session; 1 session	F_0: 1.53-3.13 MHz; I_{SPTA}: 132.85 mW/cm^2; I_{SPPA}: 34.96 W/cm^2; SD: 2 min; PRF: NR; PD: NR; DC: < 1%; Number of pulses in a sonication: NR; Peak rarefactional pressure: 1.02 MPa; MI: 0.67	MEP induced by TMS	At stimulation endpoint and 6 minutes after stimulation	An increase in MEPs amplitude	No significant difference in abnormal sensation and mood between groups
Guerra 2021	Healthy subjects	unfocused TUS; Sham (n=16 in the crossover study)	Brainstem	180 s/ session; 1 session	F_0: 1.75 MHz; I_{SPTA}: NR; I_{SPPA}: NR; SD: 180 s; PRF: NR; PD: NR; DC: NR; Number of pulses in a sonication: NR; Peak rarefactional pressure: 1.85 MPa; MI: 1.4	EMG	3 minutes after stimulation	An increase in conditioned R2 area in the superior colliculus stimulation group	No subjects reported adverse events or any skin sensation during or after stimulation
Hameroff 2013	Patients with chronic pain	unfocused TUS; Sham; (n=31 in the crossover study)	Right/left frontal-temporal cortex	15 s/ session; 1 session	F_0: 8 MHz; I_{SPTA}: 152 mW/cm^2; I_{SPPA}: NR; SD: 15 s; PRF: NR; PD: NR; DC: NR; Number of pulses in a sonication: NR; Peak rarefactional pressure: 1.98 MPa; MI: 0.7	VAMS	10 minutes and 40 minutes after stimulation	An increase in global affect score	One subject experienced an exacerbation of the headache after stimulation

TPS: transcranial pulse stimulation; MI: mechanical index; sMRI: structural magnetic resonance imaging; DTI: diffusion tensor imaging; Rs-fMRI: resting state functional magnetic resonance imaging; HDRS-17: Hamilton depression rating scale-17; fTUS: focused transcranial ultrasound stimulation; F_0: fundamental frequency; I_{SPTA}: spatial peak temporal average intensity; I_{SPPA}: spatial peak pulse average intensity; SD: stimulation duration; ISI: inter stimulation interval; PRF: pulse repetition frequency; PD: pulse duration; DC: duty cycle; QST: quantitative sensory thresholding; tb-fTUS: theta-burst focused transcranial ultrasound stimulation; NR: not reported; MEP: motor evoked potential; TMS: transcranial magnetic stimulation; SICI: short-interval intracortical inhibition; MEG: magnetoencephalography; VAMS: Visual analog mood scale; ICF: intracortical facilitation; PSWQ: Penn state worry questionnaire; unfocused TUS: unfocused transcranial ultrasound stimulation; EMG: electromyography.

Table 2. Characteristics of included animal studies

Study	Type of animals	Grouping (sample size)	Characteristics of LITUS			Outcomes			Reported adverse effect
			Target	Stimulation sessions	Parameters	Outcome measures	Timepoint of outcome measurements	Main results (Experimental group vs. control group)	
Chu 2023	Healthy rats	fTUS1, fTUS2, fTUS3, fTUS4 (n=15 for each group); Sham (n=15)	Left primary motor cortex	5 min/ session; 1 session	F_0: 0.7 MHz; I_{SPTA} (fTUS1): 0.014 mW/cm^2; I_{SPTA} (fTUS2): 0.338 mW/cm^2; I_{SPTA} (fTUS3): 3.038 mW/cm^2; I_{SPTA} (fTUS4): 12.15 mW/cm^2; I_{SPPA}: 0.175 mW/cm^2 (fTUS1); I_{SPPA}: 4.225 mW/cm^2 (fTUS2); I_{SPPA}: 37.975 mW/cm^2 (fTUS3); I_{SPPA}: 151.875 mW/cm^2 (fTUS4); SD: 5 min; PRF: 100 Hz; PD: 0.8 ms; DC: 8%; Number of pulses in a sonication: 30000; Peak rarefactional pressure: 2.5-67.8 kPa; MI: 0.003-0.081	MEPs induced by TMS	At stimulation endpoint and measured every 5 minutes for 30 minutes after stimulation	A decrease in MEP amplitude in the fTUS2 group 5, 10,15 minutes after stimulation; A decrease in MEP amplitude in the fTUS3 and fTUS4 group at all follow-up timepoints	GFAP immunohistochemical staining showed no obvious astrogliosis at or near the sonicated sites in brains
Daniels 2018	Healthy rats	fTUS1 (n=7); fTUS2 (n=15); Sham (n=3)	Inferior colliculus region	52 s/ session; 1 session	fTUS 1: F_0: 0.23 MHz; I_{SPTA}: NR; I_{SPPA}: 2.3 W/cm^2 SD: 100 ms; Trials of sonication: 17; ISI: 2900 ms; PRF: NR; PD: NR; DC: NR; Number of pulses in a sonication: NR; Pressure: 39.7 kPa; MI: 0.083 fTUS 2:	EEG	Measured for 30 minutes within 2 hours after stimulation; Measured once a week until recovery of AEP amplitude or up to 2	A decrease in AEP amplitude in fTUS1 and fTUS2 groups	T2-weighted MR image, H&E staining and histological analyses showed no brain damage, edema, tissue damage, or inflammatory response

					F_0: 0.23 mHz; I_{SPTA}: NR; I_{SPPA}: 4.6 W/cm^2; SD: 100 ms; Trials of sonication: 17; ISI: 2900 ms; PRF: NR; PD: NR; DC: NR; Number of pulses in a session: NR; Pressure: 79.3 kPa; MI: NR		months after stimulation		
Folloni 2019	Healthy macaques	fTUS for amygdala (n=4); fTUS for ACC (n=3); No fTUS (n=9)	Amygdala; ACC	40 s/ session; 1 session	F_0: 0.25 MHz; I_{SPTA}: 19.5 W/cm^2 (for amygdala); I_{SPPA}: 64.9 W/cm^2 (for amygdala); I_{SPTA}: 5.63 W/cm^2 (for ACC); I_{SPPA}: 18.8 W/cm^2(for ACC); SD: 40 s; PRF: 10 Hz; PD: 30 ms; DC: 30%; Number of pulses in a sonication: 400; Maximum pressure: 1.44 MPa (for amygdala); Maximum pressure: 0.78 MPa (for ACC); MI: 2.88 (for amygdala); MI: 1.56 (for ACC)	fMRI	At stimulation endpoint	A decrease in the amygdala activity coupling and ACC activity coupling	sMRI showed no evidence of transient edema after fTUS
Huang 2019	Healthy rats	fTUS (n=22); No fTUS (n=22)	Hippocampus	10 min/ session; 1 session per day for 10 days	F_0: 0.5 MHz; I_{SPTA}: 360 mW/cm^2; I_{SPTA}: 225 mW/cm^2 (after attenuation through skull); I_{SPPA}: 7.2 W/cm^2; I_{SPPA}: 5.1 W/cm^2(after attenuation through skull); SD: 10 min; PRF: 500 Hz; PD: 0.1 ms; DC: 5%; Number of pulses in a	Dendritic structure ESPC dynamics Levels of GluN2A Number of c-Fos positive neurons	At sonication endpoint	An increase in dendritic spine density of hippocampal neurons An increase in ESPC frequency An increase in GluN2A level in the hippocampus An increase in c-Fos positive neurons in hippocampus	H&E staining and Nissl staining showed no hemorrhaging and tissue damage in the cortex, hippocampus, and the brain regions exposed to the beam path

					sonication: 300000; Peak rarefactional pressure: 0.42 MPa; Peak rarefactional pressure: 0.35 MPa (after attenuation through skull); MI: 0.59				
Huang 2021	Healthy mice	fTUS (n=14); Sham (n=14)	Cortex and hippocampus	4 hours/ session; 1 session	F_0: 0.5 MHz; I_{SPTA}: 235 mW/cm^2 (after attenuation through skull); I_{SPPA}: 4.7 W/cm^2 (after attenuation through skull); SD: 1 s; Trials of sonication: 7200; ISI: 1 s; PRF: 500 Hz; PD: 0.1 ms; DC: 5% ; Number of pulses in a sonication: 500; Peak rarefactional pressure: 0.34 MPa (after attenuation through skull); MI: 0.48	Number of c-Fos positive neurons Level of protein marker for autophagy	At stimulation endpoint	An increase in c-Fos positive neurons in cortex and hippocampus An increase in the ratio of LC3BII/LC3BI and a decrease in p62 level in the cortex and hippocampus	H&E staining and Nissl staining showed no hemorrhaging, tissue damage or neuron loss in the cortex and hippocampus
Kim 2013	Healthy rats	fTUS (n=7); Sham (n=7)	Thalamic area	40 min/ session; 1 session	F_0: 0.35 MHz; I_{SPTA}: 3 W/cm^2; I_{SPPA}: NR; SD: 300 ms; Trials of sonication: 1045; ISI: 2 s; PRF: 1 kHz; PD: 0.5 ms; DC: NR; Number of pulses in a sonication: 300; Peak rarefactional pressure: 0.43 MPa; MI: 0.73	PET	During stimulation and up to one hour after stimulation	An increase in SUV at the center of sonication focus compared to the contralateral area	No abnormal behavior in all animals; H&E staining showed no tissue damage or hemorrhage associated with sonication in 2 selected rats

Kim 2015	Healthy rats	fTUS with various I_{SPPA} (n=9-10); fTUS with various DC (n=9-10); Sham (n=8)	Visual cortex	150 s/ session; 1 session for each parameter	Various I_{SPPA} with 5% DC: F_0: 0.35 MHz; $I_{SPTA-max}$: 250 mW/cm^2; I_{SPPA}: 1, 3, 5 W/cm^2; SD: 150 s; PRF: 100 Hz; PD: 0.5 ms; Peak rarefactional pressure: NR; MI: NR Various DC with 3 W/ cm^2 I_{SPPA}: F_0: 0.35 MHz; $I_{SPTA-max}$: 250 mW/cm^2; PRF: 20, 166 Hz; PD: 0.5 ms; DC: 1, 8.3%; Peak rarefactional pressure: NR; MI: NR	EEG	Measured every 150 seconds for 9 times including 3 times before stimulation, 1 time during stimulation, and 5 times after stimulation	A decrease in VEP magnitude during the stimulation with I_{SPPA} of 3W/cm^2 and DC of 5%; An increase in VEP magnitude during the stimulation with DC of 8.3% and I_{SPPA} of 3W/cm^2	NR
Min 2011b	Healthy rats	fTUS (n=12); No fTUS (n=10)	Thalamus	20 min/ session; 1 session	F_0: 0.65 MHz; I_{SPTA}: 175 mW/cm^2; I_{SPPA}: 3.5 W/cm^2; SD: 20 min; PRF: 100 Hz; PD: 0.5 ms; DC: 5% ; Number of pulses in a sonication: 120000; Pressure: 0.35 MPa; MI: 0.43	Extracellular level of dopamine and serotonin	During stimulation and up to 100 minutes after stimulation	An increase in dopamine level in the frontal lobe during the 100 minutes after stimulation; An increase in serotonin level in the frontal lobe 80 to 100 minutes after sonication	NR
Mohammadjavadi 2022	Healthy sheep	fTUS (n=6); Sham (n=5)	Lateral geniculate nucleus	20 min/ session; 2 consecutive sessions	F_0: 0.55 MHz; I_{SPTA}: 2.8-9.57 mW/cm^2 (after attenuation through skull); I_{SPPA}: 19.3-63.8 W/cm^2 (after attenuation through skull); SD: 300 ms; Trials of sonication: 923; ISI: 1 s; PRF: 500 Hz; PD: NR; DC: NR; Number of pulses in a sonication: 150; Peak rarefactional pressure: 0.55-1.0	EEG	During stimulation	A decrease in VEP amplitude	NR

					MPa (after attenuation through skull); MI: 0.74-1.35				
Wang 2020a	Healthy rats	fTUS (n=19); Sham (n=5)	Motor cortex	132 s/ session; 1 session	F_0: 0.5 MHz; I_{SPTA}: 440 mW/cm$^{2;}$ I_{SPPA}: 1.1 W/cm^2; SD: 400 ms; Trials of sonication: 30; ISI: 4 s; PRF: 1 kHz; PD: 0.4 ms; DC: 40%; Number of pulses in a sonication: 400; Peak rarefactional pressure: NR: MI: NR	EEG	During the stimulation and up to 2.1 seconds after sonication	An increase in LFP amplitude during stimulation and lasted 1.4 seconds after stimulation	NR
Wang 2021b	Healthy mice	fTUS (n=14); Sham (n=13)	Periaqueductal gray	20 min/ session; 1 session	F_0: 3.8 MHz; I_{SPTA}: 321 mW/cm^2; I_{SPTA}: 70 mW/cm^2 (after the attenuation through skull); I_{SPPA}: 642 mW/cm^2; I_{SPPA}: 140 mW/cm^2 (after the attenuation through skull); SD: NR; Trials of sonication: NR; ISI: NR; PRF: 1 kHz; PD: 0.5 ms; DC: 50%; Number of pulses in a sonication: NR; Peak rarefactional pressure: 136 kPa; Peak rarefactional pressure: 63.4 kPa (after the attenuation through skull); MI: 0.07	OFT	During the stimulation	An increase in the time spent moving at high speed and an increase in mean speed	The estimated elevated temperature was 0.002 °C; H&E and Nissl staining showed no brain tissue injury caused by fTUS
Yang 2012	Healthy rats	fTUS (n=9); Sham (n=9)	Thalamus	20 min/ session; 1 session	F_0: 0.65 MHz; I_{SPTA}: 175 mW/cm2; I_{SPPA}: 3.5 W/cm2; SD: NR; Trials of sonication:	Extracellular level of GABA	During stimulation and up to 100	A decrease in GABA level in the frontal lobe over time after stimulation	H&E staining showed no hemorrhaging or tissue damage at the

					NR; ISI: NR; PRF: 100 Hz; PD: 0.5 ms; DC: 5%; Number of pulses in a sonication: NR; Peak rarefactional pressure: 0.35 MPa; MI: 0.43		minutes after stimulation		sonication focus or the tissue exposed to the beam path
Yoo 2011	Healthy rats	fTUS; No fTUS; (n=15 in the crossover study)	Thalamus	20 min/ session; 1 session	F_0: 0.65 MHz; I_{SPTA}: 300 mW/cm^2; I_{SPPA}: 6 W/cm^2; SD: NR; Trials of sonication: NR; ISI: NR; PRF: 100 Hz; PD: 0.5 ms; DC: 5%; Number of pulses in a sonication: NR; Peak rarefactional pressure: 0.49 MPa; MI: 0.61	Emergence from anesthesia	After the stimulation	A decrease in the time to initiation of responses to an air puff to the eyes, hind-paw pinching, and voluntary movements of limbs	NR
Yoo 2018	Healthy rats	fTUS; Sham; (n=11 in the crossover study)	Somatosensory area	10 min/ session; 1 session	F_0: 0.65 MHz; I_{SPTA}: 210 mW/cm^2; I_{SPPA}: 4.2 W/cm^2; SD: NR; Trials of sonication: NR; ISI: NR; PRF: 100 Hz; PD: 0.5 ms; DC: 5%; Number of pulses in a sonication: 60000; Peak rarefactional pressure: NR; MI: NR	EEG	5 minutes to 35 minutes after stimulation	Differential SEP features were evident and persisted beyond 35 minutes after stimulation	The estimated temperature rise of 0.0938 °C was negligible and could not cause thermal damage
Zhao 2023	Healthy mice	fTUS (n=6); Sham (n=6)	Somatosensory cortex	25 min/ session; 1 session per day for 7 days	F_0: 1 MHz; I_{SPTA}: 430 mW/cm^2; I_{SPPA}: 8.6 W/cm^2; SD: 5 min; Trials of sonication: 3; ISI: 5 min; PRF: 1 Hz; PD: 50 ms; DC: 5%; Number of pulses in a sonication: 300; Pressure: 0.51 MPa; MI: 0.51	Whisker-dependent behavior test	At stimulation endpoint; 7, 14 days after stimulation	A better performance at stimulation endpoint	NR
	Healthy mice	fTUS (n=6); Sham (n=3)				The two-photon fluorescence imaging	At stimulation endpoint; 7, 14,	An increase in synaptic activity at the stimulation endpoint and after stimulation;	

							and 21 days after stimulation	An increase in number of spines and spines formation at stimulation endpoint	
Guo 2015	Healthy rats	fTUS; No fTUS; (n=9 in total)	Somatosensory cortex	24 min/ session; 1 session	F_0: 0.5 MHz; I_{SPPA}: 2.155 W/cm^2; I_{SPTA}: 43, 57, 72 mW/cm^2; SD: 0.4-0.67 s; Trials of sonication: 12; ISI: 2 min; PRF: 1.5 kHz; PD: NR; DC: NR; Number of pulses in a sonication: 600, 800, 1000; Peak rarefactional pressure: NR; MI: NR	LSI	Measured from 4 seconds before stimulation to 16 seconds after stimulation	An increase in cerebral blood flow velocity immediately after the stimulation and maintained up to 12 seconds after stimulation	NR
	Rat models of ischemic brain injury	fTUS (n=16); No fTUS (n=16)	Ischemic cortex	60 min/ session with 360 trials	F_0: 0.5 MHz; I_{SPTA}: 86 mW/cm^2; I_{SPTA}: NR; SD: 0.4 s; Trials of sonication: 360; ISI: 10 s; PRF: 1.5 kHz; PD: NR; DC: NR; Number of pulses: 600; Peak rarefactional pressure: NR; MI: NR	Neurological severity score Infarct volume Number of neutrophils	48 hours after stimulation	A decrease in score A decrease in infarct volume A decrease in neutrophils in lateral striatum and a part of ischemic cortex	
Niu 2020	Healthy mice	fTUS (n=14); Sham (n=18) fTUS (n=6); Sham (n=6)	Nucleus accumbens	30 min/ session; 1 session per day for 5 days	F_0: 3.4 MHz; I_{SPTA}: mW/cm^2; I_{SPTA}: ; SD: 1 s; Trials of sonication: 600; ISI: 2 s; PRF: 1 kHz; PD: 0.05 ms; DC: 5%; Number of pulses: 1000; Pressure: 304 kPa; MI: 0.75	Conditioned place preference test Level of GluA1, GluA2 and GluA3	At stimulation endpoint 7 days after stimulation	A decrease in time spent on the stimulated side An increase in GluA1, and a decrease in GluA2 and GluA3 level in nucleus accumbens	The maximum temperature increased after fTUS was estimated to be less than 0.003°C
	Mouse models of morphine addiction	fTUS (n=4); Sham (n=NR)	Nucleus accumbens	30 min/ session; 1 session per day for 5 days		Morphine-induced place preference test	After 2 days stimulation and after 5 days stimulation	A decrease in score of conditioned place preference test	

Yi 2022	Healthy mice	fTUS (n=6); Sham (n=6)	Prefrontal cortex	30 min/ session; 1 session	F_0: 0.5 MHz; I_{SPTA}: 5.05 W/cm^2; I_{SPPA}: 10.09 W/cm^2; SD: 60 s; PRF: 100 Hz; PD: 5 ms; DC: 50%; Number of pulses in a sonication: 6000; Peak rarefactional pressure: 0.62 MPa; MI:0.88	Number of c-Fos positive neurons	At stimulation endpoint	An increase in c-Fos positive neurons in prefrontal cortex	H&E and Nissl staining showed no tissue damage
	Mouse models of depression	fTUS (n=13); Sham (n=10)	Prefrontal cortex			TST, FST, EPM	17.5 hours after stimulation	A better performance in TST, FST and EPM	NR
						Level of inflammatory factors		A decrease in IL-6, IL-1β, TNF-α levels in prefrontal cortex	
Zhou 2019	Healthy rats	fTUS (n=3); Sham (n=3)	Motor cortex	40 min/ session; 1 session/ day for 7 days	F_0: 0.8 MHz; I_{SPTA}:76 mW/cm^2 (after attenuation through skull); I_{SPPA}:760 mW/cm^2 (after attenuation through skull); SD: 6 s; Trials of sonication: 150; ISI: 10 s; PRF: 100 Hz; PD: 1 ms; DC: 10%; Number of pulses in a sonication: 600; Peak rarefactional pressure: NR; MI: 0.1	Number of c-Fos positive neurons	At stimulation endpoint	A significant increase in c-Fos positive neurons in motor cortex	The estimated elevated temperature was less than 0.02 °C; H&E and Nissl staining showed no tissue damage or hemorrhage associated with fTUS
	Rat models of acute Parkinson's disease	fTUS (n=8); Sham (n=8)	Motor cortex			OFT, pole test	During the stimulation period	A better performance in OFT and pole test	
						Total SOD and GSH-PX level	1 day after stimulation	An increase in total SOD and GSH-PX in striatum	
Zhou 2021	Healthy rats	fTUS (n=4); Sham (n=4)	Subthalamic nucleus	30 min/ session; 1 session	F_0: 3.8 MHz; I_{SPTA}: 430 mW/cm^2; I_{SPPA}: 860 mW/cm^2; SD: 1 s; Trials of sonication: 360; ISI: 4 s; PRF: 1 kHz; PD: 0.5 ms; DC: 50%; Number of pulses in a sonication: 1000; Peak rarefactional pressure: 190 kPa; MI: 0.1	Number of c-Fos positive neurons	At stimulation endpoint	An increase in c-Fos positive neurons in subthalamic nucleus	H&E, Nissl and TUNEL staining showed no brain tissue injury was induced by fTUS
	Healthy rats	fTUS (n=4); Sham (n=4)	Primary visual cortex			Number of c-Fos positive neurons	At stimulation endpoint	An increase in c-Fos positive neurons in primary visual cortex	
	Mouse models of chronic Parkinson's disease	fTUS (n=13); Sham (n=12)	Subthalamic nucleus	30 min/ session; 2 sessions per week for 5 weeks		Rotarod test and, pole test	At treatment endpoint	A better performance in rotarod test and pole test	
						Number of dopaminergic neurons		An increase in dopaminergic neurons in SN	

						TNF-α, IL-1β , COX-2, NF-κB levels		A decrease in TNF-α, IL-1β, COX-2, NF-κB levels in SN and striatum	
						Amount of microglia and astrocytes		A decrease in microglia and astrocytes in SN and striatum	
						Iba1, GFAP, αSyn and iNOS levels		A decrease in Iba1, GFAP, αSyn and iNOS levels levels in SN and striatum	
						SOD level		An increase in SOD level in SN and striatum	
Baek 2018	Mouse models of ischemic brain injury	fTUS (n=12); No fTUS (n=12)	Lateral cerebellar nucleus	20 min/ session; 2 sessions with an interval of 20 min	F_0: 0.35 MHz; I_{SPTA}: 1.27 W/cm^2; I_{SPPA}: 2.54 W/cm^2; SD: 100 ms; Trials of sonication: 571; ISI: 2 s; PRF: 1 kHz; PD: 0.5 ms; DC: 50%; Number of pulses in a sonication: 100; Peak rarefactional pressure: NR; MI: 0.54	Balance beam test, adhesive removal test	At treatment endpoint and during the 4-week follow-up period	A better performance in balance beam test and adhesive removal test	Histological analysis showed no sign of bleeding or tissue damage in the cerebellum in 3 healthy rats exposed to the same fTUS as the fTUS group
						Brain edema	2 days after treatment	A decrease in brain edema in ipsilateral hemisphere	
Cao 2022	Rat models of hypertension	fTUS (n=7); No fTUS (n=7)	Solitary tract nucleus	20 min/ session; 1 session per day for 2 months	F_0: 0.6 MHz; I_{SPTA}: 1.64 W/cm^2; I_{SPPA}: 3.28 W/cm^2; SD: 200 ms; Trials of sonication: 230; ISI: 5 s; PRF: 250 Hz; PD: 2 ms; DC: 50%; Number of pulses in a sonication: 50; Peak rarefactional pressure: 0.32 MPa; MI: 0.41	Blood pressure	During the treatment period	A decrease in blood pressure	H&E staining, TUNEL assay, and Nissl staining showed no apparent morphological or cellular damage in rat brain tissue after 2 months of fTUS
						Number of c-Fos expressing neurons	During the treatment period	An increase in c-Fos expressing neurons in solitary tract nucleus	
						Blood plasma levels of hormones	At treatment endpoint	A decrease in plasma level of Aldo, ANGII, ANF, and Cor	

Chen 2020	Rat models of epilepsy	fTUS1 (n=6); fTUS2 (n=15); fTUS3 (n=6); fTUS4 (n=7); fTUS5 (n=22); Sham (n=20)	Hippocampus and thalamus regions	600 s/ session for fTUS1, fTUS2, fTUS3, fTUS5; 100 s/session for fTUS4; 1 session	fTUS1: F_0: 0.5 MHz; I_{SPTA}: 703 mW/cm^2; I_{SPPA}: 2.34 W/cm^2; SD: 600 s; PRF: 100 Hz; PD: 3 ms; DC: 30%; Number of pulses in a sonication: 60000 fTUS2: F_0: 0.5 M Hz; I_{SPTA}: 750 mW/cm^2; I_{SPPA}: 9.38 W/cm^2; SD: 600 s; PRF: 100 Hz; PD: 0.8 ms; DC: 8%; Number of pulses in a sonication: 60000 fTUS3: F_0: 0.5 M Hz; I_{SPTA}: 1.25 W/cm^2; I_{SPPA}: 4.17 W/cm^2; SD: 600 s; PRF: 100 Hz; PD: 3 ms; DC: 30%; Number of pulses in a sonication: 60000 fTUS4: F_0: 0.5 M Hz; I_{SPTA}: 2.812 W/cm^2; I_{SPPA}: 9.37 W/cm^2; SD: 100 s; PRF: 100 Hz; PD: 3 ms; DC: 30%; Number of pulses in a sonication: 10000 fTUS5: F_0: 0.5 M Hz; I_{SPTA}: 2.812 W/cm^2; I_{SPPA}: 9.37 W/cm^2; SD: 600 s; PRF: 100 Hz; PD: 3 ms;	EEG	Measured from 5 minutes before injection of pentylenetetrazol to 30 minutes after stimulation	A decrease in the number of spikes in all fTUS groups 10-15 minutes after pentylenetetrazol injection; A decrease in the number of spikes in fTUS2 and fTUS5 groups 15-20 minutes after pentylenetetrazol injection; A decrease in power spectral density of entire spectrum and decreases in alpha and theta power spectral densities in fTUS5 group 10-15 min after pentylenetetrazol injection; A decrease in beta power spectral density in fTUS4 and fTUS5 groups 10-15 min after pentylenetetrazol injection; A decrease in gamma power spectral density in fTUS2, fTUS4, fTUS5 groups 10-15 min after pentylenetetrazol injection	No behavioral abnormalities were observed, and H&E staining and low-magnification images showed no obvious tissue damage or inflammation, in rats treated with fTUS under these exposure parameters

					DC: 30%; Number of pulses in a sonication: 60000 For fTUS1-5 and sham fTUS: Peak rarefactional pressure: 0-0.53 MPa; MI: 0-0.75				
Feng 2021	Mouse models of acute neuropathic pain	fTUS1 (n=6); fTUS2 (n=6); Sham (n=6)	ACC	15 min/ session; 1 session per day for 21 days	fTUS1: F_0: 3.7 MHz; I_{SPTA}: 1.598 W/cm^2; I_{SPPA}: 15.980 W/cm^2; SD: 0.4 s; Trials of sonication: 300; ISI: 2.6 s; PRF: 1.5 kHz; PD: 0.07 ms; DC: 10%; Number of pulses in a sonication: 600; Pressure: 690 kPa; MI: 0.36 fTUS2:	Nociceptive test	During the treatment period and 4, 11, 18 days after treatment	An increase in mechanical withdrawal threshold in contralateral side in the fTUS1 group 11 days after treatment; An increase in mechanical withdrawal threshold in surgical side in the fTUS2 group during the follow-up period; An increase in mechanical withdrawal threshold and an increase in thermal withdrawal threshold in contralateral side in the fTUS2 group 4 days after treatment	H&E staining showed no abnormal findings in ACC after fTUS
	Mouse models of chronic neuropathic pain	fTUS2 (n=12); Sham (n=12)			F_0: 3.7 MHz; I_{SPTA}: 3.498 W/cm^2; I_{SPPA}: 34.982 W/cm^2; SD: 15 min; PRF: 1.5 kHz; PD: 0.07 ms; DC: 10%; Number of pulses in a sonication: 600; Pressure: 950 kPa; MI: 0.49	Nociceptive test	During the treatment period and 3 days after treatment	An increase in mechanical withdrawal threshold in the surgical side during treatment period	
						Expression of genes	At treatment endpoint	A decrease in expression of Hnrnph1 and Hnrnpd	
Guo 2021	Mouse models of depression	fTUS (n=8-9); Sham (n=8-9)	NR	20 min/ session; 1 session per day for 22 days	F_0: 1.5 MHz; Intensity: 25 mW/cm^2; SD: NR; Trials of sonication: NR; ISI: NR; PRF: 1 kHz; PD: 0.2 ms; DC: 20%; Number of pulses in a sonication: NR; Peak	SPT Doublecortin level	24 hours after treatment	An increase in SPI An increase in doublecortin level in the hippocampus	NR
	Mouse models of demyelination	fTUS (n=3-4); Sham (n=3-4)				MBP level and NG2 level	24 hours after treatment	An increase in MBP and NG2 levels in the corpus callosum	

					rarefactional pressure: NR; MI: NR				
Hakimova 2015	Mouse models of epilepsy	fTUS (n=13); No fTUS (n=10)	Hippocampus	30 s/ session; Many sessions per day in 5h, for 35 days	F_0: 0.2 MHz; I_{SPTA}: NR; I_{SPPA}: NR; SD: 30 s; PRF: 500 Hz; PD: 1 ms; DC: 50%; Number of pulses in a sonication: 15000; Peak rarefactional pressure: NR; MI: NR	Sociability task, FST	During stimulation period (day 21 to day 35)	A better performance in sociability task and FST	NR
	Mouse models of epilepsy	fTUS (n=7); No fTUS (n=9)	Hippocampus	30s/ session; Many sessions per day in 5h, for 21 days		EEG	During the stimulation	An increase in latency to status epilepsy; A decrease in spike frequency during status epilepsy	
						EEG	Measured for 2 weeks after stimulation	A decrease in spontaneous recurrent seizure	
Min 2011a	Rat models of epilepsy	fTUS (n=9); Sham (n=9)	Thalamus	3 min/ session; 2 sessions with a 10-minute interval	F_0: 0.65 MHz; I_{SPTA}: 130 mW/cm^2; I_{SPPA}: 2.6 W/cm^2; SD: 3 min; PRF: 100 Hz; PD: 0.5 ms; DC: 5%; Number of pulses in a sonication: 18000; Peak rarefactional pressure: 0.27 MPa; MI: 0.33	EEG	During stimulation and up to 10 minutes after stimulation	A decrease in number of epileptic bursts after 1st session, during and after the 2nd session; A decrease in theta activity after the 2nd session	H&E staining and TUNEL assay showed no damage in the brain tissue in healthy rats subjected to the same experimental procedure as the fTUS group
						Racine score	At stimulation endpoint	A decrease in score	
Pang 2021	Aging mice	fTUS1 (n=14); fTUS2 (n=15); Sham (n=15)	Ventromedial hypothalamic nucleus	15 min/ session; 1 session per day for two 14 days, with 2.5 months in between	fTUS1: F_0: 1 MHz; I_{SPTA}: 540 mW/cm^2; I_{SPPA}: 5.4 W/cm^2; SD: 1 s; Trials of sonication: 150; ISI: 5 s; PRF: 1 kHz; PD: 100 μs;	Grip strength	During the stimulation period and at stimulation endpoint	An increase in grip strength at stimulation endpoint in fTUS2 group	H&E staining showed no tissue damage or hemorrhaging in the hypothalamus after fTUS1 or fTUS2

					DC: 10%; Number of pulses in a sonication: 1000; Peak rarefactional pressure: 0.13 MPa; MI: 0.13 fTUS2: F_0: 1 MHz; I_{SPTA}: 540 mW/cm^2; I_{SPPA}: 5.4 W/cm^2; SD: 1 s; Trials of sonication: 150; ISI: 5 s; PRF: 10 Hz; PD: 10 ms; DC: 10%; Number of pulses in a sonication: 100; Peak rarefactional pressure: 0.13 MPa; MI: 0.13	Level of apoptosis factors Level of NMDA receptors and inflammatory cytokines	At stimulation endpoint	A decrease in Bax and an increase in Bcl-2/Bax ratio in fTUS2 group A decrease in NMDAR2B level in fTUS1 and fTUS2 groups; A decrease in TNF, IL-1β in fTUS1 group	
Park 2021	Mouse models of Alzheimer's disease	fTUS (n=6); Sham (n=6)	Entire brain	2 h/ session (repeated in stimulation blocks of 10-s ON and 30-s OFF periods); 1 session per day for 2 weeks	F_0: 0.3 MHz; I_{SPTA}: 14.4 mW/cm^2; I_{SPPA}: 1.2 W/cm^2; SD: 200 ms; Trials of sonication: 10; ISI: 800 ms; PRF: 40 Hz; PD: 3 ms; DC: 12%; Number of pulses in a sonication: 8; Peak rarefactional pressure: NR; MI: NR	Aβ42 level EEG	At treatment endpoint During the treatment period and at treatment endpoint	A decrease in total Aβ42 level in the pre- and infra-limbic cortex An increase in spontaneous gamma power at treatment endpoint	Perls' Prussian blue staining showed no significant difference in micro-bleeding between groups
Peng 2021	Rat models of TBI	fTUS (n=15); No fTUS (n=15)	Brain damage area (in the parietal lobe)	10 min/ session; 1 session per day for 10 days	F_0: 0.5 MHz; Intensity: 1.2 W/cm^2; SD: 400 ms; PRF: 1 Hz; PD: 0.5 ms; DC: 0.05%; Number of pulses in a sonication: 0.4; Peak rarefactional pressure: NR; MI: NR	DWI Neurological function score Loss rate of Nissl body	During the treatment period; At treatment endpoint At treatment endpoint	A decrease in ADC value during treatment period and at treatment endpoint; An increase in FA value at any timepoints An increase in neurological function score during the treatment period A decrease in loss rate of Nissl body	NR

Sharabi 2019	Rat models of essential tremor	fTUS (n=13); Sham (n=3)	Olivo-cerebellar system	52 s/ session; 1-3 sessions	F_0: 0.23 mHz; I_{SPTA}: NR; I_{SPPA}: 27.2 W/cm^2; SD: 100 ms; Trials of sonication: 17; ISI: 2900 ms; PRF: NR; PD: NR; DC: NR; Number of pulses in a sonication: NR; Peak rarefactional pressure: NR; MI: NR	EMG	During stimulation and up to 5 minutes after stimulation or until tremor recovered	A decrease in tremor frequency during or after the sonication in 12 responding rats, with complete tremor suppression in 6 responding rats; A decrease in average tremor frequency of the responding rats compared to baseline	No signs of neurological damage or reduction in well-being in all rats; The MR images of all scanned rats showed no abnormalities, or signs of treatment-induced toxicity
Song 2022	Rat models of Parkinson's disease	fTUS (n=4); No fTUS (n=4)	Right striatum	25 min/ session; 1 session/ day; 5 days per week for 6 weeks	F_0: 1 MHz; I_{SPTA}: 528 mW/cm^2; I_{SPPA}: 10.56 W/cm^2; SD: 5 min; Trials of sonication: 3; ISI: 5 min; PRF: 1 Hz; PD: 50 ms; DC: 5%; Number of pulses in a sonication: 300; Peak rarefactional pressure: NR; MI: NR	Amount of astroglia and microglia, and level of IL-1β and p-NF-κB p65 GDNF level Amount of dopamine transporter ZO-1 and claudin-5 level	At treatment endpoint	A decrease in astroglia and microglia and a decrease in IL-1β and p-NF-κB p65 levels in the substantia nigra pars compacta An increase in GDNF level in the substantia nigra pars compacta An increase in dopamine transporter in the substantia nigra pars compacta An increase in ZO-1 and claudin-5 level in the substantia nigra pars compacta	H&E and Nissl staining showed no fTUS-induced brain tissue injury in healthy rats subjected to the same experimental procedure as the fTUS group
Tsai 2022	Rat models of schizophrenia	fTUS (n=8); No fTUS (n=8)	3.0 mm posterior and 2.5 mm lateral to	25 min/ session; 1 session/ day for 5 days	F_0: 1 MHz; I_{SPTA}: 528 mW/cm^2; I_{SPPA}: 10.56 W/cm^2; SD: 5 min; Trials of sonication: 3; ISI: 5 min; PD: 50 ms; PRF: 1 Hz;	NOR, MWM Level of calbindin and parvalbumin	24 hours after the treatment	A better performance in NOR and MWM An increase in hippocampal calbindin and parvalbumin level	NR

			the bregma of the brain		DC: 5%; Number of pulses in a sonication: 300; Peak rarefactional pressure: NR; MI: NR	Number of parvalbumin-positive and calbindin-positive cells		An increase in and parvalbumin-positive and calbindin-positive cells in cingulate cortex	
						BDNF level		A decrease in hippocampal BDNF level and an increase in BDNF level in prefrontal cortex	
Wang 2020b	Mouse models of Parkinson's disease	fTUS (n=11); Sham (n=6)	Subthalamic nucleus	5 min/ session; 1 session	F_0: 0.5 MHz; I_{SPTA}: 379.5 mW/cm^2; I_{SPPA}: 7.59 W/cm^2; SD: 50 ms; Trials of sonication: 286; ISI: 1 s; PRF: 1 kHz; PD: 0.05 ms; DC: 5%; Number of pulses in a sonication: 50; Maximum pressure: 0.39 MPa; MI: 0.55	EEG	5 minutes after stimulation	A decrease in power spectrum of LFPs in beta band; A decrease in PACI of LFPs of beta/high gamma band and a decrease in PACI of LFPs of beta/ripple band	NR
Wang 2021a	Mouse models of ischemic brain injury	fTUS (n=6); No fTUS (n=6)	Ischemic hemisphere	10 min/ session; 1 session per day for 7 days	F_0: 0.5 MHz; I_{SPTA}: 60 mW/cm^2; I_{SPPA}: 120 mW/cm^2; SD: 300 ms; Trials of sonication: 360; ISI: 2.7 s; PRF: 1 kHz; PD: 0.5 ms; DC: 50%; Number of pulses in a sonication: 300; Peak rarefactional pressure: NR; MI: NR	Brain atrophy volume	At treatment endpoint	A decrease in brain atrophy volume	NR
						Neurological severity score		A decrease in neurological severity score	
						EBST, corner test		A better performance in EBST and corner test	
						Number of M2 microglia, level of IL-10 and IL-10R		An increase in M2 microglia and an increase in IL-10 and IL-10R levels	
Wang 2023a	Rat models of ADHD		Prefrontal cortex	15 min/ session; 1 session/ day; 6	F_0: 0.5 MHz; I_{SPTA}: 468 mW/cm^2; I_{SPPA}: 9.36 W/cm^2;	OFT, MYM, Y-maze	1-4 days after the treatment	A better performance in OFT, MYM and Y-maze spontaneous alternation test	NR

		fTUS (n=6); No fTUS (n=6)		days per week for 2 weeks	SD: 50 ms; Trials of sonication: 857; ISI: 1 s; PRF: 1 Hz; PD: 50 ms; DC: 5%; Number of pulses in a sonication: 0.05; Maximum pressure: 0.53 MPa; MI: 0.75	spontaneous alternation test T-maze EEG BDNF level	During the treatment period During the treatment period; 1 day and 7 days after treatment At treatment endpoint	A higher percentage of correct choices from day 3 to day 12 An increase in average of spike firing rates of all neurons on day 7, and 1 day, 7 days after treatment; A lower LFPs at theta bands and higher LFPs at beta bands 1 day and 7 days after treatment; Higher LFPs 7 days after treatment An increase in BDNF level	
Yang 2022	Rat models of demyelination	fTUS (n=5); No fTUS (n=5)	Demyelination lesion in the brain (CA1 region of the right hippocampus)	25 min/ session; 1 session per day for 5 days	F_0: 1 MHz; I_{SPTA}: 500 mW/cm^2; I_{SPPA}: 2.5 W/cm^2; SD: 5 min; Trials of sonication: 25 min; ISI: 5 min; PRF: 100 Hz; PD: 2 ms; DC: 20%; Number of pulses in a sonication: 30000; Peak rarefactional pressure: NR; MI: NR	Amount of remyelination fibers Number of astrocytes and microglia Microglial morphology Number of oligodendrocytes BDNF level	At treatment endpoint	An increase in remyelination fibers in hippocampus A decrease in microglia and astrocytes in hippocampus An increase in the ramified microglia and a decrease in the hypertrophic, dystrophic, rod-shaped and amoeboid microglia in hippocampus A decrease in oligodendrocyte progenitor cells and an increase in mature oligodendrocytes in hippocampus An increase in hippocampal BDNF level	NR
Yao 2022	Rat models of migraine	Pre-fTUS (n=7); Post-	Whole brain	15 min/ session; 1 session	F_0: 0.5 MHz; I_{SPTA}: 415 mW/cm^2; I_{SPPA}: 8.3 W/cm^2; SD:	Number of head scratches	Measured before, during	A decrease in the number of head scratches in the pre-fTUS group and the post-fTUS groups	NR

		fTUS (n=7); No fTUS (n=7)			15 min; PRF: 1 Hz; PD: 50 ms; DC: 5%; Number of pulses in a sonication: 900000; Peak-to-peak pressure: 0.5 MPa; MI: 0.71	LSI	and after stimulation for a total of 135 minutes	No significant difference in average cerebral blood flow velocity between groups	
Yuan 2020	Mouse models of Parkinson's disease	fTUS (n=8); Sham (n=8)	Subthalamic nucleus	5 min/ session; 1 session per day for 2 weeks	F_0: 0.5 MHz; I_{SPTA}: 255 mW/cm^2; I_{SPPA}: 5.1 W/cm^2; SD: 50 ms; Trials of sonication: 286; ISI: 1 s; PRF: 1 kHz; PD: 0.05 ms; DC: 5%; Number of pulses in a sonication: 50; Maximum pressure: 0.39 MPa; MI: 0.55	Wire hanging test, OFT, FST	During the treatment period (day 1, 2, 3, 4, 7) and at treatment endpoint (day 14)	A better performance on day 4, day 7, and at treatment endpoint	NR
Zhang 2019	Rat models of depression	fTUS (n=17); Sham (n=16)	Left prelimbic cortex	15 min/ session; 1 session per day for 2 weeks	F_0: 0.5 MHz; I_{SPTA}: 4.55 W/cm^2; I_{SPPA}: 7.59 W/cm^2; SD: 400 ms; Trials of sonication: 265; ISI: 3 s; PRF: 1.5 kHz; PD: 0.4 ms; DC: 60%; Number of pulses in a sonication: 600; Spatial-peak temporal-peak pressure: 0.38 MPa; MI: 0.54	SPT, OFT BDNF level	At treatment endpoint	A better performance in SPT and OFT An increase in BDNF level in hippocampus	H&E staining showed no fTUS-induced brain tissue injury
Zhang 2022b	Rat models of pain	fTUS (n=6); No fTUS (n=6)	Periaqueductal gray	5 min/ session; 1 session	F_0: 0.65 MHz; I_{SPTA}: 691 mW/cm^2 (after attenuation through skull); SD: 5 s; Trials of sonication: 30; ISI: 5 s; PRF: 100 Hz; PD: 1 ms; DC: 10%; Number of pulses in a sonication: 500; Peak	EEG	Measured before stimulation to 25 minutes after stimulation	A decrease in LFP intensity of delta, theta, beta, and gamma waves during stimulation	H&E staining showed no notable brain tissue injury

					rarefactional pressure: 0.47 MPa (after attenuation through skull); MI: 0.58				
Zhu 2023	Mouse models of depression	fTUS (n=11); Sham (n=11)	Dorsal raphe nucleus	30 min/ session; 1 session per day for 3 weeks	F_0: 1.1 MHz; I_{SPTA}: 2.84 W/cm^2 (after attenuated through skull); I_{SPPA}: 5.68 W/cm^2 (after attenuated through skull); SD: 1 s; Trials of sonication: 900; ISI: 1 s; PRF: 1 kHz; PD: 0.5 ms; DC: 50%; Number of pulses in a sonication: 1000; Maximum pressure: 484 kPa; MI: 0.46	TST 5-HT level	At stimulation endpoint	A decrease in tail suspension immobility duration An increase in 5-HT level in dorsal raphe nucleus	H&E staining showed no brain tissue damage
	Healthy mice	fTUS (n=3); Sham (n=3)	Dorsal raphe nucleus	30 min/ session; 1 session		Number of c-Fos positive neurons	1 hour after stimulation	An increase in c-Fos positive neurons	
Wang 2023b	Healthy mice	unfocused TUS (n=10); Sham (n=10)	Motor cortex	25 min/ session; 1 session per day for 7 days	F_0: 0.5 MHz; I_{SPTA}: 466 mW/cm^2; I_{SPPA}: 9.3 W/cm^2; PRF: 1 Hz; SD: 5 min; Trials of sonication: 3; ISI: 5 min; PD: 50 ms; DC: 5%; Number of pulses in a sonication: 300; Pressure: 0.53 MPa; MI: 0.75	NREM sleep ratio, REM sleep ratio LFP changes in NREM sleep LFP changes in REM sleep	During the stimulation period (day 1, day 3) and at stimulation endpoint (day 7)	An increase in NREM sleep ratio and a decrease in REM sleep ratio on day 3 and day 7 An increase in power of delta bands on day 3 and day 7; A decrease in power of spindle bands on day 1, day 3 and day 7; A decrease in sample entropy of delta bands and an increase in sample entropy of spindle bands on day 7 A decrease in power of theta bands and an increase in sample entropy of theta bands on day 7;	NR

					An increase in power of gamma bands and a decrease in sample entropy of gamma bands on day 3 and day 7	
Healthy mice	unfocused TUS (n=6); Sham (n=6)	Hippocampus	LFP changes in NREM sleep LFP changes in REM sleep	During the stimulation period (day 1, day 3) and at stimulation endpoint (day 7)	An increase in power of delta and spindle bands on day 3 and day 7 A decrease in power of theta and gamma bands on day 3 and day 7	NR
Mouse models of sleep disorders	unfocused TUS (n=6); Sham (n=6)	Motor cortex	REM sleep ratio LFP changes in REM sleep	During the stimulation period (day 1, day 3) and at stimulation endpoint (day 7)	A decrease in REM sleep ratio on day 7 A decrease in power of theta bands on day 3	NR
Mouse models of sleep disorder	unfocused TUS (n=6); Sham (n=6)	Hippocampus	Total sleep time, LFP changes in NREM and REM sleep	During the stimulation period (day 1, day 3) and at stimulation endpoint (day 7)	No significant difference between groups	NR
Mouse models of Alzheimer's disease with sleep disorder	unfocused TUS (n=6); Sham (n=6)	Motor cortex	Total sleep time NREM sleep ratio, REM sleep ratio LFP changes in NREM sleep	During the stimulation period (day 1, day 3) and at stimulation endpoint (day 7)	An increase in total sleep time on day 7 A significant increase in NREM and REM sleep ratio on day 7 An increase in power of delta bands and a decrease in sample entropy of delta bands on day 3 and day 7;	NR

						LFP changes in REM sleep		A decrease in sample entropy of spindle bands on day 7 A decrease in power of theta bands and an increase in sample entropy of gamma bands on day 7; An increase in sample entropy of theta bands on day 3 and day 7	
Xu 2020	Mouse models of Parkinson's disease	unfocused TUS (n=6); No unfocused TUS (n=6)	NR	5 min/ session; 1 session per day for 10 days	F_0: 1 MHz; Intensity: 0.3 W/cm^2; SD: 5 min; PRF: NR; PD: NR; DC: 100%; Number of pulses in a sonication: NR; Peak rarefactional pressure: NR; MI: 1.43	Number of dopaminergic neurons	At treatment endpoint	An increase in dopaminergic neurons in the striatum	H&E staining showed no pathological difference between groups

fTUS: focused transcranial ultrasound stimulation; F_0: fundamental frequency; I_{SPTA}: spatial peak temporal average intensity; I_{SPPA}: spatial peak pulse average intensity; SD: sonication duration; PRF: pulse repetition frequency; PD: pulse duration; DC: duty cycle; MI: mechanical index; MEPs: motor evoked potentials; TMS: transcranial magnetic stimulation; GFAP: glial fibrillary acidic protein; NR: not reported; ISI: inter stimulation interval; EEG: electroencephalogram; AEP: auditory evoked potential; MR: magnetic resonance; H&E: hemetoxylin and eosin; ACC: anterior cingulate cortex; fMRI: functional magnetic resonance imaging; sMRI: structural magnetic resonance imaging; ESPCs: excitatory spontaneous postsynaptic currents; PET: positron emission tomography; SUV: standardized uptake value; VEP: visual evoked potential; LFP: local field potential; OFT: open field test; GABA: γ-aminobutyric acid; SEP: somatosensory evoked potential; LSI: Laser speckle imaging; TST: tail suspension test; FST: forced swimming test; EPM: elevated plus maze; IL-6: interleukin-6; IL-1β: interleukin-1β; TNF-α: tumor necrosis factor-α; SOD: superoxide dismutase; GSH-PX: glutathione peroxidase; COX-2: cyclooxygenase-2; NF-κB: nuclear factor κB; SN: substantia nigra; αSyn: α-synuclein; iNOS: inducible nitric-oxide synthase; TUNEL: terminal deoxynucleotidyl transferase-mediated nick end labeling; Aldo: aldosterone; ANGII: angiotensin II; ANF: atrial natriuretic factor; Cor: cortisol; SPT: sucrose preference test; SPI: sucrose preference index; MBP: myelin basic protein; NG2: neural/glial antigen 2; NMDA: N-methyl-D-aspartate; TBI: traumatic brain injury; DWI: diffusion weighted imaging; ADC: apparent diffusion coefficient; FA: fractional anisotropy; EMG: electromyography; p- NF-κB p65: phosphorylation of nuclear factor κB p65; GDNF: glial cell line-derived neurotrophic factor; ZO-1: zonula occludens-1; NOR: novel object recognition; MWM: Morris water maze; BDNF: brain derived neurotrophic factor; PACI: phase-amplitude coupling index; EBST: elevated body swing test; IL-10: interleukin-10; IL-10R: interleukin-10 receptor; ADHD: attention deficit hyperactivity disorder; MYM: modified Y-maze; 5-HT: 5-hydroxytryptamine; unfocused TUS: unfocused transcranial ultrasound stimulation; NREM: non-rapid eye movement; REM: rapid eye movement.

2.5.2 Risk of bias within included studies

According to Cochrane RoB 2, four of eleven human studies were rated as having an overall high risk of bias, six studies as having a moderate risk of bias, and one study as having a low risk of bias (Figure 2A, Table 3). The 10-item SYRCLE's RoB tool was used to assess the quality of 44 animal studies. The item prevalence was rated as follows: "no" (3.9%), indicating a high risk of bias; "unclear" (58.5%), indicating insufficient details; "yes" (37.6%), indicating a low risk of bias (Figure 2B, Table 4).

The results of the risk of bias assessment for human and animal studies are summarized in Figure 2. See Table 3 and Table 4 for the full criteria for each tool and a full breakdown for each study.

Figure 2A

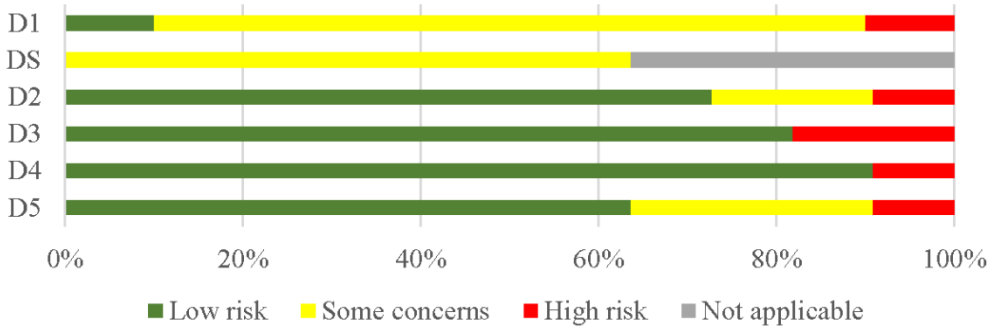

Figure 2B

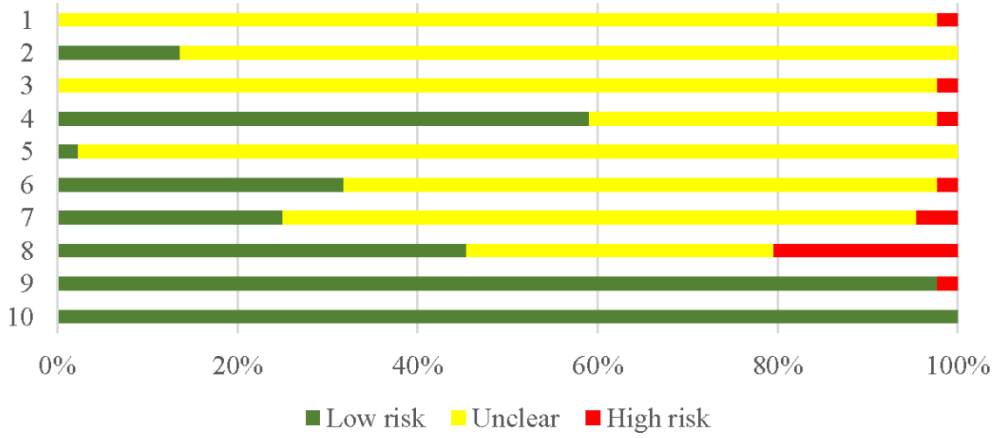

Figure 2. Risk of bias assessment for the included studies (Study 1)

Table 3. Full breakdown of study quality assessment for the included human studies using the Cochrane Risk of Bias 2 tool for randomized trials and for randomized crossover trials

Author, Year	D1	DS	D2	D3	D4	D5	Overall
Badran 2020	Some concerns	Some concerns	Low risk	Low risk	Low risk	Low risk	Some concerns
Cheung 2023	Low risk	Not applicable	Some concerns	Low risk	High risk	Some concerns	High risk
Gibson 2018	Some concerns	Not applicable	Some concerns	Low risk	Low risk	Low risk	Some concerns
Guerra 2021	High risk	Some concerns	Low risk	High risk	Low risk	Low risk	High risk
Hameroff 2013	Some concerns	Some concerns	Low risk	Low risk	Low risk	High risk	High risk
Matt 2022	Some concerns	Some concerns	Low risk	Low risk	Low risk	Low risk	Some concerns
Reznik 2020	Some concerns	Not applicable	High risk	High risk	Low risk	Some concerns	High risk
Samuel 2022	Some concerns	Some concerns	Low risk	Low risk	Low risk	Low risk	Some concerns
Sanguinetti 2020	Low risk	Not applicable	Low risk	Low risk	Low risk	Low risk	Low risk
Zeng 2022	Some concerns	Some concerns	Low risk	Low risk	Low risk	Some concerns	Some concerns
Zhang 2022a	Some concerns	Some concerns	Low risk	Low risk	Low risk	Low risk	Some concerns

Domains for the Cochrane Rob of Bias tool 2: D1: risk of bias arising from the randomization process; DS: risk of bias arising from period and carryover effects (applicable for crossover trials); D2: risk of bias due to deviations from the intended interventions; D3: risk of bias due to missing outcome data; D4: risk of bias in measurement of the outcome; D5: risk of bias in selection of the reported result.

Criteria for the overall risk-of-bias judgement: "Low risk": the study is judged to be low risk of bias for all domains for this result; "Some concerns": The study is judged to raise some concerns in at least one domain for this result, but not at high risk of bias for any domain; "High risk": The study is judged to be at high risk of bias in at least one domain for this result, or the study is judged to have some concerns for multiple domains in a way that substantially lowers confidence in the result.

Table 4. Full breakdown of study quality assessment for the included animal studies using the Systematic Review Center for Laboratory Animal Experimentation Risk of Bias tool.

Author, Year	Selection bias			Performance bias		Detection bias		Attrition bias	Reporting bias	Others
	1	2	3	4	5	6	7	8	9	10
Baek 2018	Unclear	Unclear	Unclear	Yes	Unclear	Unclear	Yes	Unclear	Yes	Yes
Cao 2022	Unclear	Unclear	Unclear	Unclear	Unclear	Unclear	Unclear	Unclear	Yes	Yes
Chen 2020	Unclear	Unclear	Unclear	Yes	Unclear	Unclear	Yes	No	Yes	Yes
Chu 2023	Unclear	Unclear	Unclear	Yes	Unclear	Unclear	Unclear	Unclear	Yes	Yes
Daniels 2018	Unclear	Unclear	Unclear	Unclear	Unclear	Unclear	Unclear	Unclear	Yes	Yes
Feng 2021	Unclear	Unclear	Unclear	Yes	Unclear	Unclear	Unclear	Unclear	Yes	Yes
Folloni 2019	No	Unclear	No	Yes	Unclear	Yes	No	Yes	Yes	Yes
Guo 2015	Unclear	Unclear	Unclear	Yes	Unclear	Yes	Yes	Yes	Yes	Yes
Guo 2021	Unclear	Unclear	Unclear	Unclear	Unclear	Yes	Unclear	No	Yes	Yes
Hakimova 2015	Unclear	Unclear	Unclear	Yes	Unclear	Unclear	Unclear	Unclear	Yes	Yes
Huang 2019	Unclear	Unclear	Unclear	Yes	Unclear	Unclear	Yes	Unclear	Yes	Yes
Huang 2021	Unclear	Unclear	Unclear	Yes	Unclear	Unclear	Unclear	Unclear	Yes	Yes
Kim 2013	Unclear	Unclear	Unclear	Yes	Unclear	Yes	Unclear	Yes	Yes	Yes
Kim 2015	Unclear	Yes	Unclear	Unclear	Unclear	Unclear	Unclear	Unclear	Yes	Yes
Niu 2020	Unclear	Unclear	Unclear	Unclear	Unclear	Unclear	Unclear	Unclear	Yes	Yes
Min 2011a	Unclear	Yes	Unclear	Yes	Unclear	Unclear	Unclear	Yes	Yes	Yes
Min 2011b	Unclear	Yes	Unclear	Yes	Unclear	Unclear	Unclear	Unclear	Yes	Yes

Mohammadjavadi 2022	Unclear	Unclear	Unclear	Yes	Yes	Unclear	Yes	Yes	Yes	Yes
Pang 2021	Unclear	Unclear	Unclear	Unclear	Unclear	Unclear	Unclear	No	Yes	Yes
Park 2021	Unclear	Unclear	Unclear	Unclear	Unclear	Unclear	Unclear	Yes	Yes	Yes
Peng 2021	Unclear	Unclear	Unclear	Unclear	Unclear	Yes	Yes	Yes	Yes	Yes
Sharabi 2018	Unclear	Unclear	Unclear	Yes	Unclear	Yes	Unclear	Yes	Yes	Yes
Song 2022	Unclear	Unclear	Unclear	Unclear	Unclear	Unclear	Yes	Unclear	Yes	Yes
Tsai 2022	Unclear	Unclear	Unclear	Unclear	Unclear	Unclear	Unclear	No	Yes	Yes
Wang 2020a	Unclear	Unclear	Unclear	Yes	Unclear	No	Unclear	No	No	Yes
Wang 2020b	Unclear	Unclear	Unclear	Yes	Unclear	Unclear	Unclear	Unclear	Yes	Yes
Wang 2021a	Unclear	Unclear	Unclear	Unclear	Unclear	Yes	Yes	Yes	Yes	Yes
Wang 2021b	Unclear	Unclear	Unclear	Yes	Unclear	Unclear	Unclear	No	Yes	Yes
Wang 2023a	Unclear	Unclear	Unclear	Yes	Unclear	Yes	Unclear	Yes	Yes	Yes
Wang 2023b	Unclear	Unclear	Unclear	Yes	Unclear	Yes	Unclear	Yes	Yes	Yes
Xu 2020	Unclear	Unclear	Unclear	Yes	Unclear	Yes	Unclear	Yes	Yes	Yes
Yang 2012	Unclear	Yes	Unclear	Yes	Unclear	Unclear	Unclear	Yes	Yes	Yes
Yang 2022	Unclear	Unclear	Unclear	Unclear	Unclear	Yes	Yes	Yes	Yes	Yes
Yao 2022	Unclear	Unclear	Unclear	Yes	Unclear	Yes	Unclear	Yes	Yes	Yes

Yi 2022	Unclear	Unclear	Unclear	Yes	Unclear	Unclear	Unclear	No	Yes	Yes
Yoo 2011	Unclear	Yes	Unclear	Unclear	Unclear	Unclear	No	Yes	Yes	Yes
Yoo 2018	Unclear	Yes	Unclear	Yes	Unclear	Unclear	Unclear	Yes	Yes	Yes
Yuan 2020	Unclear	Unclear	Unclear	Unclear	Unclear	Unclear	Unclear	Unclear	Yes	Yes
Zhang 2019	Unclear	Unclear	Unclear	Unclear	Unclear	Unclear	Yes	No	Yes	Yes
Zhang 2022b	Unclear	Unclear	Unclear	Unclear	Unclear	Unclear	Unclear	Unclear	Yes	Yes
Zhao 2023	Unclear	Unclear	Unclear	Yes	Unclear	Yes	Unclear	Yes	Yes	Yes
Zhou 2019	Unclear	Unclear	Unclear	Yes	Unclear	Unclear	Unclear	No	Yes	Yes
Zhou 2021	Unclear	Unclear	Unclear	Unclear	Unclear	Unclear	Yes	Yes	Yes	Yes
Zhu 2023	Unclear	Unclear	Unclear	No	Unclear	Yes	Unclear	Yes	Yes	Yes

Criteria for each item: Item 1: sequence generation, item 2: baseline characteristics, item 3: Allocation concealment (selection bias); item 4: random housing, item 5: blinding (performance bias); item 6: random outcome assessment, item 7: blinding (detection bias); item 8: incomplete outcome data (attrition bias); item 9: selective outcome reporting (reporting bias). item 10: other sources of bias (other bias).

Judgement: "Yes" indicates a low risk of bias; "No" indicates a high risk of bias; "Unclear" indicates an unclear risk of bias

2.5.3 Neuromodulation effects of LITUS

The neuromodulation effects of LITUS were categorized under four domains: clinical and pre-clinical, neuroimaging, neurophysiological, and histological and biochemical outcomes. A Sankey diagram (Figure 3) illustrates the main neuromodulation effects of LITUS in human subjects. Two sunburst charts (Figure 4, Figure 5) illustrate the main neuromodulation effects of LITUS in healthy animals and in disease models, respectively.

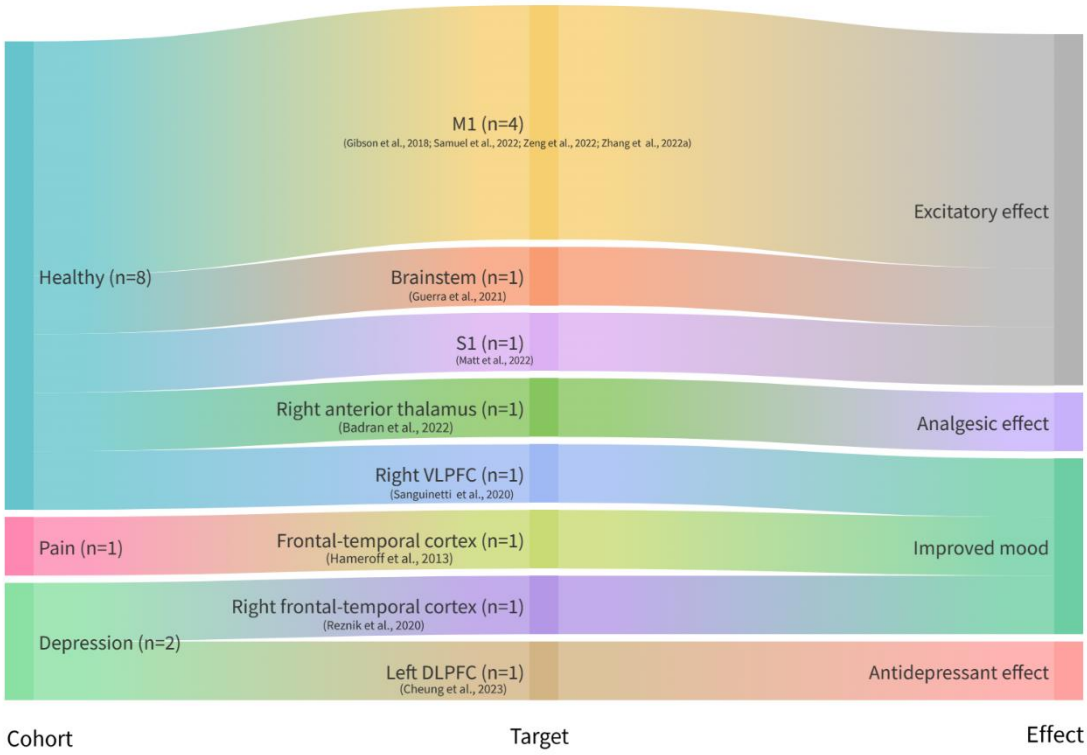

Figure 3. Neuromodulation effects of LITUS in human subjects (Study 1)

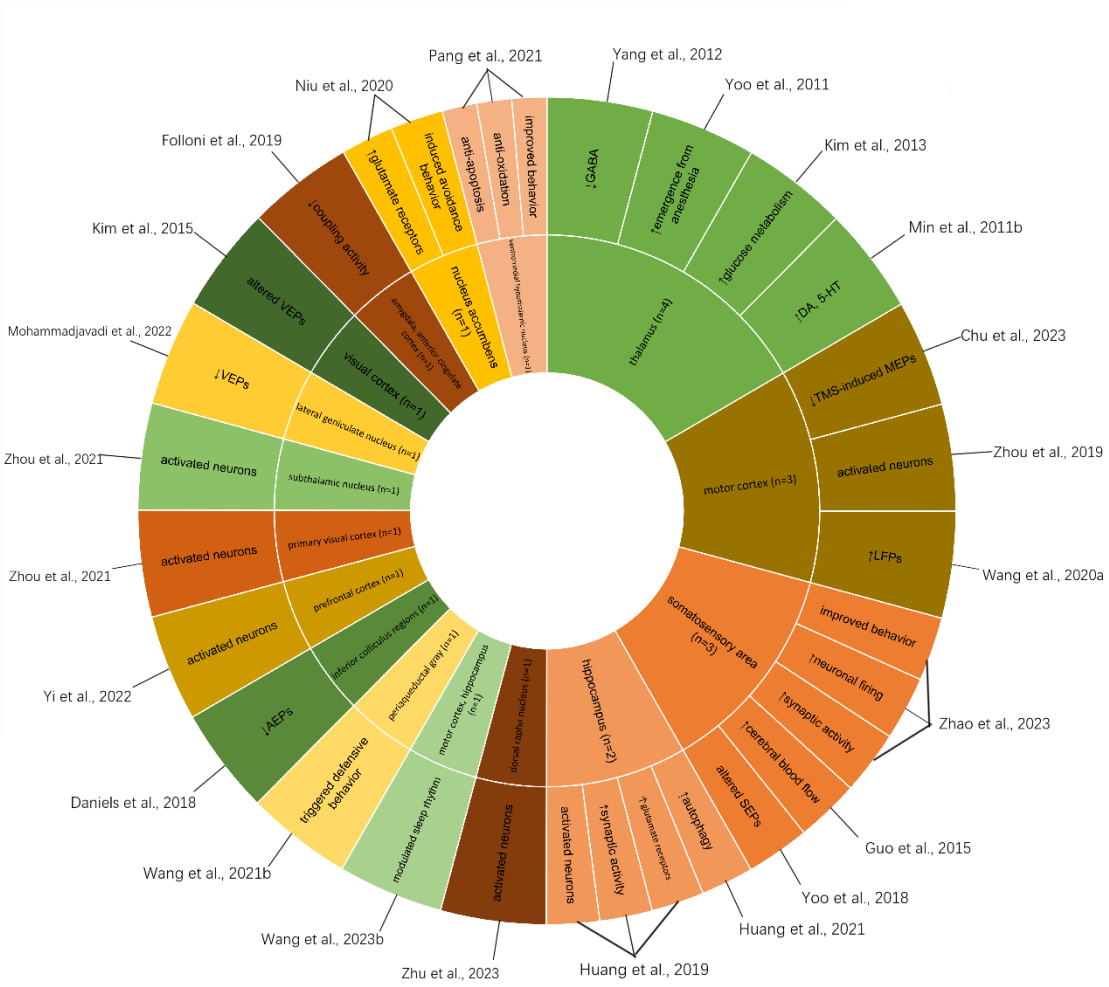

Figure 4. Neuromodulation effects of LITUS in healthy animals (Study 1)

Figure 5. Neuromodulation effects of LITUS in animal disease models (Study 1)

2.5.3.1 Clinical and pre-clinical outcomes

LITUS effects were investigated for a variety of clinical and pre-clinical outcomes, including pain, mood, motor function, cognitive functions, and others.

Regarding pain, one human study and two animal studies investigated the analgesic effects of fTUS. A study demonstrated that two sessions of 10-minute fTUS in the right anterior thalamus reduced pain sensitivity in healthy subjects (Badran et al., 2020). Animal studies found that a 10-minute whole-brain fTUS (Yao et al., 2022) and a 21-day anterior

cingulate cortex (ACC) fTUS (Feng et al., 2021) alleviated pain in rodent disease models. Notably, fTUS showed a differential impact on acute and chronic neuropathic pain (Feng et al., 2021). An online analgesic effect was found in chronic neuropathic pain, whereas an offline analgesic effect was found in acute neuropathic pain (Feng et al., 2021).

Regarding mood, four human studies and four animal studies investigated the antidepressive effects of LITUS. A 30-second right ventrolateral prefrontal cortex (VLPFC) fTUS in healthy subjects (Sanguinetti et al., 2020) and a 15-second frontal-temporal cortex unfocused TUS in patients with chronic pain (Hameroff et al., 2013) resulted in a short-term improvement in mood for 10-40 minutes after sonication. Another study performed five 30-second fTUS sessions on the right fronto-temporal cortex in depressed patients and observed that the trait worry was mitigated after treatment (Reznik et al., 2020). Notably, six TPS sessions on the left dorsolateral prefrontal cortex (DLPFC) reduced depressive symptoms in patients with depression (Cheung et al., 2023). Animal studies found that fTUS reduced depressive behavior by stimulating the medial prefrontal cortex (Yi et al., 2022), left prelimbic cortex (Zhang et al., 2019), dorsal raphe nucleus (Zhu et al., 2023), and hippocampus (Hakimova et al., 2015).

Two human studies and ten animal studies investigated the modulation effect of fTUS on motor function. Two studies in healthy subjects targeting the left primary motor cortex revealed improvements in movement speed on visuomotor tasks after 10-minute fTUS (Zhang et al., 2022a) and after 80-second theta-burst fTUS (tb-fTUS) (Zeng et al.,

2022). The restoration of motor function was found in rodent disease models after sonication. Tail muscle strength, movement duration and distance, motor coordination, bradykinesia and balance disorders were improved in rodent PD models by administration of fTUS in the motor cortex (Zhou et al., 2019) and subthalamic nucleus (STN) (Yuan et al., 2020; Zhou et al., 2021). Motor function recovery was also seen in the rat models of TBI (Peng et al., 2021) and rodent models of ischemic stroke (Baek et al., 2018; Guo et al., 2015; Wang et al., 2021a) following sonication. Ultrasound treatment was applied to the injured area of the brain, except for one study where sonication was directed to the lateral cerebellar nucleus (LCN) (Baek et al., 2018). In aging rats, 28 sessions of 10 Hz-fTUS administered to the hypothalamic nucleus enhanced the grip strength (Pang et al., 2021). A short-term effect on reducing hyperactivity in rat models of ADHD was observed 2-4 days after 12 fTUS sessions targeting the prefrontal cortex (Wang et al., 2023a).

Five animal studies investigated the effect of fTUS on cognitive function. Healthy mice (Zhao et al., 2023), aging mice (Pang et al., 2021), and rodent disease models, including ADHD (Wang et al., 2023a), schizophrenia (Tsai et al., 2022) and epilepsy (Hakimova et al., 2015) were involved in the studies, where the stimulated targets varied. In summary, an improvement in cognitive function was shown after fTUS targeting the barrel cortex (a region of the somatosensory cortex in mice) (Zhao et al., 2023), the prefrontal cortex (Wang et al., 2023a), the hippocampus (Hakimova et al., 2015) and a brain area lying 3.0 mm

posterior and 2.5 mm lateral to the bregma of the mouse brain (Tsai et al., 2022).

Other modulation effects of fTUS were demonstrated in individual animal studies. These effects included a reduction in epileptic behavior (Min et al., 2011a) by targeting the thalamus and downregulation of systolic blood pressure by targeting the solitary tract nucleus in rodent disease models (Cao et al., 2022); as well as induction of avoidance behavior by targeting nucleus accumbens in healthy mice and mouse models of addictive disorder (Niu et al., 2020), triggering of defensive behavior by targeting the periaqueductal gray (Wang et al., 2021b) and the facilitation of recovery from anesthesia by targeting thalamus (Yoo et al., 2011) in healthy rodents.

2.5.3.2 Neurophysiological outcomes

LITUS effects were investigated for a variety of neurophysiological outcomes by recording electromyography (EMG) and electroencephalography (EEG) and by measuring excitatory spontaneous postsynaptic currents.

Seven studies investigated the stimulation effect of LITUS by using EMG. Four out of five human studies evaluated motor cortical excitability after sonication by measuring the TMS-induced motor-evoked potentials (MEPs). fTUS (Zhang et al., 2022a), unfocused TUS (Gibson et al., 2018) and tb-fTUS (Samuel et al., 2022; Zeng et al., 2022) increased the MEPs after one sonication at the hotspot in the left primary motor cortex in healthy subjects. The excitatory effect lasted 6 minutes

after unfocused TUS (Gibson et al., 2018) and 30 minutes after tb-fTUS (Zeng et al., 2022). The tb-fTUS protocol also attenuated TMS-induced short-interval intracortical inhibition (SICI) up to 30 minutes and facilitated TMS-induced intracortical facilitation (ICF) up to 5 minutes after sonication (Samuel et al., 2022; Zeng et al., 2022). A similar excitatory effect of unfocused TUS on the trigeminal blink reflex was found in the remaining human study in which the superior colliculus was stimulated, and EMG was recorded in the orbicularis oculi muscle induced by electrical stimulation in the supraorbital nerve (Guerra et al., 2021). In contrast, animal studies demonstrated a suppressive effect on TMS-induced MEPs after fTUS in the left primary motor cortex in healthy rats (Chu et al., 2023) and showed online inhibition of EMG signal in tremor muscles after fTUS in the olivo-cerebellar system in mouse models of essential tremor (Sharabi et al., 2019). Overall, LITUS exhibited bidirectional (excitatory or suppressive) neuromodulation effects measured using EMG.

Thirteen animal studies evaluated modulation the effect of LITUS using EEG. In healthy rats, a suppressive effect of fTUS on auditory evoked potentials (AEPs) (Daniels et al., 2018) and visual evoked potentials (VEPs) (Mohammadjavadi et al., 2022) was demonstrated by targeting the inferior colliculus and the lateral geniculate nucleus, respectively. Whereas one study revealed that the fTUS-induced VEP amplitude change was dose-dependent by targeting the visual cortex (Kim et al., 2015). While the I_{SPPA} of 3 W/cm^2 was constant, a duty cycle (DC) of 5% suppressed the VEPs and 8.3% DC facilitated the VEPs, and 1% DC had

no effect on the VEP amplitude (Kim et al., 2015). fTUS was also found to modulate somatosensory evoked potentials (SEPs) by targeting the somatosensory cortex, and the differential SEP features persisted beyond 35 minutes after a 10-minute fTUS (Yoo et al., 2018). Moreover, an online excitatory effect of fTUS was found in the motor cortex by exhibiting higher local field potential (LFP) amplitudes (Wang et al., 2020a). Overall, studies in healthy animals examining LITUS effects using EEG showed an evident modulation of brain excitability, and the direction of the modulation (excitation or suppression) might be affected by the sonication parameters. Furthermore, animal studies found that LITUS reversed disease-related LFPs in several rodent disease models, including sleep-deprived models (Wang et al., 2023b), AD models (Park et al., 2021), PD models (Wang et al., 2020b), ADHD models (Wang et al., 2023a), pain models (Zhang et al., 2022b) and epilepsy models (Chen et al., 2020; Hakimova et al., 2015; Min et al., 2011a).

One animal study detected the fTUS-induced functional synaptic plasticity in healthy rats by recording excitatory spontaneous postsynaptic currents. The frequency of spontaneous excitatory postsynaptic current of hippocampal neurons increased after ten daily 10-minute fTUS sessions in the hippocampus (Huang et al., 2019).

2.5.3.3 Neuroimaging outcomes

LITUS effects were investigated for a variety of neuroimaging outcomes, including magnetic resonance imaging (MRI), magnetoencephalogram

(MEG), positron emission tomography (PET), laser speckle image and two-photon fluorescence imaging.

One human study and two animal studies utilized MRI to investigate the modulatory effect of LITUS. Structural magnetic resonance imaging (sMRI), resting state functional MRI (rs-fMRI) and diffusion tensor imaging (DTI) were measured in healthy subjects after three sessions of TPS targeting the left primary somatosensory cortex (Matt et al., 2022). No change in grey matter volume was found in sMRI; whereas, rs-fMRI revealed an increase in functional connectivity in the left sensorimotor network one week after the last stimulation. Furthermore, DTI revealed decreased axial diffusivity in the primary somatosensory region and primary motor region after TPS. The authors claimed that the reduced axial diffusivity could indicate axonal formation. Rs-fMRI was also examined in an animal experiment but demonstrated a suppressive effect of fTUS on functional connectivity between the target areas (amygdala and ACC) and their interconnected areas in healthy macaques (Folloni et al., 2019). In Folloni's study, high I_{SPTA} of 19.5 W/cm^2 and 5.63 W/cm^2 were used, which could induce a possible thermal effect and result in reversible neuroinhibition (Darrow et al., 2019). In TBI rat models, DWI revealed a decrease in apparent diffusion coefficient and higher fractional anisotropy during the treatment period (Peng et al., 2021). The authors claimed that fTUS effectively reduced cerebral edema and white matter damage.

One human study applied MEG to assess oscillatory brain responses and network connectivity after tb-fTUS in the left motor cortex (Samuel et al.,

2022). The results showed that tb-fTUS produced movement-associated changes in alpha and beta spectral power in distinct regions. Alpha spectral power decreased in the left limbic region, left cerebellum, bilateral sensorimotor cortices, and right supplementary motor area, while beta spectral power reduced prominently in the right parietal area and right basal ganglia. The authors concluded that the findings indicated the involvement of regions within motor networks in the response to tb-fTUS.

In an animal study on healthy rats, local glucose metabolism in the sonication target (thalamus) was examined using FDG (18-fludeoxyglucose) PET (Kim et al., 2013). After a 40-minute fTUS, higher local glucose metabolism was observed in the center of the sonication focus but not in other areas.

Two animal studies used laser speckle image to investigate the effect of fTUS on cerebral blood flow in rat models of pain (Yao et al., 2022) and healthy rats (Guo et al., 2015). After sonication with various numbers of tone bursts (600, 800, 1000), a rise of cerebral blood flow velocity was noticed immediately after fTUS at the ischemic cortex, and it maintained at a higher level up to 4-12 seconds after sonication, depending on the parameter (Guo et al., 2015). However, whole-brain fTUS did not alter cerebral blood flow velocity in the rat models of pain (Yao et al., 2022).

One animal study used two-photon fluorescence imaging in healthy rats. It showed that fTUS at the barrel cortex induced an enhancement in

neuronal firing activity and an increase in the dendritic spine growth rate in the barrel cortex (Zhao et al., 2023).

2.5.3.4 Histological and biological outcomes

LITUS effects were studied for a variety of histological and biological outcomes involving anti-inflammatory responses, neurogenesis processes, antioxidant responses, and other disease-specific changes.

Seven animal studies examined the anti-inflammatory effect of fTUS in rodent disease models, including PD models (Song et al., 2022; Zhou et al., 2021), ischemic brain injury models (Guo et al., 2015; Wang et al., 2021a), aging models (Pang et al., 2021), depression models (Yi et al., 2022), and demyelination models (Yang et al., 2022). Reduction of inflammatory neurons such as astroglia and microglia (Song et al., 2022; Yang et al., 2022; Zhou et al., 2021), inflammatory cells such as neutrophils (Guo et al., 2015), and reduction of inflammatory cytokines (TNF-α, IL-1β) (Pang et al., 2021; Song et al., 2022; Yi et al., 2022; Zhou et al., 2021) and protein markers of neuroinflammation (COX-2, NF-κB) (Song et al., 2022; Zhou et al., 2021) were observed after fTUS at right striatum (Song et al., 2022), demyelination lesion area (Yang et al., 2022), subthalamic nucleus (Zhou et al., 2021), ischemic cortex (Guo et al., 2015), ventromedial hypothalamic nucleus (Pang et al., 2021), and prefrontal cortex (Yi et al., 2022). On the other hand, an increment in anti-inflammatory M2 microglia and an increment in anti-inflammatory cytokines (IL-10 and IL-10R) were detected after fTUS at the ischemic hemisphere (Wang et al., 2021a).

Twelve animal studies investigated the neurogenesis effect of fTUS in rodent disease models and healthy rodents. LITUS increased levels of neurotrophic factors, including brain-derived neurotrophic factor (BDNF) and glial cell line-derived neurotrophic factor (GDNF), as well as expression of neurogenesis-related proteins in depression models (Guo et al., 2021; Zhang et al., 2019), PD models (Song et al., 2022; Xu et al., 2020), ADHD models (Wang et al., 2023a), and demyelination models (Yang et al., 2022), by targeting prelimbic cortex (Zhang et al., 2019), right striatum (Song et al., 2022), prefrontal cortex (Wang et al., 2023a), and demyelination lesion area (Yang et al., 2022). In a study on schizophrenia models, fTUS simultaneously reversed BDNF levels in the hippocampus and prefrontal cortex (Tsai et al., 2022). Furthermore, fTUS facilitated the remyelination process by increasing myelin basic protein (Guo et al., 2021; Yang et al., 2022) and the hippocampal fTUS activated hippocampal neurons by increasing dendritic spine density (Huang et al., 2019). LITUS also modulated the dopamine and GABA signaling pathways. Dopaminergic neurons (Xu et al., 2020; Zhou et al., 2021) and dopamine transporters (Song et al., 2022) in the substantia nigra increased in PD models following fTUS in the subthalamic nucleus (Zhou et al., 2021) and right striatum (Song et al., 2022). In schizophrenia models, an increase in GABAergic neurons in the medial prefrontal lobe was detected 24 hours after fTUS (Tsai et al., 2022). In healthy rats, extracellular dopamine levels in the frontal lobe increased up to 100 minutes after a 20-minute thalamic fTUS (Min et al., 2011b), while extracellular GABA levels declined (Yang et al., 2012). In healthy

rodents, fTUS-induced increase in synaptic proteins was detected in target regions by stimulating the hippocampus (Huang et al., 2019) and nucleus accumbens (Niu et al., 2020). Moreover, fTUS activated the autophagy process in healthy mice by increasing the LC3BII/LC3BI ratio and decreasing p62 levels in the sonicated areas (cortex and hippocampus) (Huang et al., 2021). The authors speculated that fTUS had a neuroprotection effect on neurodegenerative diseases by increasing self-digestion of abnormal constituents in obsolete cells. Taken together, fTUS demonstrated a neurogenesis effect on regulating the level of neurotrophic factors and neurogenesis-related proteins, facilitating the remyelination process, increasing the dendritic spine density of neurons, modulating dopamine and GABA signaling pathways, inducing the synaptic plasticity, and activating the autophagy process.

Three animal studies examined the antioxidant effect of fTUS in rodent PD models and aging models. Antioxidant enzymes comprising superoxide dismutase and glutathione peroxidase in the substantia nigra and striatum were increased, while inducible nitric-oxide synthase, one of the oxidant enzymes, was reduced after fTUS in PD models by targeting the motor cortex (Zhou et al., 2019) and subthalamic nucleus (Zhou et al., 2021). In aging models, decreased expression in NMDA R2B receptors and reduced expression in the promotor of cell apoptosis (Bax) were observed after sonication at the ventromedial hypothalamic nucleus (Pang et al., 2021). Taken together, fTUS exhibited antioxidant effects by increasing antioxidant enzymes, decreasing oxidant enzymes, and inhibiting the age-related apoptosis process.

Eight animal studies found disease-specific changes induced by fTUS. In rodent brain injury models, recovery in the injured area was shown after fTUS in the injured cortex (Guo et al., 2015; Peng et al., 2021; Wang et al., 2021a) and LCN (Baek et al., 2018). In mouse models of AD, fTUS reduced total Aβ42 levels in the limbic cortex (Park et al., 2021). In mouse models of neuropathic pain, ACC-fTUS downregulated the highly expressed Hnrnph1 and Hnrnpd (Feng et al., 2021). In rat models of hypertension, a therapeutic effect of solitary tract nucleus-fTUS on reducing plasma levels of aldosterone (Aldo), angiotensin II (ANGII), endothelin (ET-1), atrial natriuretic factor (ANF) and cortisol (Cor) was found (Cao et al., 2022).

2.5.4 Adverse effects reported in the included studies

A total of 282 participants received LITUS in 11 human studies. Three fTUS studies (Badran et al., 2020; Samuel et al., 2022; Zeng et al., 2022), one unfocused TUS study (Guerra et al., 2021), and one TPS study (Matt et al., 2022) reported that no adverse events were observed throughout the experiment period. Two fTUS studies did not examine the adverse effects (Reznik et al., 2020; Sanguinetti et al., 2020). Two studies reported no significant difference in terms of discomfort or abnormal sensations between verum and sham groups, with one unfocused TUS study mentioning tingling as a common sensation (Gibson et al., 2018) and one fTUS study not mentioning any details (Zhang et al., 2022a). In a TPS study, headaches were reported in a few subjects (4%) and one subject complained of nausea and vomiting after the first treatment, but the

symptoms resolved within 2 hours without the necessity for medication and no further symptoms occurred (Cheung et al., 2023). Another unfocused TUS study reported that one subject experienced an exacerbation of headache after sonication, which subsided quickly without sequelae (Hameroff et al., 2013). In summary, no adverse events were reported in four fTUS studies; three unfocused and two TPS studies reported adverse events in 1% and 5% of subjects, respectively.

Of 44 animal experiments, 25 fTUS studies and one unfocused TUS study conducted safety evaluations by performing by H&E staining, Nissl staining, Perls' Prussian blue staining, TUNEL staining, glial fibrillary acidic protein immunohistochemical staining, thermal monitoring, MRI, and behavioral testing (Baek et al., 2018; Cao et al., 2022; Chen et al., 2020; Chu et al., 2023; Daniels et al., 2018; Feng et al., 2021; Folloni et al., 2019; Huang et al., 2019; Huang et al., 2021; Kim et al., 2013; Min et al., 2011a; Niu et al., 2020; Pang et al., 2021; Park et al., 2021; Sharabi et al., 2019; Song et al., 2022; Wang et al., 2021b; Xu et al., 2020; Yang et al., 2012; Yi et al., 2022; Yoo et al., 2018; Zhang et al., 2019; Zhang et al., 2022b; Zhou et al., 2021; Zhou et al., 2019; Zhu et al., 2023). None of them reported abnormal histological, biochemical, or behavioral findings after LITUS.

Regarding the mechanical index (MI), 36 out of 39 included studies (MI was not available in 16 included studies) utilized LITUS with MI < 1.9, while two human studies used TPS with an MI of 10.95 (Cheung et al., 2023; Matt et al., 2022) and an animal study used fTUS with an MI of 2.88 (Folloni et al., 2019)."

2.6 Discussion

In this review, we comprehensively summarized the neuromodulation effects of LITUS on clinical and pre-clinical, neurophysiological, neuroimaging, histological and biochemical outcomes in human and animal research. In the reviewed articles, the treatment effects were demonstrated in neurological disorders (including PD, AD, demyelination, epilepsy, brain injury, and essential tremor), psychiatric disorders (including depression, ADHD, schizophrenia, addictive disorder), pain, sleep disorders, and hypertension. LITUS also modulated pain threshold, improved mood and enhanced motor function in healthy subjects, elicited defensive and avoidance behavior, improved cognitive function, modulated sleep rhythms, and facilitated awakening from anesthesia in healthy animals. LITUS-induced changes in neuronal excitability were found in the targeted areas and their connected regions, including the motor cortex, brainstem, hippocampus, olivo-cerebellar system, prefrontal cortex, visual cortex, inferior colliculus region, somatosensory cortex, periaqueductal gray, thalamus, amygdala, and anterior cingulate cortex. From a histological and biochemical point of view, LITUS modulated neurological function by regulating the anti-inflammatory reaction, neurogenesis process, antioxidant response, apoptosis process and autophagy process.

No histological, biochemical, or behavioral side effects were identified in the animal studies included in this review. In two human studies, reversible adverse events such as headache, nausea, and vomiting were described in a few subjects.

LITUS comprises fTUS, unfocused TUS and TPS. The mechanism of action of fTUS and unfocused TUS is similar. According to several hypotheses, ultrasonic waves interact with the intra- and extra- cellular environment through acoustic cavitation, acoustic radiation force and acoustic streaming, activating membrane gating kinetics, altering membrane capacitance, triggering synaptic transmission, and inducing NMDA-dependent synaptic plasticity (Brohawn et al., 2014; Chen et al., 2019; Jerusalem et al., 2019; Tyler, 2011; Shamli Oghli et al., 2023). Despite similar mechanisms, the different sonication parameters and the devices involved between fTUS and unfocused TUS could lead to different stimulation effects (Di Biase et al., 2019). Of note, the neuromodulation mechanism of TPS likely differs from fTUS and unfocused TUS, as TPS retains the intrinsic character of shockwaves. Low-energy extracorporeal shockwaves promote anti-inflammatory effects as well as the angiogenesis process and regeneration through mechanotransduction (d'Agostino et al., 2015). Studies revealed that the biological mechanism of low-energy extracorporeal shockwaves involves upregulation of BDNF and vascular endothelial growth factor (VEGB) (Hatanaka et al., 2016; Matsuda et al., 2020; Yahata et al., 2016) and facilitation of shifting endothelial nitrogen oxides to a tyrosine-dephosphorylated form, increasing NO production and suppressing nuclear-factor κB (Mariotto et al., 2005). Given the diversity of therapeutic modalities and different biomechanisms of LITUS, future research needs to specify the type of LITUS and the sonication

parameters employed in studies, and investigate the neuromodulation effect of fTUS, unfocused TUS and TPS individually.

To establish a reliable therapeutic framework for LITUS, several issues need to be addressed. First, the investigation of the effective and safe dosage of acoustic waves to be delivered into the target is required. Various intensities of acoustic waves were applied in the included studies. In animal studies, I_{SPPA} from 120 mW/cm^2 to 64.9 W/cm^2 and I_{SPTA} from 0.014 mW/cm^2 to 19.5 W/cm^2 were used. In human studies, fTUS was performed using a range of I_{SPPA} values, ranging from 2.26 W/cm^2 to 14 W/cm^2, and I_{SPTA} values ranging from 71 mW/cm^2 to 995 mW/cm^2; unfocused TUS utilized an I_{SPPA} of 34.96 W/cm^2 and I_{SPTA} values ranging from 132.85 mW/cm^2 to 152 mW/cm^2; Regarding TPS, it employed an I_{SPPA} of 111 W/cm^2 and an I_{SPTA} of 100 mW/cm^2. Using too low ultrasound intensity may not be sufficient to exhibit a neuromodulation effect. An animal study showed that weak fTUS with 0.014 mW/cm^2 I_{SPTA} did not alter motor cortex excitability in healthy rats, while fTUS with 0.338-12.15 mW/cm^2 increased the cortex excitability (Chu et al., 2023). For humans, the lowest effective stimulation intensity should be higher, as 69-87% of ultrasound waves are attenuated by the human skull (Riis et al., 2022). Besides, the attenuation of acoustic waves at the skull increases with higher acoustic frequencies; therefore, unfocused TUS with a higher acoustic frequency can further diminish the sonication transmitted to the brain. On the other hand, the risk of mechanical and thermal damage to the brain increases with higher acoustic intensities. MI is commonly used to estimate the risk of

mechanical damage caused by ultrasound, and an MI < 1.9 has been recommended by the FDA when using cephalic ultrasound devices (FDA, 2019). Based on current knowledge, there is no consensus on what intensity of LITUS is appropriate to guarantee robust neuronal effects while avoiding side effects. Simulation studies and in vitro studies can be performed prior to clinical trials to determine the appropriate dosage of ultrasound treatment. Second, the sonication parameters that mediate the treatment effect need to be clarified. Dose-response studies revealed that higher acoustic intensity increased the likelihood of motor responses (King et al., 2013) and that the magnitude of fTUS-induced VEPs increased with acoustic intensity (Lee et al., 2016). Furthermore, studies found that higher intensity fTUS had a stronger analgesic effect (Feng et al., 2021) and a stronger inhibitory effect on cortical excitability (Chu et al., 2023; Daniels et al., 2018). Aside from acoustic intensity, other sonication parameters such as pulse repetition frequency and pulse duration (Pang et al., 2021), number of tone bursts (Guo et al., 2015), duty cycle (Chen et al., 2020; Kim et al., 2015) and stimulation duration (Chen et al., 2020; Wang et al., 2020a) could influence the neuronal modulation effect. Specifically, Kim et al. (Kim et al., 2015) discovered that 5% DC combined with 3 W/cm^2 I_{SPPA} inhibited VEPs, whereas 8.3% DC combined with 3 W/cm^2 I_{SPPA} enhanced the VEPs amplitude. However, the factors that determine the bidirectional effect are uncertain. Further, a tb-fTUS with an 80-s sonication duration with 20-ms ultrasound pulses repeated every 200 ms (pulse repetition frequency: 5 Hz, DC: 10%, number of pulses: 400) was developed and demonstrated a

superior excitatory effect compared to a conventional fTUS with the same intensity (Zeng et al., 2022). Third, proper target selection is critical for determining treatment outcomes of LITUS, given its highly region-specific nature (Folloni et al., 2019; Kim et al., 2013). Several potential targets were proposed in the included studies, including thalamus and ACC for pain modulation (Badran et al., 2020; Feng et al., 2021); DLPFC, medial prefrontal cortex, prelimbic cortex and dorsal raphe nucleus for treating depression (Cheung et al., 2023; Yi et al., 2022; Zhang et al., 2019; Zhu et al., 2023;); VLPFC and the right fronto-temporal cortex for improving mood (Reznik et al., 2020; Sanguinetti et al., 2020; Hameroff et al., 2013); motor cortex, the subthalamic nucleus and the lateral cerebellar nucleus for improving motor function (Zeng et al., 2022; Zhang et al., 2022a; Zhou et al., 2021; Yuan et al., 2020; Zhou et al., 2019; Baek et al., 2018). Fourth, a precise neuro-navigation should be prioritized when performing LITUS. Empirical localization using landmarks on the head may compromise the precision and efficacy of LITUS; hence, real-time neuro-navigation approaches such as MRI-guided (Badran et al., 2020) and optical tracking (Cheung et al., 2023; Matt et al., 2022) should be adopted.

Regarding the limitation of the current review, first, given the strict inclusion/exclusion criteria, some potentially important pilot studies were not included in the current review. Darmani et al. (2022) and Sarica et al. (2022) can be referred to for a summary of these studies. Second, we did not search for studies that exclusively investigated the adverse consequences of LITUS. The included randomized controlled human

trials and controlled animal studies were insufficient to assess the occurrence of adverse events of LITUS (Peryer G, 2023). Third, the methodological quality of the included studies is not adequate. Ten out of eleven human studies have a moderate to high risk of bias. In 44 animal studies, most items in SYRCLE were rated as “unclear”, suggesting that there is no sufficient detail to assess the potential risk of bias. Fourth, the high heterogeneity among studies on therapy modalities, stimulation targets, and sonication parameters affects the generalizability of the results. Therefore, the results of this study must be interpreted with caution.

2.7 Conclusions

LITUS is a promising non-invasive technique that modulates brain circuits in animals and humans. The neuromodulation effects induced by LITUS include altering neuronal excitability and regulating biochemical processes such as inflammatory responses and neurogenesis, which contribute to the improvement of clinical behavior and clinical symptoms and signs. No significant adverse events were identified in the included studies; however, reversible symptoms such as headache, nausea, and vomiting were reported in a few human subjects. Future research is required to investigate the optimal sonication parameters and treatment strategies using the precise target and real-time neuro-navigation technique.

2.8 References

Badran, B.W., Caulfield, K.A., Stomberg-Firestein, S., Summers, P.M., Dowdle, L.T., Savoca, M., Li, X., Austelle, C.W., Short, E.B., Borckardt, J.J., Spivak, N., Bystritsky, A., George, M.S., 2020. Sonication of the anterior thalamus with MRI-Guided transcranial focused ultrasound (tFUS) alters pain thresholds in healthy adults: A double-blind, sham-controlled study. Brain Stimul. 13, 1805-1812. https://doi.org/10.1016/j.brs.2020.10.007.

Baek, H., Pahk, K.J., Kim, M.J., Youn, I., Kim, H., 2018. Modulation of cerebellar cortical plasticity using low-Intensity focused ultrasound for poststroke sensorimotor function recovery. Neurorehabil Neural Repair. 32, 777-787. https://doi.org/10.1177/1545968318790022.

Brohawn, S.G., Su, Z., MacKinnon, R., 2014. Mechanosensitivity is mediated directly by the lipid membrane in TRAAK and TREK1 K+channels. Proc Natl Acad Sci U S A. 111, 3614-3619. https://doi.org/10.1073/pnas.1320768111.

Cao, F., Zhang, J., Li, D., Wang, M., Lai, C., Xu, T., Bouakaz, A., Ren, P., Wan, M., Han, J., Zhang, S., 2022. Non-invasive ultrasound modulation of solitary tract nucleus exerts a sustainable antihypertensive effect in spontaneously hypertensive rats. IEEE Trans Biomed Eng. 70, 1869-1878. https://doi.org/10.1109/TBME.2022.3231343.

Chen, H., Garcia-Gonzalez, D., Jérusalem, A., 2019. Computational model of the mechanoelectrophysiological coupling in axons with application to neuromodulation. Phys Rev E. 99, 032406. https://doi.org/10.1103/PhysRevE.99.032406.

Chen, S.G., Tsai, C.H., Lin, C.J., Lee, C.C., Yu, H.Y., Hsieh, T.H., Liu, H.L., 2020. Transcranial focused ultrasound pulsation suppresses pentylenetetrazol induced epilepsy in vivo. Brain Stimul. 13, 35-46. https://doi.org/10.1016/j.brs.2019.09.011.

Cheung, T., Li, T.M.H., Ho, Y.S., Kranz, G., Fong, K.N.K., Leung, S.F., Lam, S.C., Yeung, W.F., Lam, J.Y.T., Fong, K.H., Beisteiner, R., Xiang, Y.T., Cheng, C.P.W., 2023. Effects of transcranial pulse stimulation (TPS) on adults with symptoms of depression-A pilot randomized controlled trial. Int J Environ Res Public Health. 20, 2333. https://doi.org/10.3390/ijerph20032333.

Chu, P.C., Huang, C.S., Chang, P.K., Chen, R.S., Chen, K.T., Hsieh, T.H., Liu, H.L., 2023. Weak ultrasound contributes to neuromodulatory effects in the rat motor cortex. Int J Mol Sci. 24, 2578. https://doi.org/10.3390/ijms24032578.

Cochrane, 2022. Cochrane handbook for systematic reviews of interventions version 6.3 (updated February 2022), in: Higgins JPT, T.J., Chandler J, Cumpston M, Li T, Page MJ, Welch VA (Ed.). Cochrane. Available from www.training.cochrane.org/handbook.

d'Agostino, M.C., Craig, K., Tibalt, E., Respizzi, S., 2015. Shock wave as biological therapeutic tool: From mechanical stimulation to recovery and healing, through mechanotransduction. Int JSurg. 24, 147-153. https://doi.org/10.1016/j.ijsu.2015.11.030.

Daniels, D., Sharabi, S., Last, D., Guez, D., Salomon, S., Zivli, Z., Castel, D., Volovick, A., Grinfeld, J., Rachmilevich, I., Amar, T., Liraz-Zaltsman, S., Sargsyan, N., Mardor, Y.,

Harnof, S., 2018. Focused ultrasound-induced suppression of auditory evoked potentials in vivo. Ultrasound Med Biol. 44, 1022-1030. https://doi.org/10.1016/j.ultrasmedbio.2018.01.010.

Darmani, G., Bergmann, T.O., Butts Pauly, K., Caskey, C.F., de Lecea, L., Fomenko, A., Fouragnan, E., Legon, W., Murphy, K.R., Nandi, T., Phipps, M.A., Pinton, G., Ramezanpour, H., Sallet, J., Yaakub, S.N., Yoo, S.S., Chen, R., 2022. Non-invasive transcranial ultrasound stimulation for neuromodulation. Clin Neurophysiol. 135, 51-73. https://doi.org/10.1016/j.clinph.2021.12.010.

Darrow, D.P., O'Brien, P., Richner, T.J., Netoff, T.I., Ebbini, E.S., 2019. Reversible neuroinhibition by focused ultrasound is mediated by a thermal mechanism. Brain Stimul. 12, 1439-1447. https://doi.org/10.1016/j.brs.2019.07.015.

Di Biase, L., Falato, E., Di Lazzaro, V., 2019. Transcranial focused ultrasound (tFUS) and transcranial unfocused ultrasound (tUS) neuromodulation: From theoretical principles to stimulation practices. Front Neurol. 10, 549-549. https://doi.org/10.3389/fneur.2019.00549.

Duck, F.A., 2007. Medical and non-medical protection standards for ultrasound and infrasound. Prog Biophys Mol Biol. 93, 176-191. https://doi.org/10.1016/j.pbiomolbio.2006.07.008.

FDA, 2019. Marketing clearance of diagnostic ultrasound systems and transducers; Guidance for industry and food and drug administration staff. Available from https://www.fda.gov/regulatory-information/search-fda-guidance-documents/marketing-clearance-diagnostic-ultrasound-systems-and-transducers

Feng, X., Niu, L., Long, M., Luo, K., Huang, X., Chen, M., Lin, Z., Zhou, W., Yi, S., Ao, L., 2021. Transcranial ultrasound stimulation of the anterior cingulate cortex reduces neuropathic pain in mice. Evid Based Complement Alternat Med. 2021, 6510383. https://doi.org/10.1155/2021/6510383.

Fini, M., Tyler, W.J., 2017. Transcranial focused ultrasound: a new tool for non-invasive neuromodulation. Int Rev Psychiatry. 29, 168-177. https://doi.org/10.1080/09540261.2017.1302924.

Folloni, D., Verhagen, L., Mars, R.B., Fouragnan, E., Constans, C., Aubry, J.F., Rushworth, M.F.S., Sallet, J., 2019. Manipulation of subcortical and deep cortical activity in the primate brain using transcranial focused ultrasound stimulation. Neuron. 101, 1109-1116. https://doi.org/10.1016/j.neuron.2019.01.019.

Fomenko, A., Neudorfer, C., Dallapiazza, R.F., Kalia, S.K., Lozano, A.M., 2018. Low-intensity ultrasound neuromodulation: An overview of mechanisms and emerging human applications. Brain Stimul. 11, 1209-1217. https://doi.org/10.1016/j.brs.2018.08.013.

Gibson, B.C., Sanguinetti, J.L., Badran, B.W., Yu, A.B., Klein, E.P., Abbott, C.C., Hansberger, J.T., Clark, V.P., 2018. Increased excitability induced in the primary motor

cortex by transcranial ultrasound stimulation. Front Neurol. 9, 1007. https://doi.org/10.3389/fneur.2018.01007.

Guerra, A., Vicenzini, E., Cioffi, E., Colella, D., Cannavacciuolo, A., Pozzi, S., Caccia, B., Paparella, G., Di Stefano, G., Berardelli, A., Bologna, M., 2021. Effects of transcranial ultrasound stimulation on trigeminal blink reflex excitability. Brain Sci. 11, 645. https://doi.org/10.3390/brainsci11050645.

Guo, H., Baker, G., Hartle, K., Fujiwara, E., Wang, J., Zhang, Y., Xing, J., Lyu, H., Li, X.M., Chen, J., 2021. Exploratory study on neurochemical effects of low-intensity pulsed ultrasound in brains of mice. Med Biol Eng Comput. 59, 1099-1110. https://doi.org/10.1007/s11517-021-02351-9.

Guo, T., Li, H., Lv, Y., Lu, H., Niu, J., Sun, J., Yang, G.Y., Ren, C., Tong, S., 2015. Pulsed transcranial ultrasound stimulation immediately after the ischemic brain injury is neuroprotective. IEEE Trans Biomed Eng. 62, 2352-2357. https://doi.org/10.1109/TBME.2015.2427339.

Hakimova, H., Kim, S., Chu, K., Lee, S.K., Jeong, B., Jeon, D., 2015. Ultrasound stimulation inhibits recurrent seizures and improves behavioral outcome in an experimental model of mesial temporal lobe epilepsy. Epilepsy Behav. 49, 26-32. https://doi.org/10.1016/j.yebeh.2015.04.008.

Hameroff, S., Trakas, M., Duffield, C., Annabi, E., Gerace, M.B., Boyle, P., Lucas, A., Amos, Q., Buadu, A., Badal, J.J., 2013. Transcranial ultrasound (TUS) effects on mental states: A pilot study. Brain Stimul. 6, 409-415. https://doi.org/10.1016/j.brs.2012.05.002.

Hatanaka, K., Ito, K., Shindo, T., Kagaya, Y., Ogata, T., Eguchi, K., Kurosawa, R., Shimokawa, H., 2016. Molecular mechanisms of the angiogenic effects of low-energy shock wave therapy: roles of mechanotransduction. Am J Physiol Cell Physiol. 311, C378-C385. https://doi.org/10.1152/ajpcell.00152.2016.

Hooijmans, C.R., Rovers, M.M., de Vries, R.B., Leenaars, M., Ritskes-Hoitinga, M., Langendam, M.W., 2014. SYRCLE's risk of bias tool for animal studies. BMC Med Res Methodol. 14, 43. https://doi.org/10.1186/1471-2288-14-43.

Huang, X., Lin, Z., Wang, K., Liu, X., Zhou, W., Meng, L., Huang, J., Yuan, K., Niu, L., Zheng, H., 2019. Transcranial low-intensity pulsed ultrasound modulates structural and functional synaptic plasticity in rat hippocampus. IEEE Trans Ultrason Ferroelectr Freq Control. 66, 930-938. https://doi.org/10.1109/TUFFC.2019.2903896.

Huang, X., Niu, L., Meng, L., Lin, Z., Zhou, W., Liu, X., Huang, J., Abbott, D., Zheng, H., 2021. Transcranial low-intensity pulsed ultrasound stimulation induces neuronal autophagy. IEEE Trans Ultrason Ferroelectr Freq Control. 68, 46-53. https://doi.org/10.1109/TUFFC.2020.3028619.

Jerusalem, A., Al-Rekabi, Z., Chen, H., Ercole, A., Malboubi, M., Tamayo-Elizalde, M., Verhagen, L., Contera, S., 2019. Electrophysiological-mechanical coupling in the neuronal

membrane and its role in ultrasound neuromodulation and general anaesthesia. Acta Biomater. 97, 116-140. https://doi.org/10.1016/j.actbio.2019.07.041.

Kim, H., Park, M.A., Wang, S., Chiu, A., Fischer, K., Yoo, S.S., 2013. PET⁄CT imaging evidence of FUS-mediated (18)F-FDG uptake changes in rat brain. Med Phys. 40, 033501. https://doi.org/10.1118/1.4789916.

Kim, H., Park, M.Y., Lee, S.D., Lee, W., Chiu, A., Yoo, S.S., 2015. Suppression of EEG visual-evoked potentials in rats through neuromodulatory focused ultrasound. Neuroreport. 26, 211-215. https://doi.org/10.1097/WNR.0000000000000330.

King, R.L., Brown, J.R., Newsome, W.T., Pauly, K.B., 2013. Effective parameters for ultrasound-induced in vivo neurostimulation. Ultrasound Med Biol. 39, 312-331. https://doi.org/

Lee, W., Lee, S.D., Park, M.Y., Foley, L., Purcell-Estabrook, E., Kim, H., Fischer, K., Maeng, L.-S., Yoo, S.-S., 2016. Image-guided focused ultrasound-mediated regional brain stimulation in sheep. Ultrasound Med Biol. 42, 459-470. https://doi.org/10.1016/j.ultrasmedbio.2012.09.009.

Mariotto, S., Cavalieri, E., Amelio, E., Ciampa, A.R., de Prati, A.C., Marlinghaus, E., Russo, S., Suzuki, H., 2005. Extracorporeal shock waves: from lithotripsy to anti-inflammatory action by NO production. Nitric Oxide. 12, 89-96. https://doi.org/10.1016/j.niox.2004.12.005.

Matsuda, M., Kanno, H., Sugaya, T., Yamaya, S., Yahata, K., Handa, K., Shindo, T., Shimokawa, H., Ozawa, H., Itoi, E., 2020. Low-energy extracorporeal shock wave therapy promotes BDNF expression and improves functional recovery after spinal cord injury in rats. Exp Neurol. 328, 113251-113251. https://doi.org/10.1016/j.expneurol.2020.113251.

Matt, E., Kaindl, L., Tenk, S., Egger, A., Kolarova, T., Karahasanovic, N., Amini, A., Arslan, A., Saricicek, K., Weber, A., Beisteiner, R., 2022. First evidence of long-term effects of transcranial pulse stimulation (TPS) on the human brain. J Transl Med. 20, 26. https://doi.org/10.1186/s12967-021-03222-5.

Min, B.-K., Bystritsky, A., Jung, K.-I., Fischer, K., Zhang, Y., Maeng, L.-S., In Park, S., Chung, Y.-A., Jolesz, F.A., Yoo, S.-S., 2011a. Focused ultrasound-mediated suppression of chemically-induced acute epileptic EEG activity. BMC Neurosci. 12, 23. https://doi.org/10.1186/1471-2202-12-23.

Min, B.-K., Yang, P.S., Bohlke, M., Park, S., R.Vago, D., Maher, T.J., Yoo, S.-S., 2011b. Focused ultrasound modulates the level of cortical neurotransmitters: Potential as a new functional brain mapping technique. Int J Imaging Syst Technol. 21, 232-240. https://doi.org/10.1002/ima.20284.

Mohammadjavadi, M., Ash, R.T., Li, N., Gaur, P., Kubanek, J., Saenz, Y., Glover, G.H., Popelka, G.R., Norcia, A.M., Pauly, K.B., 2022. Transcranial ultrasound neuromodulation

of the thalamic visual pathway in a large animal model and the dose-response relationship with MR-ARFI. Sci Rep. 12, 19588. https://doi.org/10.1038/s41598-022-20554-4.

Niu, L., Guo, Y., Lin, Z., Shi, Z., Bian, T., Qi, L., Meng, L., Grace, A.A., Zheng, H., Yuan, T.F., 2020. Noninvasive ultrasound deep brain stimulation of nucleus accumbens induces behavioral avoidance. Sci China Life Sci. 63, 1328-1336. https://doi.org/10.1007/s11427-019-1616-6.

O'Brien, W.D., 2007. Ultrasound–biophysics mechanisms. Prog Biophys Mol Biol. 93, 212-255. https://doi.org/10.1016/j.pbiomolbio.2006.07.010.

Page, M.J., Moher, D., Bossuyt, P.M., Boutron, I., Hoffmann, T.C., Mulrow, C.D., Shamseer, L., Tetzlaff, J.M., Akl, E.A., Brennan, S.E., Chou, R., Glanville, J., Grimshaw, J.M., Hróbjartsson, A., Lalu, M.M., Li, T., Loder, E.W., Mayo-Wilson, E., McDonald, S., McGuinness, L.A., Stewart, L.A., Thomas, J., Tricco, A.C., Welch, V.A., Whiting, P., McKenzie, J.E., 2021. PRISMA 2020 explanation and elaboration: Updated guidance and exemplars for reporting systematic reviews. BMJ. 372, n160. https://doi.org/10.1136/bmj.n160.

Pang, N., Huang, X., Zhou, H., Xia, X., Liu, X., Wang, Y., Meng, W., Bian, T., Meng, L., Xu, L., Niu, L., 2021. Transcranial ultrasound stimulation of hypothalamus in aging mice. IEEE Trans Ultrason Ferroelectr Freq Control. 68, 29-37. https://doi.org/10.1109/TUFFC.2020.2968479.

Park, M., Hoang, G.M., Nguyen, T., Lee, E., Jung, H.J., Choe, Y., Lee, M.H., Hwang, J.Y., Kim, J.G., Kim, T., 2021. Effects of transcranial ultrasound stimulation pulsed at 40 Hz on Abeta plaques and brain rhythms in 5xFAD mice. Transl Neurodegener. 10, 48. https://doi.org/10.1186/s40035-021-00274-x.

Peng, Y., Zhao, Y., Huang, Y., Liu, X., Zhang, H., Zhao, Z., Cheng, Y., Liu, L., 2021. Neuroprotective effects of low-intensity transcranial ultrasound stimulation combined with Baicalin intervention on traumatic brain injury in animals. Brain Res Bull. 175, 246-253. https://doi.org/10.1016/j.brainresbull.2021.07.028.

Peryer G, G.S., Junqueira D, Vohra S, Loke YK., 2023. Adverse effects, in: Higgins JPT, T.J., Chandler J, Cumpston M, Li T, Page MJ, Welch VA (Ed.), Cochrane handbook for systematic reviews of interventions version 6.4 (updated August 2023). Cochrane, 2023. Available from www.training.cochrane.org/handbook.

Reznik, S.J., Sanguinetti, J.L., Tyler, W.J., Daft, C., Allen, J.J.B., 2020. A double-blind pilot study of transcranial ultrasound (TUS) as a five-day intervention: TUS mitigates worry among depressed participants. Neurol Psychiatry Brain Res. 37, 60-66. https://doi.org/10.1016/j.npbr.2020.06.004.

Riis, T.S., Webb, T.D., Kubanek, J., 2022. Acoustic properties across the human skull. Ultrasonics. 119, 106591. https://doi.org/10.1016/j.ultras.2021.106591.

Samuel, N., Zeng, K., Harmsen, I.E., Ding, M.Y.R., Darmani, G., Sarica, C., Santyr, B., Vetkas, A., Pancholi, A., Fomenko, A., Milano, V., Yamamoto, K., Saha, U., Wennberg, R., Rowland, N.C., Chen, R., Lozano, A.M., 2022. Multi-modal investigation of transcranial ultrasound-induced neuroplasticity of the human motor cortex. Brain Stimul. 15, 1337-1347. https://doi.org/10.1016/j.brs.2022.10.001.

Sanguinetti, J.L., Hameroff, S., Smith, E.E., Sato, T., Daft, C.M.W., Tyler, W.J., Allen, J.J.B., 2020. Transcranial focused ultrasound to the right prefrontal cortex improves mood and alters functional connectivity in humans. Front Hum Neurosci. 14, 52. https://doi.org/10.3389/fnhum.2020.00052.

Sarica, C., Nankoo, J.F., Fomenko, A., Grippe, T.C., Yamamoto, K., Samuel, N., Milano, V., Vetkas, A., Darmani, G., Cizmeci, M.N., Lozano, A.M., Chen, R., 2022. Human studies of transcranial ultrasound neuromodulation: A systematic review of effectiveness and safety. Brain Stimul. 15, 737-746. https://doi.org/10.1016/j.brs.2022.05.002.

Sharabi, S., Daniels, D., Last, D., Guez, D., Zivli, Z., Castel, D., Levy, Y., Volovick, A., Grinfeld, J., Rachmilevich, I., Amar, T., Mardor, Y., Harnof, S., 2019. Non-thermal focused ultrasound induced reversible reduction of essential tremor in a rat model. Brain Stimul. 12, 1-8. https://doi.org/10.1016/j.brs.2018.08.014.

Shamli Oghli, Y., Grippe, T., Arora, T., Hoque, T., Darmani, G., Chen, R., 2023. Mechanisms of theta burst transcranial ultrasound induced plasticity in the human motor cortex. Brain Stimul. 16, 1135-1143. https://doi.org/10.1016/j.brs.2023.07.056.

Song, W.S., Sung, C.Y., Ke, C.H., Yang, F.Y., 2022. Anti-inflammatory and neuroprotective effects of transcranial ultrasound stimulation on Parkinson's disease. Ultrasound Med Biol. 48, 265-274. https://doi.org/10.1016/j.ultrasmedbio.2021.10.001.

Sterne, J.A.C., Savović, J., Page, M.J., Elbers, R.G., Blencowe, N.S., Boutron, I., Cates, C.J., Cheng, H.-Y., Corbett, M.S., Eldridge, S.M., Emberson, J.R., Hernán, M.A., Hopewell, S., Hróbjartsson, A., Junqueira, D.R., Jüni, P., Kirkham, J.J., Lasserson, T., Li, T., McAleenan, A., Reeves, B.C., Shepperd, S., Shrier, I., Stewart, L.A., Tilling, K., White, I.R., Whiting, P.F., Higgins, J.P.T., 2019. RoB 2: a revised tool for assessing risk of bias in randomised trials. BMJ. 366, l4898. https://doi.org/10.1136/bmj.l4898.

Tsai, C.W., Tsai, S.J., Pan, Y.J., Lin, H.M., Pan, T.Y., Yang, F.Y., 2022. Transcranial ultrasound stimulation reverses behavior changes and the expression of calcium-binding protein in a rodent model of schizophrenia. Neurotherapeutics. 19, 649-659. https://doi.org/10.1007/s13311-022-01195-x.

Tsui, P.-H., Wang, S.-H., Huang, C.-C., 2005. In vitro effects of ultrasound with different energies on the conduction properties of neural tissue. Ultrasonics. 43, 560-565. https://doi.org/10.1016/j.ultras.2004.12.003.

Tufail, Y., Matyushov, A., Baldwin, N., Tauchmann, M.L., Georges, J., Yoshihiro, A., Tillery, S.I.H., Tyler, W.J., 2010. Transcranial pulsed ultrasound stimulates intact brain circuits. Neuron. 66, 681-694. https://doi.org/10.1016/j.neuron.2010.05.008.

Tyler, W.J., 2011. Noninvasive neuromodulation with ultrasound? A continuum mechanics Hypothesis. The Neuroscientist. 17, 25-36. https://doi.org/10.1177/1073858409348066.

Tyler, W.J., Tufail, Y., Finsterwald, M., Tauchmann, M.L., Olson, E.J., Majestic, C., 2008. Remote excitation of neuronal circuits using low-intensity, low-frequency ultrasound. PloS One. 3, e3511. https://doi.org/10.1371/journal.pone.0003511.

Wang, J., Li, G., Deng, L., Mamtilahun, M., Jiang, L., Qiu, W., Zheng, H., Sun, J., Xie, Q., Yang, G.Y., 2021a. Transcranial focused ultrasound stimulation improves neurorehabilitation after middle cerebral artery occlusion in mice. Aging Dis. 12, 50-60. https://doi.org/10.14336/AD.2020.0623.

Wang, M., Wang, T., Ji, H., Yan, J., Wang, X., Zhang, X., Li, X., Yuan, Y., 2023a. Modulation effect of non-invasive transcranial ultrasound stimulation in an ADHD rat model. J Neural Eng. 20, 16003. https://doi.org/10.1088/1741-2552/acb014.

Wang, P., Zhang, J., Yu, J., Smith, C., Feng, W., 2019. Brain Modulatory effects by low-intensity transcranial ultrasound stimulation (TUS): A systematic review on both animal and human studies. Front Neurosci. 13, 696. https://doi.org/10.3389/fnins.2019.00696.

Wang, T., Wang, X., Tian, Y., Gang, W., Li, X., Yan, J., Yuan, Y., 2023b. Modulation effect of low-intensity transcranial ultrasound stimulation on REM and NREM sleep. Cereb Cortex. 33, 5238-5250. https://doi.org/10.1093/cercor/bhac413.

Wang, X., Yan, J., Wang, Z., Li, X., Yuan, Y., 2020a. Neuromodulation effects of ultrasound stimulation under different parameters on mouse motor cortex. IEEE Trans Biomed Eng. 67, 291-297. https://doi.org/10.1109/TBME.2019.2912840.

Wang, Y., Niu, L., Meng, W., Lin, Z., Zou, J., Bian, T., Huang, X., Zhou, H., Meng, L., Xie, P., Zheng, H., 2021b. Ultrasound stimulation of periaqueductal gray induces defensive behaviors. IEEE Trans Ultrason Ferroelectr Freq Control. 68, 38-45. https://doi.org/10.1109/TUFFC.2020.2975001.

Wang, Z., Yan, J., Wang, X., Yuan, Y., Li, X., 2020b. Transcranial ultrasound stimulation directly influences the cortical excitability of the motor cortex in parkinsonian mice. Mov Disord. 35, 693-698. https://doi.org/10.1002/mds.27952.

Xu, T., Lu, X., Peng, D., Wang, G., Chen, C., Liu, W., Wu, W., Mason, T.J., 2020. Ultrasonic stimulation of the brain to enhance the release of dopamine - A potential novel treatment for Parkinson's disease. Ultrason Sonochem. 63, 104955. https://doi.org/10.1016/j.ultsonch.2019.104955.

Yahata, K., Kanno, H., Ozawa, H., Yamaya, S., Tateda, S., Ito, K., Shimokawa, H., Itoi, E., 2016. Low-energy extracorporeal shock wave therapy for promotion of vascular endothelial growth factor expression and angiogenesis and improvement of locomotor and

sensory functions after spinal cord injury. J Neurosurg Spine. 25, 745-755. https://doi.org/10.3171/2016.4.Spine15923.

Yang, F.Y., Huang, L.H., Wu, M.T., Pan, Z.Y., 2022. Ultrasound neuromodulation reduces demyelination in a rat model of multiple sclerosis. Int J Mol Sci. 23, 10034. https://doi.org/10.3390/ijms231710034.

Yang, P.S., Kim, H., Lee, W., Bohlke, M., Park, S., Maher, T.J., Yoo, S.S., 2012. Transcranial focused ultrasound to the thalamus is associated with reduced extracellular GABA levels in rats. Neuropsychobiology. 65, 153-160. https://doi.org/10.1159/000336001.

Yao, L., Chen, R., Ji, H., Wang, X., Zhang, X., Yuan, Y., 2022. Preventive and therapeutic effects of low-intensity ultrasound stimulation on migraine in rats. IEEE Trans Neural Syst Rehabil Eng. 30, 2332-2340. https://doi.org/10.1109/TNSRE.2022.3199813.

Yi, S.S., Zou, J.J., Meng, L., Chen, H.M., Hong, Z.Q., Liu, X.F., Farooq, U., Chen, M.X., Lin, Z.R., Zhou, W., Ao, L.J., Hu, X.Q., Niu, L.L., 2022. Ultrasound stimulation of prefrontal cortex improves lipopolysaccharide-induced depressive-like behaviors in mice. Front Psychiatry. 13, 864481. https://doi.org/10.3389/fpsyt.2022.864481.

Yoo, S.S., Kim, H., Min, B.K., Franck, E., Park, S., 2011. Transcranial focused ultrasound to the thalamus alters anesthesia time in rats. Neuroreport. 22, 783-787. https://doi.org/10.1097/WNR.0b013e32834b2957.

Yoo, S.S., Yoon, K., Croce, P., Cammalleri, A., Margolin, R.W., Lee, W., 2018. Focused ultrasound brain stimulation to anesthetized rats induces long-term changes in somatosensory evoked potentials. Int J Imaging Syst Technol. 28, 106-112. https://doi.org/10.1002/ima.22262.

Yuan, Y., Zhao, Z., Wang, Z., Wang, X., Yan, J., Li, X., 2020. The Effect of low-intensity transcranial ultrasound stimulation on behavior in a mouse model of Parkinson's disease induced by MPTP. IEEE Trans Neural Syst Rehabil Eng. 28, 1017-1021. https://doi.org/10.1109/TNSRE.2020.2978865.

Zeng, K., Darmani, G., Fomenko, A., Xia, X., Tran, S., Nankoo, J.F., Shamli Oghli, Y., Wang, Y., Lozano, A.M., Chen, R., 2022. Induction of human motor cortex plasticity by theta burst transcranial ultrasound stimulation. Ann Neurol. 91, 238-252. https://doi.org/10.1002/ana.26294.

Zhang, D., Li, H., Sun, J., Hu, W., Jin, W., Li, S., Tong, S., 2019. Antidepressant-like effect of low-intensity transcranial ultrasound stimulation. IEEE Trans Biomed Eng. 66, 411-420. https://doi.org/10.1109/TBME.2018.2845689.

Zhang, M.F., Chen, W.Z., Huang, F.B., Peng, Z.Y., Quan, Y.C., Tang, Z.M., 2022a. Low-intensity transcranial ultrasound stimulation facilitates hand motor function and cortical excitability: A crossover, randomized, double blind study. Front Neurol. 13, 926027. https://doi.org/10.3389/fneur.2022.926027.

Zhang, T., Wang, Z., Liang, H., Wu, Z., Li, J., Ou-Yang, J., Yang, X., Peng, Y.B., Zhu, B., 2022b. Transcranial focused ultrasound stimulation of periaqueductal gray for analgesia. IEEE Trans Biomed Eng. 69, 3155-3162. https://doi.org/10.1109/TBME.2022.3162073.

Zhao, Z., Ji, H., Zhang, C., Pei, J., Zhang, X., Yuan, Y., 2023. Modulation effects of low-intensity transcranial ultrasound stimulation on the neuronal firing activity and synaptic plasticity of mice. Neuroimage. 270, 119952. https://doi.org/10.1016/j.neuroimage.2023.119952.

Zhou, H., Meng, L., Xia, X., Lin, Z., Zhou, W., Pang, N., Bian, T., Yuan, T., Niu, L., Zheng, H., 2021. Transcranial ultrasound stimulation suppresses neuroinflammation in a chronic mouse model of Parkinson's disease. IEEE Trans Biomed Eng. 68, 3375-3387. https://doi.org/10.1109/TBME.2021.3071807.

Zhou, H., Niu, L., Xia, X., Lin, Z., Liu, X., Su, M., Guo, R., Meng, L., Zheng, H., 2019. Wearable ultrasound improves motor function in an MPTP mouse model of Parkinson's disease. IEEE Trans Biomed Eng. 66, 3006-3013. https://doi.org/10.1109/TBME.2019.2899631.

Zhu, Y., He, J., Wu, C., Wu, J., Cheng, Z., Chen, Y., Yuan, M., Zeng, L., Ji, X., 2023. Transcranial ultrasound stimulation relieves depression in mice with chronic restraint stress. J Neural Eng. 20, 36011. https://doi.org/10.1088/1741-2552/ac8bfd

Chapter 3 Transcranial pulse stimulation for major depressive disorder: A randomized, double-blind, sham-controlled clinical trial (Study 2)

3.1 Introduction

Major depressive disorder (MDD) is a severe mental disorder with a lifetime prevalence of 2 to 21% (Gutierrez-Rojas et al., 2020) and is projected to become the leading cause of global disease burden by 2030 (Mathers, 2008). Non-invasive brain stimulation (NIBS), such as transcranial magnetic stimulation (TMS) and transcranial direct current stimulation (tDCS), has emerged as a promising adjunct therapy for MDD due to its noninvasiveness and clinical efficacy (Fregni et al., 2021; Lefaucheur et al., 2020).

Transcranial pulse stimulation (TPS) (NEUROLITH, Storz Medical AG, Tagerwilen, Switzerland) is a novel CE-approved NIBS device that employs shock waves to modulate brain function (Truong et al., 2022). Developed from focused low-energy extracorporeal shock wave therapy (Lohse-Busch et al., 2014; Lohse-Busch, Reime, and Falland, 2014), TPS delivers single high-pressure, short-duration (3 μs) sonication pulses characterized by a large positive peak amplitude, followed by a small negative-amplitude pulse, minimizing risks of brain heating and secondary stimulation maxima (Sarica et al., 2022). The pulses have energy flux densities (EFD) of 0.01- 0.25 mJ/ mm^2, pulse frequencies of 1 - 8 Hz, and a maximum peak pressure of 25 MPa, yielding a maximum

spatial-peak-temporal-average intensity ($I_{SPTA-max}$) of 100 mW/cm^2, a maximum spatial-peak-pulse-average intensity ($I_{SPPA-max}$) of 111 W/cm^2, a mechanical index (MI) of 10.95, and a thermal index (TI) < 0.7 (Matt et al., 2022). The current TPS system restricts the maximum EFD for human application to 1 mJ/mm^2 per second (EFD_{max} = 0.2 mJ/ mm^2 at 5 Hz; or EFD_{max} = 0.25 mJ/ mm^2 at 4 Hz), well below preclinical safety thresholds (Beisteiner et al., 2020).

Although TPS was first investigated for Alzheimer's disease (AD), where it demonstrated clinical and neural efficacy (Beisteiner et al., 2020; Matt et al., 2025; Radjenovic et al., 2025; Beisteiner and Matt, 2025; Karakatsani et al., 2025), the discovery of an antidepressive effect of TPS in AD patients (Matt, Dorl, and Beisteiner, 2022) paved the way for its research in depression. Recently, an open-label pilot randomized controlled trial (RCT) demonstrated the antidepressive effect of TPS in adults with depressive symptoms (Cheung et al., 2023). Although promising, these findings require cautious interpretation due to potential biases from placebo effects, unblinded assessment, participant heterogeneity, imprecise targeting, and small sample size.

Here, we conducted the first randomized, double-blind, sham-controlled trial to assess the antidepressive efficacy of lDLPFC-TPS in MDD patients and to explore its neuromodulatory effect using resting-state functional magnetic resonance imaging (rs-fMRI).

3.2 Methods

3.2.1 Study overview

Study 2 is a prospective, randomized, double-blind (participants, therapists, and assessors blinded), two-arm parallel, sham-controlled trial to investigate the antidepressive and neural effects of 4-week active TPS versus sham TPS in patients with MDD. The study was conducted at The Hong Kong Polytechnic University from June 2023 to October 2025. The study protocol was approved by the Institutional Review Board of The Hong Kong Polytechnic University (Reference No: HSEARS20220816001-02) and was registered on ClinicalTrial.gov (Identifier: NCT05551585). The study was unblinded once the posttreatment assessment and magnetic resonance imaging (MRI) measurement were completed at Week 4. Participants in the sham group were subsequently offered 4 weeks of active TPS. An open-label follow-up assessment was scheduled for 3 months after the active treatment in both groups. This trial followed the Consolidated Standards of Reporting Trials reporting guideline (Hopewell et al., 2025). The study procedure is shown in Figure 6.

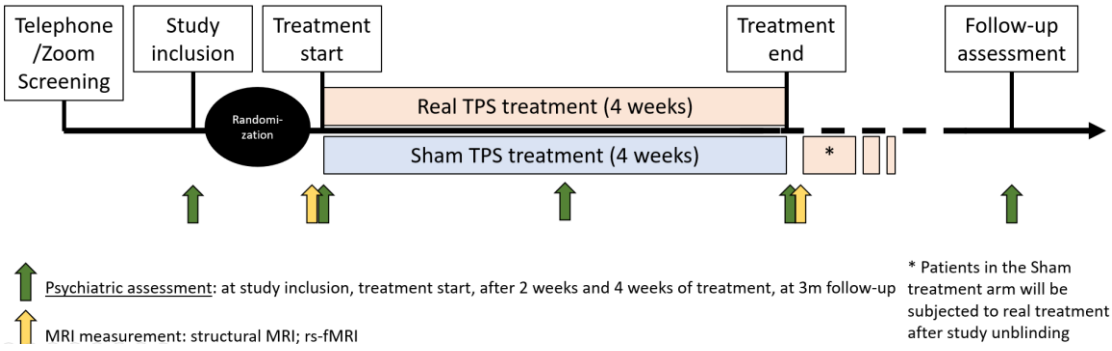

Figure 6. Study procedure of Study 2

3.2.2 Sample size

To our knowledge, no randomized, double-blind, sham-controlled TPS study in MDD has been conducted so far. With an assumption of a medium to large effect size (0.65), a power of 0.85, and an error probability of 0.05, the total sample size was calculated to be 70. Considering an estimated 10% dropout rate, around 78 participants would be required. Finally, a total sample size of 80 was determined, with a 1:1 allocation ratio between the two groups.

3.2.3 Inclusion and exclusion criteria

We recruited MDD patients with the following key inclusion criteria: (1) age 18 to 65; (2) a clinical diagnosis of MDD according to psychiatrist visit records or a clinical interview using the Chinese version of the Mini International Neuropsychiatric Interview (MINI) (司天梅 et al., 2009); (3) a baseline Hamilton depression scale-17 (HAMD-17) score ≥14; and (4) treatment naivety or stable (≥ 4 weeks) psychopharmacological treatment. Key exclusion criteria were: (1) any coagulation disorders, neurological disorders, or severe psychiatric comorbidities, including addiction, bipolar disorder, and schizophrenia; (2) pregnancy; (3) common NIBS and MRI exclusion criteria, such as a history of brain surgery, cardiac pacemaker, deep brain stimulation, and intracranial metallic particles. The study was performed following the Declaration of Helsinki (Gandevia and Tovell, 1964), including current revisions. All participants were asked for written informed consent before inclusion.

3.2.4 Randomization and allocation concealment

Participants were randomized 1:1 using a computer-based algorithm. Each participant was assigned a unique randomization identification number, determining their treatment allocation. Sealed envelopes containing the treatment allocation codes were securely held by an independent researcher throughout the study period.

3.2.5 TPS procedure and blinding

TPS treatment consisted of three sessions per week for four weeks. In each session, 1000 pulses were delivered to the lDLPFC with a pulse frequency of 4 Hz and EFD of 0.2 - 0.25 mJ/mm^2 (0.2 mJ/mm^2 during the first 2 weeks; 0.25 mJ/mm^2 during the subsequent 2 weeks). The lDLPFC was identified by transforming Montreal Neurological Institute (MNI) coordinates (x = -38, y = +44, z = +26 mm) (Blumberger et al., 2018; Fox et al., 2012) to the individual T1 space. Specifically, a 15-mm radius sphere (the smallest region that can be set in the TPS device) was created centered at x = -38, y = +44, z = +26 mm in MNI space and then transformed into individual T1-weighted space. For each voxel within the transformed sphere, the adjusted target voxels were calculated based on the 30-mm depth (the distance between the pulse location and the scalp is 30 mm by default on the TPS display). Finally, the center of mass of all these adjusted target voxels was used as the center to create a 15-mm radius sphere on the T1-weighted image. A 6.6 mm stand-off device was used to ensure sufficient penetration depth of the focus zone (43.4 mm). Precise targeting was achieved through MR-based near-infrared real-time navigation and the predefined target of a 15-mm-radius sphere. Plenty of

bubble-free ultrasound gel was applied to cover the scalp at the stimulation area to avoid acoustic impedance borders. In addition, the handpiece was maintained perpendicular to the scalp surface, and slow manual movement of the handpiece was applied to ensure adequate coupling and even energy distribution within the target sphere. The sham stimulation was performed using a sham stand-off device, which was placed in the handpiece before treatment by an independent researcher responsible for holding the sealed allocation envelopes. These procedures preserved blinding of participants and investigators. After 4-week treatment, blinding integrity was assessed by asking participants to report their group allocation guesses and their confidence levels (range: 0-10; 0: no confidence; 10: full confidence).

Adverse events were assessed by using a predefined checklist after each treatment session. Participants were additionally instructed to report any unlisted symptoms.

3.2.6 Clinical outcome measures

The primary outcome was change in the Montgomery-Åsberg Depression Rating Scale (MADRS) score at posttreatment (Week 4). Secondary outcomes included: (1) changes in HAMD-17 and patient Health Questionnaire-9 (PHQ-9) scores at posttreatment; (2) response (a reduction of ≥ 50% MADRS score) and remission (MADRS score ≤ 10) rates at posttreatment (Cole et al., 2022); and (3) changes in clinical outcomes at 3-month follow-up (3 months after the active treatment). The

exploratory outcome was the changes in MADRS score at Week 2 (midpoint).

3.2.7 Neuroimaging measures

The neuroimaging outcome was changes in lDLPFC-seeded voxel-wise resting-state functional connectivity (rsFC) at posttreatment.

MRI measurements were performed using PolyU's Siemens 3T MAGNETOM Prisma system. High-resolution sMRI was performed using a magnetization-prepared rapid gradient echo (MPRAGE, T1-weighted) sequence with the following parameters: TR/TE = 2300/2.98 ms, inversion time = 900 ms, flip angle = 9°, 208 slices, acquisition matrix = 240x256, slice thickness = 1 mm, voxel size = 1 x 1x 1 mm. Rs-fMRI was performed with a 64-channel head coil, using a single-shot gradient-recalled echoplanar imaging sequence with the following parameters: TR/TE = 607/32 ms, matrix size = 88 x 88, field-of-view = 220 x 220 mm, voxel size = 2.5 x 2.5 x 2.5 mm, 64 slices, slice thickness = 2.5 mm, interleaved series. A resting-state scan of 8 minutes was performed, during which subjects were instructed to relax with their eyes open and gaze at a cross displayed on the screen in front of them, allowing their mind to wander without focusing on anything specific.

3.2.8 Statistical analysis

All participants were included in an intention-to-treat (ITT) analysis of clinical outcomes during the RCT phase. A linear mixed-effects model (LMM) with repeated measures was used to examine the changes in

clinical scores. The model was estimated using Restricted Maximum Likelihood (REML). Group (active vs. sham), Time (baseline vs. posttreatment), and Group × Time interaction were included as fixed effects. To account for within-subject correlations, a random intercept for each participant was specified using a variance components covariance structure. The residual covariance structure across time points was specified as diagonal. The between-group effect size (Cohen's d) for the difference in change from baseline to posttreatment was calculated by comparing the estimated mean change in the active group to the estimated mean change in the sham group. Specifically, the difference between the active group's mean change and the sham group's mean change (the Group x Time interaction estimate from the LMM) was divided by their estimated standard deviation of the change scores. Chi-square tests were used to compare between-group differences in the response and remission rates. Participants who dropped out during the treatment period were viewed as non-responders. Considering a high dropout rate and the ambiguous nature of the missing data, the 3-month follow-up analysis followed a per-protocol approach. Changes in clinical outcomes from baseline to 3-month posttreatment were evaluated using a two-tailed paired t-test, with statistical significance set at $p < 0.05$.

Per-protocol rs-fMRI analyses were conducted using Statistical Parametric Mapping 12 (SPM12) and RESTplus version 1.28 (a toolbox based on SPM12 [23]) in MATLAB (2023a), encompassing preprocessing, postprocessing, and group-level statistical analyses. The default preprocessing pipeline comprised slice-timing correction,

realignment, spatial normalization, spatial smoothing (6 mm FWHM kernel), detrending, nuisance covariates regression (removal of motion confounds, white matter, and cerebrospinal fluid signal), and denoising (a band-pass filter: 0.01-0.08 Hz). lDLPFC-seeded voxel-wise rsFC was calculated as the Pearson correlation coefficient between the lDLPFC and whole-brain voxels. Group-level statistical analysis of two-way repeated ANOVA was conducted to test the interaction between Group (active vs. sham) and Time (posttreatment vs. baseline) in rsFC changes. For clusters showing a significant interaction effect, post-hoc tests were performed on extracted average rsFC values (z-scores) to assess within- and between-group differences using SPSS. Correlation analysis was conducted to investigate the association between changes in average rsFC values (z-scores) and improvements in clinical scores.

3.3 Study results

3.3.1 Participant characteristics

Of 349 screened subjects, 89 were eligible and recruited. Two had incidental MRI findings at baseline, and 7 declined participation before the first treatment session and were thus excluded from the study. In total, 80 MDD patients were randomized into two treatment groups (n = 40 active/ n = 40 sham), with 74 completing the study and 6 withdrawing (n = 2 active/n = 4 sham). Withdrawal reasons included: adverse events (n = 2 sham), unwillingness to leave home (n = 1 sham), physical health issues (n = 1 active), and lost contact (n = 1 active/n = 1 sham) (see Figure 7 for the CONSORT diagram). Seventy-two participants completed

posttreatment MRI measurements (n = 36 active/n = 36 sham). Following exclusion of six baseline scans (n = 4 active/ n = 2 sham) and 3 endpoint scans (n = 1 active/ n = 2 sham) due to problematic alignment or normalization during preprocessing, the final fMRI analysis included complete data (including both baseline and endpoint fMRI data) from 69 participants (n = 33 active/ n = 33 sham). Among 74 completers, 66% adhered to the study protocol (active: 23/38 vs. sham: 25/36; $\chi^2 = 0.422$, p = 0.645) (See details of treatment compliance in the Appendices). Demographic and clinical characteristics of participants are presented in Table 5.

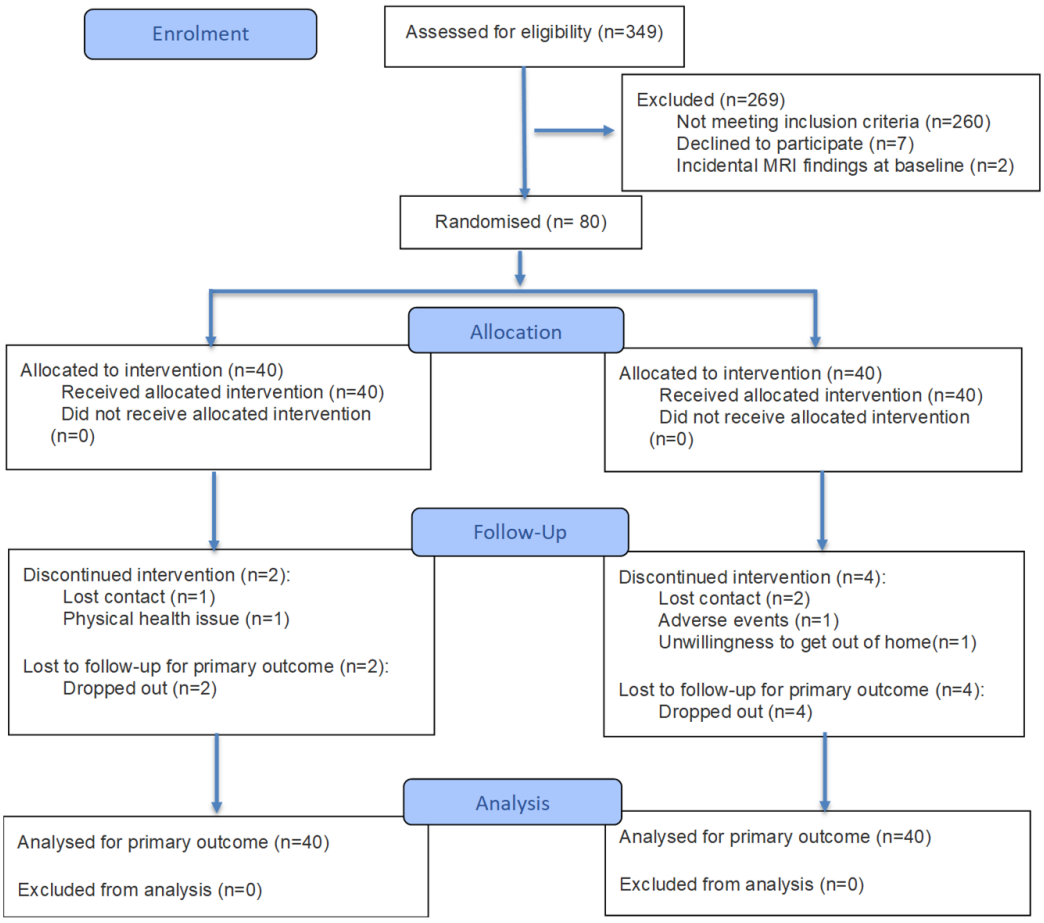

Figure 7. CONSORT flow diagram for Study 2

Table 5. Demographic and clinical characteristics of participants in Study 2

Variable	**Active TPS (n=40)**		**Sham TPS (n=40)**		
	N	%	N	%	p value
Male	17	42.5	10	25	0.098
With an MDD diagnosis	37	92.5	35	87.5	0.456
On regular antidepressants	28	70	25	62.5	0.478
	Mean	SD	Mean	SD	
Age (years)	34.3	10.94	36.8	12.41	0.174
Years of education	15.9	2.87	15.1	3.66	0.136
Baseline HAMD-17 score	19.55	4.41	19.98	4.73	0.339
Baseline MADRS score	27.35	7.07	27.85	7.81	0.382
Baseline PHQ-9 score	15.85	4.55	16.35	4.89	0.319

3.3.2 Clinical outcomes

3.3.2.1 Primary outcomes

LMM analysis for MADRS scores yielded a significant Group (active vs. sham) x Time (baseline vs. posttreatment) interaction effect (difference = -4.19, 95% CI = -8.33 to -0.04, p = 0.048, Cohen's d = 0.45) and a significant main effect of Time (difference = 10.00, 95% CI = 7.93 to 12.08, p < 0.001), with no significant main effect of Group (difference = -2.59, 95% CI = -5.85 to 0.67, p = 0.117) (Table 6). Post-hoc pairwise analyses indicated that, compared to the sham group, the active group demonstrated a greater reduction in MADRS score over the 4-week treatment period, with a mean reduction of 12.10 compared with 7.91, respectively (Table 6). Moreover, the posttreatment MADRS score was significantly lower in the active group compared to the sham group (difference = -4.69, 95% CI = -9.03 to -0.35, p = 0.035 (Table 6). Exploratory analyses showed that the active group demonstrated a significant continuous decrease in MADRS scores over the 4-week treatment course, while the sham group showed improvement from baseline at Week 2, but not from Week 2 to Week 4 (Appendices, Table S6). Changes in MADRS score over time in both groups are presented in Figure 8.

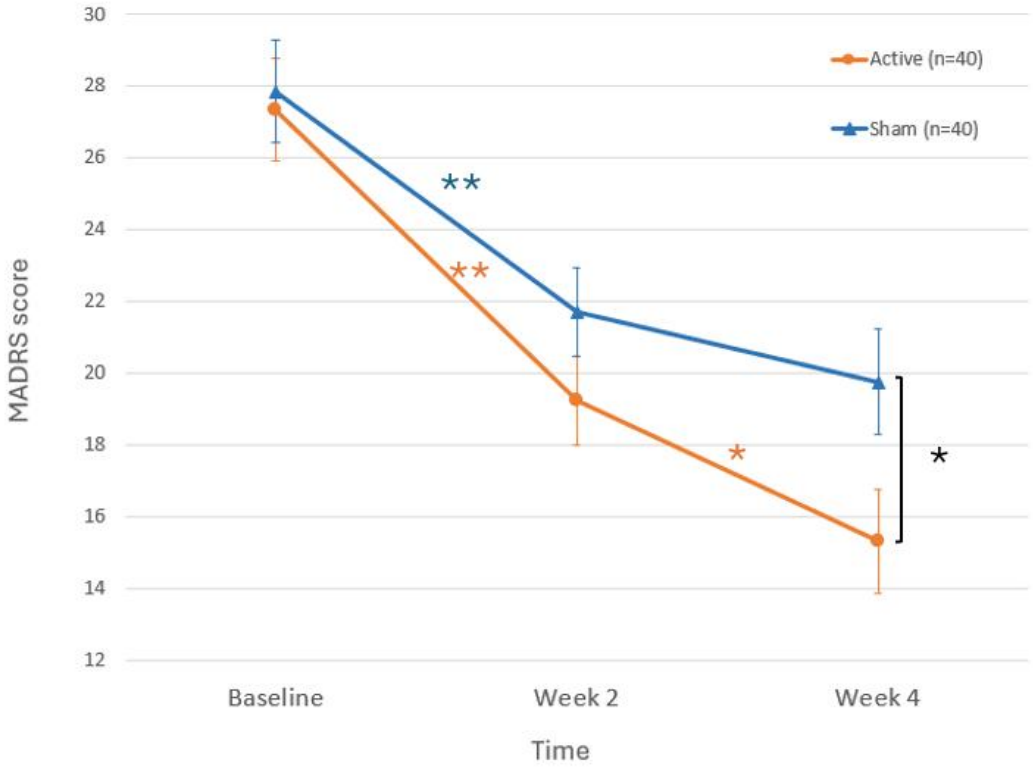

Figure 8. Montgomery-Åsberg Depression Rating Scale (MADRS) score changes in the active and sham groups. Error bars represent standard errors. *: $p < 0.05$, **: $p < 0.001$ (Bonferroni corrected p-value).

3.3.2.2 Secondary outcomes

3.3.2.2.1 Changes in HAMD-17 and PHQ-9 scores

A significant main effect of Time emerged for both HAMD-17 (difference = 6.40, 95% CI = 5.30 to 7.71, $p < 0.001$) and PHQ-9 (difference = 4.86, 95% CI = 3.58 to 6.15, $p < 0.001$) scores, with no significant Group main effect or Group x Time interaction (Table 6). Post-hoc analyses revealed that both groups demonstrated significant reductions in HAMD-17 and PHQ-9 scores during the 4-week treatment (Table 6). Changes in HAMD-17 and PHQ-9 scores over time in both groups are shown in Figures 9-10.

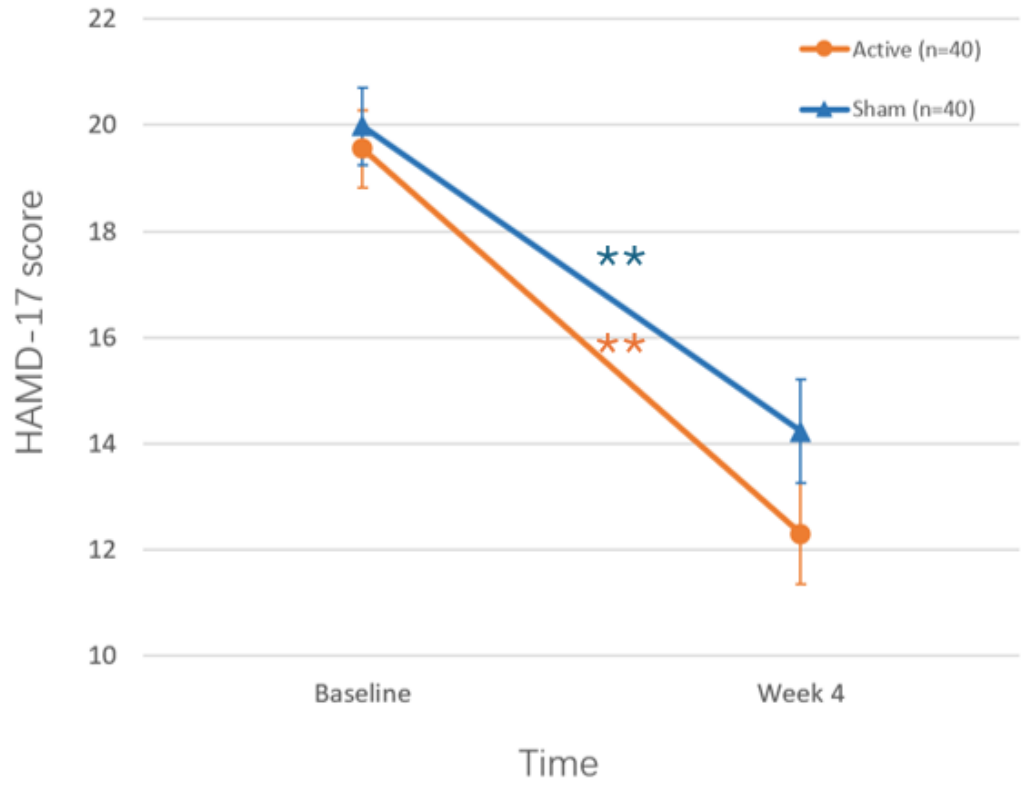

Figure 9. Hamilton depression scale-17 (HAMD-17) score changes in the active and sham groups. Error bars represent standard errors. **: $p < 0.001$

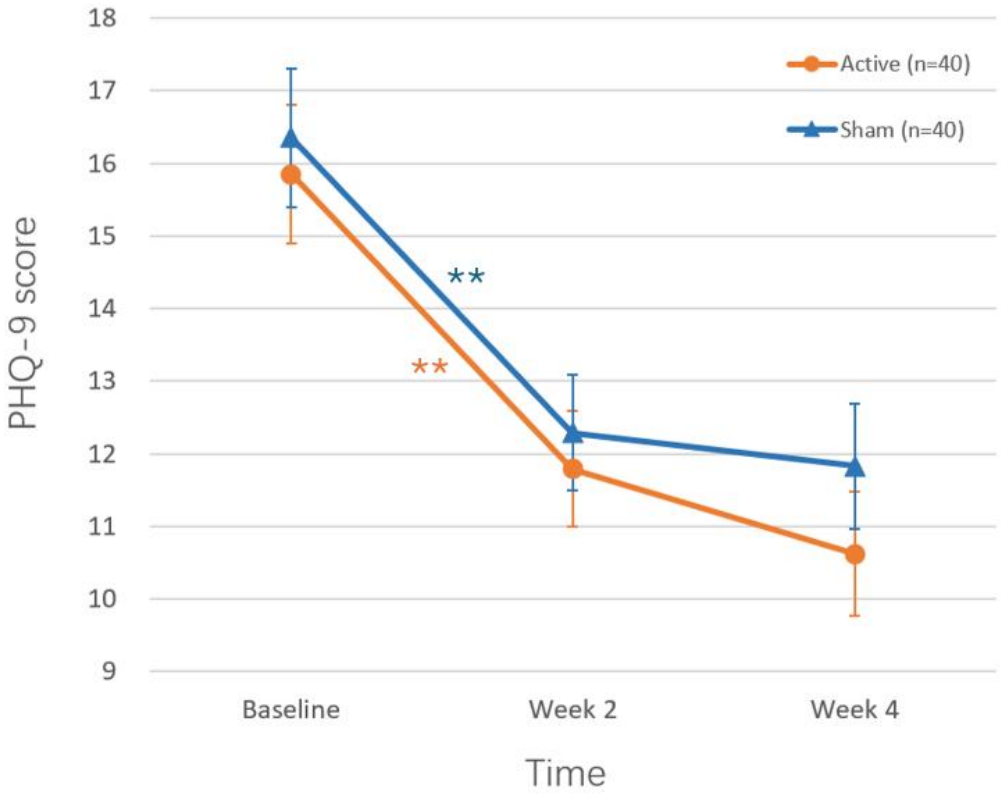

Figure 10. Patient health questionnaire-9 (PHQ-9) score changes in the active and sham groups. Error bars represent standard errors. **: $p < 0.001$ (Bonferroni corrected p-value)

Table 6. Linear mixed model analysis of change from baseline to post-treatment by Group interaction and the post-hoc analyses in Study 2

	Mean (SE)		**Time-by-Group Interaction**		**Active vs. sham**		**Baseline vs. posttreatment**
	Active TPS	**Sham TPS**	**Mean difference (95% CI)**	**P value**	**Mean difference (95% CI)**	**P value**	**Mean difference (95% CI); p value**
Primary outcome							
MADRS score							
Baseline	27.35 (1.18)	27.85 (1.18)	-4.19 (-8.33, -0.04)	0.048	-0.50 (-3.82, 2.82)	0.765	Active: 12.10 (9.20, 15.00); p < 0.001;
Posttreatment	15.25 (1.52)	19.93 (1.56)			-4.69 (-9.03, -0.36)	0.035	Sham: 7.91 (4.95, 10.88); p < 0.001
Secondary outcome							
HAMD-17 score							
Baseline	19.55 (0.72)	20.0 (0.72)	-1.51 (-3.93, 0.91)	0.217	-0.43 (-2.47, 1.61)	0.679	Active: 7.25 (5.57, 8.94); p < 0.001;
Posttreatment	12.30 (0.95)	14.23 (0.97)			-1.94 (-4.65, 0.77)	0.159	Sham: 5.74 (4.01, 7.47); p < 0.001
PHQ-9 score							
Baseline	15.85 (0.75)	16.35 (0.75)	-0.859 (-3.44, 1.72)	0.509	-0.50 (-2.60, 1.60)	0.637	Active: 5.30 (3.50, 7.10); p < 0.001;

Posttreatment	10.56 (0.89)	11.92 (0.91)	-1.36 (-3.90, 1.18)	0.289	Sham: 4.43 (2.59, 6.28); p < 0.001

TPS: transcranial pulse stimulation; MADRS: Montgomery-Åsberg Depression Rating Scale; HAMD-17: Hamilton Depression Rating Scale-17; PHQ-9: Patient Health Questionnaire-9

3.3.2.2.2 Response and remission rates

The response and remission rates at posttreatment were significantly higher in the active group compared to the sham group (response rate: active vs. sham: 52.5% (21/40) vs. 25% (10/40), $\chi^2 = 6.38$, $p = 0.012$; remission rate: active vs. sham: 40.0% (16/40) vs. 17.5% (7/40), $\chi^2 = 4.90$, $p = 0.026$).

3.3.2.3 Safety

Mild to moderate adverse events were significantly more frequent in the active TPS group (37/40) than the sham group (22/40) ($\chi^2 = 14.53$, $p < 0.001$). The most common events were tingling and pain, with all adverse events resolving spontaneously within 24 hours after treatment without medication. Complete adverse event data are shown in Table 7.

Table 7. Adverse events occurred in Study 2

	Number of participants reporting each adverse event during stimulation (%)	
	Active TPS (n=40)	Sham TPS (n=40)
Tingling[+]	23 (57.5%)	7 (17.5%)
Pain[+]	19 (47.5%)	4 (10%)
Numbness[+]	5 (12.5%)	NA
Striking sensation[+]	3 (7.5%)	NA
Dizziness	3 (7.5%)	3 (7.5%)
Nausea	3 (7.5%)	1 (2.5%)
Sleepiness	2 (5%)	6 (15%)
Neck pain	2 (5%)	1 (2.5%)

Pressure+/vibration+	1 (2.5%)	1 (2.5%)
Heaviness in the head	1 (2.5%)	NA
Tightness+	1 (2.5%)	NA
Blurred eyes	1 (2.5%)	NA
Dry eyes	1 (2.5%)	NA
Headache	1 (2.5%)	4 (10%)
Numbness in the right limbs	1 (2.5%)	NA
Sweating	1 (2.5%)	NA
Rapid heart rate	1 (2.5%)	NA
Panic attack	1 (2.5%)	NA
Warmth+	NA	4 (10%)
Sourness+	NA	1 (2.5%)

	Number of participants reporting each adverse event after stimulation (%)	
	Active TPS (n=40)	Sham TPS (n=40)
Headache	6 (15%)	3 (7.5%)
Pain+	6 (15%)	1 (2.5%)
Sleepiness	6 (15%)	4 (10%)
Dizziness	4 (10%)	4 (10%)
Numbness+	4 (10%)	NA
Nausea	2 (5%)	1 (2.5%)
Striking sensation+	1 (2.5%)	NA
Tightness+	1 (2.5%)	2 (5%)
Fatigue	1 (2.5%)	NA
Feeling heaviness in the body	1 (2.5%)	NA

Blurred eyes	1 (2.5%)	NA
Sourness^{+}	NA	1 (2.5%)
Stomach	NA	1 (2.5%)
Decreased appetite	NA	1 (2.5%)
Deteriorated mood	NA	1 (2.5%)
Numbness at the head and face	NA	1 (2.5%)
Tingling^{+}	NA	1 (2.5%)

$^{+}$: occurred at the stimulated area; NA: not applicable

3.3.2.4 Integrity of the blind

Of 80 participants, 70 provided treatment allocation guesses (n = 35 active; n = 35 sham), while 6 dropped out and 4 declined to respond. Overall, 48.6% (34/70) guessed their group allocation correctly, with no between-group difference in the guesses of active treatment (active vs. sham: 62.9% (22/35) vs. 65.7% (23/35), $\chi^2 = 0.062$, p = 0.803). Binomial tests revealed the correct guesses did not exceed chance levels for either group (active: 22/35, p = 0.175; sham: 12/35, p = 0.090). Confidence levels in guessing showed no significant between-group differences.

3.3.3 Neuroimaging outcomes

3.3.3.1 lDLPFC-seeded rsFC changes

A significant Group x Time interaction was observed for lDLPFC-seeded rsFC with several brain regions (threshold: F = 11.86, P = 0.001, k = 40 voxels, $P_{\text{cluster-level FDR-corrected}} < 0.05$). Post-hoc analyses revealed that active TPS increased rsFC between the lDLPFC and most of these brain regions,

whereas the sham group showed decreases in most regions. Notably, the active group showed a significant enhancement in the lDLPFC-seeded rsFC with the bilateral precuneus, calcarine, and left posterior cingulate cortex (Cluster 5), and the left orbitofrontal, superior medial prefrontal, and pregenual anterior cingulate cortices (Cluster 6). In addition, the active group also showed significantly enhanced rsFC within lDLPFC (Cluster 10). Conversely, the sham group showed a significant decrease in lDLPFC-seeded rsFC with the right inferior frontal cortex (orbital and triangular part) (Cluster 12). See rs-fMRI results of the interaction effect and post-hoc analyses in Table 8 and Figure 11.

Table 8. Rs-fMRI results displaying significant clusters for the group x time interaction effect for the completers (n=33 active; n=33 sham).

	Interaction effect ($P_{Cluster\text{-}level\ FDR\text{-}corrected} < 0.05$)				**Post-hoc analysis, post vs. pre**		**Post-hoc analysis, active vs. sham**	
	Brain regions defined by AAL	**F**	**k**	**Peak MNI coordinates, x y z**	**active**	**sham**	**pre-TPS**	**post-TPS**
Cluster 1	Left inferior frontal gyrus, orbital part, triangular part; Left middle temporal gyrus; Left temporal pole: superior & middle temporal gyrus	46.1	688	-36 36 -12	t = 1.114, p = 0.273	t = -0.900, p = 0.375	t = -0.914, p = 0.364	t = 0.263, p = 0.794
Cluster 2	Right superior & middle temporal gyrus; Right angular gyrus; Right inferior parietal gyrus; Right supramarginal gyrus	43.4	385	48 -45 21	t = 1.313, p = 0.199	t = -1.160, p = 0.255	t = -0.083, p = 0.934	t = 1.487, p = 0.142

Cluster 3	Left middle & superior temporal gyrus; Left supramarginal gyrus; Left angular gyrus; Left inferior parietal gyrus	40.6	383	-54 -57 24	t = 1.394, p = 0.173	t = -2.000, p = 0.054	t = -1.007, p = 0.318	t = 0.975, p = 0.333
Cluster 4	Right temporal pole: superior & middle temporal gyrus; Right middle temporal gyrus	34	287	45 21 -27	t = 1.399, p = 0.171	t = -0.029, p = 0.977	t = -0.931, p = 0.355	t = 0.043, p = 0.966
Cluster 5	Left posterior cingulum gyrus; Left & right precuneus; Left calcarine	39	268	-6 -51 27	**t = 2.376, p = 0.024***	t = 0.044, p = 0.965	t = -1.389, p = 0.170	t = 0.205, p = 0.838
Cluster 6	Left middle frontal gyrus, orbital part; Left superior frontal gyrus, medial; Left anterior cingulum gyrus	33.4	97	-12 60 -3	**t = 3.766, p < 0.001***	t = -1.441, p = 0.159	**t = -2.498, p = 0.015***	t = 0.037, p = 0.970
Cluster 7	Right superior & middle temporal gyrus	25.5	58	48 -27 0	t = -0.499, p = 0.621	t = -0.463, p = 0.646	t = 0.097, p = 0.923	t = 0.055, p = 0.956

Cluster 8	Left & right superior frontal gyrus, medial	23.5	58	0 51 42	t = 1.211, p = 0.235	t = -1.478, p = 0.149	t = -1.253, p = 0.215	t = 0.338, p = 0.737
Cluster 9	Right inferior frontal gyrus, triangular part	26	52	57 36 12	t = 0.619, p = 0.541	t = -0.954, p = 0.347	t = -0.383, p = 0.703	t = 0.911, p = 0.366
Cluster 10	Left superior & middle frontal gyrus	23.4	52	-24 39 51	**t = 2.802, p = 0.009***	t = 1.171, p = 0.250	t = -1.869, p = 0.066	t = -0.354, p = 0.725
Cluster 11	Right & left supplementary motor area;	21.3	43	3 0 75	t = -0.779, p = 0.442	t = -0.729, p = 0.472	t = 0.419, p = 0.677	t = 0.345, p = 0.731
Cluster 12	Right inferior frontal gyrus, orbital & triangular part	21.5	40	54 42 -3	t = -0.112, p = 0.911	**t = -2.542, p = 0.016***	t = 0.635, p = 0.527	**t = 2.709, p = 0.009***

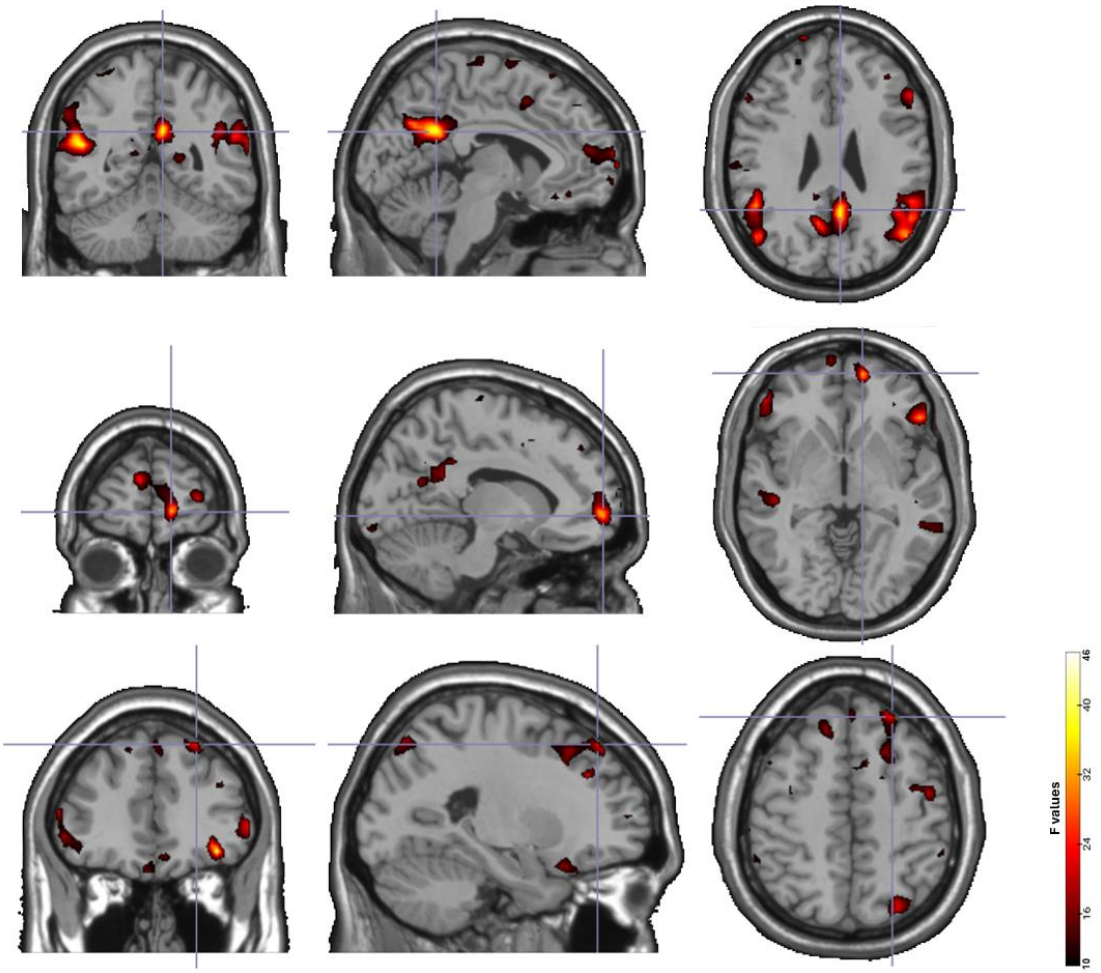

Figure 11. Post-hoc analysis results (posttreatment vs. baseline) of significant clusters with an interaction effect (threshold: F = 11.86, P = 0.001, k = 40 voxels, $P_{\text{cluster-level FDR-corrected}} < 0.05$). Brain regions marked with a cross indicate the peak MNI coordinates of clusters demonstrating a substantial increase in left DLPFC-seeded rsFC following the active group (n = 33, completers). Upper panel (Cluster 5 with a cluster size of 268 voxels, F = 34.02, $P_{\text{cluster-level FDR-corrected}} < 0.0001$): the left posterior cingulum gyrus, bilateral precuneus and calcarine gyrus; middle panel (Cluster 6 with a cluster size of 97 voxels, F = 33.40, $P_{\text{cluster-level FDR-corrected}} = 0.001$): the left orbitofrontal cortex and superior medial prefrontal, and pregenual anterior cingulate gyrus; lower panal (Cluster 10 with a cluster size of 52 voxels, F = 23.43, $P_{\text{cluster-level FDR-corrected}} = 0.013$): the left dorsolateral prefrontal cortex.

3.3.3.2 Association between lDLPFC-seeded rsFC changes and treatment response

Correlation analyses showed that, in the active group, the improvement in

total MADRS scores was positively correlated with the changes in lDLPFC-seeded rsFC with the right temporal pole and superior and middle temporal gyrus (Clusters 4 and 7), albeit only at an uncorrected significance level. No correlation survived after correction for multiple comparisons (See Appendices, Table S7).

3.3.4 Open-label treatment

Of the 36 participants who completed the sham treatment, 30 proceeded to receive active TPS treatment in the open-label phase, with 27 completing treatment. These completers showed an initial MADRS improvement of 7.7 points (95% CI = 2.88 to 8.97) after receiving sham TPS, and a further improvement of 5.0 points (95% CI = 2.10 to 7.98) after receiving active TPS. Taken together, of the 65 of 80 patients who completed active TPS treatment, 29 (44.6%) participants showed a response, and 25 (38.5%) achieved remission.

3.3.5 3-month follow-up

The 3-month follow-up assessment was completed by two unblinded cohorts: 32 of the 38 completers from the active group in the RCT phase and 24 of the 27 completers in the open-label phase. In total, 26 participants (46.4%) responded, and 22 (39.3%) were in remission at 3-month follow-up. Specifically, in the first cohort, 16 of 19 responders and 10 of 14 who had remitted maintained their status, while 3 of 13 non-responders and 4 of 18 non-remitters subsequently achieved response or remission; Similarly, in the second cohort, 3 of 7 initial responders and 6 of 8 who had remitted maintained their status, while 4 of 17 non-responders and 2 of 16 non-remitters later met these criteria.

3.4 Discussion

3.4.1 The feasibility and clinical efficacy of TPS for treating major depression

This first randomized, double-blind, sham-controlled trial demonstrates that 12 sessions of lDLPFC-TPS over four weeks significantly reduced depressive symptoms and modulated rsFC in patients with MDD compared to sham stimulation. While adverse events (primarily transient tingling and pain) were more frequent with active TPS, the low overall dropout rate of 7.5% confirms its feasibility and tolerability.

The antidepressive efficacy of TPS was supported by several key findings. First, the active TPS group showed a significantly greater reduction in MADRS scores than sham treatment at posttreatment, with a mean reduction of 12.10 versus 7.91 (effect size = 0.45), suggesting a clinically meaningful benefit (Leucht et al., 2017; Turkoz et al., 2021). Our observed effect size (0.45) contrasts with a previous open-label, waitlist-controlled RCT reporting a much larger effect (0.93) (Cheung et al., 2023), suggesting a substantial placebo effect in the prior trial. In Study 2, this placebo response was most prominent during the first two weeks, with a significant between-group difference in symptom improvement only emerging between the midpoint (Week 2) and the posttreatment (Week 4). This trajectory suggests that longer treatment durations or increased session frequencies may be necessary to optimize TPS outcomes. Second, active TPS achieved a response rate of 52.5%

and a remission rate of 40.0%, comparable to the outcomes of active rTMS in MDD (Barnes et al., 2023; Blumberger et al., 2021). Furthermore, TPS demonstrated a favorable profile relative to TMS, with fewer adverse events, lower reported pain intensity (mean score on verbal analogue scale: TPS: 2.7 vs. repetitive TMS: 3.4 vs. intermittent theta burst stimulation (iTBS): 3.8 (Blumberger et al., 2018)), and fewer treatment sessions (TPS: 12 vs. TMS: 20), suggesting that TPS may offer a more favorable cost-effectiveness ratio. However, future studies are needed to investigate the efficacy of TPS in treatment-resistant MDD populations. Third, the open-label phase demonstrated the sustained therapeutic effect of TPS, as evidenced by the majority of treatment responders and remitters maintaining their clinical status at 3-month follow-up.

3.4.2 The neural effects of lDLPFC-TPS

Our rs-fMRI results provide the first evidence of the neural effects of lDLPFC-TPS. The active TPS reversed several neural circuit dysfunctions that are frequently reported to underly the pathology of depression, specifically the hypoconnectivity between the DLPFC and the medial prefrontal cortex (Goldstein-Piekarski et al., 2022), rostral anterior cingulate cortex (Pantazatos et al., 2020), orbitofrontal cortex (Han et al., 2023), precuneus (Rueda et al., 2025), and visual cortex (Kita et al., 2025). Of note, TPS-induced enhancement in rsFC between lDLPFC and the medial prefrontal and pregenual anterior cingulate cortices aligns with the neural effects of treatment responses to other treatment strategies,

including serotonin (Arnone et al., 2018) and cognitive behavioral therapy (Pantazatos et al., 2020).

3.4.3 Implementation of standardized MNI-coordinate targeting

Our methodological advances in precise targeting distinguish this study from prior TPS research. As TPS was initially designed to target large brain regions in patients with AD (Beisteiner et al., 2020), most clinical studies used anatomical landmarks for targeting or simply applied whole-brain, broad stimulation. Recently, more TPS trials have been conducted to target the specific brain regions and have shown promising clinical effectiveness and neuromodulation effect (Manganotti et al., 2025; Cheung, Li, Ho, et al., 2023; Cheung, Li, Lam, et al., 2023; Matt et al., 2022); however, none of them illustrated targeting details of the TPS application. To our knowledge, we are the first to implement standardized MNI-coordinate targeting with individual T1-space transformation - an approach common in TMS studies (Blumberger et al., 2018; Fox et al., 2012). This enhanced methodological rigor addresses important concerns about reliability and reproducibility in the field.

3.4.4 Study limitations

Study 2 has several limitations. First, although patient and assessor blinding was successful, the therapists administering TPS could sometimes distinguish between active and sham conditions due to inherent tactile and auditory differences - a common challenge also encountered in TMS trials. Second, protocol adherence was suboptimal at

66%; however, this figure includes nine cases influenced by device malfunctions that were beyond the control of either participants or research personnel. Third, while participants were instructed to maintain stable medication regimens, six out of 80 reported changes to their regimen during the trial. Specifically, two participants (n = 1 active/ n = 1 sham) increased their antidepressant dosage, three (active group) decreased their antidepressant dosage, and one (active group) increased anti-anxiety medication dosage to control somatic symptoms during treatment visits. We made a deliberate choice to retain these participants in our intention-to-treat analysis, as their inclusion better reflects the clinical realities of treating MDD in real-world settings.

3.5 References

Arnone, D., T. Wise, C. Walker, P. J. Cowen, O. Howes, and S. Selvaraj. 2018. 'The effects of serotonin modulation on medial prefrontal connectivity strength and stability: A pharmacological fMRI study with citalopram', *Progress in Neuro-Psychopharmacology and Biological Psychiatry*, 84: 152-59.

Barnes, R., D. Skvarc, P. B. Fitzgerald, M. Berk, O. M. Dean, S. Dodd, T. Schriemer, and A. B. Singh. 2023. 'Equal remission rates and reduced length of hospital stay with twice-daily repetitive transcranial magnetic stimulation (rTMS) for major depression - A large naturalistic retrospective cohort association study', *Prog Neuropsychopharmacol Biol Psychiatry*, 127: 110820.

Beisteiner, R., and E. Matt. 2025. 'Ultrasound neuromodulation - How deep can we stimulate?', *Brain Stimul*, 18: 15-18.

Beisteiner, R., E. Matt, C. Fan, H. Baldysiak, M. Schonfeld, T. Philippi Novak, A. Amini, T. Aslan, R. Reinecke, J. Lehrner, A. Weber, U. Reime, C. Goldenstedt, E. Marlinghaus, M. Hallett, and H. Lohse-Busch. 2020. 'Transcranial Pulse Stimulation with Ultrasound in Alzheimer's Disease-A New Navigated Focal Brain Therapy', *Adv Sci (Weinh)*, 7: 1902583.

Blumberger, D. M., F. Vila-Rodriguez, K. E. Thorpe, K. Feffer, Y. Noda, P. Giacobbe, Y. Knyahnytska, S. H. Kennedy, R. W. Lam, Z. J. Daskalakis, and J. Downar. 2018. 'Effectiveness of theta burst versus high-frequency repetitive transcranial magnetic

stimulation in patients with depression (THREE-D): a randomised non-inferiority trial', *Lancet*, 391: 1683-92.

Blumberger, D. M., F. Vila-Rodriguez, W. Wang, Y. Knyahnytska, M. Butterfield, Y. Noda, S. Yariv, M. Isserles, D. Voineskos, N. J. Ainsworth, S. H. Kennedy, R. W. Lam, Z. J. Daskalakis, and J. Downar. 2021. 'A randomized sham controlled comparison of once vs twice-daily intermittent theta burst stimulation in depression: A Canadian rTMS treatment and biomarker network in depression (CARTBIND) study', *Brain Stimul*, 14: 1447-55.

Cheung, T., T. M. H. Li, Y. S. Ho, G. Kranz, K. N. K. Fong, S. F. Leung, S. C. Lam, W. F. Yeung, J. Y. T. Lam, K. H. Fong, R. Beisteiner, Y. T. Xiang, and C. P. W. Cheng. 2023. 'Effects of Transcranial Pulse Stimulation (TPS) on Adults with Symptoms of Depression-A Pilot Randomized Controlled Trial', *Int J Environ Res Public Health*, 20.

Cheung, T., T. M. H. Li, J. Y. T. Lam, K. H. Fong, L. Y. Chiu, Y. S. Ho, A. C. Tse, C. T. Li, C. P. Cheng, and R. Beisteiner. 2023. 'Effects of transcranial pulse stimulation on autism spectrum disorder: a double-blind, randomized, sham-controlled trial', *Brain Commun*, 5: fcad226.

Cheung, T., B. K. Yee, B. Chau, J. Y. T. Lam, K. H. Fong, H. Lo, T. M. H. Li, A. M. Li, L. Sun, R. Beisteiner, and C. P. W. Cheng. 2024. 'Efficacy and safety of transcranial pulse stimulation in young adolescents with attention-deficit/hyperactivity disorder: a pilot, randomized, double-blind, sham-controlled trial', *Front Neurol*, 15: 1364270.

Cole, Eleanor J., Angela L. Phillips, Brandon S. Bentzley, Katy H. Stimpson, Romina Nejad, Fahim Barmak, Clive Veerapal, Naushaba Khan, Kirsten Cherian, Emily Felber, Randi Brown, Elizabeth Choi, Sinead King, Heather Pankow, James H. Bishop, Azeezat Azeez, John Coetzee, Rachel Rapier, Nicole Odenwald, David Carreon, Jessica Hawkins, Maureen Chang, Jennifer Keller, Kristin Raj, Charles DeBattista, Booil Jo, Flint M. Espil, Alan F. Schatzberg, Keith D. Sudheimer, and Nolan R. Williams. 2022. 'Stanford Neuromodulation Therapy (SNT): A Double-Blind Randomized Controlled Trial', *American Journal of Psychiatry*, 179: 132-41.

Fox, M. D., R. L. Buckner, M. P. White, M. D. Greicius, and A. Pascual-Leone. 2012. 'Efficacy of transcranial magnetic stimulation targets for depression is related to intrinsic functional connectivity with the subgenual cingulate', *Biol Psychiatry*, 72: 595-603.

Fregni, F., M. M. El-Hagrassy, K. Pacheco-Barrios, S. Carvalho, J. Leite, M. Simis, J. Brunelin, E. M. Nakamura-Palacios, P. Marangolo, G. Venkatasubramanian, D. San-Juan, W. Caumo, M. Bikson, and A. R. Brunoni. 2021. 'Evidence-Based Guidelines and Secondary Meta-Analysis for the Use of Transcranial Direct Current Stimulation

in Neurological and Psychiatric Disorders', *Int J Neuropsychopharmacol*, 24: 256-313.

Gandevia, B., and A. Tovell. 1964. 'DECLARATION OF HELSINKI', *Med J Aust*, 2: 320-1.

Goldstein-Piekarski, A. N., T. M. Ball, Z. Samara, B. R. Staveland, A. S. Keller, S. L. Fleming, K. A. Grisanzio, B. Holt-Gosselin, P. Stetz, J. Ma, and L. M. Williams. 2022. 'Mapping Neural Circuit Biotypes to Symptoms and Behavioral Dimensions of Depression and Anxiety', *Biol Psychiatry*, 91: 561-71.

Gutierrez-Rojas, L., A. Porras-Segovia, H. Dunne, N. Andrade-Gonzalez, and J. A. Cervilla. 2020. 'Prevalence and correlates of major depressive disorder: a systematic review', *Braz J Psychiatry*, 42: 657-72.

Han, Sizhu, Xing-Xing Li, Shuochi Wei, Di Zhao, Jinjun Ding, Yongming Xu, Chang Yu, Zan Chen, Dong-Sheng Zhou, and Ti-Fei Yuan. 2023. 'Orbitofrontal cortex-hippocampus potentiation mediates relief for depression: A randomized double-blind trial and TMS-EEG study', *Cell Reports Medicine*, 4.

Hopewell, Sally, An-Wen Chan, Gary S. Collins, Asbjørn Hróbjartsson, David Moher, Kenneth F. Schulz, Ruth Tunn, Rakesh Aggarwal, Michael Berkwits, Jesse A. Berlin, Nita Bhandari, Nancy J. Butcher, Marion K. Campbell, Runcie C. W. Chidebe, Diana Elbourne, Andrew Farmer, Dean A. Fergusson, Robert M. Golub, Steven N. Goodman, Tammy C. Hoffmann, John P. A. Ioannidis, Brennan C. Kahan, Rachel L. Knowles, Sarah E. Lamb, Steff Lewis, Elizabeth Loder, Martin Offringa, Philippe Ravaud, Dawn P. Richards, Frank W. Rockhold, David L. Schriger, Nandi L. Siegfried, Sophie Staniszewska, Rod S. Taylor, Lehana Thabane, David Torgerson, Sunita Vohra, Ian R. White, and Isabelle Boutron. 2025. 'CONSORT 2025 statement: updated guideline for reporting randomized trials', *Nature Medicine*.

Jia, X. Z., J. Wang, H. Y. Sun, H. Zhang, W. Liao, Z. Wang, C. G. Yan, X. W. Song, and Y. F. Zang. 2019. 'RESTplus: an improved toolkit for resting-state functional magnetic resonance imaging data processing', *Sci Bull (Beijing)*, 64: 953-54.

Karakatsani, M. E., I. Gezginer, D. Nozdriukhin, S. Tiemann, H. A. I. Yoshihara, R. Storz, M. Belau, R. Ni, X. L. Dean-Ben, and D. Razansky. 2025. 'Transcranial pulse stimulation modulates neuronal activity and functional network dynamics', *Brain Stimul*, 18: 1834-42.

Kita, A., T. Ishida, N. Kita, M. Tabata, A. Tamaki, S. Uenishi, K. Yasuda, S. Takahashi, H. Matsuura, S. Yamada, and S. Kimoto. 2025. 'Exploring the capabilities of repetitive transcranial magnetic stimulation in major depressive disorder: Dynamic causal modeling of the neural network', *Transl Psychiatry*, 15: 257.

Lefaucheur, J. P., A. Aleman, C. Baeken, D. H. Benninger, J. Brunelin, V. Di Lazzaro, S. R. Filipovic, C. Grefkes, A. Hasan, F. C. Hummel, S. K. Jaaskelainen, B. Langguth, L. Leocani, A. Londero, R. Nardone, J. P. Nguyen, T. Nyffeler, A. J. Oliveira-Maia, A.

Oliviero, F. Padberg, U. Palm, W. Paulus, E. Poulet, A. Quartarone, F. Rachid, I. Rektorova, S. Rossi, H. Sahlsten, M. Schecklmann, D. Szekely, and U. Ziemann. 2020. 'Evidence-based guidelines on the therapeutic use of repetitive transcranial magnetic stimulation (rTMS): An update (2014-2018)', *Clin Neurophysiol*, 131: 474-528.

Leucht, S., H. Fennema, R. R. Engel, M. Kaspers-Janssen, P. Lepping, and A. Szegedi. 2017. 'What does the MADRS mean? Equipercentile linking with the CGI using a company database of mirtazapine studies', *J Affect Disord*, 210: 287-93.

Lohse-Busch, H., E. Marlinghaus, U. Reime, and U. Mowis. 2014. 'Focused low-energy extracorporeal shock waves with distally symmetric polyneuropathy (DSPNP): a pilot study', *NeuroRehabilitation*, 35: 227-33.

Lohse-Busch, H., U. Reime, and R. Falland. 2014. 'Symptomatic treatment of unresponsive wakefulness syndrome with transcranially focused extracorporeal shock waves', *NeuroRehabilitation*, 35: 235-44.

Manganotti, P., M. Liccari, T. Maria Isabella Lombardo, J. Della Toffola, V. Cenacchi, M. Catalan, and P. Busan. 2025. 'Effect of a single session of transcranial pulse stimulation (TPS) on resting tremor in patients with Parkinson's disease', *Brain Res*, 1850: 149405.

Mathers, Colin. 2008. *The global burden of disease: 2004 update* (World Health Organization).

Matt, E., G. Dorl, and R. Beisteiner. 2022. 'Transcranial pulse stimulation (TPS) improves depression in AD patients on state-of-the-art treatment', *Alzheimers Dement (N Y)*, 8: e12245.

Matt, E., L. Kaindl, S. Tenk, A. Egger, T. Kolarova, N. Karahasanovic, A. Amini, A. Arslan, K. Saricicek, A. Weber, and R. Beisteiner. 2022. 'First evidence of long-term effects of transcranial pulse stimulation (TPS) on the human brain', *J Transl Med*, 20: 26.

Matt, Eva, Michael Mitterwallner, Sonja Radjenovic, Daria Grigoryeva, Alexandra Weber, Elisabeth Stögmann, Alina Domitner, Anna Zettl, Sarah Osou, and Roland Beisteiner. 2025. 'Ultrasound Neuromodulation With Transcranial Pulse Stimulation in Alzheimer Disease', *JAMA Network Open*, 8.

Pantazatos, Spiro P., Ashley Yttredahl, Harry Rubin-Falcone, Ronit Kishon, Maria A. Oquendo, J. John Mann, and Jeffrey M. Miller. 2020. 'Depression-related anterior cingulate prefrontal resting state connectivity normalizes following cognitive behavioral therapy', *European Psychiatry*, 63.

Radjenovic, S., L. Bender, M. Gaal, D. Grigoryeva, M. Mitterwallner, S. Osou, A. Zettl, N. Plischek, P. Lachmair, K. Herzhauser, E. Matt, and R. Beisteiner. 2025. 'A retrospective analysis of ultrasound neuromodulation therapy using transcranial pulse stimulation in 58 dementia patients', *Psychol Med*, 55: e70.

Rueda, A., I. Demchenko, V. K. Tassone, F. Gholamali Nezhad, V. Peters, N. W. Churchill, B. N. Frey, S. Hassel, R. W. Lam, R. V. Milev, D. J. Muller, T. A. Schweizer, S. C. Strother, V. H. Taylor, S. H. Kennedy, S. A. Anteraper, V. Bhat, and Can-Bind Investigator Team. 2025. 'Multi-voxel pattern analysis for characterizing functional connectivity and neurocognitive function in major depression: A CAN-BIND-1 report', *Neuroimage Clin*, 48: 103840.

Sarica, C., J. F. Nankoo, A. Fomenko, T. C. Grippe, K. Yamamoto, N. Samuel, V. Milano, A. Vetkas, G. Darmani, M. N. Cizmeci, A. M. Lozano, and R. Chen. 2022. 'Human Studies of Transcranial Ultrasound neuromodulation: A systematic review of effectiveness and safety', *Brain Stimul*, 15: 737-46.

Truong, D. Q., C. Thomas, B. M. Hampstead, and A. Datta. 2022. 'Comparison of Transcranial Focused Ultrasound and Transcranial Pulse Stimulation for Neuromodulation: A Computational Study', *Neuromodulation*, 25: 606-13.

Turkoz, I., L. Alphs, J. Singh, C. Jamieson, E. Daly, M. Shawi, J. J. Sheehan, M. H. Trivedi, and A. J. Rush. 2021. 'Clinically meaningful changes on depressive symptom measures and patient-reported outcomes in patients with treatment-resistant depression', *Acta Psychiatr Scand*, 143: 253-63.

司天梅, 舒良, 党卫民, 苏允爱, 陈景旭, 董问天, 孔庆梅, and 张卫华. 2009. '简明国际神经精神访谈中文版的临床信效度', *中国心理卫生杂志*, 23: 493-97.

Chapter 4: Effects of transcranial pulse stimulation of the primary motor cortex on motor performance in healthy adults: A randomized crossover pilot study (Study 3)*

*Published on *CNS Neuroscience & Therapeutics* in December 2025

4.1 Introduction

Transcranial pulse stimulation (TPS) is a novel non-invasive brain stimulation technique that uses high-pressure ultrashort ultrasound pulses to modulate brain function (Truong et al., 2022). Developed from low-energy extracorporeal shock wave therapy (ESWT), TPS influences cellular processes through mechanotransduction, promoting neovascularization, tissue regeneration, and anti-inflammatory processes (d'Agostino et al., 2015). In vitro studies demonstrate that ESWT enhances the expression of vascular endothelial growth factor, brain-derived neurotrophic factor, and endogenous nitric oxide synthase, supporting neurovascular health (Ito, Fukumoto, and Shimokawa, 2009; Hatanaka et al., 2016; Wang et al., 2017; Mariotto et al., 2009).

TPS is a CE-approved device for Alzheimer's disease (AD) treatment (Beisteiner et al., 2020). Early pilot studies reported cognitive improvements following 6 - 12 TPS sessions with benefits lasting up to three months, correlating with increased functional connectivity within the memory network and cortical thickness in the left superior parietal lobule (Popescu, Pernet, and Beisteiner, 2021). Subsequent research has investigated TPS across several neurological and psychiatric disorders, including mild neurocognitive disorder, depression, Parkinson's disease

(PD), Autism Spectrum Disorder (ASD), and Attention Deficit Hyperactivity Disorder (ADHD) (Fong et al., 2023; Lo et al., 2024; Cheung, Li, Ho, et al., 2023; Osou et al., 2024; Cheung et al., 2024). Notably, a recent RCT demonstrated the therapeutic and neuromodulatory effects of a 2-week verum TPS treatment in younger AD patients (Matt et al., 2025).

Despite promising findings, most TPS studies have been uncontrolled and distributed stimulation across several cortical regions. This approach has left the region-specific behavioral effects and the underlying neuromodulatory mechanisms unclear. To date, only three randomized controlled TPS trials have investigated target-specific neuromodulatory and behavioral effects (Manganotti et al., 2025; Beisteiner et al., 2020; Matt et al., 2022). Beisteiner et al. demonstrated that a single session (1000 pulses at 4 Hz) over the primary somatosensory cortex (S1) induced immediate neurophysiological alterations in healthy individuals, as measured by somatosensory evoked potentials (Beisteiner et al., 2020). Furthermore, three sessions of S1-TPS led to a long-lasting enhancement in global sensorimotor efficiency one week later (Matt et al., 2022). More recently, a clinical trial demonstrated the behavioral modulatory effects of TPS, finding that a single session (1500 pulses at 4 Hz) of the primary motor cortex (M1) immediately reduced tremor amplitude in PD patients compared to sham stimulation (Manganotti et al., 2025).

Since the aftereffects of a single TPS session are largely unexplored and motor function serves as an objective readout of behavioral modulation, we conducted this randomized, subject- and analyst-blind, crossover pilot

trial. The aim was to investigate whether TPS over the right primary motor cortex (rM1) enhances left-hand motor performance in healthy individuals. Based on analogous effects shown by transcranial current direct stimulation and low-intensity transcranial ultrasound stimulation (Ferrucci et al., 2013; Hameroff et al., 2013; Ehsani et al., 2016), we hypothesized that rM1-TPS would improve left-hand performance with aftereffects lasting 30-40 minutes.

4.2 Methods

4.2.1 Study overview

Study 3 is a two-visit, randomized, subject- and analyst-blind, controlled, crossover pilot trial conducted at the Hong Kong Polytechnic University. Thirty-five right-handed (as assessed by the Edinburgh Handedness Inventory score > 40) healthy adults aged between 18 and 65 years were recruited from posters posted at the Hong Kong Polytechnic University from March 2024 to December 2024. Eligible participants signed the written informed consent after the experimental procedures were fully explained. This study was performed according to the Declaration of Helsinki (Gandevia and Tovell 1964), and the study protocol was approved by the Human Subjects Ethics Sub-committee of The Hong Kong Polytechnic University (Reference No: HSEARS20240319001-03). This study was registered in ClinicalTrial.gov in April 2024 (NCT06312930).

After enrollment, participants were randomly assigned to receive a single TPS session of 1000 pulses at either the rM1 or the vertex during the first visit, followed by the alternative target during the second visit in a randomized, counterbalanced order. The two experimental visits were scheduled 24 hours apart. Before each TPS session, both the active target (hotspot in the rM1) and the control target (vertex) were identified and marked on the scalp. Motor performance was assessed using the nine-hole peg test (NHPT) and the Deary-Liewald simple reaction time task (SRTT) at baseline and at multiple post-TPS time points (immediate, 10, 20, 30, and 40 minutes after stimulation) to examine changes over time. The study procedure of Study 3 is illustrated in Figure 12.

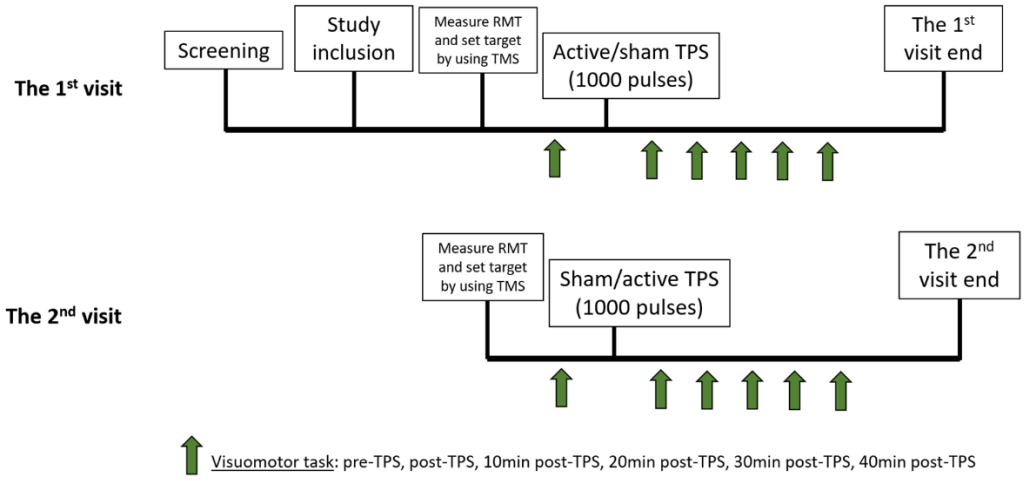

Figure 12. Experimental design of Study 3

4.2.2 Sample size

To date, no TPS study has been conducted to investigate the modulation effect on the motor cortex. With an expected medium effect size of 0.5 (Cohen's d), a power of 0.8, and an error probability of 0.05, the calculated sample size for the current crossover Study 3 should be 34.

Considering a 5% dropout rate, a total sample size of 36 has been determined.

4.2.3 Inclusion and exclusion criteria

The inclusion criteria were: (1) age 18 to 65; (2) no neurological, musculoskeletal, or psychiatric disorders based on a clinical interview; (3) right-handedness confirmed by Edinburgh Handedness Inventory score > 40. Exclusion criteria are as follows: (1) history of any neurological, musculoskeletal, or psychiatric disorders; (2) history of brain injury or cranial bone defects; (3) untreated coagulopathies (hemophilia); (4) thrombosis in the stimulated area; (5) pregnancy; (6) malignant tumor in the stimulated area; (7) cortisone therapy up to 6 weeks before first TPS session; (8) metallic objects in the head; (9) pacemakers that are not authorized for focused shock wave therapy; (10) simultaneous utilization of medication that lower the seizure threshold; (11) implanted deep brain stimulation device; (12) history of substance abuse or alcohol dependence; (13) with neuroscience or medical background.

4.2.4 Randomization, allocation concealment, and blinding

Randomization tables generated via a computer-based algorithm assigned participants to two counterbalanced visits, each receiving a unique randomization ID that determined the sequence of active and control stimulation. These IDs and sequences were recorded in an Excel sheet and managed by the TPS operator, who administered TPS according to

the predetermined order – though the operator was not blinded in this study.

Participants, lacking neuroscience or medical backgrounds, were blinded to the study hypothesis. They were informed that they would receive stimulation at two different targets during two visits, but they were not informed of the existence of a control condition (vertex stimulation). Before stimulation, both active and control targets were determined and marked during both visits to ensure the integrity of participants' blinding. To assess blinding effectiveness, they were asked at the end of their second visit whether they expected a performance difference between visits.

Two blinded analysts independently processed behavioral data. They recorded NHPT completion times via video analysis, extracted SRTT reaction times from the computer program, and excluded outliers from the reaction time dataset.

4.2.5 TPS procedure

4.2.5.1 Locating stimulation targets

The active target of the hotspot in the rM1 was identified using single-pulse TMS (MagVenture MagPro X100). A figure-of-eight TMS coil was positioned with its handle oriented 45° laterally and posteriorly to the sagittal plane. Starting at a low stimulation intensity, single TMS pulses were delivered at different scalp locations over the primary motor cortex. Motor-evoked potentials (MEPs) of the left first dorsal interosseous (FDI)

were recorded at rest using a pair of 25 mm x 20 mm surface electrodes in a belly-tendon montage with the TMS device's MEP monitor. The hotspot was defined as the scalp location where single-pulse TMS consistently elicited the largest MEP amplitude in the left FDI muscle at the lowest stimulation intensity. The location was then marked on the scalp with a brown eyebrow pencil to ensure precise TPS targeting. Figure 13 illustrates the hotspot marking procedure.

The control target of the vertex was defined as the midpoint between the nasion and inion along the midline. The marking procedure followed the same protocol as used for the hotspot. Before each TPS session, both the active and control targets were marked to minimize potential bias in the marking process.

Figure 13. Procedure for marking the hotspot in the right primary motor cortex. Left: A circular ring removed from the TPS handpiece was used for marking, with its center indicating the TPS handpiece's focal point; Middle: The hotspot was positioned at the center of the circular ring; Right: The ring's circumference was marked on the scalp using a brown eyebrow pencil.

4.2.5.2 TPS parameters and administration

TPS was delivered using the NEUROLITH system (Storz Medical AG, Tagerwilen, Switzerland). During active stimulation sessions, 1000 TPS pulses were delivered at a pulse frequency of 4 Hz with an energy flux density (EFD) of 0.20 mJ/mm^2 to the hotspot in the rM1 (Figure 14, left), similar to the parameters utilized in previous research (Beisteiner et al., 2020; Matt et al., 2022). The TPS pulse has a focus size of 5 mm (lateral) x 5mm (sagittal) x 56 mm (axial) (Karakatsani et al., 2025) and a focus depth of 43.4 mm (with a 6.6 mm stand-off device). To ensure optimal acoustic coupling, a generous amount of bubble-free ultrasound gel was applied to the stimulation site. The TPS handpiece, equipped with the circular ring, was carefully aligned with the marked circumference and maintained perpendicular to the scalp throughout stimulation. Control stimulation sessions followed the same procedural setup and parameters, with the only difference being the target location: the vertex rather than the motor hotspot (Figure 14, right). An adverse event checklist was used

after each TPS session to assess the side effects.

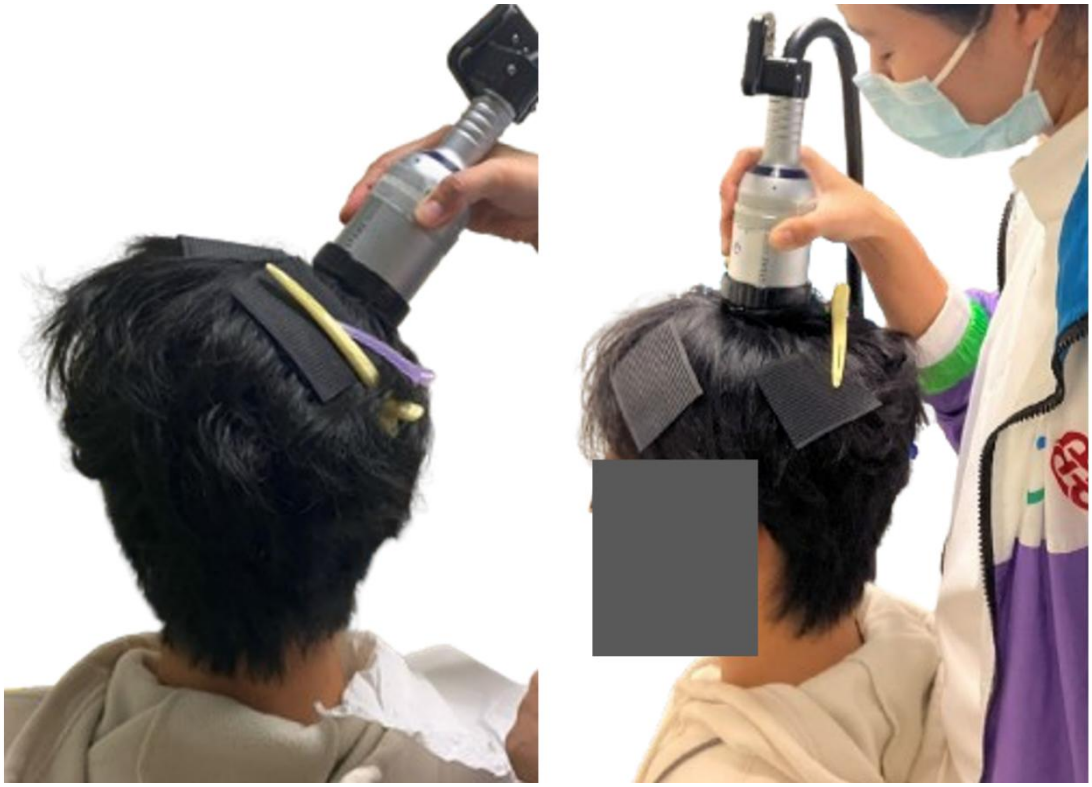

Figure 14. TPS handpiece positioning for (left) hotspot in the right primary motor cortex and (right) vertex stimulation. Hair stickers and clips were used to keep hair out of the way and expose the markers.

4.2.6 Behavioral assessment

The Deary-Liewald SRTT and NHPT were used to assess the motor performance at baseline (T0) and immediately after (T1), as well as 10 (T2), 20 (T3), 30 (T4), and 40 minutes (T5) following TPS. The tests were given in a fixed sequence: first the SRTT, then the NHPT.

The SRTT assesses processing speed by measuring reaction times to a diagonal cross appearing on a computer screen (Deary et al., 2011). Participants pressed the space key as quickly as possible after the stimulus appeared. The stimulus remained on the screen until the participant responded, and the interval between stimuli varied randomly

between 1 to 3 seconds. Each session included 10 practice trials and 20 test trials, performed first with the left hand and then with the right. Reaction times were automatically recorded, and outliers – responses exceeding 1s or below 0.1s – were excluded. Two independent analysts extracted the data and calculated the mean and standard deviation for analysis.

The NHPT assesses hand dexterity utilizing the Jamar 9-Hole Pegboard (Mathiowetz et al., 1985; Kellor et al., 1971). The square pegboard (12 cm x 12 cm) has nine holes (7 mm diameter, 26 mm apart from each other) and comes with pegs (32 mm length, 6 mm diameter). The pegboard and a dish were placed at the participant's midline, with the dish oriented toward the tested hand (first with the left hand, then the right hand). During the test, participants took pegs one by one, placed them into the holes, then returned them to the dish as quickly as possible, without retrieving dropped pegs. Before testing, a practice trial was conducted for each hand, followed by two consecutive test trials per hand, with the mean time recorded for analysis. The procedure was video-recorded, and two independent analysts used a stopwatch to measure the time from first peg touch to last peg hitting the dish (Mathiowetz et al., 1985; Oxford et al., 2003). If a participant paused after placing all pegs, retrieved fallen pegs, or deviated from instructions, the trial was discarded and repeated, with the reason documented. Any interruptions or errors, such as dropped pegs or talking, were noted. Additionally, if the time divergence between analysts exceeded 0.2431 seconds (based on the

simple reaction time (Deary et al., 2011), the trial was re-reviewed until the discrepancy was ≤ 0.2431 seconds.

4.2.7 Statistical analysis

A linear mixed-effects model was used to analyze the effects of time, stimulation condition, and their interaction, while accounting for potential confounding factors. Stimulation conditions (active vs. control), time points (T0-T5), and their interaction were set as fixed factors, with subject number as a random effect. The stimulation sequence (active-control vs. control-active) and baseline NHPT/SRTT performance were included as covariates. When significant main effects or interaction effects were found for NHPT or SRTT, post-hoc tests were performed to examine between- and within-group differences.

4.3 Study results

4.3.1 Participants' characteristics

A total of 36 healthy subjects have been recruited, with 34 completing two visits, one withdrawing from the study (due to factors unrelated to the study procedure), and one excluded due to an unmeasurable hotspot target. Of the 34 completers, 53% were males; the average age was 36.9 ± 17.66 (mean ± SD), and the average education year was 15.3 ± 2.72 (mean ± SD). The baseline characteristics were similar in the two visits (Table 9).

Table 9. Baseline characteristics of participants (completers, n = 34) in Study 3

Variable	Active TPS visit (n = 34)	Sham TPS visit (n = 34)

		N	%	N	%	
1st visit		17	50	17	50	
		Mean	SD	Mean	SD	P value
Baseline NHPT (second)	Left hand	19.94	2.32	19.81	2.15	0.732#
	Right hand	18.11	2.02	17.80	1.69	0.330#
Baseline SRTT (second)	Left hand	0.292543	0.035573	0.284121	0.026387	0.106&
	Right hand	0.292922	0.032739	0.287700	0.028509	0.489&

Paired t-test; &Wilcoxon signed-rank test

4.3.2 NHPT performance

For left-hand NHPT performance, the linear mixed-effects model revealed a significant main effect of time ($F = 10.872$, $p < 0.001$), but no significant main effect of stimulation condition (active vs. control, $F = 0.002$, $p = 0.967$) or interaction effect ($F = 0.244$, $p = 0.943$). Post-hoc paired t-tests examined changes from baseline across post-TPS time points for both active and control visits. During the active visit (rM1-TPS), left-hand NHPT performance significantly improved 10 to 40 minutes post-TPS with medium to large effect sizes:

10 min: $t = 3.29$, $p_{corrected} = 0.01$, Cohen's $d = 0.56$

20 min: $t = 5.07$, $p_{corrected} < 0.001$, Cohen's $d = 0.87$

30 min: $t = 4.71$, $p_{corrected} < 0.001$, Cohen's $d = 0.81$

40 min: $t = 5.08$, $p_{corrected} < 0.001$, Cohen's $d = 0.87$.

During the control visit (vertex-TPS), similar significant improvements were observed between 10 and 40 minutes, with medium effect sizes:

10 min: $t = 3.40$, $p_{corrected} = 0.01$, Cohen's $d = 0.58$

20 min: $t = 3.37$, $p_{corrected} = 0.01$, Cohen's $d = 0.58$

30 min: $t = 3.86$, $p_{corrected} < 0.001$, Cohen's $d = 0.67$

40 min: $t = 3.54$, $p_{corrected} = 0.005$, Cohen's $d = 0.61$.

Therefore, rM1-TPS did not significantly enhance NHPT performance compared to vertex-TPS, although effect sizes were larger for rM1 stimulation between 20 and 40 minutes post-TPS. Changes in left-hand NHPT performance over time for both visits are shown in Figure 15 and Table 10.

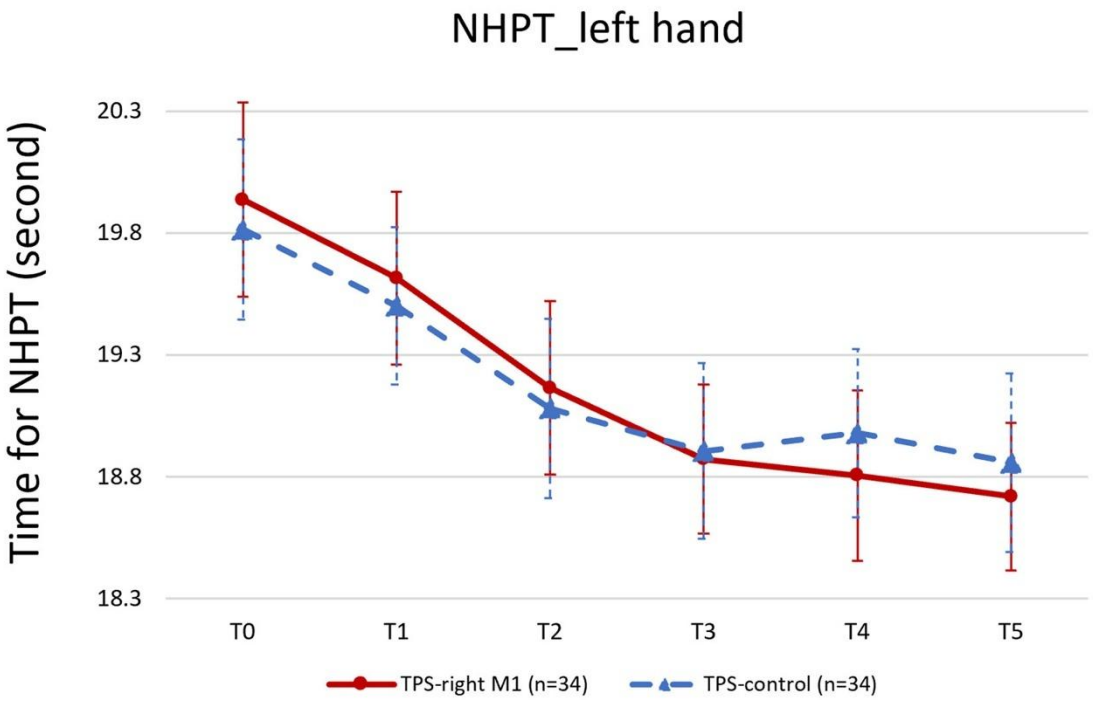

Figure 15. Changes in left-hand NHPT performance over time after the active and control TPS. The dots and triangles indicate the mean time for NHPT, and the bars indicate the standard errors (SEs) for each session. T0: baseline; T1: immediately after TPS; T2: 10 minutes after TPS; T3: 20 minutes after TPS; T4: 30 minutes after TPS; T5: 40 minutes after TPS.

Table 10. The numerical data of NHPT for both visits for the left hand

		Baseline	Immediately post-TPS	10min post-TPS	20min post-TPS	30min post-TPS	40min post-TPS
Left hand	rM1-TPS visit	19.94 ± 0.40	19.61 ± 0.35 (p = 0.084)	19.16 ± 0.36* (p = 0.002, Cohen's d = 0.564)	18.87 ± 0.31* (p < 0.001, Cohen's d = 0.869)	18.80 ± 0.35* (p < 0.001, Cohen's d = 0.808)	18.72 ± 0.30* (p < 0.001, Cohen's d = 0.871)
	Vertex-TPS visit	19.81± 0.37	19.50 ± 0.32 (p = 0.144)	19.10 ± 0.37* (p = 0.002, Cohen's d = 0.582)	18.90 ± 0.36* (p = 0.002, Cohen's d = 0.578)	18.98 ± 0.35* (p < 0.001, Cohen's d = 0.662)	18.86 ± 0.37* (p = 0.001, Cohen's d = 0.607)

Data is shown as mean ± SE. p-values were calculated by using paired t-tests to investigate the difference between the baseline. *: The significance level of corrected p-values should be < 0.01 by using Bonferroni correction.

4.3.3 SRTT performance

For SRTT performance, no significant main effects or interaction effects were observed during either visit. Changes in left-hand SRTT performance over time for both visits are illustrated in Figure 16, with numerical data available in Table 11.

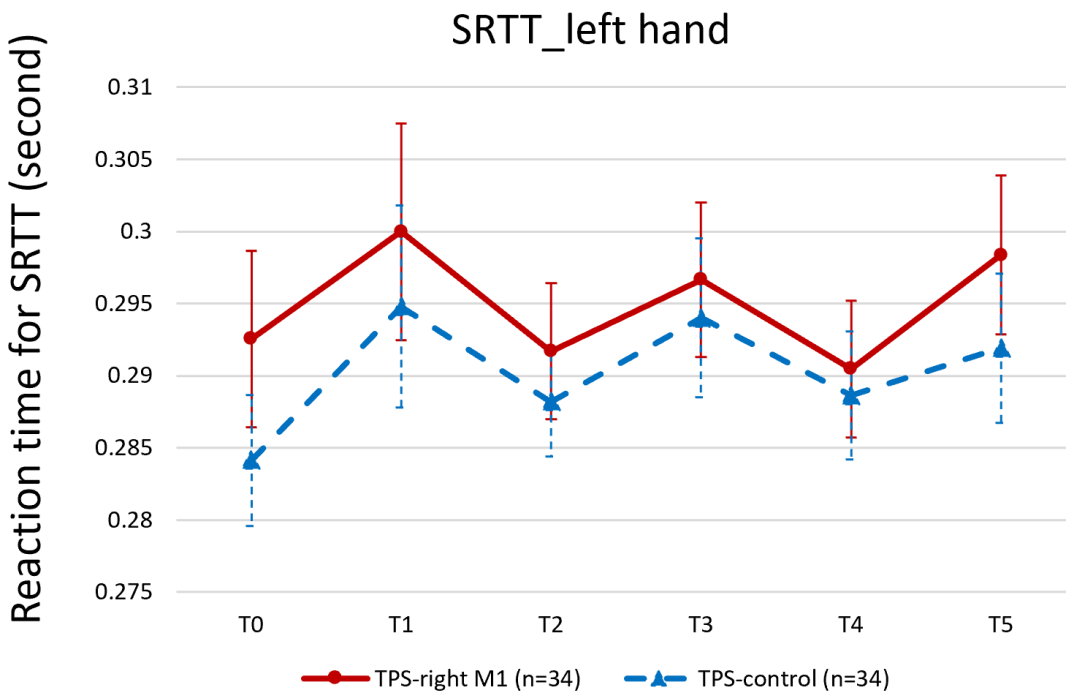

Figure 16. Changes in left-hand SRTT performance over time after the active and control TPS. The dots and triangles indicate the mean reaction time for SRTT, and the bars indicate the standard errors (SEs) for each session. T0: baseline; T1: immediately after TPS; T2: 10 minutes after TPS; T3: 20 minutes after TPS; T4: 30 minutes after TPS; T5: 40 minutes after TPS.

Table 11. The numerical data of SRTT for both visits for the left hand

		Baseline	**Immediately post-TPS**	**10min post-TPS**	**20min post-TPS**	**30min post-TPS**	**40min post-TPS**
Left hand	rM1-TPS visit	0.2925 ± 0.0061	0.3000 ± 0.0075 (p = 0.447)	0.2917 ± 0.0047 (p = 0.544)	0.2967 ± 0.0053 (p = 0.197)	0.2905 ± 0.0047 (p = 0.993)	0.2984 ± 0.0055 (p = 0.169)
	Vertex-TPS visit	0.2841 ± 0.0045	0.2948 ± 0.0070 (p = 0.071)	0.2882 ± 0.0038 (p = 0.135)	0.2940 ± 0.0055 (p = 0.077)	0.2886 ± 0.0044 (p = 0.263)	0.2919 ± 0.0052 (p = 0.103)

Data is shown as mean ± SE. p-values were calculated using the Wilcoxon test to investigate differences from baseline. *: The significance level of corrected p-values should be < 0.01 by using Bonferroni correction.

4.3.4 Integrity of the blind

Participants were asked whether they thought they were expected to perform better during one of the two visits. Nine (27%) of the 34 participants believed they were expected to perform better during the rM1-TPS visit, while 12 (35%) expected better performance during the vertex-TPS visit; the remaining 13 participants (38%) reported uncertainty. A binary test confirmed that participants' expectations (rM1-TPS visit vs. vertex-TPS visit) were no better than chance ($p = 0.664$), demonstrating successful blinding of participants to the stimulation condition.

4.3.5 Safety

Among the 34 participants, 25 (74%) in the rM1-TPS visit and 25 (74%) in the vertex-TPS visit reported side effects, with the most common ones being tingling and pressure sensation at the stimulation site. See details in the Supplementary Table 12. All symptoms resolved within 24 hours without medication.

Table 12. Adverse events occurred in Study 3

	Number of participants reporting each adverse event during stimulation (%)	
	rM1-TPS	Vertex-TPS
Tingling	8 (24%)	8 (24%)
Pressure sensation	3 (9%)	5 (15%)
pain	3 (9%)	5 (15%)
numbness	2 (6%)	3 (9%)
Striking sensation	2 (6%)	1 (3%)

Vibration in the ears	2 (6%)	2 (6%)
Unpleasant noise	1 (3%)	1 (3%)
Dizziness	1 (3%)	1 (3%)
Decreased hearing	1 (3%)	NA
Headache	1 (3%)	NA
Pain around the left ear	NA	2 (6%)
Irritation	NA	1 (3%)
	Number of participants reporting each adverse event after stimulation (%)	
Fatigue	1 (3%)	NA
Decreased hearing	1 (3%)	NA
Dizziness	1 (3%)	NA
Headache	1 (3%)	NA
Sourness in the arm and hand	1 (3%)	NA
Pain around the left ear	NA	1 (3%)
Muscle tightness in the right face	NA	1 (3%)

rM1-TPS: transcranial pulse stimulation over the right primary motor cortex; Vertex-TPS: transcranial pulse stimulation over the vertex; NA: not applicable.

4.4 Discussion

4.4.1 The feasibility and behavioral effects of a single-session TPS

This randomized, controlled, subject- and analyst-blind crossover study assessed the feasibility of a single-session TPS protocol and its modulatory effects on motor performance in healthy adults. The results confirm that delivering 1000 pulses of TPS to the right primary motor cortex is both feasible and safe, with no serious adverse events reported. No significant difference was observed between active and control stimulation, with left-hand NHPT performance demonstrating larger effect sizes between 20 to 40 minutes post rM1-TPS (Cohen's d = 0.808-0.871) than vertex-TPS (Cohen's d = 0.578-0.662). A post hoc power analysis indicated that a total sample size of 180 participants would be required to detect a significant interaction between stimulation condition and time, with an alpha of 0.05 and 80% power.

A recent study demonstrated immediate tremor amplitude reduction in PD patients following a single-session TPS applied to the motor cortex contralateral to the most affected body side (Manganotti et al., 2025). They found that active TPS significantly decreased the amplitude of resting tremor immediately after stimulation, compared with sham stimulation, with a large effect size (Cohen's d = 1.341). While promising, these results await replication. In any case, our study has several key differences from Manganotti et al.'s study (Manganotti et al., 2025) that may explain the differences in results. First, while Mangonotti

et al. examined clinical populations and symptom changes, we investigated behavioral performance in healthy adults, making direct comparisons between these two studies difficult. Second, our protocol delivered 1000 pulses at the TMS-defined hotspot, whereas Manganotti et al. administered 1500 pulses over the motor cortex without a detailed illustration of the targeting method or the size of the stimulation area. On the other hand, the potential dose-dependent effect of TPS may partly explain their larger effect size. Third, methodological limitation in Manganotti et al.'s study may have influenced their results. Their non-randomized trial treated 16 PD patients with active TPS first, followed by sham treatment in only 9 patients, potentially introducing selection and blinding biases that could compromise reliability. Fourth, Manganotti et al. did not assess the time course of TPS's immediate effects on motor function. Our study is the first to investigate the short-term behavioral effects of a single-session TPS for up to 40 minutes post-stimulation.

No significant improvement in SSRT performance was detected following either rM1-TPS or vertex-TPS. One possible explanation is that SSRT relies not only on sensory-motor processing but also on attentional demand, which is closely linked to frontal cortex function (Stuss et al., 2005). Additionally, the ceiling effect observed in healthy participants may have limited detectable improvements.

4.4.2 Study limitations

Study 3 has several limitations. First, the washout period may have been insufficient. However, Manganotti et al. (Manganotti et al., 2025) found

that the active TPS group demonstrated significantly greater improvement in tremor amplitude compared to the sham group immediately after TPS, rather than 24 hours post-stimulation. This suggests that a single session of TPS may modulate motor function more effectively than a placebo in the immediate period. In addition, several crossover trials on transcranial ultrasound stimulation also included a 24-hour washout period (Guerra et al., 2021; Zhang et al., 2022). Second, we used vertex stimulation as a control to maintain participant blinding, but this control stimulation may have induced a general stimulation effect, potentially confounding our results. Third, a single TPS session may not be sufficient to demonstrate effectiveness in behavioral improvements. Most TPS studies have employed multiple sessions administered over 2-4 weeks (Beisteiner et al., 2020; Fong et al., 2023; Cheung, Li et al., 2023; Cheung, Yee et al., 2024; Matt et al., 2025). Moreover, our unpublished data in MDD patients showed greater clinical improvement with active TPS than with sham treatment, particularly during weeks 2-4 of continued therapy.

4.4.3 Implications for future studies

Although no short-term behavioral effects of rM1-TPS were observed when compared to vertex-TPS, our findings illuminate potential directions for future TPS research. First, given that a recent animal study found real-time neurovascular effects during TPS (Karakatsani et al., 2025), future studies should investigate the online and short-term effects of TPS using combined neurophysiological and neuroimaging assessments. Second, including a sham control condition is essential to clarify the target-specific modulatory effects of TPS. Third, the efficacy

of multiple TPS sessions should be explored to determine if they induce stronger aftereffects.

4.5 References

Beisteiner R, Matt E, Fan C, Baldysiak H, Schönfeld M, Philippi Novak T, et al. *Transcranial Pulse Stimulation with Ultrasound in Alzheimer's Disease-A New Navigated Focal Brain Therapy.* Adv Sci (Weinh), 2020. **7**(3): p. 1902583. https://doi.org/10.1002/advs.201902583.

Cheung T, Li TMH, Ho YS, Kranz G, Fong KNK, Leung SF, et al. *Effects of Transcranial Pulse Stimulation (TPS) on Adults with Symptoms of Depression-A Pilot Randomized Controlled Trial.* Int J Environ Res Public Health, 2023. **20**(3). https://doi.org/10.3390/ijerph20032333.

Cheung T, Yee BK, Chau B, Lam JYT, Fong KH, Lo H, et al. *Efficacy and safety of transcranial pulse stimulation in young adolescents with attention-deficit/hyperactivity disorder: a pilot, randomized, double-blind, sham-controlled trial.* Front Neurol, 2024. **15**: p. 1364270. https://doi.org/10.3389/fneur.2024.1364270.

d'Agostino MC, Craig K, Tibalt E, Respizzi S. *Shock wave as biological therapeutic tool: From mechanical stimulation to recovery and healing, through mechanotransduction.* Int J Surg, 2015. **24**(Pt B): p. 147-53. https://doi.org/10.1016/j.ijsu.2015.11.030.

Deary IJ, Liewald D, Nissan J. *A free, easy-to-use, computer-based simple and four-choice reaction time programme: the Deary-Liewald reaction time task.* Behav Res Methods, 2011. **43**(1): p. 258-68. https://doi.org/10.3758/s13428-010-0024-1.

Ehsani F, Bakhtiary AH, Jaberzadeh S, Talimkhani A, Hajihasani A. *Differential effects of primary motor cortex and cerebellar transcranial direct current stimulation on motor learning in healthy individuals: A randomized double-blind sham-controlled study.* Neurosci Res, 2016. **112**: p. 10-19. https://doi.org/10.1016/j.neures.2016.06.003.

Ferrucci R, Brunoni AR, Parazzini M, Vergari M, Rossi E, Fumagalli M, et al. *Modulating human procedural learning by cerebellar transcranial direct current stimulation*. Cerebellum. 2013. **12**(4): p. 485-492. https://doi.org/10.1007/s12311-012-0436-9.

Fong TKH, Cheung T, Ngan STJ, Tong K, Lui WYV, Chan WC, et al. *Transcranial pulse stimulation in the treatment of mild neurocognitive disorders.* Ann Clin Transl Neurol, 2023. **10**(10): p. 1885-1890. https://doi.org/10.1002/acn3.51882.

Gandevia B, Tovell A. *DECLARATION OF HELSINKI.* Med J Aust, 1964. **2**: p. 320-1.

Guerra A, Vicenzini E, Cioffi E, Collella D, Cannavacciuolo A, Pozzi S, et al. *Effects of Transcranial Ultrasound Stimulation on Trigeminal Blink Reflex Excitability.* Brain Sci, 2021. **11**(5): p. 645. https://doi.org/10.3390/brainsci11050645.

Hameroff S, Trakas M, Duffield C, Annabi E, Gerace MB, Boyle P, et al. *Transcranial ultrasound (TUS) effects on mental states: a pilot study.* Brain Stimul, 2013. **6**(3): p. 409-415. https://doi.org/15.10.1016/j.brs.2012.05.002.

Hatanaka K, Ito K, Shindo T, Kagaya Y, Ogata T, Eguchi K, et al. *Molecular mechanisms of the angiogenic effects of low-energy shock wave therapy: roles of mechanotransduction.* Am J Physiol Cell Physiol, 2016. **311**(3): p. C378-85. https://doi.org/10.1152/ajpcell.00152.2016.

Ito K, Fukumoto Y, Shimokawa H. *Extracorporeal shock wave therapy as a new and non-invasive angiogenic strategy.* Tohoku J Exp Med, 2009. **219**(1): p. 1-9. https://doi.org/10.1620/tjem.219.1.

Karakatsani ME, Gezginer I, Nozdriukhin D, Tiemann S, Yoshihara HAI, Storz R, et al. (2025). *Transcranial pulse stimulation modulates neuronal activity and functional network dynamics*. Brain stimulation, 2025. **18**(6): p. 1834–1842. Advance online publication. https://doi.org/10.1016/j.brs.2025.09.021

Karakatsani ME, Nozdriukhin D, Tiemann S, Yoshihara HAI, Storz R, Belau M, Ni R, et al. *Multimodal imaging of murine cerebrovascular dynamics induced by transcranial pulse stimulation.* Alzheimer's & Dementia, 2025. **21**(2): e14511. https://doi.org/10.1002/alz.14511.

Kellor M, Frost J, Silberberg N, Iversen I, Cummings R. *Hand strength and dexterity.* Am J Occup Ther, 1971. **25**(2): p. 77-83.

Lo HK, Fong TK, Cheung T, Ngan SJ, Lui WV, Chan WC, et al. *Enhanced Cognition and Modulation of Brain Connectivity in Mild Neurocognitive Disorder: The Promise of Transcranial Pulse Stimulation.* Biomedicines, 2024. **12**(9). https://doi.org/10.3390/biomedicines12092081.

Manganotti P, Liccari M, Maria Isabella Lombardo T, Della Toffola J, Cenacchi V, et al. *Effect of a single session of transcranial pulse stimulation (TPS) on resting tremor in patients with Parkinson's disease.* Brain Res, 2025. **1850**: p. 149405. https://doi.org/10.1016/j.brainres.2024.149405.

Mariotto S, de Prati AC, Cavalieri E, Amelio E, Marlinghaus E, Suzuki H. *Extracorporeal shock wave therapy in inflammatory diseases: molecular mechanism that triggers anti-inflammatory action.* Curr Med Chem, 2009. **16**(19): p. 2366-72. https://doi.org/10.2174/092986709788682119.

Mathiowetz V, Weber K, Kashman N, Volland G. *Adult norms for the nine hole peg test of finger dexterity.* The Occupational Therapy Journal of Research, 1985. **5**(1): p. 24-38. https://doi.org/10.1177/153944928500500102.

Matt E, Kaindl L, Tenk S, Egger A, Kolarova T, Karahasanović N, et al. *First evidence of long-term effects of transcranial pulse stimulation (TPS) on the human brain.* J Transl Med, 2022. **20**(1): p. 26. https://doi.org/10.1186/s12967-021-03222-5.

Matt E, Mitterwallner M, Radjenovic S, Grigoryeva D, Weber A, Stögmann E, et al. *Ultrasound Neuromodulation With Transcranial Pulse Stimulation in Alzheimer Disease.* JAMA Network Open, 2025. **8**(2). https://doi.org/10.1001/jamanetworkopen.2024.59170.

Osou S, Radjenovic S, Bender L, Gaal M, Zettl A, Dörl G, et al. *Novel ultrasound neuromodulation therapy with transcranial pulse stimulation (TPS) in Parkinson's disease: a first retrospective analysis.* J Neurol, 2024. **271**(3): p. 1462-1468. https://doi.org/10.1007/s00415-023-12114-1.

Oxford Grice K, Vogel KA, Le V, Mitchell A, Muniz S, Vollmer MA. *Adult norms for a commercially available Nine Hole Peg Test for finger dexterity.* The American journal of occupational therapy, 2003. **57**(5): p. 570-573. https://doi.org/10.5014/ajot.57.5.570.

Popescu T, Pernet C, Beisteiner R. *Transcranial ultrasound pulse stimulation reduces cortical atrophy in Alzheimer's patients: A follow-up study.* Alzheimers Dement (N Y), 2021. **7**(1): p. e12121. https://doi.org/10.1002/trc2.12121.

Stuss DT, Alexander MP, Shallice T, Picton TW, Binns MA, Macdonald R, et al. *Multiple frontal systems controlling response speed.* Neuropsychologia, 2005. **43**(3): p. 396-417. https://doi.org/10.1016/j.neuropsychologia.2004.06.010.

Truong DQ, Thomas C, Hampstead BM, Datta A. *Comparison of Transcranial Focused Ultrasound and Transcranial Pulse Stimulation for Neuromodulation: A Computational Study.* Neuromodulation, 2022. **25**(4): p. 606-13. https://doi.org/10.1016/j.neurom.2021.12.012.

Wang B, Ning H, Reed-Maldonado AB, Zhou J, Ruan Y, Zhou T, et al. *Low-Intensity Extracorporeal Shock Wave Therapy Enhances Brain-Derived Neurotrophic Factor Expression through PERK/ATF4 Signaling Pathway.* Int J Mol Sci, 2017. **18**(2). https://doi.org/10.3390/ijms18020433.

Zhang MF, Chen WZ, Huang FB, Peng ZY, Quan YC, Tang ZM. *Low-intensity transcranial ultrasound stimulation facilitates hand motor function and cortical excitability: A crossover, randomized, double blind study.* Front Neurol, 2022. **13**: p. 926027. https://doi.org/10.3389/fneur.2022.926027.29. Karakatsani ME, Nozdriukhin D, Tiemann S, Yoshihara HAI, Storz R, Belau M, Ni R, et al. *Multimodal imaging of murine cerebrovascular dynamics induced by transcranial pulse stimulation.* Alzheimer's & Dementia, 2025. **21**(2): e14511. https://doi.org/10.1002/alz.14511.

Chapter 5: Efficacy and safety of transcranial stimulation of the dorsal cingulate cortex and anterior insula cortex in healthy adults: A prospective, randomized, sham-controlled, pilot trial (Study 4)

5.1 Introduction

Non-invasive brain stimulation (NIBS) techniques, such as transcranial magnetic stimulation (TMS) and transcranial direct current stimulation (tDCS), are widely used as complementary treatments for depression (Lefaucheur et al., 2020; Wang, 2019). The most common target is the left dorsolateral prefrontal cortex (lDLPFC), based on its established efficacy in reducing depressive symptoms. A fundamental limitation of these techniques, however, is their inability to directly stimulate deeper brain regions. This restriction prevents the exploration of alternative therapeutic targets in deeper neural circuits. Crucially, evidence from invasive deep brain stimulation suggests several deep brain regions—including the subcallosal cingulate gyrus, ventral capsule/ventral striatum, medial forebrain bundle, nucleus accumbens, and bed nucleus of the stria terminalis—that can produce promising long-term antidepressant effects (Reddy et al., 2024). This highlights a significant gap between the therapeutic potentials of these validated deeper targets and the technical limitations of conventional NIBS techniques.

Notably, the dorsal anterior cingulate cortex (dACC) and anterior insula cortex (AIC) are core nodes of the salience network (SN). This network is responsible for identifying the most relevant stimuli among internal and external inputs to guide attention and behavioral responses (Menon and

Uddin, 2010). Dysfunction of the SN is implicated in the pathophysiology of various mental disorders, including depression, anxiety, autism spectrum disorder, obsessive-compulsive disorder, post-traumatic stress disorder, and schizophrenia (Goldstein-Piekarski et al., 2022; Segal et al., 2023; Williams, 2016; Lynch et al., 2024). In depression, insula hypoconnectivity within SN (Mulders, van Eijndhoven et al., 2015) and hypoconnectivity between the dACC node of SN and the precuneus node of the attention circuit (Kaiser et al., 2015) have been noted. Notably, and degree of insular hypoconnectivity is inversely related to symptom severity (Mulders et al., 2015). These SN dysfunctions may underlie clinical symptoms of anxious avoidance, characterized by difficulty in discerning relevant salient cues and withdrawing from situations that could cause sensory or interoceptive overload (Williams, 2016). Structural neuroimaging provides convincing evidence for the SN's central role. A landmark meta-analysis of over 15,000 individuals with various psychiatric disorders identified reduced grey matter volume in the bilateral AIC and dACC as the only structural abnormalities common to schizophrenia, bipolar disorder, depression, addiction, obsessive-compulsive disorder, and anxiety (Goodkind et al., 2015).

Transcranial pulse stimulation (TPS) was first investigated in Alzheimer's disease, where it demonstrated clinical and neural effects (Beisteiner et al., 2020; Matt et al., 2025; Radjenovic et al., 2025; Beisteiner and Matt, 2025; Karakatsani et al., 2025). Afterwards, more and more TPS clinical studies have been conducted across various disease cohorts, including MCI (Fong et al., 2023; Lo et al., 2024), depression

(Cheung, Li, Ho, et al., 2023), PD (Osou et al., 2024; Manganotti et al., 2025), ADHD (Cheung et al., 2024), and ASD (Cheung, Li, Lam, et al., 2023). However, a critical limitation persists in this literature: most trials apply stimulation broadly across multiple cortical regions (Beisteiner et al., 2020; Matt et al., 2025; Fong et al., 2023; Lo et al., 2024; Osou et al., 2024). Only a handful of studies have employed region-specific targeting, focusing on surface cortex areas such as the somatosensory cortex (Beisteiner et al., 2020; Matt et al., 2022), the primary motor cortex (Manganotti et al., 2025), DLPFC (Cheung, Li, Ho, et al., 2023), and temporoparietal junction (Cheung, Li, Lam, et al., 2023). Consequently, the precise modulatory effects and underlying mechanisms of region-specific TPS remain poorly understood. Moreover, although TPS is capable of non-invasively stimulating deeper brain regions up to 8 cm deep (Matt, Kaindl et al., 2022), the feasibility and efficacy of targeting specific subcortical regions remain unexplored.

Given the research gap and the established relevance of the dACC and AIC in depression, this study aimed to assess the feasibility, safety, and modulatory effects of TPS targeting these deeper regions in healthy adults. To probe AIC and dACC function, we selected four well-validated psychological tasks based on prior task-fMRI studies: the counting Stroop task (assessing conflict monitoring) (Bush et al., 1998), the Go/NoGo test (GNGT) (response inhibition) (Wager et al., 2005), the balloon analog risk task (BART) (risk-taking) (Rao et al., 2008), and the reading the mind in the eyes test (RMET) (theory of mind) (Moor et al., 2012). In addition, subjective affective state was assessed using mood scales. Our

goal was to provide foundational evidence for TPS as a tool for non-invasive deeper brain stimulation and to identify potential therapeutic targets for depression.

5.2 Methods

5.2.1 Study overview

A single-blind, sham-controlled randomized pilot trial was conducted to investigate the effects of TPS on AIC and dACC function. The study was conducted at The Hong Kong Polytechnic University between August 2024 and August 2025. The study protocol was approved by the Institutional Review Board of The Hong Kong Polytechnic University (Reference No: HSEARS20240319006) and registered at ClinicalTrial.gov (Identifier: NCT06635161). Eligible healthy participants were randomized to receive AIC-TPS, dACC-TPS, or vertex-sham TPS for 10 sessions over 2 weeks. Task performance and subjective mood were evaluated at three time points: baseline, midpoint (one week after the first TPS session), and endpoint (upon completion of the final session). Structural magnetic resonance imaging (sMRI) and resting-state functional magnetic resonance imaging (rs-fMRI) were performed at baseline and endpoint. sMRI was used for individualized targeting, while rs-fMRI was employed to examine TPS-induced changes in voxel-wise, target-seeded resting-state functional connectivity (rsFC). The study procedure is shown in Figure 17.

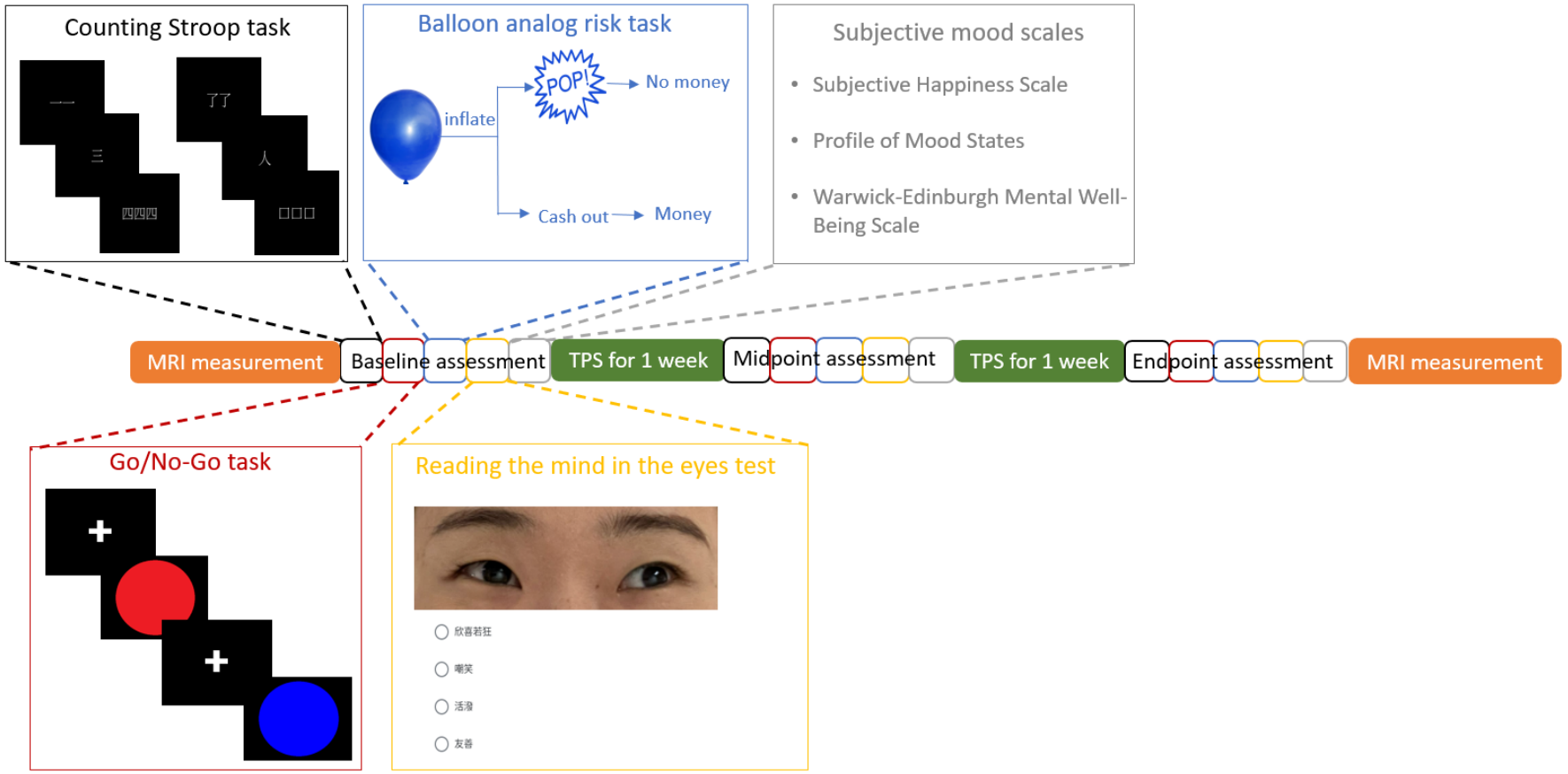

Figure 17. Study procedure of Study 4

5.2.2 Sample size

Until now, no TPS trial has specifically targeted AIC or dACC. As a pilot study, the sample size was set at 20 participants per group, following the conventional rule of thumb. This resulted in a total sample size of 60, allocated in a 1:1:1 ratio across the dACC, AIC, and sham groups.

5.2.3 Inclusion and exclusion criteria

Healthy participants were included in this study. Inclusion criteria were: (1) age between 18 and 65 years; (2) good physical and mental health, confirmed through a clinical interview; and (3) the ability to comprehend and follow instructions provided by the study team. Exclusion criteria included (1) the presence of intracranial metal implants; (2) corticosteroid treatment within 6 weeks prior to enrollment; (3) pregnancy or breastfeeding; (4) standard contraindications for NIBS and MRI, such as a history of brain surgery, cardiac pacemaker, deep brain stimulation, or intracranial metallic particles; (5) prior experience with TPS; (6) color blindness; and (7) a background in neuroscience. Eligible participants were enrolled in the study after obtaining written informed consent. The study was performed in accordance with the Declaration of Helsinki (Gandevia and Tovell, 1964), including its current revisions.

5.2.4 Randomization and allocation concealment

Randomization tables, generated by a computer-based algorithm with a block size of 12, were used to allocate participants to the three experimental arms in a 1:1:1 ratio. Each participant was assigned a

unique randomization identification number, which determined their assigned stimulation target. Sealed, opaque envelopes containing the group allocation corresponding to each randomization identification number were prepared and securely maintained by the TPS operator throughout the study period.

5.2.5 TPS procedure and blinding

The TPS protocol followed Study 2, except that five TPS sessions were applied per week for two weeks in Study 4. Targets in the bilateral AIC, bilateral dACC, and vertex were identified using neuronavigation based on each participant's sMRI (Figure 18). Each session consisted of 1000 pulses (500 per hemisphere for the AIC or dACC, and 1000 for the vertex) delivered at 4 Hz with an EFD of 0.2 mJ/mm^2. The left AIC (lAIC), right AIC (rAIC), left dACC (ldACC), right dACC (rdACC), and vertex were predefined as 15-mm radius spheres centered at the following MNI coordinates: lAIC (x = -41, y = 6, z = 3 mm), rAIC (x = 44, y = 9, z = 2 mm), ldACC (x = -4, y = 26, z = 45 mm), rdACC (x = 7, y = 30, z = 40 mm) (Ho et al., 2017; Yeo et al., 2011), and vertex (x = 0, y = -30, z = 60 mm). These spheres were then transformed into each participant’s individual T1-weighted space, and adjusted target voxels were calculated to match the TPS display at a penetration depth of 30 mm. Predefined 15-mm-radius spheres were then created as target zones on the individual T1-weighted image, centered at the center of mass of all adjusted target voxels. A 6.6 mm stand-off device was used for AIC targeting to achieve a focus depth of 43.4 mm, while no stand-off device was used for dACC

targeting to allow deeper penetration (a focus depth of 50 mm). Sham stimulation was delivered by placing a sham stand-off device into the handpiece. Adverse events were assessed using a predefined checklist after each session, and participants were instructed to report any additional symptoms. To assess the self-perceived efficacy of TPS, participants were asked at endpoint (Week 2) whether the stimulation had influenced their task performance or mood, and, if so, in what way.

The TPS operator could not be blinded because they needed to be aware of the stimulation targets. Participants, however, were blinded to the study hypothesis. They were provided with partial information: while informed that they would receive stimulation, they were not told about the specific targets or the primary purpose of the study. Although participants may have realized that stimulation sites varied across individuals (e.g., through conversations with other participants), their lack of a neuroscience background prevented them from discerning the precise differences among the three stimulation targets. This process guaranteed effective participant blinding throughout the study. Because participants also served as assessors for self-performed tasks and questionnaires, maintaining this level of blinding was essential to minimize bias in the subjective outcomes.

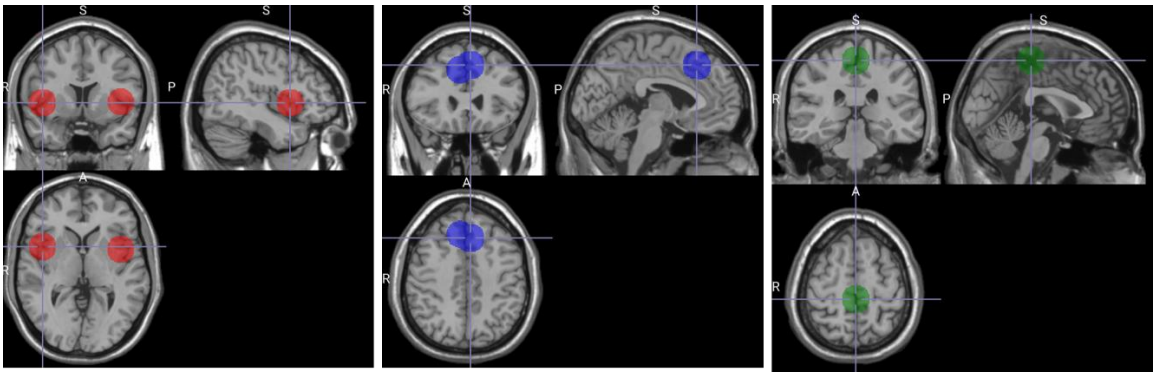

Figure 18. Stimulation targets: Left panel (red): bilateral anterior insular cortex; middle panel (blue): bilateral dorsal anterior cingulate cortex; right panel (green): vertex.

5.2.6 Psychological measurements

The Counting Stroop task was used to assess dACC function in conflict and error monitoring (Bush et al., 2006; Bush et al., 1998). Participants were instructed to report, via keypress, the number of identical words displayed on a computer screen while ignoring the words' meaning, responding as quickly and accurately as possible. The number of words (1-4) was indicated by pressing the 'A', 'S', 'K', and 'L' keys with the right middle, right index, left index, and left middle fingers, respectively. In incongruent blocks, stimuli consisted of Chinese number words ("一", "二", "三", "四"), where the quantity and semantic meaning conflicted. Neutral blocks presented matched-complexity, non-numerical Chinese characters ("了", "人", "手", "口") (Shang et al., 2018). Stimuli were presented every 1.5 seconds, with equal frequency for each word, and the trial order was randomized. The task comprised eight 30-second blocks (20 trials per block), alternating between incongruent and neutral trials, with order counterbalanced across participants. A practice session of 20 neutral and 20 incongruent trials was conducted to familiarize participants with the task (Bush et al., 1998; Hayward, Goodwin, and Harmer, 2004). Cognitive interference was measured as increased reaction time (RT) and decreased accuracy in incongruent compared to neutral trials.

The Balloon Analog Risk Task (BART) was used to assess the AIC and dACC involvement in risky decision-making (Rao et al., 2008). In this task, participants inflated a virtual balloon on-screen, earning money with each pump but simultaneously increasing the risk of explosion, which resulted in losing all earnings for that trial. Participants could stop pumping at any time to cash out accumulated earnings. The task consisted of 30 trials (balloons), each allowing a maximum of 12 pumps, with participants earning HKD 0.6 per pump for unexploded balloons. The explosion probability increased with each pump, ranging from 2% at the first pump to 90% at the last. Participants were informed that the explosion point varied across balloons (Lejuez et al., 2002). Risk-taking was quantified as the unadjusted number of pumps (average number of pumps across all 30 balloons), the adjusted number of pumps (average number of pumps across unexploded balloons), and the number of explosions.

The Chinese version of the Reading the Mind in the Eyes Test (RMET) was used to assess the AIC function related to the theory of mind (Baron-Cohen et al., 2001; Lee et al., 2023; Moor et al., 2012). In this test, participants viewed 28 photographs of the eye region, each accompanied by four mental state terms (e.g., vigorous, encouraged, excited, serene). For each trial, participants selected the word that best described what the person in the photograph was thinking or feeling. Trial order was randomized, and participants were instructed to respond based on their first impression, without time constraints.

The Go/No-go task (GNGT) was used to assess the AIC and dACC function in response inhibition (Wager et al., 2005). Participants were instructed to press the spacebar as quickly as possible for Go signals (red circles) and to withhold responses for No-Go signals (blue circles). Stimuli were randomly presented for 400 ms, separated by a 1000-ms central fixation cross. The task consisted of 280 trials across two blocks, with No-Go trial probability varying by block (high: 50%; low: 20%). A 20-trial practice session preceded the main task. The outcome measure was the false alarm rate (FAR) on No-Go trials, calculated as the proportion of No-Go trials in which participants failed to inhibit the prepotent response.

To explore the influence of TPS on affective state, mood was assessed using three validated instruments: the Subjective Happiness Scale (SHS) (Lyubomirsky and Lepper, 1999; Nan et al., 2014), the Profile of Mood States (POMS) (Lin, Hsiao, and Wang, 2014; Chen, Snyder, and Krichbaum, 2002), and the Warwick-Edinburgh Mental Well-Being Scale (WEMWBS) (Fung, 2019; Stewart-Brown and Janmohamed, 2008).

5.2.7 MRI measurements

The MRI protocol followed Study 2. Within one week prior to the first TPS session and at the conclusion of the final session, participants received a 6-minute sMRI scan using a Siemens 3T MAGNETOM Prisma system equipped with a 64-channel head coil. Standard scanning parameters were TR/TE = 2300/2.98 ms, flip angle = 9°, field-of-view = 240 x 256 x 208 mm, voxel size = 1 x 1 x 1 mm. An 8-minute rs-fMRI

scan was also performed. During this scan, participants were instructed to relax with their eyes open and to fixate on a cross displayed on the screen, allowing their minds to wander without focusing on specific thoughts. Rs-fMRI was acquired using single-shot gradient-recalled echo planar imaging with TR/TE = 607/32 ms, FOV = 220 x 220 x 160 mm, voxel size = 2.5 x 2.5 x 2.5 mm, 64 slices (slice thickness = 2.5 mm), interleaved acquisition, and a simultaneous multislice acceleration factor of 8.

5.2.8 Statistical analysis

An intention-to-treat analysis was planned using a linear mixed model (LMM) to estimate stimulation effects, given its flexibility, ability to handle missing data, and greater statistical power compared to other approaches. The stimulation effect of TPS was considered confirmed when a significant group-by-time interaction was followed by a significant post hoc comparison, demonstrating that the active groups exhibited greater improvements in task performance or mood state compared to the sham group. In addition, exploratory paired t-tests were performed to assess within-group changes from baseline for each outcome of interest.

Voxel-wise seed-based rsFC analyses were performed to investigate TPS-induced rsFC changes. Seeds were defined as the bilateral AIC (MNI coordinate: lAIC: x = -41, y = 6, z = 3 mm; rAIC: x = 44, y = 9, z = 2 mm) and bilateral dACC (MNI coordinate: ldACC: x = -4, y = 26, z = 45 mm; rdACC: x = 7, y = 30, z = 40 mm) (Ho et al., 2017; Yeo et al.,

2011). Correlation analyses were then conducted to examine the associations between changes in rsFC and improvements in task performance or mood.

5.3 Study results

5.3.1 Participants' characteristics

A total of 65 healthy participants were recruited, of whom 60 were included in the study. Five participants were excluded before the start of the first TPS session: four declined participation, and one had incidental findings on the baseline sMRI scan. Of the 60 participants included, 57 completed the 2-week experiment, and 3 withdrew. Two participants in the AIC group dropped out due to headaches, and one in the dACC group withdrew for personal reasons unrelated to the study procedures. In addition, improper data storage resulted in completely random missing data: endpoint data for the GNGT and BART from one AIC group participant; baseline data for the counting Stroop task, GNGT, and BART from one dACC group participant; and mood scales scores from 23 participants (n = 8 dACC, n = 8 AIC, n = 7 sham). Of the enrolled 60 participants, 22 (36.7%) were males; the mean age was 23.52 ± 8.60 years, and the mean years of education was 15.43 ± 2.13. Baseline characteristics across most outcome measures were comparable among the three groups (Table 13).

Table 13. Baseline characteristics of participants (n = 60) in Study 4

Variable			**AIC-TPS (n = 20)**	**dACC-TPS (n = 20)**	**Sham-TPS (n = 20)**	**p-value**
Male (n, %)			8, 40%	5, 25%	9, 45%	0.393
Age (y), mean (SD)			23.75 (9.32)	23.65 (7.76)	23.15 (9.07)	0.973
Education (y), mean (SD)			15.35 (1.90)	15.85 (1.93)	15.1 (2.54)	0.533
Baseline counting Stroop task	Interference	Accuracy (neutral vs. incongruent trials, %), mean (SD)	5.31 (4.25)	6.14 (7.62) [n=19]#	3.13 (2.98)	0.189
		RT (incongruent vs. neutral trials, s), mean (SD)	0.0730 (0.04247)	0.0621 (0.04927) [n=19]#	0.0709 (0.03674)	0.704
Baseline GNGT	50% No-Go trials	Accuracy of No-Go trials (%), mean (SD)	97.60 (3.02)	98.53 (2.39) [n=19]#	98.00 (3.18)	0.669
	20% No-Go trials	Accuracy of No-Go trials (%), mean (SD)	86.50 (12.68)	93.16 (10.57) [n=19]#	92.00 (15.76)	0.248
Baseline BART	Average Pumps (n), mean (SD)		4.69 (0.69)	4.91 (0.76) [n=19]#	4.65 (0.98)	0.560
	Adjusted average pumps (n), mean (SD)		4.70 (0.80)	4.89 (0.94) [n=19]#	4.75 (1.10)	0.803
	Exploded balloons (n), mean (SD)		12.85 (3.76)	14.05 (3.63) [n=19]#	13.70 (4.59)	0.631
Baseline RMET, mean (SD)			21.50 (2.04)	19.55 (1.91)	20.75 (3.13)	0.044*

Baseline SHS, mean (SD)	16.67 (20.85) [n=12]#	18.42 (4.87) [n=12]#	20.85 (4.39) [n=13]#	0.111
Baseline WEMWBS, mean (SD)	45.67 (9.03) [n=12]#	41.08 (7.83) [n=12]#	51.15 (11.00) [n=13]#	0.039*
Baseline POMS, mean (SD)	110.42 (26.37) [n=12]#	115.17(21.27) [n=12]#	108.23 (30.47) [n=13]#	0.802

AIC: anterior insula cortex; dACC: dorsal anterior cingulate cortex; RT: reaction time; HKD: Hong Kong dollar; BART: balloon analog risk task; REMT: reading the mind in the eyes test; SHS: subjective happiness scale; WEMWBS: Warwick-Edinburgh mental well-being scale; POMS: profile of mood states. #: exclusion of completely random missing data due to improper data storage; *: the baseline RMET score in the dACC group was significantly lower than that in the AIC group ($p_{corrected} = 0.041$); and the baseline WEMWBS score was significantly lower in the dACC group, compared to the sham group ($p_{corrected} = 0.035$).

5.3.2 Task performance and mood

Because most continuous outcome data were not normally distributed, they were not suitable for analysis with the planned LMM approach. Instead, Generalized Linear Mixed Models (GLMM) were employed. A Gamma distribution with a log link function was used for non-percentage data, while an identity link function was applied for percentage data. The model included Group (dACC x AIC x sham), Time (baseline vs. midpoint vs. endpoint), and their interaction as fixed effects. A random intercept for subjects was included to account for repeated measures, with an unstructured covariance type assumed.

5.3.2.1 Counting Stroop task performance

For both RT and accuracy interference, no significant interaction effects were found (RT interference: $p = 0.098$; accuracy interference: $p = 0.401$), nor were there significant main effects of Group (RT interference: $p = 0.557$; accuracy interference: $p = 0.448$). A significant main effect of Time was observed (RT interference: $p = 0.049$; accuracy interference: $p = 0.025$). Exploratory paired t-tests revealed no significant changes from baseline within individual groups. However, the dACC group demonstrated a marginally significant reduction in RT interference from Week 1 to Week 2 (midpoint vs. endpoint: 0.0788 ± 0.0093 vs. 0.0536 ± 0.0073 [mean±SE], $p_{corrected} = 0.054$). Changes in RT and accuracy interference across groups are presented in Appendices (Figures S1-S2).

5.3.2.2 BART performance

For the average number of pumps, no significant interaction effect ($p = 0.066$), or significant main effects of Time ($p = 0.274$) or Group ($p = 0.820$), were found. Exploratory paired t-tests revealed a significant increase in the AIC group from Week 1 to Week 2 (midpoint vs. endpoint: 4.6 ± 0.2 vs.4.9 ± 0.2 [mean ± SE], $p_{corrected} = 0.042$), with an overall effect size of 0.36 (Figure 19).

For the adjusted number of pumps, a significant interaction effect ($p = 0.026$) and main effect of Time ($p = 0.039$) were found, with no significant main effect of Group ($p = 0.838$). Post-hoc analyses showed a significant increase in the AIC group from Week 1 to Week 2 (midpoint vs. endpoint: 4.8 ± 0.2 vs. 5.2 ± 0.2 [mean ± SE], $p_{corrected} = 0.006$) and from baseline to endpoint (4.7 ± 0.2 vs. 5.2 ± 0.2 [mean ± SE], $p_{corrected} = 0.006$). The overall effect size is 0.74 (Figure 20).

For the number of exploded balloons, no significant interaction effect ($p = 0.340$) or main effect of Group ($p = 0.904$) was found; however, a significant main effect of Time ($p < 0.001$) was detected. Exploratory paired t-tests revealed a significant decrease in the dACC group after 2-week TPS (baseline vs. endpoint: 13.5 ± 1.3 vs. 11.0 ± 1.0 [mean ± SE], $p_{corrected} = 0.019$), with an overall effect size of 0.64 (Figure 21).

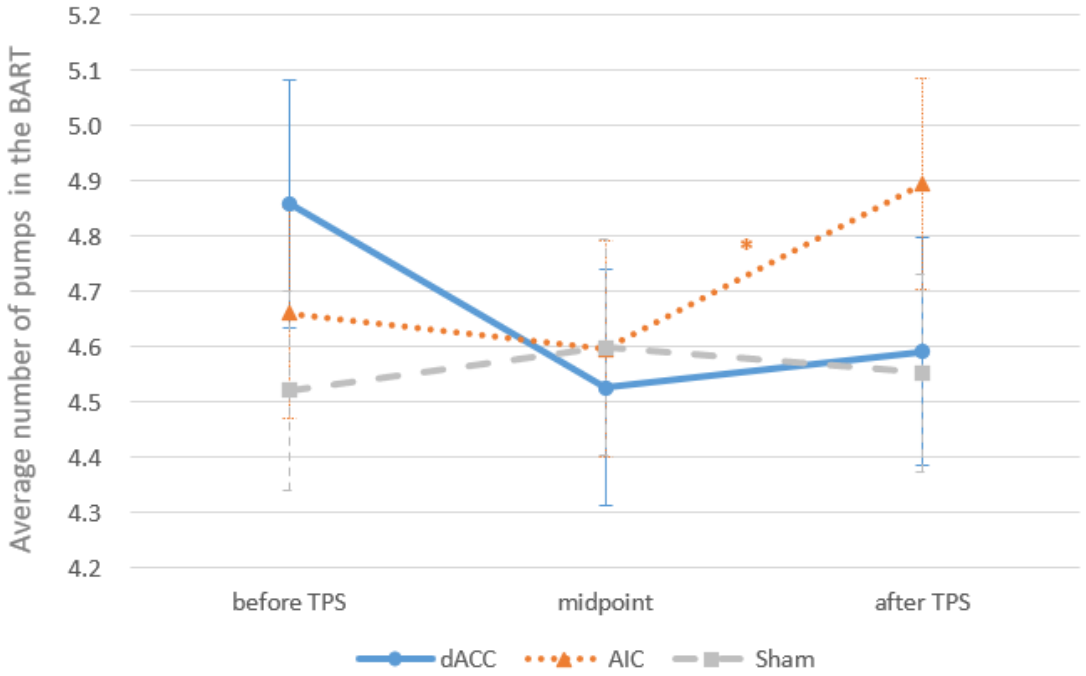

Figure 19. Average number of pumps in the BART. The dots, triangles, and squares indicate the mean values in the dACC, AIC, and sham groups, respectively; The bars indicate the standard errors. *: p-value < 0.05 after Bonferroni correction. The asterisk indicates an AIC within-group difference between the midpoint and the endpoint.

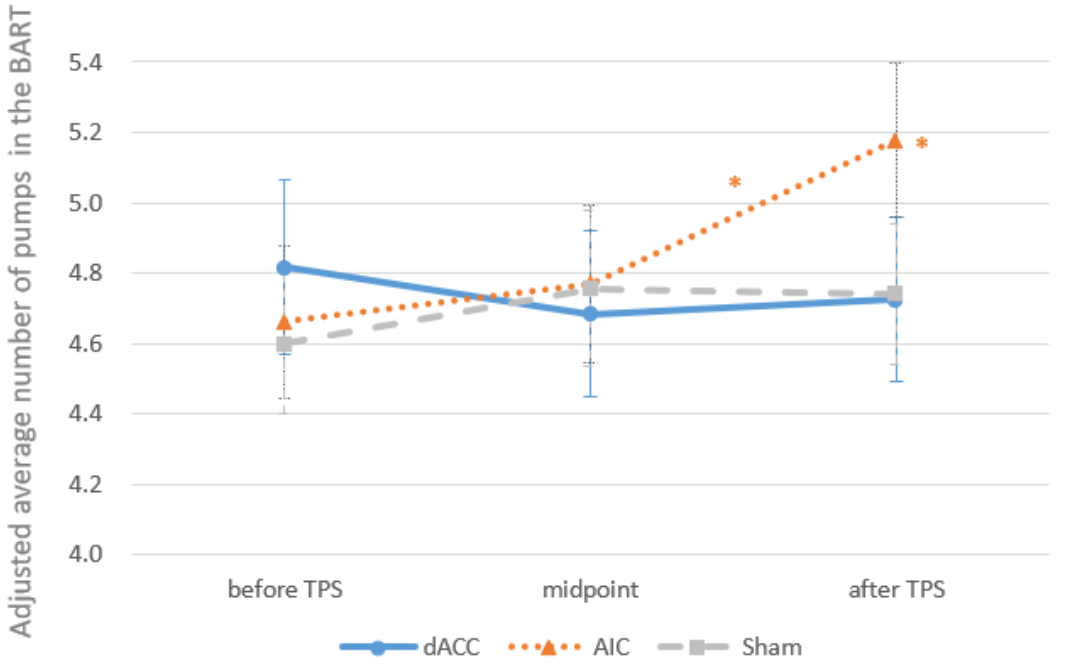

Figure 20. Adjusted average number of pumps in the BART. The dots, triangles, and squares indicate the mean values in the dACC, AIC, and sham groups, respectively; The bars indicate the standard errors. *: p-value < 0.05 after Bonferroni correction. The asterisk above the line

indicates the within-group difference between the midpoint and the endpoint. The asterisk beside the line indicates an AIC within-group difference between baseline and endpoint.

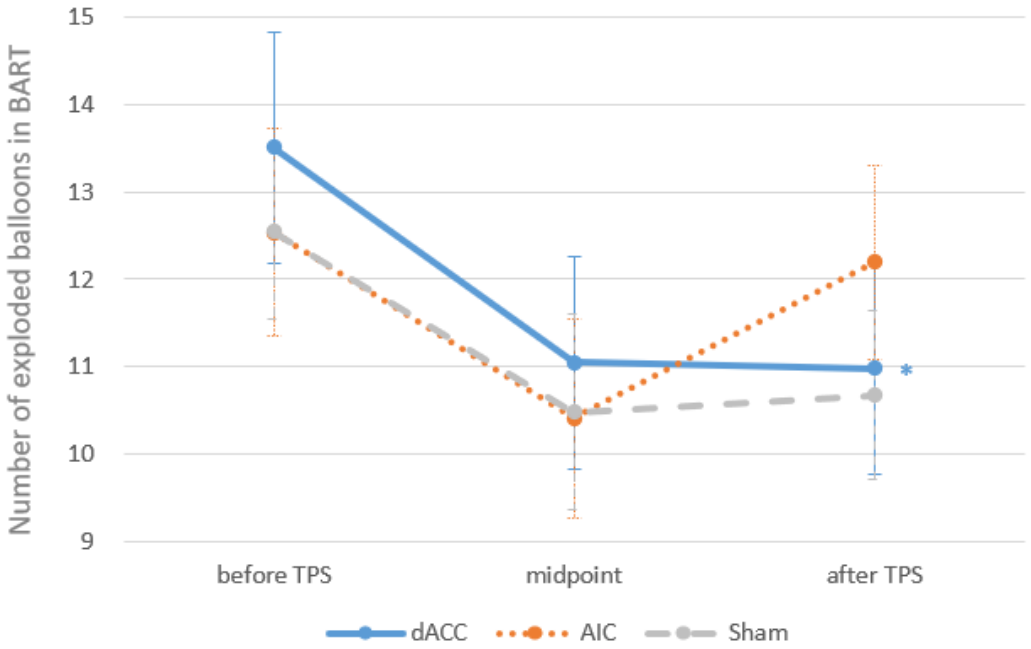

Figure 21. Number of exploded balloons in the BART. The dots, triangles, and squares indicate the mean values in dACC, AIC, and control groups, respectively; The bars indicate the standard errors. *: p-value < 0.05 after Bonferroni correction. The asterisk beside the line indicates a dACC within-group difference between baseline and endpoint.

5.3.2.3 GNGT performance

For both GNGT versions (20% No-Go trials and 50% No-Go trials), no significant interaction effects were found ($p = 0.312$ for 50% No-Go; $p = 0.781$ for 20% No-Go). Similarly, there were no significant main effects of Time ($p = 0.163$ for 50% No-Go; $p = 0.747$ for 20% No-Go) or Group ($p = 0.290$ for 50% No-Go; $p = 0.918$ for 20% No-Go). Exploratory paired t-tests also revealed no significant changes from baseline within individual groups. Changes in FAR for both GNGT versions (50% and 20% No-Go trials) across the three groups are shown in Appendices (Figures S3-S4).

5.3.2.4 RMET performance

No significant interaction effect ($p = 0.615$) was found for RMET scores; however, a significant main effect of Group ($p = 0.007$) and Time ($p = 0.037$) was found. Exploratory paired t-tests revealed that RMET scores in the dACC group were significantly lower than those in the AIC group at both baseline (dACC vs. AIC: 19.5 ± 0.5 vs. 21.4 ± 0.5 [mean ± SE], $p_{corrected} = 0.024$) and midpoint (dACC vs. AIC: 20.0 ± 0.5 vs. 22.0 ± 0.5 [mean ± SE], $p_{corrected} = 0.019$). At the midpoint, RMET scores in the dACC group were also significantly lower than those in the sham group (dACC vs. sham: 20.0 ± 0.5 vs. 22.0 ± 0.5 [mean ± SE], $p_{corrected} = 0.019$). In addition, the sham group demonstrated a significant improvement after 1 week of TPS (baseline vs. midpoint: 20.6 ± 0.5 vs. 22.0 ± 0.5 [mean ± SE], $p_{corrected} = 0.030$) (Appendices, Figure S5).

5.3.2.5 Mood

No significant interaction effects, main effects, or paired t-tests results were found for the SHS, WEMWBS, or POMS (Appendices, Figures S6-S8).

5.3.3 Rs-fMRI findings

Of the 57 participants who completed psychological assessments (n = 19 dACC, n = 18 AIC, n = 20 sham), all underwent endpoint MRI measurements. Four fMRI datasets were excluded due to poor normalization quality during preprocessing (n = 1 dACC, n = 2 sham, n = 1 AIC). Therefore, the final fMRI analysis included both baseline and

endpoint fMRI data from 53 participants (n = 18 dACC, n = 17 AIC, n = 18 sham).

5.3.3.1 Seed-based rsFC changes following TPS

Seed-based, voxel-wise rsFC analyses were conducted to evaluate target-seeded rsFC changes following TPS. The predefined seed regions were: (1) rdACC: MNI coordinates x = 7, y = 30, z = 40 mm; (2) ldACC: MNI coordinates x = -4, y = 26, z = 45 mm; (3) rAIC: MNI coordinates x = 44, y = 9, z = 2 mm; and (4) lAIC: MNI coordinates x = -41, y = 6, z = 3 mm. A spherical radius of 15 mm was applied to each seed region.

Following dACC stimulation, a significant interaction effect (dACC vs. sham x post-TPS vs. pre-TPS) was found in rdACC-seeded rsFC with the bilateral inferior frontal gyrus (orbital and triangular parts), right superior frontal gyrus (including the medial part), and bilateral cuneus. In addition, a significant interaction effect was found in ldACC-seeded rsFC with the bilateral inferior frontal gyrus (orbital and triangular parts). Post-hoc analyses revealed that, compared to the sham group, the dACC group exhibited greater rsFC enhancement between the dACC and the aforementioned regions, with the exception of the bilateral cuneus (Table 14 and Figure 22).

Table 14. Rs-FC results displaying clusters with a significant interaction effect (dACC vs. sham x post vs. pre) and the corresponding post-hoc analyses (completers: n=18 dACC group; n=18 sham group)

			Interaction effect				Post-hoc analysis, pre vs. post		Post-hoc analysis, active vs. sham	
	Cluster No.	**Brain regions defined by AAL**	**F**	**k**	**Peak MNI coordinates, x y z**	**AAL for the peak MNI**	**dACC**	**sham**	**pre-TPS**	**post-TPS**
rdACC-seeded	Cluster 1	Frontal_Inf_Orb_R; Frontal_Inf_Tri_R	44.72 ($P_{FWE-corr}$ = 0.001; $P_{FDR-corr}$ = 0.005)	99	39 36 -6	Frontal_Inf_Orb_R	t = -0.818, p = 0.425	t = -0.547, p = 0.592	t = 0.649, p = 0.521	t = 0.741, p = 0.464
	Cluster 2	Frontal_Inf_Orb_L; Frontal_Inf_Tri_L	33.68 ($P_{FWE-corr}$ = 0.004; $P_{FDR-corr}$ = 0.006)	81	-33 33 -12	Frontal_Inf_Orb_L	t = -1.192, p = 0.250	t = -0.400, p = 0.694	t = 1.471, p = 0.151	t = 1.509, p = 0.141
	Cluster 3	Frontal_Sup_Medial_R; Frontal_Sup_R; Frontal_Mid_R	30.63 ($P_{FWE-corr}$ = 0.004; $P_{FDR-corr}$ = 0.006)	80	9 54 48	Frontal_Sup_Medial_R	t = -1.766, p = 0.095	t = -0.661, p = 0.517	t = 0.394, p = 0.696	t = 1.162, p = 0.253
	Cluster 4	Cuneus_R, L	36.16 ($P_{FWE-corr}$ = 0.043; $P_{FDR-corr}$ = 0.049)	47	9 -90 30	Cuneus_R	t = -0.914, p = 0.373	t = -1.001, p = 0.331	t = 1.087, p = 0.285	t = 0.977, p = 0.336

ldACC-seeded	Cluster 1	Frontal_Inf_Orb_R; Frontal_Inf_Tri_R	47.32 ($P_{FWE\text{-}corr}$ < 0.0001; $P_{FDR\text{-}corr}$ = 0.001)	128	39 36 -6	Frontal_Inf_Orb_R	t = -1.472, p = 0.159	t = -0.305, p = 0.764	t = 0.490, p = 0.627	t = 0.938, p = 0.178
	Cluster 2	Frontal_Inf_Orb_L; Frontal_Inf_Tri_L	34.54 ($P_{FWE\text{-}corr}$ = 0.004; $P_{FDR\text{-}corr}$ = 0.008)	87	-42 33 -9	Frontal_Inf_Orb_L	t = -1.258, p = 0.225	t = -0.814, p = 0.427	t = 0.770, p = 0.446	t = 0.715, p = 0.480

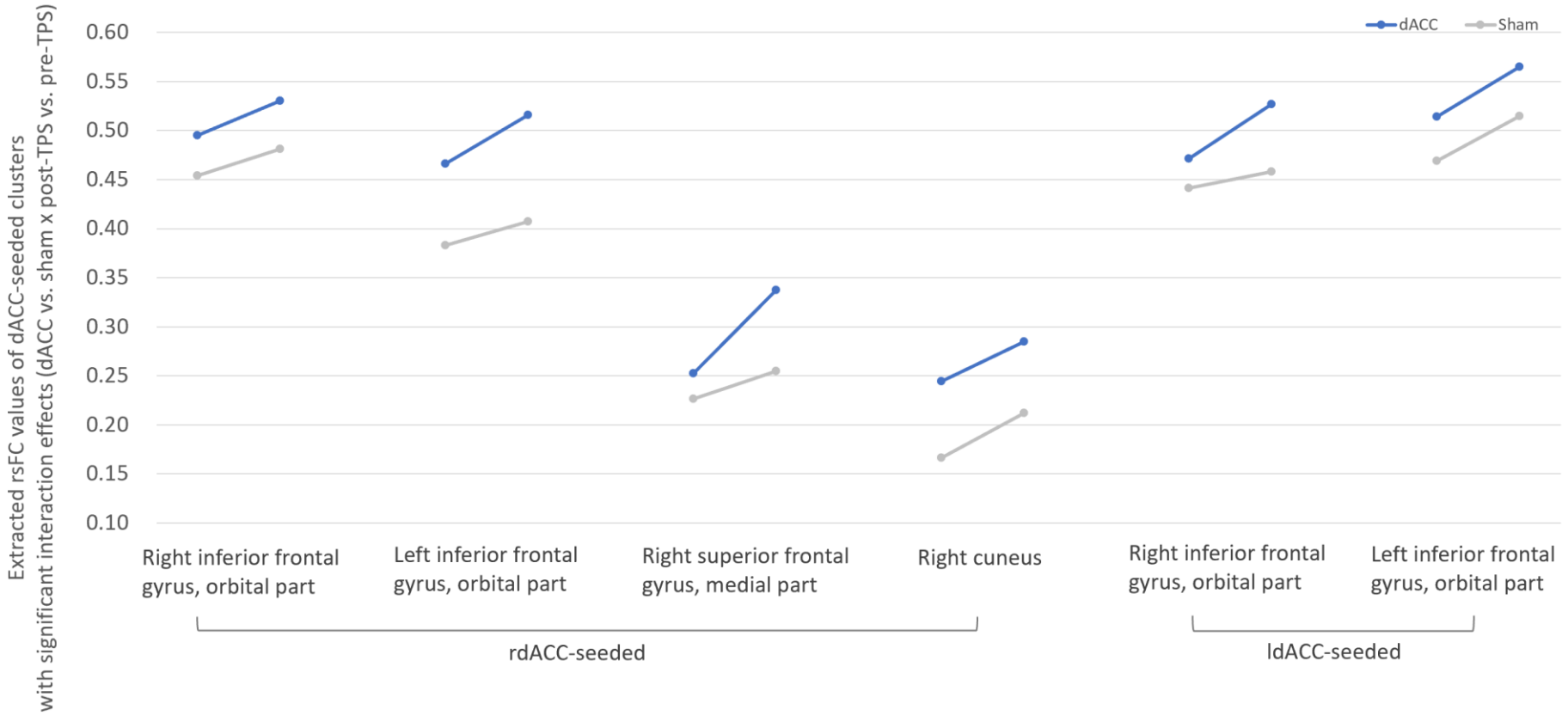

Figure 22. dACC-seeded rsFC changes in clusters showing a significant interaction effect (dACC vs. sham x post-TPS vs. pre-TPS). The dots represent mean rsFC values extracted at pre-TPS and post-TPS for individual clusters. rdACC-seeded rsFC: significant interaction effects were observed with clusters whose peak MNI coordinates were located in the bilateral inferior gyrus (orbital part), right superior frontal gyrus (medial part), and right cuneus. ldACC-seeded rsFC: significant interaction effects were observed with clusters whose peak MNI coordinates were located in the bilateral inferior gyrus (orbital part).

Following AIC stimulation, a significant interaction effect was found in rAIC-seeded rsFC with the right angular gyrus, bilateral middle temporal gyrus, bilateral middle occipital gyrus, right inferior frontal gyrus (opercular and triangular parts), right middle frontal gyrus, right precentral gyrus, left superior occipital gyrus, left cuneus, left superior parietal gyrus, and left middle cingulum. Moreover, a significant interaction effect was found in lAIC-seeded rsFC with the right angular gyrus, bilateral middle temporal gyrus, bilateral middle occipital gyrus, right superior temporal gyrus, and supramarginal gyrus. Post-hoc analyses revealed that, compared with the sham group, the AIC group showed reduced AIC-seeded rsFC enhancement or reduced AIC-seeded rsFC with all aforementioned clusters (Table 15 and Figure 23).

Table 15. Rs-FC results displaying clusters with a significant interaction effect (AIC vs. sham x post vs. pre) and the corresponding post-hoc analysis (completers: n=17 AIC group; n=18 sham group).

			Interaction effect				Post-hoc analysis, pre vs. post		Post-hoc analysis, active vs. sham	
	Cluster No.	**Brain regions defined by AAL**	**F**	**k**	**Peak MNI coordinates, x y z**	**AAL for the peak MNI**	**AIC**	**sham**	**pre-TPS**	**post-TPS**
rAIC-seeded	Cluster 1	Angular_R; Temporal_Mid_R; Occipital_Mid_R	56.05 ($P_{FWE\text{-}corr}$ < 0.0001; $P_{FDR\text{-}corr}$ < 0.0001)	574	42-48 24	Angular_R	t = -0.740, p = 0.470	t = -2.220, p = 0.040*	t = 0.621, p = 0.539	t = -0.659, p = 0.514
	Cluster 2	Temporal_Mid_L; Occipital_Mid_L	50.64 ($P_{FWE\text{-}corr}$ < 0.0001; $P_{FDR\text{-}corr}$ < 0.0001)	211	-51 -57 12	Temporal_Mid_L	t = 0.051, p = 0.960	t = -2.063, p = 0.055	t = 1.050, p = 0.305	t = -0.367, p = 0.716
	Cluster 3	Frontal_Inf_Oper_R; Frontal_Mid_R; Frontal_Inf_Tri_R Precentral_R	44.96 ($P_{FWE\text{-}corr}$ = 0.002; $P_{FDR\text{-}corr}$ = 0.004)	91	33 9 36	Frontal_Inf_Oper_R	t = 0.573, p = 0.575	t = -1.076, p = 0.297	t = 0.436, p = 0.666	t = -0.440, p = 0.663
	Cluster 4	Occipital_Sup_L; Cuneus_L; Parietal_Sup_L	41.60 ($P_{FWE\text{-}corr}$ = 0.002; $P_{FDR\text{-}corr}$ = 0.004)	88	-15 -84 42	Occipital_Sup_L	t = 0.128, p = 0.900	t = -0.397, p = 0.696	t = 0.627, p = 0.535	t = 0.169, p = 0.867

	Cluster 5	Cingulum_Mid_L	35.54 ($P_{FWE\text{-}corr}$ = 0.008; $P_{FDR\text{-}corr}$ = 0.011)	69 -12 -27 45	Cingulum_Mid_L	t = 0.294, p = 0.772	t = -0.670, p = 0.512	t = 0.723, p = 0.475	t = -0.081, p = 0.936
lAIC-seeded	Cluster 1	Angular_R; Temporal_Mid_R; Occipital_Mid_R	37.40 ($P_{FWE\text{-}corr}$ = 0.001; $P_{FDR\text{-}corr}$ = 0.003)	113 42 -48 24	Angular_R	t = -1.030, p = 0.318	t = -2.556, p = 0.020*	t = 0.359, p = 0.722	t = -0.968, p = 0.340
	Cluster 2	Temporal_Mid_L; Occipital_Mid_L	35.71 ($P_{FWE\text{-}corr}$ < 0.0001; $P_{FDR\text{-}corr}$ < 0.0001)	165 -48 -57 12	Temporal_Mid_L	t = -0.424, p = 0.677	t = -2.137, p = 0.047*	t = 0.194, p = 0.848	t = -0.830, p = 0.412
	Cluster 3	Temporal_Sup_R; SupraMarginal_R	29.10 ($P_{FWE\text{-}corr}$ = 0.035; $P_{FDR\text{-}corr}$ = 0.075)	54 66 -36 21	Temporal_Sup_R	t = 1.602, p = 0.129	t = -0.398, p = 0.696	t = 1.650, p = 0.108	t = 0.241, p = 0.811

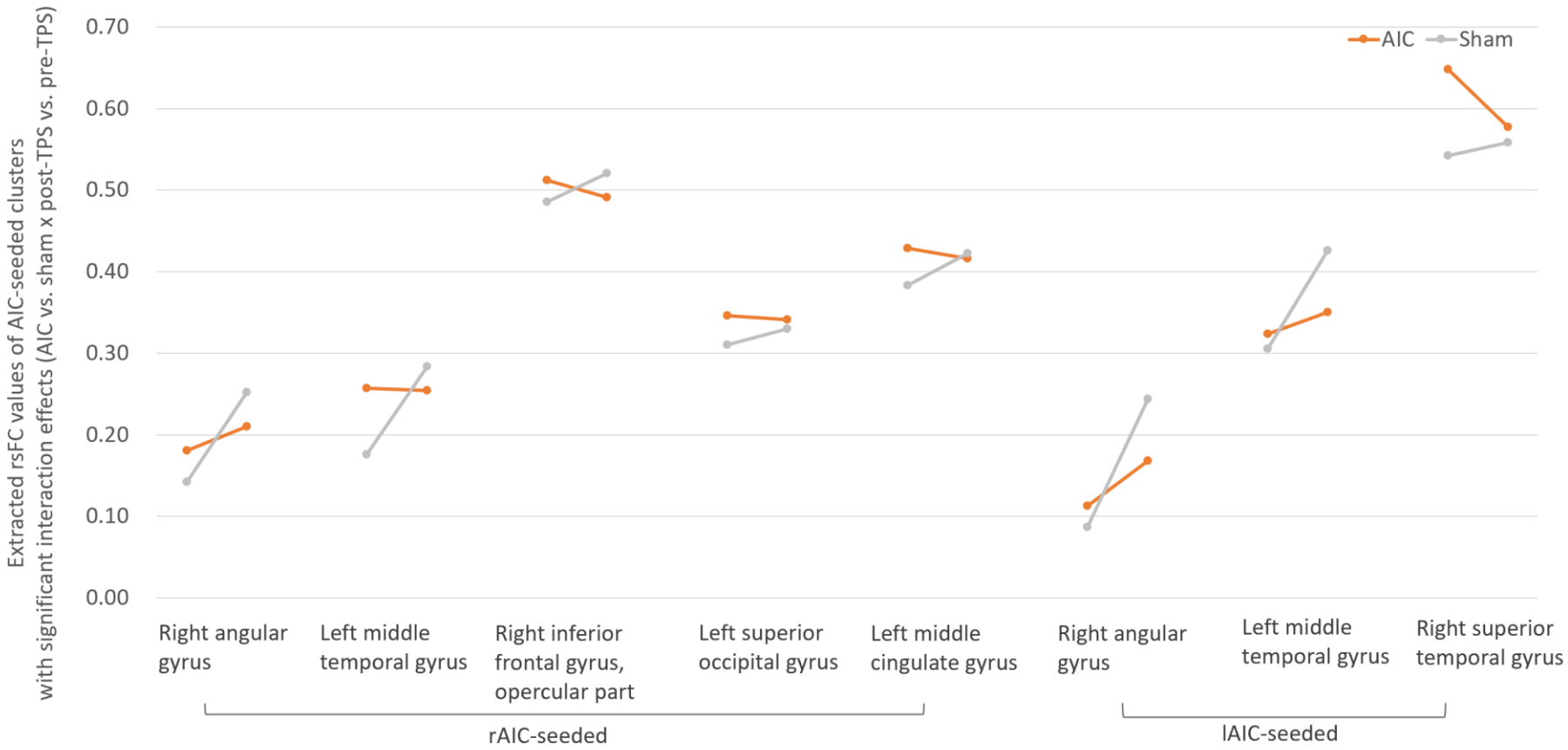

Figure 23. AIC-seeded rsFC changes in clusters showing significant interaction effects (AIC vs. sham x post-TPS vs. pre-TPS). The dots represent mean rsFC values extracted at pre-TPS and post-TPS for individual clusters. rAIC-seeded rsFC: significant interaction effects were observed with clusters whose peak MNI coordinates were located in the right angular gyrus, left middle temporal gyrus, right inferior frontal gyrus (opercular part), and left superior

occipital gyrus. lAIC-seeded rsFC: significant interaction effects were observed with clusters whose peak MNI coordinates were located in the right angular gyrus, left middle temporal gyrus, and right superior temporal gyrus.

To determine whether the rsFC changes reflected target-specific neuromodulation rather than a non-specific global stimulation effect, exploratory analyses were conducted: (1) AIC-seeded rsFC changes following dACC stimulation, and (2) dACC-seeded rsFC changes following AIC stimulation. The results showed that rsFC between the AIC and most regions with a significant interaction effect (dACC vs. sham x post-TPS vs. pre-TPS) increased following dACC stimulation (Appendices, Table S8 and Figure S9). Conversely, rsFC between the dACC and most regions with a significant interaction effect (AIC vs. sham x post-TPS vs. pre-TPS) decreased after AIC stimulation (Appendices, Table S9 and Figure S10). These divergent, target-dependent patterns of rsFC change provide evidence that TPS induced a target-specific neuromodulatory effect.

5.3.3.2 Association between changes in target-seeded rsFC and changes in psychological assessment

Correlation analyses were performed to examine associations between changes in target-seeded rsFC and changes in task performance or mood. Both cluster-wise and whole-brain-wise approaches were applied for each group. For cluster-wise correlation analysis, the average rsFC values of clusters showing significant interaction effects were extracted, and Pearson's correlations were performed with behavioral/ mood outcomes of interest using SPSS. For the whole-brain-wise correlation analysis, multiple regression analyses were conducted in SPM12 (Matlab 2023a) to identify clusters showing significant correlations with behavioral/ mood

outcomes of interest. The behavioral and mood outcomes of interest were those that had demonstrated significant changes from baseline within individual groups. Specifically, for the dACC group, the outcome of interest was the number of exploded balloons in the BART, and for the AIC group, the outcome of interest was the adjusted average pumps in the BART.

Cluster-wise correlation analyses showed that enhancement in rdACC-seeded rsFC with the right superior frontal gyrus (including the medial part) was significantly correlated with a decrease in the number of exploded balloons in the BART ($r = -0.501$, $p_{uncorrected} = 0.041$). However, this correlation did not survive correction for multiple comparisons. Regarding the AIC group, no significant cluster-wise correlations were observed between rAIC-seeded rsFC and the adjusted number of pumps in the BART. To further examine stimulation specificity, cluster-wise correlation analyses were also conducted for the sham group. No significant correlations were found between changes in dACC- or AIC-seeded rsFC and corresponding changes in the task performance following sham stimulation.

Whole-brain-wise correlation analysis revealed that, following dACC stimulation, changes in rdACC-seeded rsFC with the left superior frontal gyrus (including the medial part) were significantly negatively correlated with the changes in the number of exploded balloons in the BART. In contrast, no significant whole-brain-wise correlations were observed between AIC-seeded rsFC and the adjusted number of pumps in the BART following AIC stimulation. To further examine stimulation

specificity, whole-brain-wise correlation analyses were also conducted for the sham group. No significant correlations were found between changes in dACC- or AIC-seeded rsFC and corresponding changes in the task performance following sham stimulation.

5.3.4 Self-perception of TPS's efficacy

At the end of the experiment, participants were asked about their perceptions of TPS efficacy on task performance and mood. Among completers, 7 of 18 participants in the AIC-TPS group (39%), 8 of 19 participants in the dACC-TPS group (42%), and 5 of 20 participants in the sham group (25%) reported that TPS had affected their performance or mood. Of note, among these participants, all 8 in the dACC group, all 5 in the sham group, and 5 of 7 in the AIC group perceived improvement after stimulation, whereas 2 of 7 participants in the AIC group reported worse performance.

5.3.5 Safety

Among the 60 participants, all in the AIC-TPS and dACC-TPS groups, and 15 participants (75%) in the sham group reported mild to moderate side effects. The most common were tingling and pain at the stimulation site. Nearly all symptoms resolved spontaneously within 12 hours without the need for medication. One participant in the AIC group reported pain (VAS = 6) at the stimulated site and headache (VAS = 6) after AIC stimulation, which temporarily affected sleep quality but resolved

spontaneously within two days. Detailed information on adverse events is provided in Table 16.

Table 16. Adverse events occurred during the experimental period in Study 4

	AIC-TPS (n=20)	**dACC-TPS (n=20)**	**Sham vertex-TPS (n=20)**
	Number of participants reporting each adverse event during stimulation (%)		
Tingling	19 (95%)	15 (75%)	2 (10%)
pain	8 (40%)	3 (15%)	4 (20%)
Pressure sensation	3 (15%)	4 (20%)	1 (5%)
Striking sensation	1 (5%)	7 (35%)	1 (5%)
Dizziness	2 (10%)	2 (10%)	3 (15%)
Sleepiness	1 (5%)	2 (10%)	2 (10%)
numbness	2 (10%)	4 (20%)	
Headache	4 (20%)	1 (5%)	
Heating		3 (15%)	1 (5%)
Tinnitus		1 (5%)	2 (10%)
Blurred vision		1 (5%)	2 (10%)
Numbness in the arms/legs/hands	2 (10%)	1 (5%)	
Vibration in the ears	1 (5%)		1 (5%)
Nausea		1 (5%)	
Pain around the ears		1 (5%)	
Neck pain		1 (5%)	3 (15%)
Pain in the temple	1 (5%)	1 (5%)	
Muscle tightness in the face			1 (5%)
	Number of participants reporting each adverse event after stimulation (%)		
Headache	4 (20%)	1 (5%)	
Dizziness	1 (5%)	2 (10%)	2 (10%)

Pain	2 (10%)		1 (5%)
Tingling	1 (5%)		1 (5%)
Sleepiness		1 (5%)	1 (5%)
Numbness in the hands		1 (5%)	

AIC-TPS: transcranial pulse stimulation over the bilateral anterior insula cortex; dACC-TPS: transcranial pulse stimulation over the bilateral dorsal anterior cingulate cortex; Sham vertex-TPS: sham transcranial pulse stimulation over the vertex; NA: not applicable.

5.4 Discussion

5.4.1 Feasibility and safety of TPS for stimulating the dACC and AIC

Our findings demonstrated that ten sessions of dACC-TPS and AIC-TPS administered over a two-week period are both feasible and safe in healthy adults. Mild AEs, primarily transient tingling and pain at the stimulation site, were reported in all participants in the AIC-TPS and dACC-TPS groups and by 15 out of 20 participants in the sham group. All symptoms resolved within 12 hours without medication. One moderate AE - pain (VAS = 6) at the stimulated site, accompanied by headache (VAS = 6) following stimulation - was reported by a participant in the AIC group; this event temporarily affected sleep quality but resolved spontaneously within two days. Overall, the low dropout rate of 5% further supports the feasibility of TPS for stimulating the dACC and AIC.

The AE rate in our study was higher than that reported for fTUS in the literature. For example, in a fTUS study targeting the amygdala, only 2 out of 29 participants (6.9%) reported AEs such as headache and irritability during the treatment period (Barksdale et al., 2025). On the other hand, while all participants in our dACC-TPS and AIC-TPS groups reported AEs, the incidence of individual AEs was higher in the AIC-TPS group. Specifically, as shown in Table 16, tingling was reported by 19 of 20 participants (95%) and pain by 8 of 20 (40%) in the AIC-TPS group, compared with 75% and 15%, respectively, in the dACC-TPS group. A likely explanation for these region-specific differences in AEs is the distinct scalp locations and their relative sensitivities to pain: for dACC

stimulation, the TPS handpiece is positioned at the forehead, whereas for AIC stimulation, it is placed at the temple, a site that is more sensitive to pain.

5.4.2 Stimulation effects on behavioral performance

Study 4 provided evidence that dACC stimulation decreases impulsivity, whereas AIC stimulation increases impulsivity. Specifically, ten sessions of TPS over two weeks modulated performance on the BART following dACC and AIC stimulation, compared with sham stimulation. A significant decrease in the number of exploded balloons in the BART was observed following dACC stimulation, but not following AIC or sham stimulation. Conversely, an increase in the adjusted average number of pumps was observed following AIC stimulation, compared with both dACC and sham stimulation. These findings demonstrate that TPS modulates region-specific functions, consistent with prior fMRI evidence. Specifically, the dACC has been implicated in evaluating the value of cash-outs, and the AIC has been associated with the number of pumps in the BART (Schonberg et al., 2012).

5.4.3 Stimulation effects on rsFC

Target-specific TPS-induced changes in rsFC were observed following both dACC and AIC stimulation, compared with sham stimulation. Our results showed that dACC stimulation increased the rsFC of dACC, which aligns with the findings from a transcranial focused ultrasound study (Yaakub et al., 2023). In contrast, AIC stimulation was found to reduce the AIC-seeded rsFC. Previous studies have established the rsFC

profiles for the dACC and AIC. The dACC shows positive rsFC with prefrontal regions such as the ventrolateral prefrontal cortex and DLPFC, which is linked to higher-order cognitive function (Margulies et al., 2007). Similarly, the AIC exhibits positive rsFC with middle and inferior frontal (Cauda et al., 2011) and superior temporal cortices (Ghaziri et al., 2024), facilitating the integration of cognitive, homeostatic, and emotional processes. Taken together, our findings suggest that TPS of the dACC enhances its positive rsFC with the cognitive control network, whereas TPS of the AIC attenuates its positive rsFC with the integrative network. This discrepancy may reflect the distinct functional roles of these regions within the SN. The dACC appears to be more engaged in processing external environmental signals, while the AIC is more sensitive to internal signals (Koutsoumpari et al., 2025). This divergence – extrinsic versus intrinsic – could account for the different patterns of rsFC changes induced by external stimulation such as TPS. Similarly, prior TPS studies have reported both increases and decreases in rsFC following stimulation. For example, enhanced global efficiency within the cortical sensorimotor network was observed after somatosensory cortex-TPS in healthy adults compared with sham stimulation (Matt et al., 2022). Upregulated global efficiency in the dorsal attention network was also found following whole-brain stimulation in patients with Alzheimer's disease compared to the baseline (Matt et al., 2025). Conversely, down-regulation of rsFC (compared to the baseline) within the limbic system following whole-brain stimulation predicted improved global cognition in participants with mild cognitive impairment (Lo et al., 2024). The

predominant mechanistic framework for TPS, based on mechanotransduction (d'Agostino et al., 2015), posits that its effects are driven by neural excitation. This process enhances cellular metabolism by activating mechanosensitive ion channels and upregulating brain-derived neurotrophic factor and vascular endothelial growth factor, thereby promoting neurogenesis and angiogenesis (Ito, Fukumoto, and Shimokawa, 2009; Matsuda et al., 2020; Sun et al., 2006; Yahata et al., 2016). However, this excitatory model alone cannot fully explain the bidirectional effects observed across studies. Therefore, the target-specific effects identified in our study highlight the need for further investigation into the mechanisms underlying TPS.

5.4.4 Study limitations

Study 4 has several limitations. First, as a pilot study, the sample size was relatively small, resulting in limited statistical power to validate the efficacy of dACC-TPS or AIC-TPS. Second, although changes in behavioral performance were observed after ten sessions of dACC-TPS and AIC-TPS, the long-term efficacy of these stimulations remains uninvestigated. Third, the absence of significant correlations between behavioral and neuroimaging outcomes leaves the underlying neural mechanisms of TPS's modulatory effects uncertain.

5.4.5 Future research direction

Study 4 provides preliminary groundwork for the future clinical application of TPS for targeting deeper brain regions. However, before

clinical application in depression treatment, further studies are needed to (1) employ larger sample sizes to confirm the short-term and long-term efficacy of dACC-TPS and AIC-TPS, and (2) utilize online neuroimaging or neurophysiological investigations to further elucidate the neural mechanisms underlying these modulatory effects.

5.5 References

Barksdale, B. R., L. Enten, A. DeMarco, R. Kline, M. K. Doss, C. B. Nemeroff, and G. A. Fonzo. 2025. 'Low-intensity transcranial focused ultrasound amygdala neuromodulation: a double-blind sham-controlled target engagement study and unblinded single-arm clinical trial', *Mol Psychiatry*, 30: 4497-511.

Baron-Cohen, Simon, Sally Wheelwright, Jacqueline Hill, Yogini Raste, and Ian Plumb. 2001. 'The "Reading the Mind in the Eyes" Test revised version: a study with normal adults, and adults with Asperger syndrome or high-functioning autism', *The Journal of Child Psychology and Psychiatry and Allied Disciplines*, 42: 241-51.

Beisteiner, R., and E. Matt. 2025. 'Ultrasound neuromodulation - How deep can we stimulate?', *Brain Stimul*, 18: 15-18.

Beisteiner, R., E. Matt, C. Fan, H. Baldysiak, M. Schonfeld, T. Philippi Novak, A. Amini, T. Aslan, R. Reinecke, J. Lehrner, A. Weber, U. Reime, C. Goldenstedt, E. Marlinghaus, M. Hallett, and H. Lohse-Busch. 2020. 'Transcranial Pulse Stimulation with Ultrasound in Alzheimer's Disease-A New Navigated Focal Brain Therapy', *Adv Sci (Weinh)*, 7: 1902583.

Bush, G., P. J. Whalen, L. M. Shin, and S. L. Rauch. 2006. 'The counting Stroop: a cognitive interference task', *Nat Protoc*, 1: 230-3.

Bush, George, Paul J. Whalen, Bruce R. Rosen, Michael A. Jenike, Sean C. McInerney, and Scott L. Rauch. 1998. 'The counting stroop: An interference task specialized for functional neuroimaging-validation study with functional MRI', *Human brain mapping*, 6: 270-82.

Cauda, F., F. D'Agata, K. Sacco, S. Duca, G. Geminiani, and A. Vercelli. 2011. 'Functional connectivity of the insula in the resting brain', *Neuroimage*, 55: 8-23.

Chen, Kuei-Min, Mariah Snyder, and Kathleen Krichbaum. 2002. 'Translation and equivalence: the profile of mood states short form in English and Chinese', *International journal of nursing studies*, 39: 619-24.

Cheung, T., T. M. H. Li, Y. S. Ho, G. Kranz, K. N. K. Fong, S. F. Leung, S. C. Lam, W. F. Yeung, J. Y. T. Lam, K. H. Fong, R. Beisteiner, Y. T. Xiang, and C. P. W. Cheng.

2023. 'Effects of Transcranial Pulse Stimulation (TPS) on Adults with Symptoms of Depression-A Pilot Randomized Controlled Trial', *Int J Environ Res Public Health*, 20.

Cheung, T., T. M. H. Li, J. Y. T. Lam, K. H. Fong, L. Y. Chiu, Y. S. Ho, A. C. Tse, C. T. Li, C. P. Cheng, and R. Beisteiner. 2023. 'Effects of transcranial pulse stimulation on autism spectrum disorder: a double-blind, randomized, sham-controlled trial', *Brain Commun*, 5: fcad226.

Cheung, T., B. K. Yee, B. Chau, J. Y. T. Lam, K. H. Fong, H. Lo, T. M. H. Li, A. M. Li, L. Sun, R. Beisteiner, and C. P. W. Cheng. 2024. 'Efficacy and safety of transcranial pulse stimulation in young adolescents with attention-deficit/hyperactivity disorder: a pilot, randomized, double-blind, sham-controlled trial', *Front Neurol*, 15: 1364270.

d'Agostino, M. C., K. Craig, E. Tibalt, and S. Respizzi. 2015. 'Shock wave as biological therapeutic tool: From mechanical stimulation to recovery and healing, through mechanotransduction', *Int J Surg*, 24: 147-53.

Fong, T. K. H., T. Cheung, S. T. J. Ngan, K. Tong, W. Y. V. Lui, W. C. Chan, C. S. M. Wong, and C. P. W. Cheng. 2023. 'Transcranial pulse stimulation in the treatment of mild neurocognitive disorders', *Ann Clin Transl Neurol*, 10: 1885-90.

Fung, Sai-fu. 2019. 'Psychometric evaluation of the Warwick-Edinburgh Mental Well-being Scale (WEMWBS) with Chinese university students', *Health and Quality of Life Outcomes*, 17: 46.

Gandevia, B., and A. Tovell. 1964. 'DECLARATION OF HELSINKI', *Med J Aust*, 2: 320-1.

Ghaziri, J., P. Fei, A. Tucholka, S. Obaid, O. Boucher, I. Rouleau, and D. K. Nguyen. 2024. 'Resting-State Functional Connectivity Profile of Insular Subregions', *Brain Sci*, 14.

Goldstein-Piekarski, A. N., T. M. Ball, Z. Samara, B. R. Staveland, A. S. Keller, S. L. Fleming, K. A. Grisanzio, B. Holt-Gosselin, P. Stetz, J. Ma, and L. M. Williams. 2022. 'Mapping Neural Circuit Biotypes to Symptoms and Behavioral Dimensions of Depression and Anxiety', *Biol Psychiatry*, 91: 561-71.

Goodkind, M., S. B. Eickhoff, D. J. Oathes, Y. Jiang, A. Chang, L. B. Jones-Hagata, B. N. Ortega, Y. V. Zaiko, E. L. Roach, M. S. Korgaonkar, S. M. Grieve, I. Galatzer-Levy, P. T. Fox, and A. Etkin. 2015. 'Identification of a common neurobiological substrate for mental illness', *JAMA Psychiatry*, 72: 305-15.

Hayward, G., G. M. Goodwin, and C. J. Harmer. 2004. 'The role of the anterior cingulate cortex in the counting Stroop task', *Exp Brain Res*, 154: 355-8.

Ho, T. C., M. D. Sacchet, C. G. Connolly, D. S. Margulies, O. Tymofiyeva, M. P. Paulus, A. N. Simmons, I. H. Gotlib, and T. T. Yang. 2017. 'Inflexible Functional Connectivity of the Dorsal Anterior Cingulate Cortex in Adolescent Major Depressive Disorder', *Neuropsychopharmacology*, 42: 2434-45.

Ito, K., Y. Fukumoto, and H. Shimokawa. 2009. 'Extracorporeal shock wave therapy as a new and non-invasive angiogenic strategy', *Tohoku J Exp Med*, 219: 1-9.

Kaiser, R. H., J. R. Andrews-Hanna, T. D. Wager, and D. A. Pizzagalli. 2015. 'Large-Scale Network Dysfunction in Major Depressive Disorder: A Meta-analysis of Resting-State Functional Connectivity', *JAMA Psychiatry*, 72: 603-11.

Karakatsani, M. E., I. Gezginer, D. Nozdriukhin, S. Tiemann, H. A. I. Yoshihara, R. Storz, M. Belau, R. Ni, X. L. Dean-Ben, and D. Razansky. 2025. 'Transcranial pulse stimulation modulates neuronal activity and functional network dynamics', *Brain Stimul*, 18: 1834-42.

Koutsoumpari, Nomiki, Johannes Algermissen, Siti Yaakub, Hanneke E. M. den Ouden, Nadege Bault, and Elsa Fouragnan. 2025.

Lee, T. M. C., L. Liang, W. K. Hou, A. H. Y. Tse, and C. C. H. Chan. 2023. 'The Chinese "Reading the Mind in the Eyes" Test: A study with normal adults, and adults with Asperger syndrome/high-functioning autism', *Asian J Psychiatr*, 89: 103785.

Lefaucheur, J. P., A. Aleman, C. Baeken, D. H. Benninger, J. Brunelin, V. Di Lazzaro, S. R. Filipovic, C. Grefkes, A. Hasan, F. C. Hummel, S. K. Jaaskelainen, B. Langguth, L. Leocani, A. Londero, R. Nardone, J. P. Nguyen, T. Nyffeler, A. J. Oliveira-Maia, A. Oliviero, F. Padberg, U. Palm, W. Paulus, E. Poulet, A. Quartarone, F. Rachid, I. Rektorova, S. Rossi, H. Sahlsten, M. Schecklmann, D. Szekely, and U. Ziemann. 2020. 'Evidence-based guidelines on the therapeutic use of repetitive transcranial magnetic stimulation (rTMS): An update (2014-2018)', *Clin Neurophysiol*, 131: 474-528.

Lejuez, C. W., Jennifer P. Read, Christopher W. Kahler, Jerry B. Richards, Susan E. Ramsey, Gregory L. Stuart, David R. Strong, and Richard A. Brown. 2002. 'Evaluation of a behavioral measure of risk taking: The Balloon Analogue Risk Task (BART)', *Journal of Experimental Psychology: Applied*, 8: 75-84.

Lin, Shuqiong, Yu-Yu Hsiao, and Miao Wang. 2014. "Test review: the profile of mood states 2nd edition." In.: SAGE Publications Sage CA: Los Angeles, CA.

Lo, H. K., T. K. Fong, T. Cheung, S. J. Ngan, W. V. Lui, W. C. Chan, C. S. Wong, T. K. Wong, and C. P. Cheng. 2024. 'Enhanced Cognition and Modulation of Brain Connectivity in Mild Neurocognitive Disorder: The Promise of Transcranial Pulse Stimulation', *Biomedicines*, 12.

Lynch, C. J., I. G. Elbau, T. Ng, A. Ayaz, S. Zhu, D. Wolk, N. Manfredi, M. Johnson, M. Chang, J. Chou, I. Summerville, C. Ho, M. Lueckel, H. Bukhari, D. Buchanan, L. W. Victoria, N. Solomonov, E. Goldwaser, S. Moia, C. Caballero-Gaudes, J. Downar, F. Vila-Rodriguez, Z. J. Daskalakis, D. M. Blumberger, K. Kay, A. Aloysi, E. M. Gordon, M. T. Bhati, N. Williams, J. D. Power, B. Zebley, L. Grosenick, F. M.

Gunning, and C. Liston. 2024. 'Frontostriatal salience network expansion in individuals in depression', *Nature*, 633: 624-33.

Lyubomirsky, Sonja, and Heidi S Lepper. 1999. 'A measure of subjective happiness: Preliminary reliability and construct validation', *Social indicators research*, 46: 137-55.

Manganotti, P., M. Liccari, T. Maria Isabella Lombardo, J. Della Toffola, V. Cenacchi, M. Catalan, and P. Busan. 2025. 'Effect of a single session of transcranial pulse stimulation (TPS) on resting tremor in patients with Parkinson's disease', *Brain Res*, 1850: 149405.

Margulies, D. S., A. M. Kelly, L. Q. Uddin, B. B. Biswal, F. X. Castellanos, and M. P. Milham. 2007. 'Mapping the functional connectivity of anterior cingulate cortex', *Neuroimage*, 37: 579-88.

Matsuda, M., H. Kanno, T. Sugaya, S. Yamaya, K. Yahata, K. Handa, T. Shindo, H. Shimokawa, H. Ozawa, and E. Itoi. 2020. 'Low-energy extracorporeal shock wave therapy promotes BDNF expression and improves functional recovery after spinal cord injury in rats', *Exp Neurol*, 328: 113251.

Matt, E., L. Kaindl, S. Tenk, A. Egger, T. Kolarova, N. Karahasanovic, A. Amini, A. Arslan, K. Saricicek, A. Weber, and R. Beisteiner. 2022. 'First evidence of long-term effects of transcranial pulse stimulation (TPS) on the human brain', *J Transl Med*, 20: 26.

Matt, Eva, Michael Mitterwallner, Sonja Radjenovic, Daria Grigoryeva, Alexandra Weber, Elisabeth Stögmann, Alina Domitner, Anna Zettl, Sarah Osou, and Roland Beisteiner. 2025. 'Ultrasound Neuromodulation With Transcranial Pulse Stimulation in Alzheimer Disease', *JAMA Network Open*, 8.

Menon, V., and L. Q. Uddin. 2010. 'Saliency, switching, attention and control: a network model of insula function', *Brain Struct Funct*, 214: 655-67.

Moor, B. G., Z. A. Macks, B. Güroglu, S. A. Rombouts, M. W. Molen, and E. A. Crone. 2012. 'Neurodevelopmental changes of reading the mind in the eyes', *Soc Cogn Affect Neurosci*, 7: 44-52.

Mulders, P. C., P. F. van Eijndhoven, A. H. Schene, C. F. Beckmann, and I. Tendolkar. 2015. 'Resting-state functional connectivity in major depressive disorder: A review', *Neurosci Biobehav Rev*, 56: 330-44.

Nan, Hairong, Michael Y Ni, Paul H Lee, Wilson WS Tam, Tai Hing Lam, Gabriel M Leung, and Ian McDowell. 2014. 'Psychometric evaluation of the Chinese version of the Subjective Happiness Scale: evidence from the Hong Kong FAMILY Cohort', *International journal of behavioral medicine*, 21: 646-52.

Osou, S., S. Radjenovic, L. Bender, M. Gaal, A. Zettl, G. Dorl, E. Matt, and R. Beisteiner. 2024. 'Novel ultrasound neuromodulation therapy with transcranial pulse stimulation (TPS) in Parkinson's disease: a first retrospective analysis', *J Neurol*, 271: 1462-68.

Radjenovic, S., L. Bender, M. Gaal, D. Grigoryeva, M. Mitterwallner, S. Osou, A. Zettl, N. Plischek, P. Lachmair, K. Herzhauser, E. Matt, and R. Beisteiner. 2025. 'A retrospective analysis of ultrasound neuromodulation therapy using transcranial pulse stimulation in 58 dementia patients', *Psychol Med*, 55: e70.

Rao, H., M. Korczykowski, J. Pluta, A. Hoang, and J. A. Detre. 2008. 'Neural correlates of voluntary and involuntary risk taking in the human brain: an fMRI Study of the Balloon Analog Risk Task (BART)', *Neuroimage*, 42: 902-10.

Reddy, S., K. E. Kabotyanski, S. Hirani, T. Liu, Z. Naqvi, N. Giridharan, M. Hasen, N. R. Provenza, G. P. Banks, S. J. Mathew, W. K. Goodman, and S. A. Sheth. 2024. 'Efficacy of Deep Brain Stimulation for Treatment-Resistant Depression: Systematic Review and Meta-Analysis', *Biol Psychiatry Cogn Neurosci Neuroimaging*, 9: 1239-48.

Schonberg, T., C. R. Fox, J. A. Mumford, E. Congdon, C. Trepel, and R. A. Poldrack. 2012. 'Decreasing ventromedial prefrontal cortex activity during sequential risk-taking: an FMRI investigation of the balloon analog risk task', *Front Neurosci*, 6: 80.

Segal, A., L. Parkes, K. Aquino, S. M. Kia, T. Wolfers, B. Franke, M. Hoogman, C. F. Beckmann, L. T. Westlye, O. A. Andreassen, A. Zalesky, B. J. Harrison, C. G. Davey, C. Soriano-Mas, N. Cardoner, J. Tiego, M. Yucel, L. Braganza, C. Suo, M. Berk, S. Cotton, M. A. Bellgrove, A. F. Marquand, and A. Fornito. 2023. 'Regional, circuit and network heterogeneity of brain abnormalities in psychiatric disorders', *Nat Neurosci*, 26: 1613-29.

Shang, C. Y., C. Sheng, L. K. Yang, T. L. Chou, and S. S. Gau. 2018. 'Differential brain activations in adult attention-deficit/ hyperactivity disorder subtypes: a counting Stroop functional MRI study', *Brain Imaging Behav*, 12: 882-90.

Stewart-Brown, Sarah, and Kulsum Janmohamed. 2008. 'Warwick-Edinburgh mental well-being scale', *User guide. Version*, 1: 2.

Sun, Y., K. Jin, J. T. Childs, L. Xie, X. O. Mao, and D. A. Greenberg. 2006. 'Vascular endothelial growth factor-B (VEGFB) stimulates neurogenesis: evidence from knockout mice and growth factor administration', *Dev Biol*, 289: 329-35.

Wager, T. D., C. Y. Sylvester, S. C. Lacey, D. E. Nee, M. Franklin, and J. Jonides. 2005. 'Common and unique components of response inhibition revealed by fMRI', *Neuroimage*, 27: 323-40.

Wang, Y. 2019. 'Transcranial direct current stimulation for the treatment of major depressive disorder: A meta-analysis of randomized controlled trials', *Psychiatry Res*, 276: 186-90.

Williams, Leanne M. 2016. 'Precision psychiatry: a neural circuit taxonomy for depression and anxiety', *The Lancet Psychiatry*, 3: 472-80.

Yaakub, Siti N., Tristan A. White, Jamie Roberts, Eleanor Martin, Lennart Verhagen, Charlotte J. Stagg, Stephen Hall, and Elsa F. Fouragnan. 2023. 'Transcranial focused ultrasound-mediated neurochemical and functional connectivity changes in deep cortical regions in humans', *Nature Communications*, 14.

Yahata, K., H. Kanno, H. Ozawa, S. Yamaya, S. Tateda, K. Ito, H. Shimokawa, and E. Itoi. 2016. 'Low-energy extracorporeal shock wave therapy for promotion of vascular endothelial growth factor expression and angiogenesis and improvement of locomotor and sensory functions after spinal cord injury', *J Neurosurg Spine*, 25: 745-55.

Yeo, B. T., F. M. Krienen, J. Sepulcre, M. R. Sabuncu, D. Lashkari, M. Hollinshead, J. L. Roffman, J. W. Smoller, L. Zollei, J. R. Polimeni, B. Fischl, H. Liu, and R. L. Buckner. 2011. 'The organization of the human cerebral cortex estimated by intrinsic functional connectivity', *J Neurophysiol*, 106: 1125-65.

Chapter 6 Conclusions and Suggestions for Future Research

This research establishes TPS as a safe, well-tolerated, and effective intervention for MDD, with demonstrable neuromodulation on depression-relevant brain circuits. These findings on MDD provide a strong foundation for optimizing TPS therapeutic efficacy by increasing treatment sessions and refining targeting strategies. On the other hand, a single TPS session did not demonstrate sufficient utility as a combined therapy for modulating behaviors. Furthermore, TPS applied to the dACC and AIC was shown to be both feasible and safe in healthy adults, producing changes in risk-taking behavior and demonstrating target-specific neuromodulatory effects. Collectively, these findings provide a strong foundation for future studies to optimize TPS protocols, explore the AIC and dACC as novel therapeutic targets, and further examine the underlying neural mechanisms of its antidepressive effects.

Future studies are required to (1) investigate the neural mechanisms underlying TPS's antidepressive effect using online neuroimaging or neurophysiological approaches; (2) assess the immediate and short-term aftereffects of multiple TPS sessions; (3) confirm both the short-term and long-term efficacy of deeper brain TPS stimulation in larger samples; and (4) evaluate the feasibility and therapeutic potential of deeper brain TPS in patients with MDD.

Appendices

Table S1. Search strategy of MEDLINE through PubMed

#1	"low intensity transcranial ultrasound"
#2	"transcranial focused ultrasound"
#3	"transcranial unfocused ultrasound"
#4	"transcranial pulse stimulation"
#5	"transcranial ultrasound"
#6	"low intensity transcranial focused ultrasound"
#7	#1 OR #2 OR #3 OR #4 OR #5 OR #6
#8	"focused ultrasound"
#9	transcranial
#10	ultrasound
#11	#8 AND #9
#12	#9 AND #10
#13	#7 OR #11 OR #12
#14	neuromodulation
#15	#13 AND #14
Filters	Results by year: from 1940 to 2023 (search date: 31 May 2023)
	Language: English and Chinese
	Source: MEDLINE

Table S2. Search strategy of Embase through Embase

#1	"low intensity transcranial ultrasound"
#2	"transcranial focused ultrasound"

#3	"transcranial unfocused ultrasound"
#4	"transcranial pulse stimulation"
#5	"transcranial ultrasound"
#6	"low intensity transcranial focused ultrasound"
#7	#1 OR #2 OR #3 OR #4 OR #5 OR #6
#8	"focused ultrasound"
#9	transcranial
#10	ultrasound
#11	#8 AND #9
#12	#9 AND #10
#13	#7 OR #11 OR #12
#14	neuromodulation
#15	#13 AND #14
Filters	Publication Years from: <1966 to 2023 (search date: 31 May 2023)
	Language: English and Chinese
	Source: Embase

Table S3. Search strategy of CENTRAL through Cochrane Library

#1	"low intensity transcranial ultrasound"
#2	"transcranial focused ultrasound"
#3	"transcranial unfocused ultrasound"
#4	"transcranial pulse stimulation"
#5	"transcranial ultrasound"
#6	"low intensity transcranial focused ultrasound"
#7	#1 OR #2 OR #3 OR #4 OR #5 OR #6

#8	"focused ultrasound"
#9	transcranial
#10	ultrasound
#11	#8 AND #9
#12	#9 AND #10
#13	#7 OR #11 OR #12
#14	neuromodulation
#15	#13 AND #14
Filters	Search date: 31 May 2023
	Language: English and Chinese

Table S4. Search strategy of CINAHL through EBSCOHost

#1	"low intensity transcranial ultrasound"
#2	"transcranial focused ultrasound"
#3	"transcranial unfocused ultrasound"
#4	"transcranial pulse stimulation"
#5	"transcranial ultrasound"
#6	"low intensity transcranial focused ultrasound"
#7	#1 OR #2 OR #3 OR #4 OR #5 OR #6
#8	"focused ultrasound"
#9	transcranial
#10	ultrasound
#11	#8 AND #9
#12	#9 AND #10
#13	#7 OR #11 OR #12
#14	neuromodulation

#15	#13 AND #14
Filters	Search date: 31 May 2023
	Language: English and Chinese

Table S5. Search strategy of WOB through Web of Science

#1	"low intensity transcranial ultrasound"
#2	"transcranial focused ultrasound"
#3	"transcranial unfocused ultrasound"
#4	"transcranial pulse stimulation"
#5	"transcranial ultrasound"
#6	"low intensity transcranial focused ultrasound"
#7	#1 OR #2 OR #3 OR #4 OR #5 OR #6
#8	"focused ultrasound"
#9	transcranial
#10	ultrasound
#11	#8 AND #9
#12	#9 AND #10
#13	#7 OR #11 OR #12
#14	neuromodulation
#15	#13 AND #14
Filters	Publication date: from database inception to 2023 (search date: 31 May 2023)
	Language: English and Chinese

The treatment compliance in Study 2: Among 74 participants who completed 12 TPS treatment sessions, 48 participants (n = 23 active, n = 25 sham) adhered to the treatment protocol (3 sessions per week for 4 weeks). Among the 26 participants (n = 15 active, n = 11 sham) who failed to adhere to the treatment protocol, 25 completed 12 TPS sessions in 5 weeks (n = 14 active, n = 11 sham), while one completed the treatment sessions in 8 weeks (n = 1 active). The reasons for non-compliance were as follows: (1) time conflicts (n = 11 active, n = 7 sham); (2) unexpected breakdown of the TPS device (n = 4 active, n = 4 sham).

Table S6. Changes in MADRS scores from baseline to Week 2 and from Week 2 to posttreatment (Week 4)

	Baseline	**Week 2**	**Posttreatment**		
	Mean (SE)	**Mean (SE)**	**Mean (SE)**	**p-value (baseline vs. Week 2)**	**p-value (Week 2 vs. posttreatment)**
Active group	27.35 (1.42)	19.23 (1.23)	15.34 (1.45)	$p_{corrected} < .001$	$p_{corrected} = 0.002$
Sham group	27.85 (1.42)	21.72 (1.24)	19.77 (1.48)	$p_{corrected} < .001$	$p_{corrected} = 0.252$

Table S7. Correlation analysis between the rsFC changes in significant clusters for the Group x Time interaction effect and improved MADRS scores in Study 2 (n = 33 active group vs. n = 33 sham group for completers).

Cluster No.	Clusters with a significant interaction effect (active vs. sham x pre vs. post)	Correlation with improved total MADRS scores	p-value (uncorrected)
Cluster 1	Left inferior frontal gyrus, orbital part, triangular part; Left middle temporal gyrus; Left temporal pole: superior & middle temporal gyrus	r = 0.288	.104
Cluster 2	Right superior & middle temporal gyrus; Right angular gyrus; Right inferior parietal gyrus; Right supramarginal gyrus	r = -0.148,	.411
Cluster 3	Left middle & superior temporal gyrus; Left supramarginal gyrus; Left angular gyrus; Left inferior parietal gyrus	r = 0.043	.811
Cluster 4	Right temporal pole: superior & middle temporal gyrus; Right middle temporal gyrus	r = 0.361	.039*
Cluster 5	Left posterior cingulum gyrus; Left & right precuneus; Left & right calcarine	r = 0.04	.808
Cluster 6	Left middle frontal gyrus, orbital part; Left superior frontal gyrus, medial; Left anterior cingulum	r = 0.196	.274
Cluster 7	Right superior & middle temporal gyrus	r = 0.376	.031*
Cluster 8	Left & right superior frontal gyrus, medial	r = 0.114	.528

Cluster 9	Right inferior frontal gyrus, triangular part	r = -0.105	.561
Cluster 10	Left superior & middle frontal gyrus	r = 0.285	.108
Cluster 11	Right & left supplementary motor area;	r = 0.123	.494
Cluster 12	Right inferior frontal gyrus, orbital & triangular part	r = 0.250	.160

Figure S1. Reaction time interference (incongruent vs. neutral trials) in the counting Stroop task.

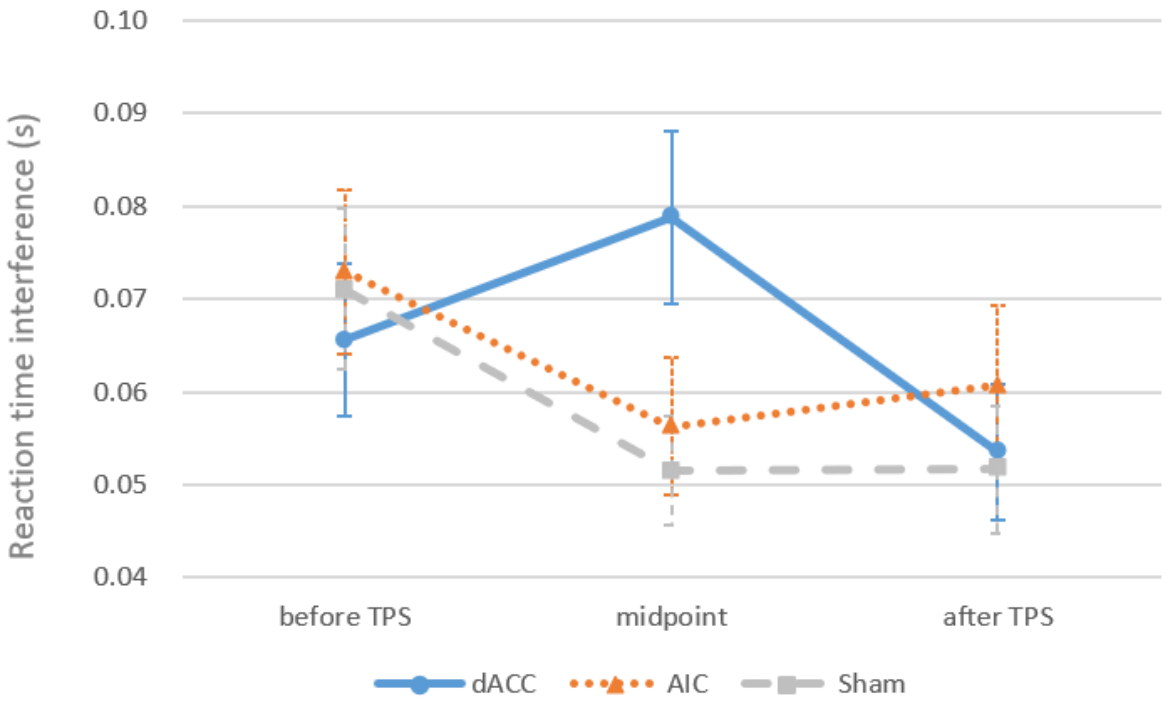

The dots, triangles, and squares indicate the mean values in the dACC, AIC, and sham groups, respectively; The bars indicate the standard errors.

Figure S2. Accuracy interference (neutral vs. incongruent trials) in the counting Stroop task.

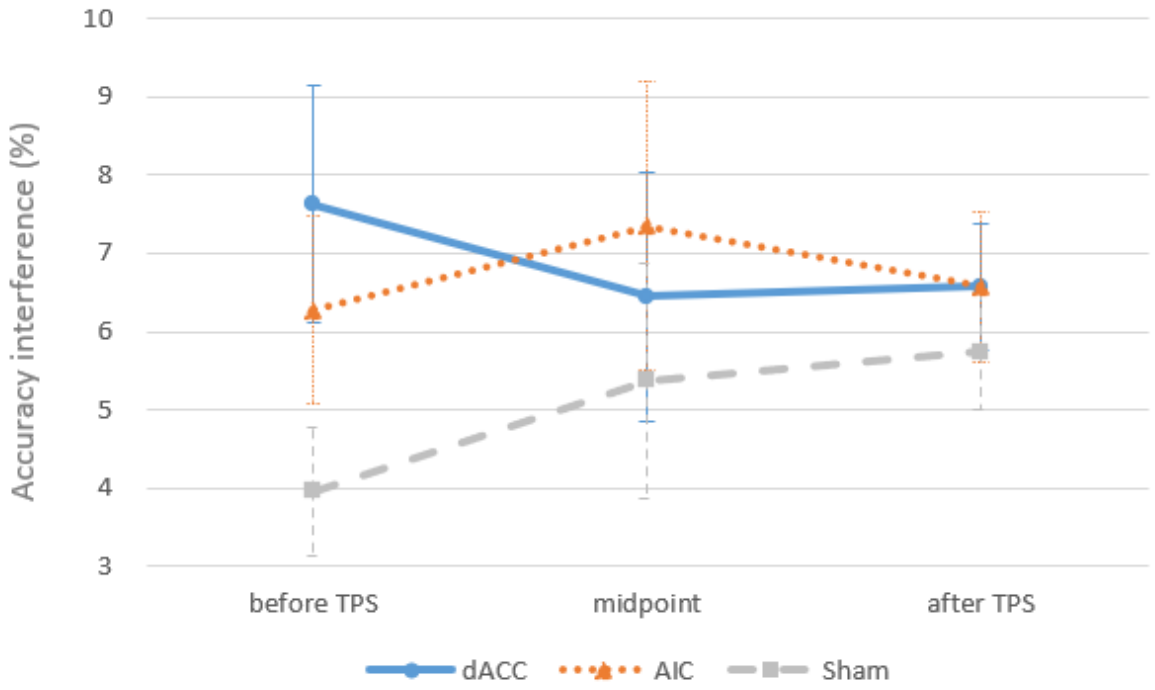

The dots, triangles, and squares indicate the mean values in the dACC, AIC, and sham groups, respectively; The bars indicate the standard errors.

Figure S3. False alarm rate (FAR) in No-Go trials in the Go/No-Go test (GNGT) with 50% No-Go trials.

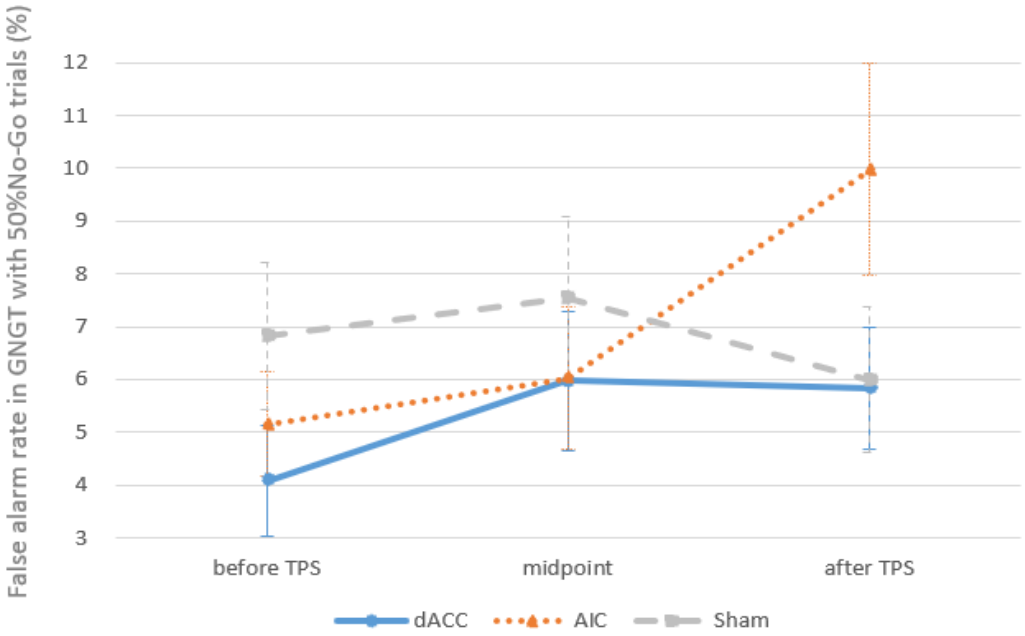

The dots, triangles, and squares indicate the mean values in the dACC, AIC, and sham groups, respectively; The bars indicate the standard error.

Figure S4. False alarm rate (FAR) in No-Go trials in the Go/No-Go test (GNGT) with 20% No-Go trials.

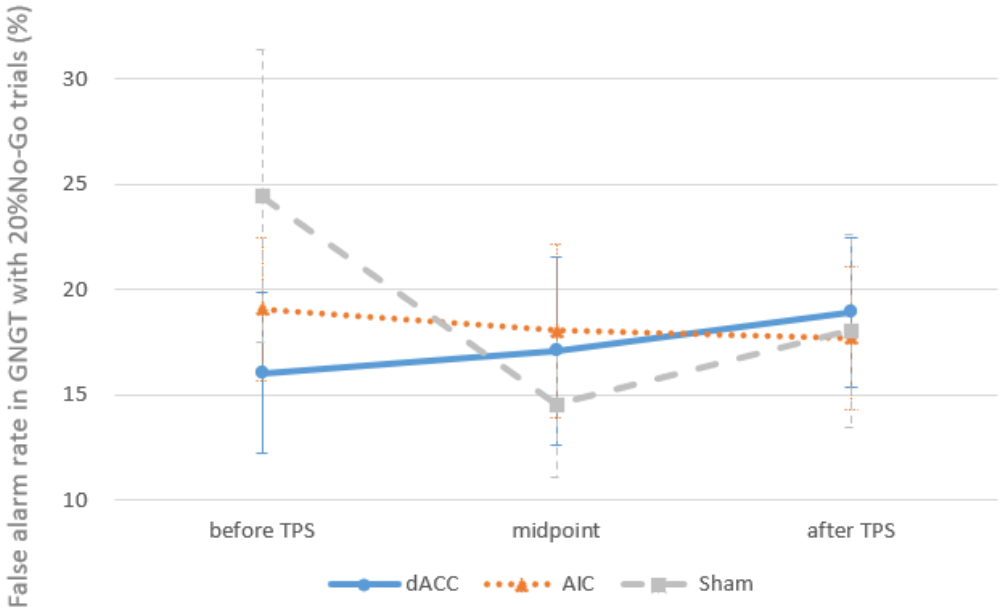

The dots, triangles, and squares indicate the mean values in the dACC, AIC, and sham groups, respectively; The bars indicate the standard error.

Figure S5. Scores of the reading mind in the eyes test (RMET) in individual groups.

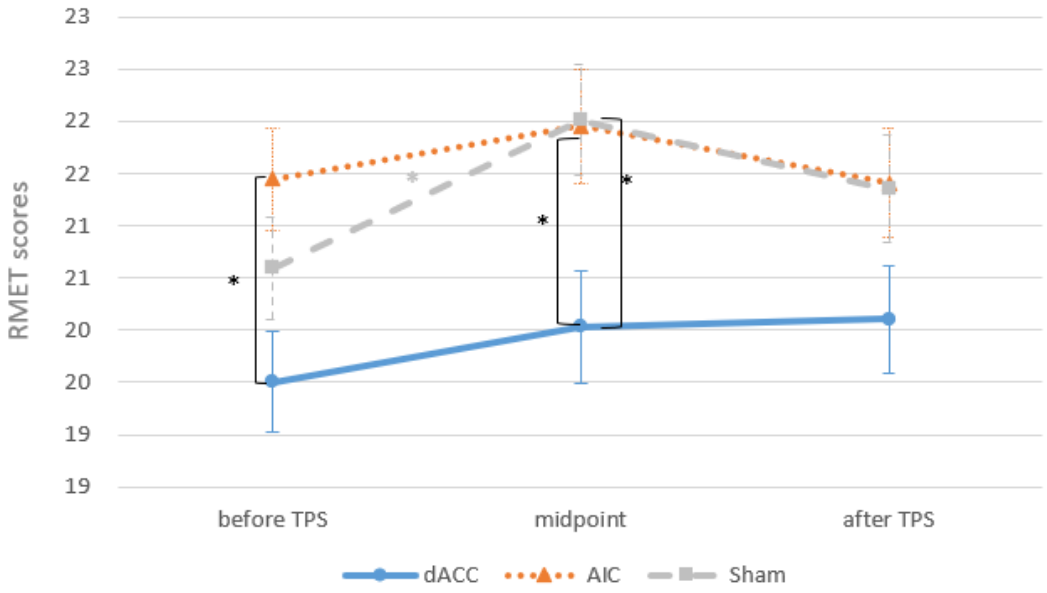

The dots, triangles, and squares indicate the mean values in the dACC, AIC, and sham groups, respectively; Bars indicate the standard errors. *: p-value < 0.05 after Bonferroni correction. Asterisks above the line indicate the within-group difference between baseline and midpoint.

Figure S6. Subjective happiness scale (SHS) scores in individual groups.

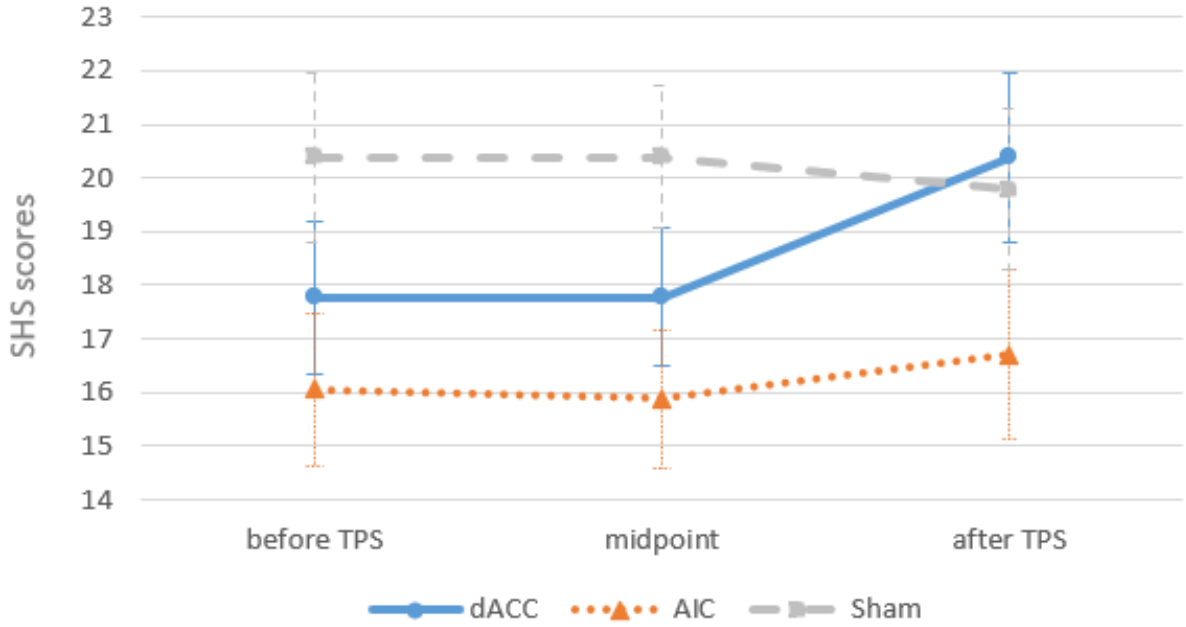

The dots, triangles, and squares indicate the mean values in the dACC, AIC, and sham groups, respectively; The bars indicate the standard errors.

Figure S7. Warwick-Edinburgh mental well-being scale (WEMWBS) scores in individual groups.

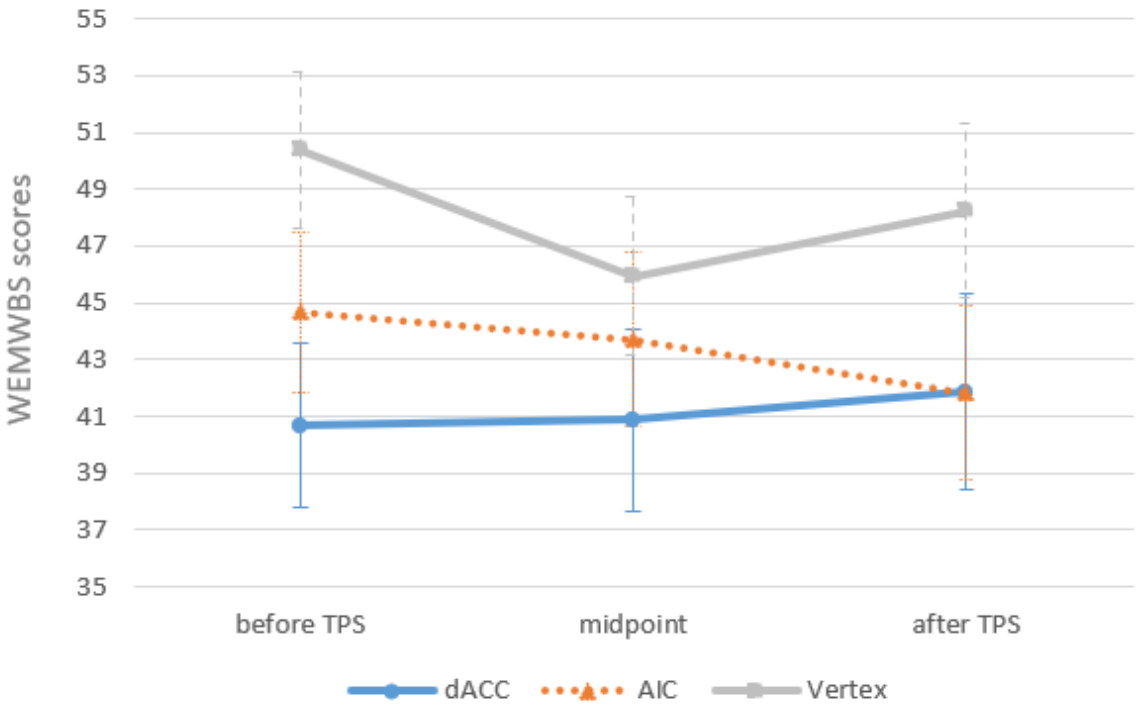

The dots, triangles, and squares indicate the mean values in the dACC, AIC, and sham groups, respectively; The bars indicate the standard errors.

Figure S8. Profile of mood scale (POMS) scores in individual groups.

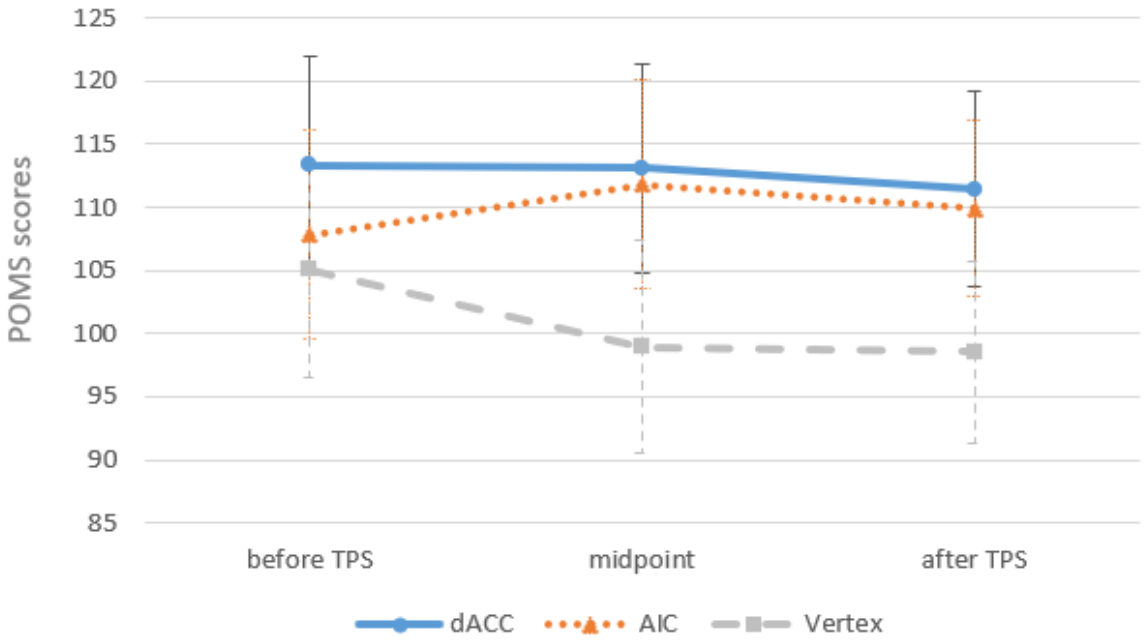

The dots, triangles, and squares indicate the mean values in the dACC, AIC, and sham groups, respectively; The bars indicate the standard errors.

Table S8. Rs-FC results displaying AIC-seeded clusters with a significant interaction effect (dACC vs. sham x post-TPS vs. pre-TPS) and the corresponding post-hoc analyses (completers: n = 18 dACC group; n = 18 sham group) in Study 4

	Interaction effect ($P_{FWE-corr} < 0.05$)						Post-hoc analysis, pre vs. post		Post-hoc analysis, active vs. sham	
	Cluster No.	**Brain regions defined by AAL**	**F**	**k**	**Peak MNI coordinates, x y z**	**AAL for the peak MNI**	**dACC**	**sham**	**pre-TPS**	**post-TPS**
rAIC-seeded	Cluster 1	Frontal_Mid_Orb_R; Frontal_Inf_Orb_R; Frontal_Inf_Tri_R; Frontal_Sup_Orb_R; Frontal_Mid_R	54.96 ($P_{FWE-corr} < 0.0001$; $P_{FDR-corr} < 0.0001$)	907	36 51 -9	Frontal_Mid_Orb_R	t = -1.430, p = 0.171	t = -1.002, p = 0.330	t = 0.256, p = 0.800	t = 0.608, p = 0.547
	Cluster 2	Frontal_Inf_Tri_R; Frontal_Mid_R; Frontal_Inf_Oper_R	43.95 ($P_{FWE-corr} < 0.0001$; $P_{FDR-corr} = 0.001$)	120	54 30 30	Frontal_Inf_Tri_R	t = -1.840, p = 0.083	t = -1.423, p = 0.173	t = -0.080, p = 0.936	t = 0.349, p = 0.719
	Cluster 3	Postcentral_R; SupraMarginal_R; Parietal_Inf_R	36.68 ($P_{FWE-corr} = 0.001$; $P_{FDR-corr} = 0.003$)	98	57 -24 54	Postcentral_R	t = 0.768, p = 0.453	t = 1.544, p = 0.141	t = -0.727, p = 0.472	t = 0.803, p = 0.428

Cluster 4	Temporal_Sup_R; Temporal_Mid_R	41.20 ($P_{FWE-corr}$ = 0.001; $P_{FDR-corr}$ = 0.003)	97	60 -42 15	Temporal_Sup_R	t = -1,892, p = 0.076	t = -0.266, p = 0.794	t = -0.519, p = 0.607	t = 0.613, p = 0.272
Cluster 5	Temporal_Mid_R; Temporal_Sup_R	28.71 ($P_{FWE-corr}$ = 0.002; $P_{FDR-corr}$ = 0.004)	87	57 -21 -6	Temporal_Mid_R	t = -1.679, p = 0.111	t = -1.404, p = 0.178	t = 0.013, p = 0.990	t = 0.330, p = 0.743
Cluster 6	Temporal_Pole_Mid_R; Temporal_Mid_R	26.18 ($P_{FWE-corr}$ = 0.003; $P_{FDR-corr}$ = 0.005)	81	51 12 -27	Temporal_Pole_Mid_R	t = -1.777, p = 0.093	t = -1.763, p = 0.096	t = 1.442, p = 0.159	t = 0.803, p = 0.427
Cluster 7	Calcarine_R; Lingual_R	27.19 ($P_{FWE-corr}$ = 0.008; $P_{FDR-corr}$ = 0.009)	69	21 -63 9	Calcarine_R	t = -1.550, p = 0.139	t = -1.247, p = 0.229	t = -0.107, p = 0.916	t = -0.040, p = 0.968
Cluster 8	Frontal_Inf_Tri_L	25.90 ($P_{FWE-corr}$ = 0.013; $P_{FDR-corr}$ = 0.014)	62	-51 27 6	Frontal_Inf_Tri_L	**t = -2.746, p = 0.014***	t = -1.284, p = 0.216	t = 0.107, p = 0.915	t = 0.789, p = 0.435
Cluster 9	Precentral_L; Postcentral_L	34.13 ($P_{FWE-corr}$ = 0.040; $P_{FDR-corr}$ = 0.038)	47	-60 0 36	Precentral_L	**t = -2.141,**	t = -1.183,	t = -0.189, p = 0.851	t = 0.549, p = 0.587

						p = 0.047*	p = 0.253		
	Cluster 10	Temporal_Mid_L	27.55 ($P_{FWE\text{-}corr}$ = 0.050; $P_{FDR\text{-}corr}$ = 0.044)	44 -54 -24 -6	Temporal_Mid_L	t = -2.115, p = 0.050	t = -1.392, p = 0.182	t = 1.569, p = 0.063	t = 1.457, p = 0.077
lAIC-seeded	Cluster 1	Frontal_Inf_Tri_R; Frontal_Inf_Orb_R; Frontal_Mid_Orb_R	36.85 ($P_{FWE\text{-}corr}$ < 0.0001; $P_{FDR\text{-}corr}$ < 0.0001)	209 51 27 6	Frontal_Inf_Tri_R	t = -0.898, p = 0.382	t = -0.037, p = 0.971	t = -0.463, p = 0.323	t = 0.241, p = 0.406
	Cluster 2	Supp_Motor_Area_R; Frontal_Sup_R; Frontal_Sup_Medial_R [little]	27.84 ($P_{FWE\text{-}corr}$ = 0.001; $P_{FDR\text{-}corr}$ = 0.005)	123 15 15 69	Supp_Motor_Area_R	t = -1.132, p = 0.273	t = -0.710, p = 0.487	t = -0.537, p = 0.297	t = 0.082, p = 0.468
	Cluster 3	Frontal_Sup_Medial_L, R; Cingulum_Mid_R	38.74 ($P_{FWE\text{-}corr}$ = 0.013; $P_{FDR\text{-}corr}$ = 0.037)	77 0 57 39	Frontal_Sup_Medial_L	t = -1.380, p = 0.185	t = -0.527, p = 0.605	t = 0.339, p = 0.368	t = 0.863, p = 0.197
	Cluster 4	Postcentral_R; Parietal_Inf_R; SupraMarginal_R	33.46 ($P_{FWE\text{-}corr}$ = 0.019; $P_{FDR\text{-}corr}$ = 0.042)	70 57 -21 54	Postcentral_R	t = -0.904, p = 0.379	t = 1.495, p = 0.153	t = -0.437, p = 0.333	t = 0.991, p = 0.164

Cluster 5	Temporal_Sup_R; Temporal_Mid_R	28.15 ($P_{FWE\text{-}corr}$ = 0.044; $P_{FDR\text{-}corr}$ = 0.079)	56	60 -39 18	Temporal_Sup_R	t = -1.700, p = 0.107	t = -1.373, p = 0.187	t = 0.219, p = 0.414	t = 0.375, p = 0.355

Figure S9. AIC-seeded rsFC changes in clusters showing significant interaction effects (dACC vs. sham x post-TPS vs. pre-TPS) in Study 4.

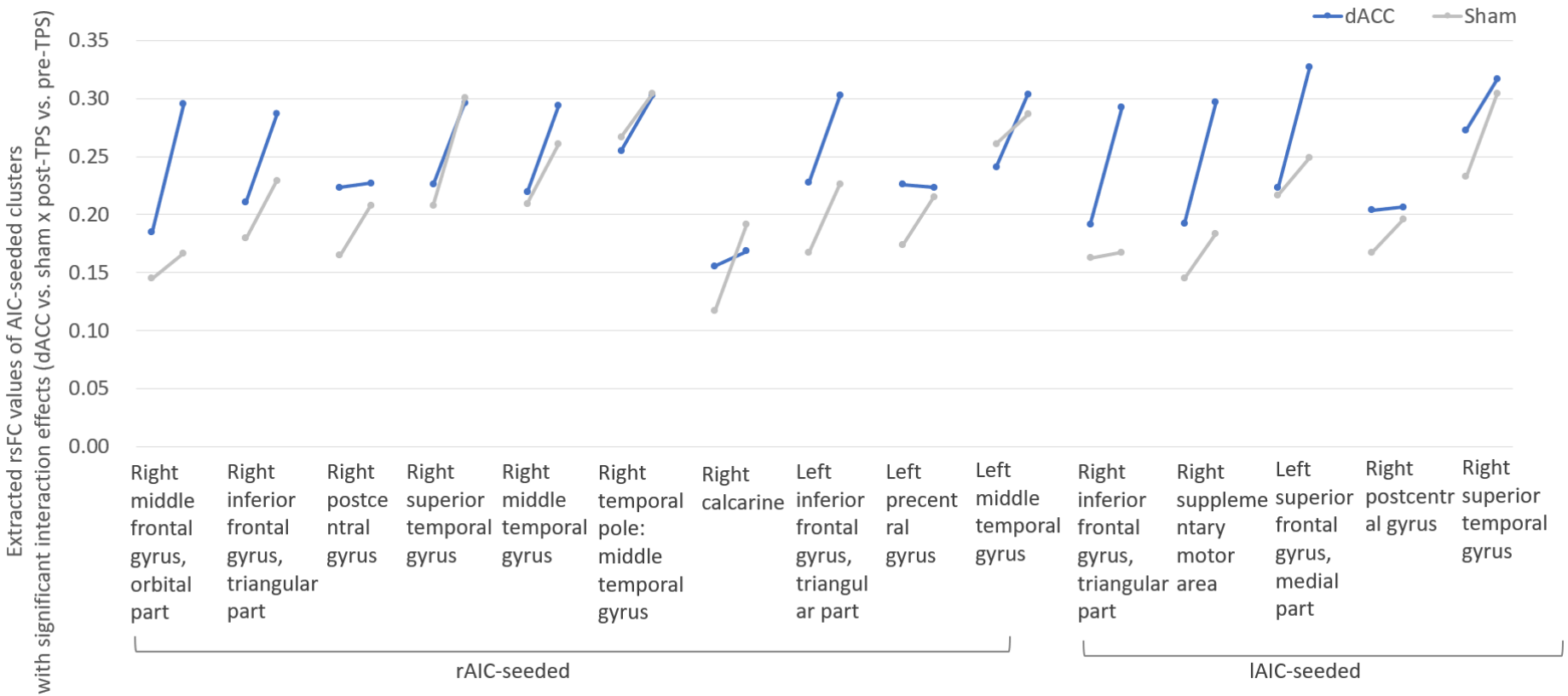

The dots represent mean rsFC values extracted at pre-TPS and post-TPS for individual clusters. rAIC-seeded rsFC: significant interaction effects were observed with clusters whose peak MNI coordinates were located in the right middle frontal gyrus (orbital part), right inferior frontal gyrus (triangular part), right postcentral gyrus, right superior and middle temporal gyrus, right temporal pole: middle temporal gyrus, right calcarine, left inferior frontal gyrus

(triangular part), and left precentral gyrus. lAIC-seeded rsFC: significant interaction effects were observed with clusters whose peak MNI coordinates were located in the right inferior frontal gyrus (triangular part), right supplementary motor area, left superior frontal gyrus (medial part), right postcentral gyrus, and right superior temporal gyrus.

Table S9. RsFC results displaying dACC-seeded clusters with a significant interaction effect (AIC vs. sham x post-TPS vs. pre-TPS) and the corresponding post-hoc analysis (completers: n=17 AIC group; n=18 sham group) in Study 4.

	Interaction effect ($P_{FWE-corr} < 0.05$)					Post-hoc analysis, pre vs. post		Post-hoc analysis, active vs. sham	
	Cluster No.	**Brain regions defined by AAL**	**F**	**k**	**Peak MNI coordinates, x y z**	**AAL for the peak MNI**	**AIC**	**sham**	**pre-TPS**	**post-TPS**
rdACC-seeded	Cluster 1	Frontal_Mid_Orb_R, L; Frontal_Sup_Orb_L [little]; Frontal_Sup_Medial_R [little]; Frontal_Sup_R [little]	33.01 ($P_{FWE-corr} < 0.0001$; $P_{FDR-corr} = 0.001$)	139	6 63 -3	Frontal_Mid_Orb_R	t = 0.139, p = 0.892	t = 0.431, p = 0.672	t = 0.803, p = 0.428	t = 1.033, p = 0.309
	Cluster 2	Frontal_Sup_Medial_R; Frontal_Sup_R; Frontal_Mid_R	42.90 ($P_{FWE-corr} < 0.0001$; $P_{FDR-corr} = 0.001$)	120	12 39 48	Frontal_Sup_Medial_R	t = 1.783, p = 0.094	t = 0.340, p = 0.738	t = 1.183, p = 0.245	t = -0.125, p = 0.901
	Cluster 3	Fronal_Mid_L; Frontal_Inf_Tri_L [little]	37.94 ($P_{FWE-corr} = 0.001$; $P_{FDR-corr} = 0.001$)	118	-36 33 33	Fronal_Mid_L	t = 0.116, p = 0.909	t = -0.324, p = 0.750	t = 0.198, p = 0.844	t = -0.124, p = 0.902

	Cluster 4	Frontal_Sup_Medial_R, L; Cingulum_Ant_R	26.47 ($P_{FWE\text{-}corr}$ = 0.006; $P_{FDR\text{-}corr}$ = 0.010)	78	6 57 21	Frontal_Sup_Medial_R	t = 0.351, p = 0.730	t = 0.071, p = 0.944	t = 0.943, p = 0.352	t = 0.706, p = 0.485
	Cluster 5	Temporal_Mid_R;	26.22 ($P_{FWE\text{-}corr}$ = 0.024; $P_{FDR\text{-}corr}$ = 0.031)	57	69 -36 -9	Temporal_Mid_R	t = 1.423, p = 0.174	t = -0.639, p = 0.531	t = 1.862, p = 0.072	t = 0.190, p = 0.851
	Cluster 6	Temporal_Mid_R; Angular_R [little]	25.43 ($P_{FWE\text{-}corr}$ = 0.025; $P_{FDR\text{-}corr}$ = 0.031)	56	48 -66 18	Temporal_Mid_R	t = 0.943, p = 0.360	t = -0.859, p = 0.402	t = 0.905, p = 0.372	t = -0.644, p = 0.524
	Cluster 7	Frontal_Mid_Orb_R; Frontal_Mid_R	31.19 ($P_{FWE\text{-}corr}$ = 0.039; $P_{FDR\text{-}corr}$ = 0.041)	50	39 54 -3	Frontal_Mid_Orb_R	t = -0.979, p = 0.342	t = 1.079, p = 0.296	t = -0.954, p = 0.347	t = 0.803 p = 0.428
ldACC-seeded	Cluster 1	Frontal_Sup_Orb_L; Frontal_Mid_Orb_L, R	33.95 ($P_{FWE\text{-}corr}$ = 0.002; $P_{FDR\text{-}corr}$ = 0.009)	90	-15 57 -6	Frontal_Sup_Orb_L	t = -0.321, p = 0.752	t = -1.602, p = 0.128	**t = 2.246, p = 0.030***	t = 1.482, p = 0.148
	Cluster 2	Temporal_Mid_R	26.78 ($P_{FWE\text{-}corr}$ = 0.005; $P_{FDR\text{-}corr}$ = 0.014)	73	48 -66 18	Temporal_Mid_R	t = -0.446,	t = -1.876,	t = -0.038, p = 0.970	t = -1.152, p = 0.257

	p = 0.662	p = 0.078

Figure S10. dACC-seeded rsFC changes in clusters showing significant interaction effects (AIC vs. sham x post-TPS vs. pre-TPS) in Study 4.

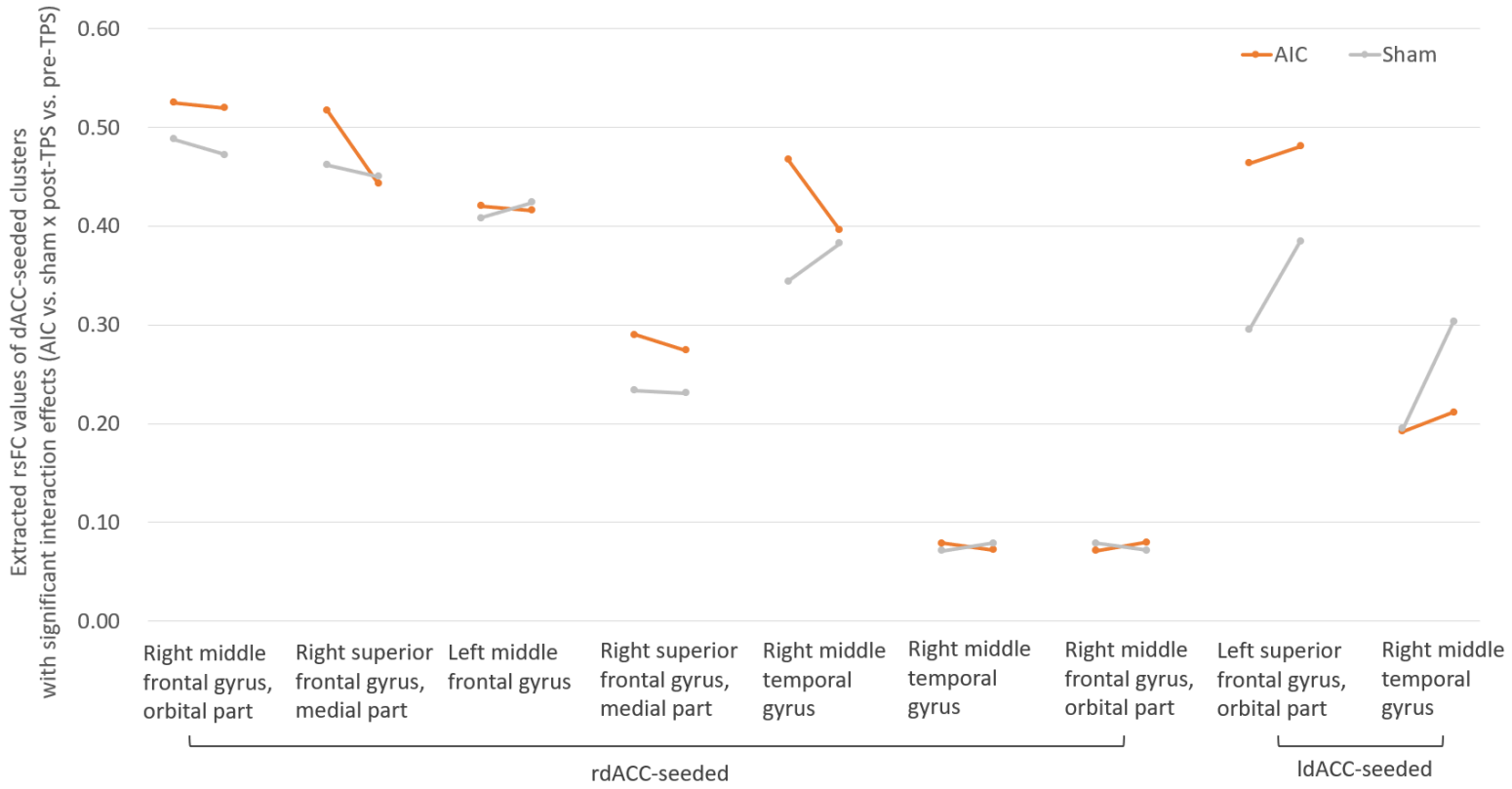

The dots represent mean rsFC values extracted at pre-TPS and post-TPS for individual clusters. rdACC-seeded rsFC: significant interaction effects were observed with clusters whose peak MNI coordinates were located in the right middle frontal gyrus (orbital part), right superior frontal gyrus (medial part), left

middle frontal gyrus, right superior frontal gyrus (medial part), right middle temporal gyrus, and right middle frontal gyrus (orbital part). lAIC-seeded rsFC: significant interaction effects were observed with clusters whose peak MNI coordinates were located in the left superior frontal gyrus (orbital part), and right middle temporal gyrus.